



HAL
open science

Impact of a +2°C climate on the emission of biogenic volatile organic compounds and on air quality

Safae Oumami

► **To cite this version:**

Safae Oumami. Impact of a +2°C climate on the emission of biogenic volatile organic compounds and on air quality. Earth Sciences. Université de Toulouse, 2024. English. NNT : 2024TLSEP013 . tel-04503172

HAL Id: tel-04503172

<https://theses.hal.science/tel-04503172>

Submitted on 13 Mar 2024

HAL is a multi-disciplinary open access archive for the deposit and dissemination of scientific research documents, whether they are published or not. The documents may come from teaching and research institutions in France or abroad, or from public or private research centers.

L'archive ouverte pluridisciplinaire **HAL**, est destinée au dépôt et à la diffusion de documents scientifiques de niveau recherche, publiés ou non, émanant des établissements d'enseignement et de recherche français ou étrangers, des laboratoires publics ou privés.

Doctorat de l'Université de Toulouse

préparé à Toulouse INP

Impact d'un climat à +2°C sur les émissions des composés
biogéniques volatils et sur la qualité de l'air

Thèse présentée et soutenue, le 13 février 2024 par

Safae OUMAMI

École doctorale

SDU2E - Sciences de l'Univers, de l'Environnement et de l'Espace

Spécialité

Océan, Atmosphère, Climat

Unité de recherche

CNRM - Centre National de Recherches Météorologiques

Thèse dirigée par

Vincent GUIDARD et Joaquim ARTETA

Composition du jury

M. Didier HAUGLUSTAINE, Rapporteur, CNRS

Mme Agnès BORBON, Rapporteur, CNRS

Mme Trissevgeni STAVRAKOU, Rapporteur, Institut d'Aéronomie Spatiale de Belgique

M. Vincent GUIDARD, Directeur de thèse, Météo France

M. Joaquim ARTETA, Co-directeur de thèse, Météo France

Mme Nadia FOURRIÉ, Présidente, CNRS

Membres invités

Mme Christine Delire, CNRS

M. Paul David Hamer, NILU

”Nothing in life is to be feared,
it is only to be understood. Now
is the time to understand more,
so that we may fear less.”

Marie Curie

Abstract

Once Volatile Organic Compounds (VOCs) are released into the atmosphere, they play a major role in altering its chemistry and composition, consequently impacting the global climate. VOCs released from natural sources account for 90% of the total emitted VOCs, which makes Biogenic Volatile Organic Compounds (BVOCs) a key contributor to the formation of several air pollutants. The influence of BVOCs goes beyond air quality concerns, as they can impact the climate through the formation of aerosols which have a cooling effect and greenhouse gases which have a warming effect, thus effecting the Earth's net radiative forcing. Conversely, climate can effect the release of biogenic species through global warming, land cover and land use change, drought and increasing atmospheric CO_2 concentrations. The present work aims to evaluate how BVOCs emission will evolve in a $+2^\circ C$ climate change conditions and how this change will effect air quality in the future.

For this purpose, a consequent work was undertaken to couple the SURFEX (SURface Externalisée in French) and MEGAN (Model of Emission of Gases and Aerosols from Nature) models. The coupled model SURFEX-MEGAN will allow the simulation of future emissions of biogenic species along with other important emission key drivers such as leaf area index, soil moisture, soil temperature, etc. The impact of climate change on isoprene emissions was assessed by conducting two global simulations representing present- and future-climate conditions over 2010-2014 and 2046-2050, respectively. The results of this study indicate a global increase of isoprene emissions by 13% (40 Tg). This change account for the effect of temperature, solar radiation and atmospheric CO_2 concentrations. Temperature have the highest positive effect. Solar radiation have a negative effect as it decreased under the SSP3-7.0 scenario and CO_2 concentrations have both positive and negative effects. The former arises from the CO_2 fertilization effect and the latter from the CO_2 inhibition effect. The SURFEX-MEGAN results were confronted to other projections from CMIP6 models. Most of the models predicted a positive trend in future isoprene emissions. The disparities in model results are attributed to variations in isoprene schemes, resolution, vegetation distribution, and density, but most importantly, each model's output of temperature and solar radiation differed, despite employing the same SSP scenario.

The study of the impact of climate change on future ozone levels showed that the ozone burden will increase by 5% in 2050 compared to 2013. This change is mainly due to the change in human-induced NO_x and VOC emissions. Although ozone's sensitivity to isoprene is high, the inclusion of future changes in isoprene emissions have only a marginal effect on global ozone trends. However, this effect is significant at regional and local scales, where ozone is positively and negatively correlated to isoprene trends in high and low NO_x regions, respectively. The impact of isoprene emissions in future air quality is most significant when neglecting the inhibitory effect of CO_2 on isoprene emissions. In this case air quality was predicted to improve at a global scale and in tropical regions particularly in the future compared to a future-climate scenario with present-climate isoprene emissions.

Résumé

Une fois libérés dans l'atmosphère, les Composés Organiques Volatils (COV) jouent un rôle majeur dans l'altération de la chimie et de la composition de l'atmosphère, impactant ainsi le climat mondial. Les COV émis par des sources naturelles représentent 90% du total des COV émis, ce qui fait des Composés Organiques Volatils Biogéniques (COVB) un contributeur clé à la formation de plusieurs polluants atmosphériques. L'influence des COVB va au-delà des préoccupations liées à la qualité de l'air, car ils peuvent affecter le climat par la formation d'aérosols et gaz à effet de serre, impactant ainsi le forçage radiatif net de la Terre. À l'inverse, le climat peut influencer les COVB par le biais de température, des changements de couverture et d'utilisation des sols et de l'augmentation des concentrations du CO₂. Le présent travail vise à évaluer comment les émissions de COVB évolueront dans un climat à +2°C et comment ce changement affectera la qualité de l'air dans le futur.

À cette fin, un travail conséquent a été entrepris pour coupler les modèles SURFEX (SURface Externalisée) et MEGAN (Model of Emission of Gases and Aerosols from Nature). Le modèle SURFEX-MEGAN permettra la simulation des émissions futures des COVB ainsi que d'autres facteurs clés d'émission tels que l'indice de surface foliaire (LAI), l'humidité du sol, la température du sol, etc. L'impact du changement climatique sur l'isoprène a été évalué en réalisant deux simulations globales représentant les conditions climatiques actuelles et futures. Les résultats de cette étude indiquent une augmentation globale des émissions d'isoprène de 13%. Cette variation prend en compte l'effet de la température, du rayonnement solaire et des concentrations du CO₂. La température a l'effet positif le plus élevé. Le rayonnement solaire a un effet négatif et les concentrations de CO₂ ont à la fois des effets positifs et négatifs. Le premier résulte de l'effet de fertilisation par le CO₂ et le second de l'effet d'inhibition du CO₂. Les résultats de SURFEX-MEGAN ont été confrontés à d'autres projections provenant des modèles CMIP6. La plupart des modèles ont prédit une tendance positive pour les émissions futures d'isoprène. Les disparités dans les résultats des modèles sont attribuées aux variations dans les schémas d'isoprène, la distribution de la végétation, mais surtout, les sorties de température et de rayonnement solaire de chaque modèle différaient, malgré l'utilisation du même scénario SSP.

L'étude de l'impact du changement climatique sur les niveaux futurs d'ozone a montré que la charge d'ozone augmentera de 5% en 2050 par rapport à 2013. Ce changement est principalement dû au changement des émissions anthropiques de NO_x et de COV. Bien que la sensibilité de l'ozone à l'isoprène soit élevée, l'inclusion des changements futurs de l'isoprène n'a qu'un effet marginal sur les tendances globales de l'ozone. Cependant, cet effet est significatif à l'échelle régionale et locale, où l'ozone est positivement et négativement corrélé aux tendances de l'isoprène dans les régions à forte et faible concentration de NO_x, respectivement. L'impact des émissions d'isoprène sur la qualité de l'air future est le plus significatif lorsque l'on néglige l'effet inhibiteur du CO₂. Dans ce cas, la qualité de l'air était prévue s'améliorer à l'échelle globale et particulièrement dans les régions tropicales, par rapport à un scénario climatique futur avec des émissions d'isoprène correspondant au climat actuel.

Acknowledgments

I would like to begin by expressing my sincere gratitude to my parents, Soukeina, Rim and Aymane for their unwavering support, unconditional love, and constant encouragement. I wouldn't be here today without you.

I would also like to express my sincere appreciation to my thesis supervisors, Vincent and Joaquim. Your unwavering faith in my potential and your guidance throughout the three-year journey have been invaluable. I feel incredibly fortunate to have had you as my supervisors. The wealth of knowledge and experience I've gained from you in the past three years is immeasurable, and I continue to learn from you every day until the completion of my PhD.

A special acknowledgment goes to the members of COMETS and PLASMA. Beatrice, your kindness during challenging times meant a lot to me. To Sophie, Flavien, Francesca, Mehdi, Jonathan.(G & A) and others, I am grateful for your kindness and support, which have enriched my experience and made this journey even more meaningful.

I want to express my appreciation to Paul for the warm welcome and enriching scientific discussions during my time in Norway. Shobitha, our shared moments of laughter, coffee, and discussions about Harry Potter created a strong connection that I deeply value. A heartfelt thank you also goes to Virginie for her assistance and support in every aspect.

Lastly, I extend my deepest thanks to my best friend and partner, Mohamed. Your unwavering presence through thick and thin, Friday dates, and Saturday movie nights have been a source of strength. Thank you for consistently supporting me. To my best friends Abdelilah, Asmaa and Najwa, words cannot capture the depth of my gratitude for your unconditional support and love. I am truly blessed to have you in my life.

Table of Contents

Introduction	1
1 Biogenic volatile organic compounds	13
1.1 Principal BVOCs	13
1.2 BVOCs emission processes	17
1.3 Eco-physiological role of BVOCs	18
1.4 BVOCs emission factors	18
1.5 Conclusion of Chapter 1	23
2 Air quality	25
2.1 Ozone	26
2.1.1 Ozone precursors	27
2.1.2 Tropospheric ozone formation	29
2.1.3 Ozone chemical regimes	31
2.1.4 Ozone transport	33
2.2 Aerosols	35
2.2.1 Primary organic aerosols	35
2.2.2 Secondary organic aerosols	36
2.2.3 Environmental impact of aerosols	37
2.3 Influence of BVOCs on atmospheric chemistry and air quality	39
2.4 Conclusion of Chapter 2	40
3 Climate change	41
3.1 Current climate change: Evidence and impact	41
3.2 Future climate: Description and impact	43
3.2.1 Shared Socioeconomic Pathways	44
3.2.2 Future climate impacts and risks	50

3.3	Change at a +2°C global warming for SSP3-7.0	51
3.4	Climate change and air quality	52
3.4.1	Pollution control in the SSP scenarios	52
3.4.2	The impact of climate change on air quality	53
3.5	The impact of a changing environment on BVOCs	56
3.6	The impact of BVOCs on climate	59
3.7	Thesis objectives	61
4	BVOCs modeling with SURFEX-MEGAN	63
4.1	MEGAN	63
4.1.1	Plant functional types	65
4.1.2	Emission factor	66
4.1.3	Activity factor	67
4.2	SURFEX	71
4.2.1	ECOCLIMAP	73
4.2.2	Land surface model ISBA	75
4.3	SURFEX-MEGAN coupling	81
4.4	Conclusion of Chapter 4	113
5	Impact of a +2°C climate on isoprene emissions	115
5.1	Methodology	115
5.2	SSP3-7.0 fields analysis	117
5.3	Isoprene in present and future climate	118
5.4	Attribution of isoprene changes	122
5.4.1	Climate change	124
5.4.2	Climate change and Leaf Area Index	126
5.4.3	Climate change and CO2 inhibition factor	128
5.4.4	Climate change, Leaf Area Index and CO2 inhibition factor	130
5.5	Comparison with CMIP6 models isoprene projections	130
5.5.1	Models description	130
5.5.2	Isoprene change analysis	132
5.6	Conclusion of Chapter 5	135
6	Impact of isoprene in a +2°C climate on air quality	137
6.1	MOCAGE	137
6.2	Methodology	139
6.3	Emission changes	140
6.4	Ozone change	141

6.5	Ozone sensitivity to isoprene emissions	144
6.6	Impact of the CO ₂ inhibition effect on air quality	146
6.7	Conclusion of Chapter 6	147
Conclusions and perspectives		151
Acronyms		167
Bibliography		169
Appendix A: The Jacobs A-gs model		181
Appendix B: Supplementary figures of Chapter 5		183

List of Figures

1.1	Different biotic and abiotic factors controlling BVOCs emission from plants (inspired by Penuelas and Llusia (2001)).	19
1.2	Isoprene emission flux variation as a function of temperature (a) and PPFD (b) for white oak (a) and sweet gum (b) leaves (adapted from Fuentes et al. (2000)).	20
1.3	Relative humidity dependence of normalized isoprene emission rates from eucalyptus leaves. Emission rates are normalized by the observed emission at a relative humidity of 40%. Measurements made with no water vapor present in the inlet air steam are presented by open circles (adapted from Guenther et al. (1991)).	21
1.4	CO_2 concentration dependence of normalized isoprene emission rates (squares) and normalized CO_2 assimilation rates (open diamonds) from eucalyptus leaves. Rates are normalized by the observed rates at a CO_2 mixing ratio of 330 ppm. (adapted from Guenther et al. (1991)).	22
1.5	Isoprene emission flux emitted by sweet gum leaves, sun leaves and shade leaves are represented with a filled square and a filled circle, respectively (adapted from Fuentes et al. (2000)).	23
2.1	Primary and secondary atmospheric pollutant.	26
2.2	Ozone formation via the interactions between the RO_x - (blue) and NO_x -cycles (black). Interfering with the RO_x - NO_x cycle are ozone degrading reactions (green) via $NMVOCs$ (non-methane volatile organic compounds) as well as terminating reactions (red); $h\nu$, light. Methane and carbon monoxide are not displayed (adapted from Fitzky et al. (2019)).	32
2.3	Ozone isopleth diagram. Isopleths show constant ozone concentrations, the ratio $[VOC]/[NO_x]$ is written at the end of isopleths. The unit of VOCs $ppmC$ refers to Parts Per Million Carbon (adapted from Sillman (1999)).	33

2.4	Average hourly O_3 concentrations in week days and week-end in Los Angeles (a) and in Southeast Desert (Calexico) (b) (adapted from Heuss et al. (2003)). . . .	34
2.5	Secondary aerosol formation processes (adapted from Delmas and Mérieu (2015)).	37
2.6	A view of Paris taken from Saint-Germain-en-Laye, December 5, 2016 (from LeMonde.fr).	38
3.1	Global surface temperature and GHGs concentration evolution during the period 1850-2020 (adapted from Arias et al. (2021)).	43
3.2	Description of the five SSPs each described by a specific level of socio-economic challenges for adaptation and mitigation (adapted from O’Neill et al. (2017)). .	45
3.3	GHG reference and transition scenarios generation scheme for a given SSP scenario.	46
3.4	Future annual emissions of CO_2 in $GtCO_2/yr$ (adapted from Arias et al. (2021)).	48
3.5	Global surface temperature change relative to 1850-1900 (adapted from Arias et al. (2021)).	49
3.6	September Arctic sea ice area (adapted from Arias et al. (2021)).	50
3.7	Global ocean surface pH (adapted from Arias et al. (2021)).	50
3.8	Simulated mean annual temperature change (in $^{\circ}C$) (a), precipitation absolute change (in %) (b), total column soil moisture change (as standard deviation) (c) relative to the period 1850-1900. Precipitation and soil moisture might have a false high change rate in dry regions (from Arias et al. (2021)).	51
3.9	Representation of the atmospheric concentration of NO_x (a) and VOCs (b) over the period 2000-2100 for the different SSPs (from Arias et al. (2021)).	53
3.10	Annual mean change in surface ozone O_3 in ppb at a $+2^{\circ}C$ warming level. Ozone change is calculated as the difference between ozone with evolving future emissions and sea surface temperature under the SSP3-7.0 scenario and ozone with the same setup but with fixed present-day sea surface temperature (from Arias et al. (2021)).	54
3.11	Percent change in global surface ozone O_3 and particulate matter $PM_{2.5}$ in 2040 (a) and in 2100 (b) relative to 2019. SSP-3.0 LL is SSP3-7.0 with low short-lived climate forcers (SLCFs) and CH_4 emissions, SSP-3.7.0 LH is SSP-3.7.0 with low SLFs emissions and high CH_4 emissions (from Arias et al. (2021)).	55
3.12	Schematic representation of the interaction between biogenic emissions, air chemistry and climate with the feedback mechanism between the three components (adapted from Paasonen et al. (2013)).	59

3.13	Radiative effect W/m^{-2} of BVOCs emission in the 1850s and the 2000s and the contribution of multiple warming and cooling climate pollutants. 2000s-1850s defines the global radiative forcing of BVOC emissions for this time period. Fix-BVOC-emis represents the radiative forcing considering the changes to anthropogenic emissions only (adapted from Unger (2014b))	60
4.1	Schematic of MEGAN2.1 model components and driving variables. (adapted from Guenther et al. (2012))	64
4.2	Representation of the canopy environment model used in MEGAN2.1.	65
4.3	Isoprene emission factor map in $\mu g m^{-2} h^{-1}$	67
4.4	MEGAN estimates of isoprene emission response to PPFD transmission for leaves exposed to different solar angles (15, 45 and 70 degrees) and for average PPFD levels for the past 24 to 240 h ($PPFD_{24} = PPFD_{240}$ in each case) that include 600 and 150 $\mu mol m^{-2} s^{-1}$ respectively, for sun leaves and shade leaves, 400 and 100 $\mu mol m^{-2} s^{-1}$ for sun and shade leaves, and 100 and 50 $\mu mol m^{-2} s^{-1}$ for sun and shade leaves, using MEGANv2.0 (adapted from Guenther et al. (2006)).	69
4.5	MEGAN estimates of isoprene emission response to temperature for leaves exposed to different average temperatures (280K, 290K, 297K and 305K) during the past 24 to 240 h ($T_{24} = T_{240}$ in each case) using MEGANv2.0 (adapted from Guenther et al. (2006)).	70
4.6	Description of the exchanges between an atmospheric model sending meteorological and radiative fields to the surface and Surfex composed of a set of physical models that compute tiled variables F_* covering a fraction f_* of a unitary grid box and an interface where the averaged variables F are sent back to the atmosphere (adapted from Le Moigne (2018)).	72
4.7	ISBA force-restore scheme.	76
4.8	ISBA diffusion scheme.	78
4.9	Differences between the standard ISBA model and the photosynthesis ISBA-A-gs model, LE is latent heat flux, R_n is the net radiation, H is sensible heat flux, T_s is the soil temperature and W is the moisture flux.	80
5.1	Mean annual global near surface air temperature change relative to 1850-1900 (a) and mean annual global surface downwelling shortwave radiation (W/m^2) (b). SSP3-7.0 temperature and shortwave radiation data are represented in red and blueviolet, respectively. The temperature and solar radiation linear regression plot is represented in dashed line.	117

5.2	Mean annual global surface CO_2 volume mixing ratio in mol/mol (a), mean annual global precipitation flux in $kg/m^2/s$ (b) and mean annual global leaf area index in m^2/m^2 (c) over the period 2015-2050. The linear regression line for the three parameters is represented in dashed line.	119
5.3	Total annual isoprene estimated with SURFEX-MEGAN over 2010-2014 (a) and 2046-2050 (b) in Tg.	120
5.4	Absolute difference of SURFEX-MEGAN isoprene mean emission flux between 2046-2055 and 2010-2014 in $kg/m^2/s$	121
5.5	Absolute difference of SURFEX-MEGAN simulated leaf area index in m^2/m^2 (a), CO_2 volume mixing ratio in mol/mol (b), near surface air temperature in $^{\circ}C$ (c) and incoming shortwave radiation in W/m^2 (d) between (2046-2055) and (2010-2014).	122
5.6	Impact of climate change (a), climate change and LAI (b), climate change and CO_2 inhibition factor (c) and climate change, LAI and CO_2 inhibition factor (d) on isoprene emissions between 2050 and 2014 for the SSP3-7.0 scenario.	124
5.7	Absolute difference of near surface air temperature in $^{\circ}C$ (a) and incoming shortwave radiation in W/m^2 (c) between 2050 and 2014.	125
5.8	Absolute difference of temperature (a) in $^{\circ}C$, precipitation flux (b) in $kg/m^2/s$, soil liquid water content at the first DIFF layer (c) in m^3/m^3 and SURFEX-MEGAN simulated leaf area index in m^2/m^2 (d) between FUT_{LAI} and $HIST_{LAI}$	126
5.9	Isoprene relative difference between 2050 and 2014 for the four scenarios for different globe regions.	127
5.10	CO_2 inhibition factor following Heald et al. (2009) parametrization.	129
5.11	Mean absolute temperature difference in 2046-2050 between CESM2-WACCM (a), GFDL-ESM4 (b), GISS-E2-1-G (c), UKESM1-0-LL (d) and CNRM-ESM2-1 temperature output.	133
5.12	Isoprene flux difference between 2046-2050 and 2010-2014 for the coupled model SURFEX-MEGAN and the 4 CMIP6 models: CESM2-WACCM, GFDL-ESM4, GISS-E2-1-G and UKESM1-0-LL.	134
5.13	Inhibition factor γ_{CO_2} over the period 1850-2100 using the SSP3-7.0 CO_2 concentrations. G2012 (Guenther et al., 2012) uses the Heald et al. (2009) CO_2 parametrization and P2011 (Pacifico et al., 2011) the (Niinemets et al., 1999) CO_2 parametrization (adapted from Cao et al. (2021)).	135
6.1	Representation of vertical level configuration of MOCAGE with 60 levels (adapted from El Aabaribaoune (2022)).	138

6.2	Difference in mean annual anthropogenic and biomass burning NO_x (a) and $NMVOCS$ (b) emissions in $kg/m^2/s$ and biogenic $NMVOCS$ in $kg/m^2/s$ (c) of SSP3-7.0 (2050) emissions and present day emissions (2013).	141
6.3	Difference in mean ozone (a,b) and NO_x concentrations (c,d) in ppv between $Sim_{ISO-CTRL}$ and $CTRL$ simulations in boreal winter (DJF: December-January-February) and boreal summer (JJA: June-July-August).	142
6.4	Distribution of mean NO_x concentrations (a,b) in ppv, difference in mean isoprene flux (c,d) in $kg/m^{-2}/s$ and in ozone net production rate in ppv/s (e,f) between Sim_{LAI,CO_2} and $Sim_{ISO-CTRL}$ in boreal winter (DJF: December-January-February) and boreal summer (JJA: June-July-August).	145
6.5	Difference in surface mean annual ozone net production rate in ppv/s between Sim_{LAI} and Sim_{LAI,CO_2}	147
6.6	Difference in mean ozone (a,b) and NO_x concentrations (e,f) in ppv and in isoprene flux (c,d) in $kg/m^{-2}/s$ between Sim_{LAI} and $CTRL$ simulations in boreal winter (DJF: December-January-February) and boreal summer (JJA: June-July-August).	148
A.1	Mean absolute difference in soil liquid water content at the fifth DIFF layer in m^3/m^3 between 2046-2050 and 2010-2014.	155
A.2	<i>Différence absolue moyenne de la teneur en eau liquide du sol à la 5ème couche DIFF en m^3/m^3 entre 2046-2050 et 2010-2014.</i>	164
B.1	Leaf area index absolute difference between 2046-2050 and 2010-2014 for the coupled model SURFEX-MEGAN and the 4 CMIP6 models: CESM2-WACCM, GFDL-ESM4, GISS-E2-1-G and UKESM1-0-LL.	184
B.2	Temperature absolute difference between 2046-2050 and 2010-2014 for the 5 CMIP6 models: CNRM-ESM2-1, CESM2-WACCM, GFDL-ESM4, GISS-E2-1-G and UKESM1-0-LL.	185
B.3	Solar radiation absolute difference between 2046-2050 and 2010-2014 for the 5 CMIP6 models: CNRM-ESM2-1, CESM2-WACCM, GFDL-ESM4, GISS-E2-1-G and UKESM1-0-LL.	186

List of Tables

1.1	The chemical structure, boiling point and molecular weight of some non-methane organic compounds (adapted from Fuentes et al. (2000)).	14
1.2	Annual global total averaged over the period of 1980–2010 for selected BVOC species simulated with MEGAN (with standard deviation σ), their relative contribution to the global total of all BVOCs expressed as emission of carbon, maximal and minimal value within the modeled period. Note that the sum of monoterpenes already includes emissions of α -pinene and β -pinene (in italics) (adapted from Sindelarova et al. (2014)).	15
2.1	Atmospheric lifetime of some <i>VOCs</i> (adapted from Ragothaman and Anderson (2017)).	28
2.2	Annual emission flux of primary organic aerosols from natural and anthropogenic sources in $\text{Mt}=10^{12}\text{g}$ (from Boucher (2012)).	36
3.1	Description of the correspondence between SSPs and RCPs (adapted from Arias et al. (2021)).	47
3.2	Qualitative framework for pollution control in the SSPs (adapted from Rao et al. (2017)).	52
4.1	Description of CLM4 plant functional types and the spatial coverage for each PFT (in 10^{12}km^2) (adapted from Guenther et al. (2012)).	66
4.2	MEGAN2.1 biogenic emission classes and emission factors ($\mu\text{gm}^{-2}\text{h}^{-1}$) for each of the plant functional types (adapted from Guenther et al. (2012)).	67
4.3	Description of the SURFEX land types (Le Moigne, 2018).	73
4.4	Surface parameters defined in ECOCLIMAP (Le Moigne, 2018).	74
5.1	Description of the present- and future-climate simulations setup.	116
5.2	Description of the simulations used in the sensitivity analysis along with the total annual isoprene emission in Tg estimated with SURFEX-MEGAN.	123

5.3	List of CMIP6 isoprene emission projections and the emission total difference between 2045-2050 and 2010-2014. G1995 refers to the Guenther et al. (1995) isoprene emission model, G2006 is a newer version developed by Guenther et al. (2006), G2012 is the algorithm used currently in the MEGANv2.1 model by Guenther et al. (2012) and P2011 is the interactive BVOC model developed by Pacifico et al. (2011). (a) The estimation of γ_{CO_2} follows the Heald et al. (2009) parametrization and (b) follows the Niinemets et al. (1999) parametrization.	131
5.4	Atmospheric CO_2 activity factor. C_i is the ambient air CO_2 concentration, $I_{max}=1.344$, $h=1.4614$, $C_*=585$ and C_{st} is the atmospheric CO_2 concentration at standard conditions =370ppm.	135
6.1	Description of the simulations used to model atmospheric composition with MOCAGE. (*) The details of the isoprene inventories used in each simulation are given in Chapter 5, Tables 5.1 and 5.2. ANT and BB represent emissions from anthropogenic and biomass burning sources, respectively.	139
6.2	Total annual NO_x and VOC emissions from anthropogenic (ANT), biomass burning (BB) sources for historical (<i>CTRL</i>) and SSP3.7-0 simulations (<i>Sim_{LAI,CO₂}</i> , <i>Sim_{ISO-CTRL}</i> and <i>Sim_{LAI}</i>). For biogenic VOCs emissions, ISO and OBVOC represent the total emissions of isoprene and other biogenic species, respectively.	140

Introduction

Since the pre-industrial era, climate change has profoundly affected various aspects of human life and the surrounding environment. Since then, extensive efforts have been dedicated to understanding the origins of climate change, assessing its current state, predicting its future course, and evaluating the associated risks to both human health and the environment. In their latest assessment report (AR6), the International Panel on Climate Change (IPCC) stated that climate change was unequivocally caused by the release of greenhouse gases from human activities. This has led to a $+1.1\text{ }^{\circ}\text{C}$ increase in global surface temperature in 2011-2020 compared to the pre-industrial era (1850-1900). With the ongoing emission of greenhouse gases, the IPCC predicts substantial alterations in future climate patterns, with temperature projected to rise between 1 and $5\text{ }^{\circ}\text{C}$ by the end of the twenty-first century depending on the considered climate change scenario. Atmospheric chemistry is also recognized as an important component of climate change studies. In particular, the prediction of future air quality is of utmost importance, as air pollutants chemistry and transport patterns are expected to change in response to climate and anthropogenic emissions change. The latter are determined by the emission control policies defined in each scenario of the Shared Socio-Economic Pathway (SSP).

Over short time scales, the release of air pollutants directly affects the quality of the air we breathe. The term "air quality" has been introduced to measure the impact of these pollutants on both health and vegetation. Since the end of the 20th century, the state of air quality has been the subject of particular attention worldwide, and especially in developed countries. In light of this recognition, there has been a heightened focus on monitoring air quality and controlling atmospheric pollution. The aim of national, and regional regulations is to estimate the rural and urban air pollution levels, evaluate the efficiency of initiatives taken to limit human-made pollutant emissions, and provide the public with pertinent information regarding air quality. These directives adapt in tandem with emerging insights into the health implications of atmospheric pollutants.

Air quality is determined by a complex interplay between the amount of pollutants emitted

into the atmosphere and the physical and chemical processes they undergo, such as dispersion, chemical transformation, and wet and dry deposition. In air quality, atmospheric pollutants can be categorized into primary and secondary pollutants. Primary pollutants are chemical species emitted directly into the atmosphere from natural sources (e.g., vegetation, volcanoes) or anthropogenic sources (e.g., vehicles, industrial plants, consumer products, power plants). The main primary pollutants are: oxides of sulfur (SO_x), oxides of nitrogen (NO_x), carbon monoxide (CO), particulate matter (PM). In contrast to primary pollutants, secondary pollutants are not emitted directly into the atmosphere, but are rather formed by chemical reactions involving primary pollutants and other atmospheric components with or without photo-activation. Examples of secondary pollutant include ozone (O_3), formaldehyde, peroxy acetyl nitrate (PAN), photochemical smog, peroxy butyl nitrate (PBN).

A special emphasis is placed on a specific secondary pollutant: ozone (O_3). When present in the troposphere, ozone is considered as one of the most harmful atmospheric pollutant as prolonged exposure to ozone leads to irreversible effects on both human health and vegetation growth. Ground-level ozone is formed through a series of complex reactions involving different compounds, most importantly Volatile Organic Compounds ($VOCs$) and nitrogen oxides (NO_x). These reactions occur under specific environmental conditions (presence of sunlight). The majority of ground-level ozone is the result of reactions between $VOCs$ and man-made NO_x only a small fraction comes from transported stratospheric ozone or from nature-induced NO_x .

The recognized importance of assessing and evaluating air quality to prevent health issues has led to the dedication of extensive efforts to predict the evolution of air quality in the future on regional and global scales. In fact, it is believed that future air quality trends will be affected by climate change for many reasons. Firstly, climate change can directly impact the atmospheric concentration of certain air pollutant precursors, mainly those originating from natural sources. Furthermore, meteorological variables such as temperature and solar radiation can directly affect air quality by altering the production rates of certain atmospheric pollutants. Indirectly, these meteorological changes can disrupt pollutant transport patterns by modifying the frequency and intensity of atmospheric blocking episodes. Lastly, climate change can modify the chemical properties of certain gases, for example the lifetime of pollutants in the atmosphere, thus altering the overall dynamics of air quality. Conversely, the chemical composition of the atmosphere affects climate through two main components of the Earth's atmosphere: greenhouse gases and aerosols. The former absorb the Earth's infrared radiation, whereas the latter reflect and absorb solar radiation and modify the microphysics and therefore the radiative properties, structure and lifetime of clouds, these effects are known as the direct effect and the indirect effect, respectively.

In the context of air quality assessment, Biogenic Volatile Organic Compounds (BVOCs)

hold a significant place in the evaluation of certain air pollutants levels. These chemical compounds account for around 90% of the total emitted VOCs, which are considered as key precursors of ozone and Secondary Organic Aerosols (SOAs). In this regard, BVOCs comprise a vast class of compounds, the most important of which are terpenoids (e.g., isoprene, monoterpenes, sesquiterpenes), alkenes, alkanes, benzoid compounds, organic sulfur compounds, etc. These biogenic compounds are emitted by plants as a part of their normal metabolic processes and are essential for the growth, development, and reproduction of plants. The most important BVOC is isoprene, as it accounts for about half of the total emitted BVOCs. Due to its abundance and high reactivity, isoprene has garnered extensive attention and has been the subject of extensive study within the scientific community.

Isoprene and other biogenic compounds are expected to change in the future as a result of climate change. These compounds are sensitive to variations in a number of meteorological variables such as temperature, solar radiation, atmospheric concentrations of CO_2 and environmental variables such as soil moisture, land cover and land use and vegetation density. Conversely, these compounds affect atmospheric chemistry through the formation of tropospheric ozone and secondary organic aerosols, and through the influence of specific greenhouse gases (e.g., methane) lifetime. The emission of ozone and the formation of atmospheric aerosols have effects that reach beyond air quality and human health concerns. They also exert a substantial influence on the current and future state of our climate. Consequently, achieving a precise estimation of BVOCs is of utmost importance. This precision is crucial for making accurate forecasts of air pollutants using chemical-transport models on both regional and global scales and also for quantifying the exact radiative forcing effects arising from ozone and aerosols under both present and future climate conditions.

Most prior and current research focusing on predicting future air quality trends has operated under the assumption that biogenic emissions remain constant. These studies predict future air pollutant levels based solely on projected meteorological conditions and on assumptions about the evolution of anthropogenic and biomass burning emissions. However, it is anticipated that biogenic VOCs, which account for over 90% of the total emitted VOCs, will experience significant alterations due to rising temperatures and shifts in vegetation distribution and density. Therefore, to improve the accuracy of air chemistry forecasting in general, and ozone and secondary organic aerosols levels in particular, it is crucial to incorporate the evolving dynamics of biogenic VOCs when modeling future air quality.

The IPCC, dedicated to examining all aspects of climate change, is complemented by specialized projects with narrower focuses. The **IMPACT2C** initiative, launched in 2011, specifically focuses on the consequences of global warming attributable to climate change. This project aimed to understand the impacts of a potential $2^\circ C$ temperature increase on specific economic sectors and to assess projected climate change impact in Europe and vulnerable regions. This

evaluation was based on various regional climate models and global projections. The importance of the 2°C threshold is underlined by the international agreement achieved in the December 2015 Paris Agreement, in which countries committed to limit global warming to levels below this critical threshold.

This thesis falls within the scope of this project, as it aims to predict the evolution of biogenic emissions and air quality in a climate change level of $+2^{\circ}\text{C}$. The models that have been used in this study, methods, state of the art as well as sensitivity studies will be presented in detail throughout the manuscript, which will be organized as follows:

- **Chapter 1** provides a comprehensive overview of biogenic volatile organic compounds, including their emission processes, chemical properties, eco-physiological role, and the various meteorological and environmental factors influencing their release. This chapter discusses also the role played by biogenic volatile organic compounds serving as a link between the Earth's physical, chemical and biological components.
- **Chapter 2** provides a scientific overview of atmospheric chemistry, with a specific focus on air quality. This chapter specifically discusses the chemical formation processes linked to ozone and secondary organic aerosols. These two air pollutants are of particular importance to our study as they originate both from BVOCs. The health and environmental impacts of these pollutants will be also discussed as well as the influence of aerosols on the Earth's radiative balance and on clouds formation and physical properties.
- **Chapter 3** describes the current state and the evidence of the observed climate change. Based on the IPCC's latest assessment report, this chapter provides a description of climate change in the future following the different shared socioeconomic pathways, with a specific focus on temperature, precipitation and soil moisture predicted levels in a $+2^{\circ}\text{C}$ climate change level. The impact of climate change on BVOCs and air quality will be also discussed, particularly the impact of land use, global warming, water stress and CO_2 atmospheric concentrations. At the end of this chapter, the objectives of this thesis will be outlined.
- **Chapter 4** provides a comprehensive description of the models used in this study mainly MEGAN (Model of Emission of Gases and Aerosols from Nature) and SURFEX (Surface Externalisée in french). MEGAN is the model used to simulate the emission of biogenic compounds and SURFEX is a surface modeling interface used to simulate surface-atmosphere exchanges. To estimate future biogenic emissions, we have coupled the SURFEX and MEGAN models. The objectives of this coupling are provided in this chapter as well as a comprehensive representation of the technical implementation, the validation

and the sensitivity studies performed with the coupled model SURFEX-MEGAN. The evaluation of isoprene emissions from the coupled model SURFEX-MEGAN have been the subject of a scientific paper presented in this chapter.

- **Chapter 5** evaluates the future changes in isoprene emissions using the coupled model SURFEX-MEGAN according to a warming level of $+2^{\circ}\text{C}$ relative to 1850-1900. The methodology as well as an extensive analysis of the scenario SSP3-7.0 fields will be given. This specific scenario was used to derive future isoprene emissions. A sensitivity analysis will be driven to determine the individual contribution of climate, leaf area index (LAI) and atmospheric CO_2 inhibition factor to the observed changes in future isoprene emissions. Finally, this chapter will provide a comparison of the SURFEX-MEGAN predicted isoprene changes with CMIP6 models isoprene projections over the same study period and using the same SSP scenario.
- **Chapter 6** describes MOCAGE, which is the atmospheric-chemistry model used to simulate air quality in present and future-climate simulations. The simulated isoprene emissions from Chapter 5, will be used as inputs to the MOCAGE model along with the SSP3-7.0 NO_x and VOCs anthropogenic and biomass burning emissions. This chapter will first evaluate surface ozone levels in a $+2^{\circ}\text{C}$ climate change level by considering fixed isoprene emissions. The contribution of the latter to future ozone trends will be assessed later. Since the inhibitory effect of atmospheric CO_2 offsets the increase in future isoprene emissions driven by high temperatures, we will test the sensitivity of excluding this factor on future air quality in general and surface ozone levels in particular.

Finally, the study will conclude with the drawing of relevant conclusions from the gathered findings. These will be followed by future prospects for a potential follow-up to the present study.

Introduction

Depuis l'ère pré-industrielle, le changement climatique a profondément affecté divers aspects de la vie humaine et de l'environnement. Depuis lors, d'importants efforts ont été consacrés à la compréhension des origines du changement climatique, à l'évaluation de son état actuel, à la prédiction de son évolution future et à l'évaluation des risques associés à la fois pour la santé humaine et pour l'environnement. Dans leur dernier rapport d'évaluation (AR6), le Groupe d'experts Intergouvernemental sur l'Évolution du Climat (GIEC) a affirmé que le changement climatique était sans équivoque causé par les émissions de gaz à effet de serre provenant des activités humaines. Cela a entraîné une augmentation de $+1,1^{\circ}\text{C}$ des températures à la surface en 2011-2020 par rapport à l'ère pré-industrielle (1850-1900). Avec la poursuite des émissions de gaz à effet de serre, le GIEC prévoit des modifications substantielles dans les schémas climatiques futurs, les températures étant projetées à augmenter entre 1 et 5°C d'ici la fin du XXI^e siècle, selon le scénario de changement climatique considéré. La chimie atmosphérique est également considérée comme un élément important des études sur le changement climatique. La prédiction de la qualité de l'air, en particulier, revêt une importance capitale, car on s'attend à ce qu'elle change en réponse aux variations climatiques et aux changements d'émissions d'origine anthropique. Ces derniers sont déterminés par les politiques de contrôle des émissions définies dans chaque scénario de la trajectoire socio-économiques partagée (SSP).

Les émissions de polluants atmosphériques affectent directement la qualité de l'air que nous respirons. Le terme "qualité de l'air" a été introduit à la fin XX^e siècle pour évaluer l'impact de ces polluants sur la santé et la végétation. Depuis, la qualité de l'air a fait l'objet d'une surveillance particulière à l'échelle mondiale, et notamment dans les pays développés. De ce fait, la surveillance de la qualité de l'air et la lutte contre la pollution atmosphérique sont devenues des priorités. Ainsi, des réglementations régionales et nationales ont été mises en place pour fournir au public des informations pertinentes sur la qualité de l'air, évaluer l'efficacité des initiatives prises pour limiter les émissions de polluants anthropiques et mesurer les niveaux de pollution de l'air dans les zones rurales et urbaines.

La qualité de l'air est déterminée par une interaction complexe entre la quantité de polluants émis dans l'atmosphère et les processus physiques et chimiques qu'ils subissent, tels que le dépôt sec et humide, la transformation chimique et la dispersion. À cet égard, les polluants atmosphériques peuvent être classés en polluants primaires et secondaires. Les polluants primaires sont des espèces chimiques émises directement dans l'atmosphère par des sources naturelles (la végétation, les volcans) ou des sources anthropiques (les véhicules, les installations industrielles, les produits de consommation, les centrales électriques). Les principaux polluants primaires sont : les oxydes de soufre (SO_x), les oxydes d'azote (NO_x), le monoxyde de carbone (CO), les particules (PM). Contrairement aux polluants primaires, les polluants secondaires ne sont pas émis directement dans l'atmosphère, mais sont plutôt formés par des réactions chimiques impliquant des polluants primaires et d'autres composants atmosphériques, avec ou sans photo-activation. Parmi les exemples de polluants secondaires, on peut citer l'ozone (O_3), le formaldéhyde, le nitrate de peroxyacétyle (PAN), le smog photochimique, le nitrate de peroxybutyle (PBN).

Une importance particulière est accordée à un polluant secondaire spécifique : l'ozone (O_3). Lorsqu'il est présent dans la troposphère, l'ozone est considéré comme l'un des polluants atmosphériques les plus nocifs pour la santé humaine. L'ozone est formé par une série de réactions complexes impliquant différents composés, dont les plus importants sont les composés organiques volatils (VOCs) et les oxydes d'azote (NO_x). Ces réactions se produisent dans des conditions environnementales spécifiques (présence de lumière solaire). La majorité de l'ozone troposphérique est le résultat de réactions entre les VOC et les NO_x produits par l'homme ; seule une petite partie provient de l'ozone stratosphérique transporté ou des NO_x d'origine naturelle.

La nécessité d'évaluer la qualité de l'air pour prévenir les problèmes de santé a conduit à déployer des efforts considérables pour prévoir l'évolution de la qualité de l'air dans le futur à l'échelle régionale et mondiale. En fait, on estime que les tendances futures de la qualité de l'air seront affectées par le changement climatique pour de nombreuses raisons. Tout d'abord, le changement climatique peut avoir un impact direct sur la concentration atmosphérique de certains précurseurs de polluants atmosphériques, principalement ceux provenant des sources naturelles. En outre, les variables météorologiques telles que la température et le rayonnement solaire peuvent affecter directement la qualité de l'air en modifiant les taux de production de certains polluants atmosphériques. Indirectement, ces changements météorologiques peuvent également perturber les schémas de transport des polluants en modifiant la fréquence et l'intensité des épisodes de blocage atmosphérique. Enfin, les changements chimiques induits par le climat peuvent encore modifier la durée de vie des polluants dans l'atmosphère, affectant ainsi la dynamique globale de la qualité de l'air. Inversement, la composition chimique de l'atmosphère affecte le climat par l'intermédiaire des gaz à effet de serre et des aérosols. Les

premiers absorbent le rayonnement infrarouge de la Terre, tandis que les seconds absorbent et réfléchissent le rayonnement solaire et modifient la microphysique et donc la durée de vie, la structure et les propriétés radiatives des nuages ; ces effets sont connus sous le nom "d'effet direct" et "d'effet indirect", respectivement.

Dans le contexte de la modélisation de la qualité de l'air, les composés organiques volatils biogéniques (COVB) occupent une place importante dans l'évaluation des niveaux d'ozone (O_3) et d'aérosols organiques secondaires (AOS). Ces composés chimiques représentent environ 90% du total des COV émis, qui sont considérés comme des précurseurs clés de l'ozone et des AOS. À cet égard, les COVB comprennent une vaste catégorie de composés, dont les plus importants sont les terpénoïdes (isoprène, monterpènes, sesquiterpènes), les alcènes, les alcanes, les composés benzoïdes, les composés organiques soufrés, etc. Ces composés biogéniques sont émis par les plantes en raison de leurs processus métaboliques normaux et sont essentiels à la croissance, au développement et à la reproduction des plantes. Le COVB le plus important est l'isoprène, qui représente environ la moitié du total des COVB émis. En raison de son abondance et de sa grande réactivité, l'isoprène a suscité beaucoup d'attention et fait l'objet d'études approfondies au sein de la communauté scientifique.

Le changement climatique entraînerait une modification dans l'émission d'isoprène et d'autres composés biogéniques dans le futur. Ces composés sont sensibles aux variations d'un certain nombre de variables météorologiques et environnementales telles que la température, le rayonnement solaire, les concentrations atmosphériques de CO_2 , l'humidité du sol, l'occupation et l'utilisation des sols et la densité de la végétation. Inversement, ces composés affectent la chimie atmosphérique par la formation d'ozone troposphérique et d'aérosols organiques secondaires, et par l'influence sur la durée de vie de certains gaz à effet de serre (par exemple, le méthane). L'émission d'ozone et la formation d'aérosols atmosphériques ont des effets qui vont au-delà des problèmes de qualité de l'air et de santé humaine. Elles exercent également une influence considérable sur l'état actuel et futur de notre climat. Par conséquent, il est de la plus haute importance de parvenir à une estimation précise des COVB. Cette précision est essentielle pour établir des prévisions exactes des polluants atmosphériques à l'aide de modèles de chimie-transport à l'échelle régionale et globale, ainsi que pour quantifier les effets exacts du forçage radiatif dû à l'ozone et aux aérosols dans les conditions climatiques actuelles et futures.

La plupart des recherches antérieures et actuelles sur la prédiction des tendances futures de la qualité de l'air se fondent sur l'idée que les émissions biogéniques resteront constantes. Ces études projettent les futurs niveaux de polluants atmosphériques en se basant uniquement sur les conditions météorologiques à venir, ainsi que sur les émissions anthropiques et de combustion de biomasse provenant des scénarios SSP. Cependant, il est prévu que les COV biogéniques, qui représentent plus de 90% du total des COV émis, subissent des modifications significatives en raison de l'élévation des températures et des changements dans la distribution et la densité de

la végétation. Par conséquent, afin d'améliorer la précision de la prédiction de l'état chimique de l'air en général, et des niveaux d'ozone et d'aérosols organiques secondaires en particulier, il est impératif d'intégrer la dynamique évolutive des COV biogéniques lors de la modélisation de la qualité de l'air dans le futur.

Le GIEC, dédié à l'examen de tous les aspects du changement climatique, est complété par des projets spécialisés avec des objectifs plus restreints. L'initiative **IMPACT2C**, lancée en 2011, se concentre spécifiquement sur les conséquences du changement climatique. Ce projet vise à comprendre les impacts d'une augmentation potentielle de la température de 2°C sur des secteurs économiques spécifiques et à évaluer l'impact projeté du changement climatique en Europe et dans les régions vulnérables. Cette évaluation était basée sur divers modèles climatiques régionaux et globaux. L'importance du seuil de 2°C est soulignée par l'accord international conclu dans l'Accord de Paris de décembre 2015, dans lequel les pays se sont engagés à limiter le réchauffement global à des niveaux inférieurs à ce seuil critique.

Cette thèse s'inscrit dans le cadre de ce projet, car elle vise à prédire l'évolution des émissions biogéniques et de la qualité de l'air dans un contexte de changement climatique de +2°C. Les modèles utilisés dans cette étude, les méthodes, l'état de l'art ainsi que les études de sensibilité seront présentés en détail tout au long du manuscrit, qui sera organisé comme suit:

- **Chapitre 1** présente un aperçu détaillé des composés organiques volatils biogéniques, notamment leurs processus d'émission, leurs propriétés chimiques, leur rôle éco-physiologique, ainsi que les divers facteurs météorologiques et environnementaux influençant leur émission. Ce chapitre aborde également le rôle joué par les composés organiques volatils biogéniques en tant que lien entre les composants physiques, chimiques et biologiques de la Terre. Il se plonge spécifiquement dans l'impact considérable des COVB sur la chimie atmosphérique et le climat.
- **Chapitre 2** fournit un aperçu scientifique de la chimie atmosphérique, en mettant l'accent sur la qualité de l'air. Ce chapitre aborde les processus de formation chimique liés à l'ozone (O_3) et aux aérosols organiques secondaires (AOS). Ces deux polluants atmosphériques revêtent une importance particulière pour notre étude car ils proviennent tous deux des COVB. Les impacts sur la santé et l'environnement de ces polluants seront également discutés, ainsi que l'influence des aérosols sur le bilan radiatif de la Terre et sur la formation et les propriétés physiques des nuages.
- **Chapitre 3** décrit l'état actuel et les preuves du changement climatique observé. Basé sur le dernier rapport d'évaluation du GIEC, ce chapitre propose une description du changement climatique futur selon les différentes trajectoires socio-économiques partagées (SSP),

en mettant l'accent sur les niveaux prédits de température, de précipitations et d'humidité du sol dans un contexte de changement climatique de $+2^{\circ}\text{C}$. L'impact du changement climatique sur les COVB et la qualité de l'air sera également discuté, en mettant particulièrement l'accent sur l'impact de l'utilisation des terres, du réchauffement global, du stress hydrique et des concentrations atmosphériques du CO_2 . À la fin de ce chapitre, les objectifs de cette thèse seront exposés.

- **Chapitre 4** offre une description complète des modèles utilisés dans cette étude, principalement MEGAN (Model of Emission of Gases and Aerosols from Nature) et SURFEX (Surface Externalisée). MEGAN est le modèle utilisé pour simuler les émissions des composés biogéniques et SURFEX est une interface de modélisation de surface utilisée pour simuler les échanges surface-atmosphère. Pour estimer les futures émissions biogéniques, nous avons couplé les modèles SURFEX et MEGAN. Les objectifs de ce couplage sont fournis dans ce chapitre, ainsi qu'une représentation technique du couplage, de la validation et des études de sensibilité réalisées avec le modèle couplé SURFEX-MEGAN. L'évaluation des émissions d'isoprène à partir du modèle couplé SURFEX-MEGAN a fait l'objet d'un article scientifique présenté dans ce chapitre.
- **Chapitre 5** présente les résultats de l'évaluation des émissions futures d'isoprène en utilisant le modèle couplé SURFEX-MEGAN selon un niveau de réchauffement de $+2^{\circ}\text{C}$ par rapport à la période 1850-1900. La méthodologie ainsi qu'une analyse approfondie des champs du scénario SSP3-7.0 seront présentées. Ce scénario spécifique a été utilisé pour dériver les futures émissions d'isoprène. Une analyse de sensibilité sera menée pour déterminer la contribution individuelle du climat, de l'indice de surface foliaire (LAI) et du facteur d'inhibition atmosphérique du CO_2 aux changements observés dans les futures émissions d'isoprène. Enfin, ce chapitre fournira une comparaison des changements d'isoprène prédits par SURFEX-MEGAN avec les projections d'isoprène des modèles CMIP6 sur la même période d'étude et en utilisant le même scénario SSP.
- **Chapitre 6** décrit MOCAGE, qui est le modèle de chimie-transport utilisé pour simuler la qualité de l'air dans les simulations du climat actuel et futur. Les émissions d'isoprène simulées avec SURFEX-MEGAN seront utilisées comme entrées pour le modèle MOCAGE, ainsi que les émissions anthropiques et de combustion de biomasse provenant du scénario SSP3-7.0. Ce chapitre évaluera d'abord les niveaux d'ozone de surface dans un contexte de changement climatique de $+2^{\circ}\text{C}$ en considérant des émissions d'isoprène actuelles. La contribution de ces dernières aux tendances futures de l'ozone sera évaluée ultérieurement. Étant donné que l'effet inhibiteur du CO_2 atmosphérique compense l'augmentation des émissions futures d'isoprène induite par les températures élevées, nous testerons la sensibilité de l'exclusion de ce facteur sur la qualité de l'air future en général et les niveaux

d'ozone de surface en particulier.

Enfin, le travail sera conclu en dressant des conclusions appropriées à partir des résultats obtenus. Celles-ci seront suivies de perspectives futures pour une éventuelle suite à l'étude actuelle.

Biogenic volatile organic compounds

Biogenic volatile organic compounds (BVOCs) are organic chemicals composed of carbon that are primarily released by the biosphere. These compounds originate from various sources within terrestrial ecosystems, such as soils, oceans, and vegetation components like leaf litter, roots, trunks, stems, and flowers (Greenberg et al. (2012), Baghi et al. (2012)). Among these sources, vegetation is considered as the largest contributor to the global total emission of BVOCs (Guenther, 2013).

The importance of studying BVOCs stems from their high reactivity and hence the significant role they play in atmospheric chemistry. These chemicals can influence the oxidation capacity of the atmosphere, as they are considered a major sink for hydroxyl radicals (OH). Additionally, BVOCs can also impact regional and global air quality, as they account for about 90% of total global emissions of volatile organic compounds. In this regard, the oxidation of VOCs in a NO_x (Nitrogen Oxides) emitting area can lead to the formation of ground-level ozone, considered an important tropospheric pollutant. VOCs oxidation can also lead to the formation of secondary organic aerosols (SOA), which can effect visibility, climate and air quality.

1.1 Principal BVOCs

BVOCs are essential for the growth, development, and reproduction of plants. However, for the majority of plant species, BVOCs play an essentially defensive and protective role. These chemicals act as well as a communication tool among plants and between plants and insects. Table 1.1 and 1.2 list the properties and the annual emission of different BVOCs, respectively. According to Kesselmeier and Staudt (1999) and Fuentes et al. (2000), BVOCs can be grouped in multiple categories, including:

Terpenoids: This category comprises the most extensive collection of plant secondary metabolites, accounting for 60% of recognized biogenic substances. Terpenoids include a large group

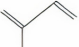
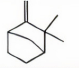
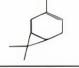
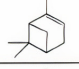
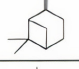
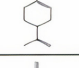
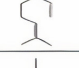
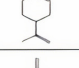
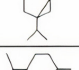
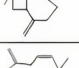
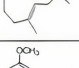
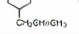
Compound name	Chemical formula	Molecular weight (g mol ⁻¹)	Boiling point (K)	Chemical structure
Isoprene	C ₅ H ₈	68.12	307	
Camphene	C ₁₀ H ₁₆	136.24	320	
3-Carene	C ₁₀ H ₁₆	136.24	441	
α-Pinene	C ₁₀ H ₁₆	136.24	428	
β-Pinene	C ₁₀ H ₁₆	136.24	436	
Limonene	C ₁₀ H ₁₆	136.24	448	
Myrcene	C ₁₀ H ₁₆	136.24	440	
Terpinolene	C ₁₀ H ₁₆	136.24	459	
Sabinene	C ₁₀ H ₁₆	136.24	437	
β-Caryophyllene	C ₁₅ H ₂₄	204.35	396	
α-Humulene	C ₁₅ H ₂₄	204.35	396	
Methyl chavicol		148.20	489	

Table 1.1: The chemical structure, boiling point and molecular weight of some non-methane organic compounds (adapted from Fuentes et al. (2000)).

of chemical species: Hemiterpenoids (Isoprene: C₅H₈), Monoterpenoids (C₁₀H₁₆), Sesquiterpenoids (C₁₅H₂₄), Diterpenoids (C₂₀H₃₂), Sesterterpenoids (C₂₅H₄₀), Triterpenoids (C₃₀H₄₈), Tetraterpenoids (C₄₀H₆₄) and Polyterpenoid (C₅H₈)_n.

- **Isoprene:**

Due to its substantial contribution to biogenic emissions, isoprene (C₅H₈) is considered as one of the most important biogenic volatile organic compounds, accounting for roughly half of these emissions (Guenther et al., 2012). It is also known as the most volatile compound among BVOCs. Due to its abundance and high reactivity, isoprene has garnered extensive attention and is the subject of extensive study within the scientific community. The primary sources of isoprene are plants, with tropical broadleaf trees being the most significant contributors. These trees, found in regions with high temperatures and abundant rainfall, are responsible for more than 70% of global isoprene emissions. This is

Global totals Species	mean Tg (species) yr ⁻¹	rel. contribution %	minimum Tg yr ⁻¹	maximum Tg yr ⁻¹
isoprene	594 ± 34	69.2	520	672
sum of monoterpenes	95 ± 3	10.9	89	103
<i>α-pinene</i>	32 ± 1	3.7	30	34
<i>β-pinene</i>	16.7 ± 0.6	1.9	15.6	17.9
sesquiterpenes	20 ± 1	2.4	18	23
methanol	130 ± 4	6.4	121	138
acetone	37 ± 1	3.0	35	40
ethanol	19 ± 1	1.3	17	21
acetaldehyde	19 ± 1	1.3	17	21
ethene	18.1 ± 0.5	2.0	17.1	19.2
propene	15.0 ± 0.4	1.7	14.1	15.9
formaldehyde	4.6 ± 0.2	0.2	4.3	5.1
formic acid	3.5 ± 0.2	0.1	3.2	3.8
acetic acid	3.5 ± 0.2	0.1	3.2	3.8
2-methyl-3-buten-2-ol	1.6 ± 0.1	0.1	1.4	1.8
toluene	1.5 ± 0.1	0.2	1.4	1.6
other VOC species	8.5 ± 0.3	0.8	7.9	9.0
CO	90 ± 4	–	82	97

Table 1.2: Annual global total averaged over the period of 1980–2010 for selected BVOC species simulated with MEGAN (with standard deviation σ), their relative contribution to the global total of all BVOCs expressed as emission of carbon, maximal and minimal value within the modeled period. Note that the sum of monoterpenes already includes emissions of α -pinene and β -pinene (in italics) (adapted from Sindelarova et al. (2014)).

mainly due to their high rates of photosynthesis, which is directly linked to isoprene production. The remainder of isoprene emissions, primarily comes from broadleaf temperate trees and shrubs (Guenther et al., 2012).

The estimated total annual isoprene emissions present a wide range of variations depending on input parameters and model assumptions. Isoprene reported values in 2019 ranged from 311Tg to 637Tg. (Sindelarova et al. (2014) - Sindelarova et al. (2022) - Opacka et al. (2021)).

- **Monoterpenes:**

Monoterpenes are a family of biogenic compounds characterized with the chemical formula $C_{10}H_{16}$. They have been the subject of several studies due to their high reactivity in the atmosphere. They can be linear or cyclic (monocyclic or bicyclic), among the latter, a distinction is made between the so-called endo- and exocyclic molecules, depending on whether the unsaturation is located inside or outside the ring structure. These aromatic compounds are present mainly in the form of essential oils because of their low weight characteristics and are responsible for plant odors. Citrus, for example, owes its characteristic fragrance to monoterpenes called limonenes. Among the most common

monoterpenes are compounds such as 3-carene, myrcene, limonene, camphene and most importantly α -pinene and β -pinene. There are also a few oxygenated monoterpenes such as linalool or α -terpineol. According to Guenther et al. (2012) and Sindelarova et al. (2014), monoterpenes are responsible of 11% of total annual biogenic emissions, with tropical broadleaf trees being the largest monoterpene emitters (80%).

- **Sesquiterpenes:**

Sesquiterpenes, characterized by the molecular formula $C_{15}H_{25}$ are mostly emitted by broadleaf trees. This family is the most important element in the essential oils that certain plants produce. It comprises a wide range of compounds consisting of three isoprene units. Few studies have focused on understanding the chemical properties of these compounds, one of the uncertainties surrounding sesquiterpenes is their vegetation emission potential, which makes the estimation of their emission flux hard to assess.

Oxygenated volatile organic compounds (OVOCs): OVOCs are a class of organic chemicals that contain carbon, hydrogen, and oxygen atoms, they can be produced by natural processes and human activities. The most important OVOCs are:

- **Methanol:**

Methanol (CH_3OH) ranks among the most abundant oxygenated volatile organic compounds (OVOCs) present in the atmosphere. According to Sindelarova et al. (2014), it contributes over 6% to global annual BVOC emissions. The sources of methanol production are diverse, with approximately 28% to 35% originating from oceans, 37% to 42% from terrestrial ecosystems, 15% to 29% from the atmospheric oxidation of VOCs, 5% from biomass burning, and 1% to 2% from urban sources (Guenther, 2013). Although plants release methanol through leaf expansion, the precise emission mechanism remains unknown.

- **Carbonyl compounds and organic acids:**

Carbonyl compounds are emitted by forest trees, these compounds include: acetone, propanal, acetaldehyde, formaldehyde, i-butenal, butenal, i-butanal, 2-butanone, 2-methyl-2-pentenal, 2-pentanone, crotonaldehyde, benzaldehyde, methyl-vinyl-ketone (MVK), hexanal, (E)-2-hexenal and (Z)-3-hexenal. Organic acids come from forest, the most prominent organic acids are acetic and formic acids. With the exception of acetone, the contribution of carbonyl compounds and organic acids to total BVOC emissions is relatively low (less than 0.2%), acetone represents more than 3% of this contribution.

Alkenes (including Oxygenated Alkenes): Alkenes (C_nH_{2n}) like terpenoids, butene, propene are emitted into the atmosphere by terrestrial ecosystems. Propene is emitted mainly from agriculturally used crops (Guenther, 2013).

Alkanes (including Oxygenated Alkanes): Multiple alkanes (C_nH_{2n+2}) originate from biogenic sources. Grass, crops and trees are responsible of emitting ethane, propane, pentane, hexane, heptane, pyruvic acid, ketones, alcohols and C6 to C10 saturated aldehydes. Several studies have shown that living plants emit relatively small amounts of methane (Dueck et al., 2007). However, terrestrial ecosystems such as termites and soil microbes are considered as significant contributors to methane emissions (Keppler et al., 2006).

Benzenoid Compounds: Several benzenoid compounds such as benzyl alcohol, anisole, benzaldehyde are emitted from plants in the form of floral scents. Their contribution to annual regional *BVOC* emissions is believed to be relatively small, but may be significant on a local scale.

Organic Sulfur Compounds: In clean environments, atmospheric sulfur compounds originate mainly from biogenic organic sulfur arising from terrestrial and marine ecosystems. Dimethyl disulfide, dimethyl sulfide and methyl mercaptan are emitted by plants and soil microbes. According to Guenther (2013), 85% of the global dimethyl sulfide flux comes from oceans with the remainder coming from terrestrial ecosystems.

1.2 BVOCs emission processes

BVOCs are emitted by plants as a part of their normal metabolic processes. After being produced in plant cells in a liquid form, these compounds can be emitted into the atmosphere by three different release processes: diffusion through stomata, diffusion through cuticles or release through plant storage structures.

Isoprene, like many other BVOCs, is released directly after synthesis via diffusion resulting from a high concentration gradient between the plant leaves (high concentrations) and the surrounding air (low concentrations). Additionally, isoprene is known to lack a storage mechanism in plants. Consequently, the isoprene emission rate is always equal to the biosynthesis rate (Lerdau et al., 1997).

Unlike isoprene, monoterpenes can be stored in specialized structures such as the storage cavities in eucalyptus leaves, the glandular dots of the rutaceae, the resin canals in pines needles the resin blisters in coniferous trees and the glandular hairs on mints (Lerdau et al., 1997). These stored monoterpenes are released into the atmosphere when environmental conditions

change or the plant is damaged. Monoterpenes release commonly occurs by passive diffusion, with monoterpenes evaporating from the plant surface and diffusing into the surrounding air.

1.3 Eco-physiological role of BVOCs

Plants release a variety of volatile organic compounds for various purposes, including communication, protection, and defense. Several studies have revealed the key role that isoprene plays in protecting plants from short high-temperature episodes that can affect the plant's photosynthetic functions. In these particular conditions, isoprene can act as a shield against thermal stress, reducing the detrimental effects of excessive heat on plant tissues (Sharkey and Singaas (1995), Behnke et al. (2007)).

Monoterpenes have also multiple functions, most importantly protection (Mihaliak et al., 1991). These compounds are released as a defense mechanism against pathogens and herbivores, as their antimicrobial properties can inhibit the growth of potential attackers, serving as a chemical barrier (Wang et al., 2013). Monoterpenes also have an allelopathic function, effecting the germination, growth, and survival of neighboring plants. This allelopathic¹ function helps plants to alter the growth of nearby plants, giving the emitting plant a competitive advantage in resource acquisition (Tarayre et al. (1995), Fischer (1991)). Monoterpenes also serve as attractants for pollinators, as different oxygenated monoterpenes are released by plants to attract bees and guarantee their reproduction (Wright and Schiestl (2009), Dobson (2017)). Monoterpenes can also serve as a means of interplant communication. This form of communication helps plants in sharing valuable information about potential threats, resource availability, or other physiological states (Shulaev et al., 1997).

1.4 BVOCs emission factors

VOCs emission from vegetation vary largely as a result of a series of complex interactions between the plant and its environment. The spacial and temporal variability of emissions is controlled by a variety of factors that can be synthesized in Figure 1.1. The most important factors are detailed below.

Light and temperature:

¹Allelopathic refers to the biochemical interactions between plants, where one plant species releases chemicals into the environment that can inhibit the growth or development of other nearby plants.

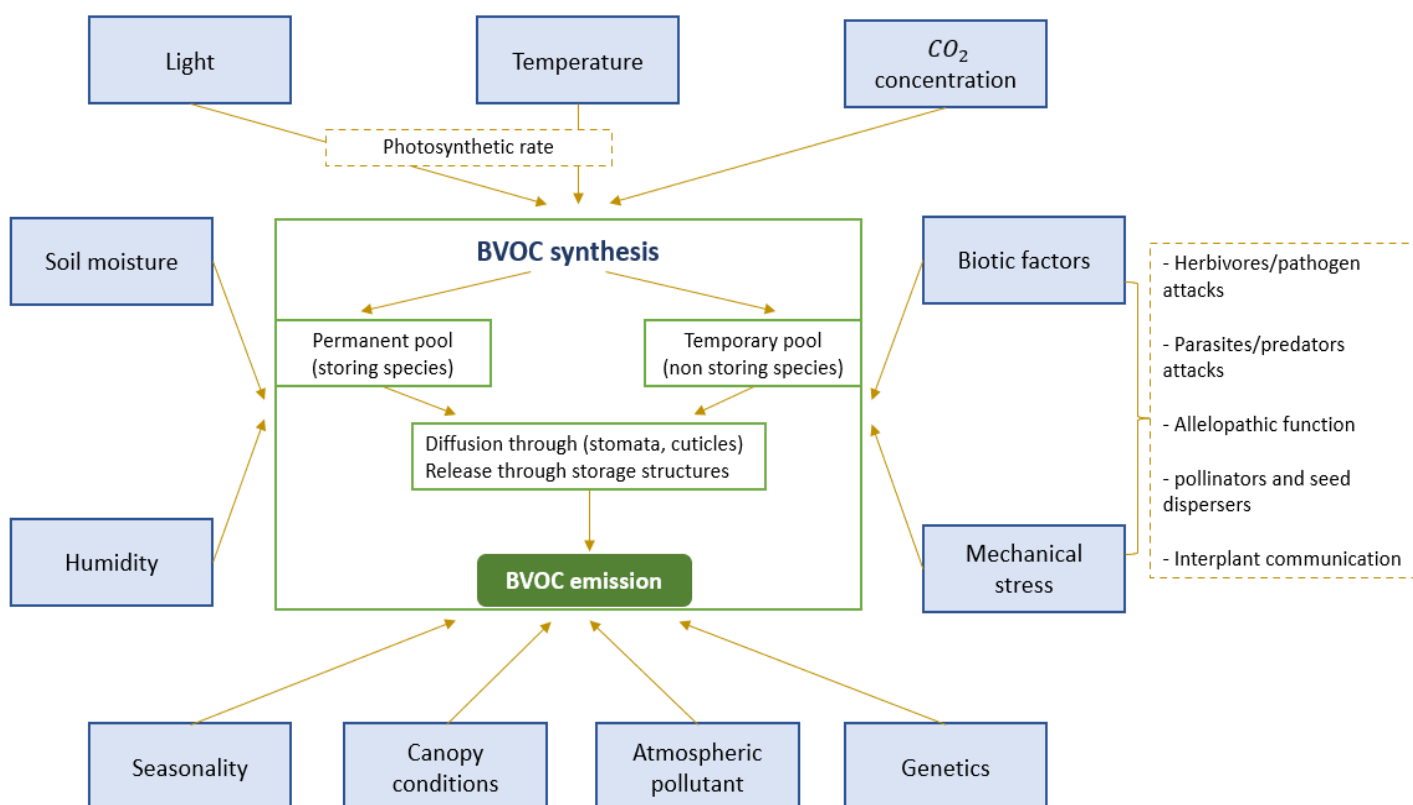


Figure 1.1: Different biotic and abiotic factors controlling BVOCs emission from plants (inspired by Penuelas and Llusia (2001)).

Temperature and light are the most important factors in BVOCs emission. Rising temperatures have several impacts on plants: decreasing the resistance of emission pathways, increasing BVOCs vapor pressure levels and enhancing enzymatic synthesis activities. These factors lead to an exponential increase in BVOCs emission with temperature up to an optimum. However, at higher temperatures, enzyme inactivation leads to a further decrease (Guenther et al., 1991). The effect of temperature on emissions is in line with the relationship between temperature and vapor pressure curves, Tingey et al. (1980) provided a formula that describes the response of emissions to increasing temperatures:

$$F = F_s \times \exp(\alpha \times (T - T_s)) \quad (1.1)$$

Where F is the emission at temperature T , F_s is the emission at standard temperature T_s and α is the slope $= \frac{d \ln F}{dT}$.

For species stored in plant reservoirs, such as monoterpenes, temperature is the dominant factor in biogenic emissions, these compounds are called light-independent. For other species with no existing storage pool, such as isoprene, biogenic emissions are also light-driven, these compounds are called light-dependent. For all existing plants, synthesis requires the presence of

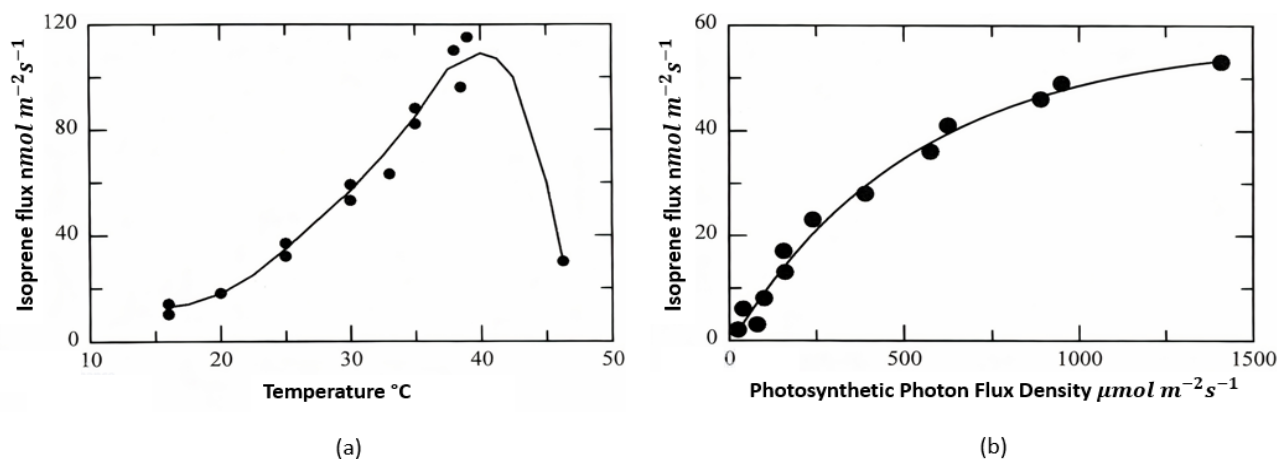


Figure 1.2: Isoprene emission flux variation as a function of temperature (a) and PPFD (b) for white oak (a) and sweet gum (b) leaves (adapted from Fuentes et al. (2000)).

light, hence the emission of non-stored VOCs will cease within minutes under dark conditions. Figure 1.2 shows the influence of temperature and photosynthetic photon flux density (PPFD²) for white oak and liquidambar leaves.

Atmospheric relative humidity:

Several studies have reported that atmospheric humidity can have a positive effect on the emission rate of certain BVOCs. Aspen and eucalyptus isoprene emissions (Guenther et al. (1991)) and oak, mint and sage monoterpenes emissions (Loreto et al. (1996), Dement et al. (1975)) have been shown to increase with atmospheric humidity. This effect could be explained by a change in the permeability of the leaf cuticula when hydrated. However, other studies have shown that the contribution of atmospheric humidity in controlling monoterpenes emission rates in eucalyptus, spruce and pine is relatively small (Guenther et al. (1991), Janson (1993)). Figure 1.3 shows the influence of atmospheric humidity on isoprene emission rates from eucalyptus leaves.

Atmospheric CO₂ concentration:

Guenther et al. (1991) have demonstrated that isoprene emission variation linked to CO₂ concentrations variation was only observed at very high (> 600 ppm) or very low (< 100 ppm) CO₂ mixing ratio. At these concentrations, isoprene emissions decreased relatively. As shown in Figure 1.4, isoprene emission rates from eucalyptus leaves are constant for CO₂ mixing ratios between 50 and 600 ppm, but at very low or very high CO₂ concentrations, isoprene emission

²PPFD measures the intensity of light that is needed by plants for photosynthesis, this light is within the wavelength range $400\text{nm} < \lambda < 700\text{nm}$.

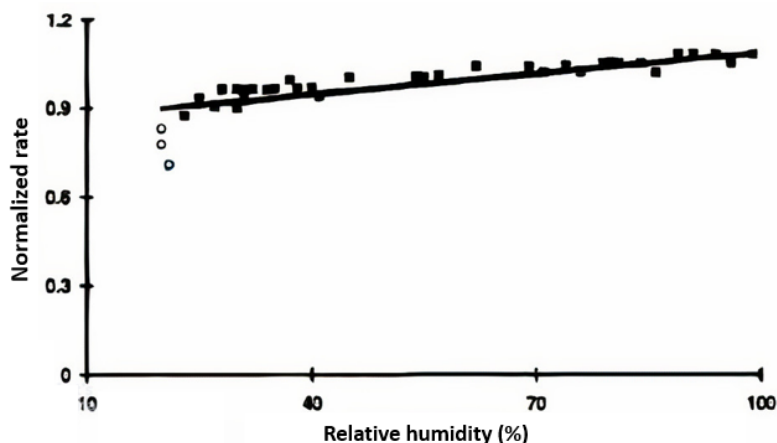


Figure 1.3: Relative humidity dependence of normalized isoprene emission rates from eucalyptus leaves. Emission rates are normalized by the observed emission at a relative humidity of 40%. Measurements made with no water vapor present in the inlet air stream are presented by open circles (adapted from Guenther et al. (1991)).

rates decrease slightly.

Atmospheric pollutant:

There is some disagreement as to the influence of air pollutants on BVOCs emission rate. Some studies focusing on BVOCs emission from conifers under ozone exposure, have reported unchanged monoterpenes emissions (Lindskog and Potter (1995), Juuti et al. (1990)). However, other studies that investigated the impact of plant exposure to elevated levels of air pollutants (e.g., ozone and SO_2), have reported high monoterpenes and ethylene emissions under air pollution conditions (Bucher (1981), Renwick and Potter (1981)). The discrepancies between the results of these studies may be explained by differences in plant species, BVOC species and seasons.

Soil moisture:

Several studies have conducted experiments aiming to investigate the impact of soil moisture on BVOCs emission from various vegetation types (Holm oak, conifers, live oak, kudzu wine and sweet gum). These studies came up with a common finding: isoprenoids (isoprene and monoterpenes) response to drought shows constant emission rate under moderate stress conditions with declining H_2O and CO_2 gas exchange. Under extreme soil moisture deficit conditions, isoprenoids emissions are reduced. However, increasing soil moisture after a severe drought can largely enhance isoprene and monoterpenes emissions (Bertin and Staudt (1996), Tingey et al. (1980), Sharkey and Loreto (1993)).

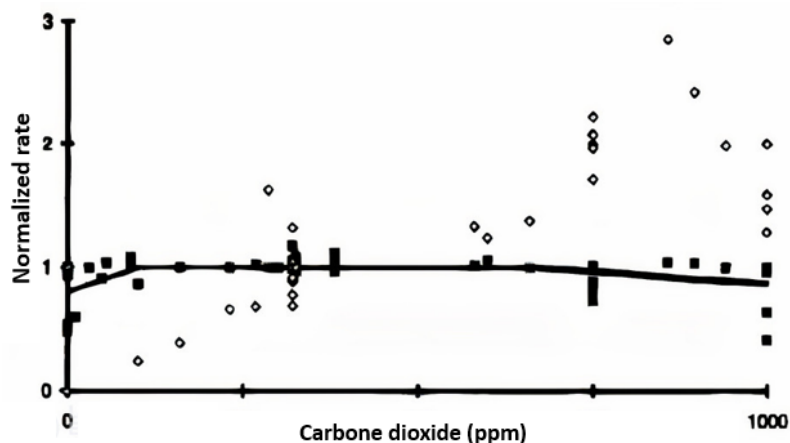


Figure 1.4: CO_2 concentration dependence of normalized isoprene emission rates (squares) and normalized CO_2 assimilation rates (open diamonds) from eucalyptus leaves. Rates are normalized by the observed rates at a CO_2 mixing ratio of 330 ppm. (adapted from Guenther et al. (1991)).

Seasonality and canopy conditions:

Seasons play an important role in BVOCs emission. According to Guenther et al. (1991), BVOCs emission rate follows a general seasonal pattern where emissions are insignificant during winter, rapidly rising to a maximum during the growing season (in spring and summer), followed then by a rapid decrease during autumn. This seasonal pattern is observed for various BVOCs, including isoprene.

The seasonal variations in *BVOC* emissions are influenced by several factors including light, temperature, and species development stage. For instance, isoprene-emitting plants (e.g., aspen) release important quantities of monoterpenes and other alkenes during spring at the early stages of leaf development. In summer, when the foliage has reached maturity, isoprene is emitted at high levels. In fact, isoprene emission only begins once the leaf is fully developed, and more precisely after several days of exposure to sufficiently warm temperatures.

The living and development conditions of plants can also impact their BVOCs emission rate. Several studies have investigated the influence of a luminous environment on isoprene and monoterpenes emissions from leaves, as shown in Figure 1.5, leaves located at the top of the canopy in a very bright environment produce greater quantities of isoprene than leaves in the canopy (Street et al. (1997); Bertin and Staudt (1996); Fuentes et al. (2000)).

Biotic factors:

In some plants, BVOCs are emitted as a defense mechanism against intruders. One example is corn leaves, which activate their terpene production when the plant is eaten by a caterpillar.

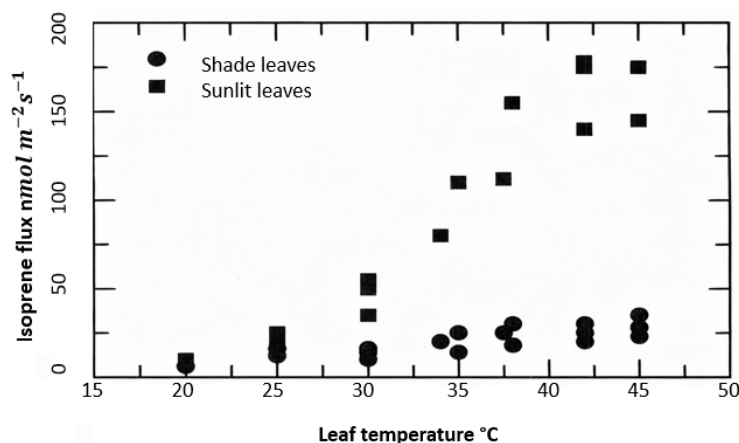


Figure 1.5: Isoprene emission flux emitted by sweet gum leaves, sun leaves and shade leaves are represented with a filled square and a filled circle, respectively (adapted from Fuentes et al. (2000)).

Here, VOC emissions are triggered by the presence of an elicitor³. The induced emissions enable a parasitoid wasp, which uses the caterpillar as a host for its larvae, to locate the attacked plants. This limits the damage to maize plants caused by an invasion of caterpillars (Turlings et al., 1990). Other BVOCs are released to attract pollinators, for example some oxygenated monoterpenes (linalool) help plants to attract bees.

Mechanical stress:

Attacks by pathogens and herbivores as well as injuries can have several short and long-term effects on BVOCs emissions. Unlike isoprene, which does not appear to be affected or altered by plant damages (Loreto and Sharkey (1993), Monson et al. (1994)), monoterpenes are found to be produced in large quantities by plants subjected to mild mechanical stress (Guenther et al. (1991), Juuti et al. (1990)).

1.5 Conclusion of Chapter 1

BVOCs include a wide range of compounds. These chemicals are emitted mainly from terrestrial biosphere for communication, protection and as a defense mechanism. The emission of these compounds is influenced by a variety of factors, the most important of which are temperature, light, soil moisture and atmospheric CO_2 concentrations. BVOCs are emitted in large quantities accounting for about 90% of the total VOCs. Due to their abundance and high reactivity, these compounds can serve as a link between the Earth's physical, chemical and biological

³In biology, elicitors are substances that trigger a defense or protective reaction in plants when they come into contact with them.

components. In the next Chapter we will explore how biogenic compounds can affect the Earth's chemical component and particularly atmospheric chemistry and air quality.

Air quality

Since the 19th century, the global population has experienced significant growth, leading to a substantial increase in the number of people living in cities, as the urban population has increased by more than a factor of four. This rapid urbanization, coupled with industrialization and technological advancements, has brought significant changes in energy consumption and transportation modes. Global energy consumption, for instance, has risen by nearly a factor of five, driven by the growing demand for power in various sectors. The use of motor vehicles has also increased significantly with the rise of automobile ownership.

The impact of increasing industrial and transportation emissions on public health has thus become a pressing issue, the notion of **air quality** has emerged and considerable efforts were conducted in the implementation of environmental regulations and the development of environment friendly technologies.

In this context, the **World Health Organization (WHO)** was established in 1948 to address the global health challenges arising from these changes. The WHO took on the responsibility of promoting and coordinating international efforts to improve health, prevent diseases, and provide healthcare services worldwide. As part of its mission, the organization also recognized the importance of addressing environmental factors, including air pollution, in safeguarding public health. According to the latest estimations of the WHO, 6.7 million annual deaths are caused by indoor and outdoor air pollution, with outdoor air pollution contributing to more than 4.2 million deaths in 2019.

In line with its objectives, the WHO has played a crucial role in setting strict emissions standards for industries and automobiles. These standards are designed to regulate and reduce pollutant levels, including sulfur dioxide (SO_2), nitrogen dioxide (NO_2), ozone (O_3) and particulate matter (PM) contributing to improve air quality and protecting public health.

In this chapter, we will provide a general overview of primary and secondary air pollutants, with a particular focus on ground-level ozone and secondary organic aerosols. The chemical formation processes of these two air pollutants are linked to VOCs.

Atmospheric pollutants can be divided into two categories: **primary pollutants** and **secondary pollutants**.

Primary pollutants are chemical species emitted directly into the atmosphere from natural sources (e.g., vegetation, volcanoes) or anthropogenic sources (e.g., vehicles, industrial plants, consumer products, power plants). The main primary pollutants are: oxides of sulfur (SO_x), nitrogen oxides (NO_x), carbon monoxide (CO), particulate matter (PM), etc.

In contrast to primary pollutants, secondary pollutants are not emitted directly into the atmosphere, but are rather formed by chemical reactions involving primary pollutants and other atmospheric components with or without photo-activation. Examples of secondary pollutant include ozone (O_3), nitric acid (HNO_3), peroxy acetyl nitrate (PAN), photochemical smog, peroxy butyl nitrate (PBN), etc. A representation of primary and secondary pollutant is shown in Figure 2.1.

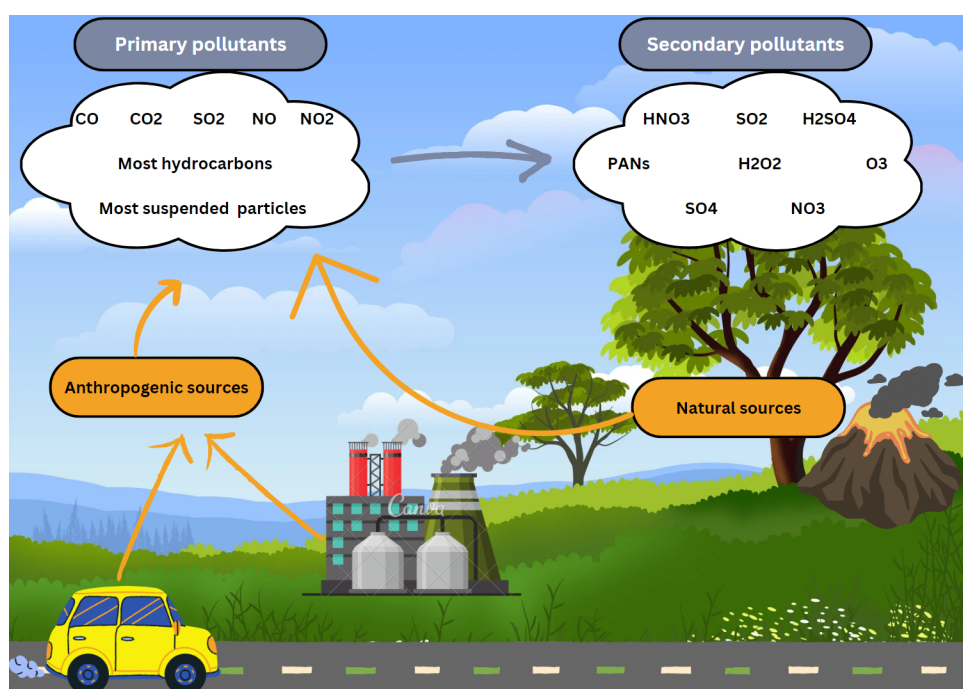


Figure 2.1: Primary and secondary atmospheric pollutant.

2.1 Ozone

Ozone is a highly reactive trace gas and one of the most studied secondary pollutants. It is present in large quantities in the upper-atmosphere (stratosphere) and in small quantities in the lower-atmosphere (troposphere).

Stratospheric ozone, also known as the ozone layer, plays a crucial role in shielding the Earth from harmful ultraviolet (UV) radiation. This protective layer is located approximately

10 to 50 km above the Earth's surface and comprises the largest fraction of atmospheric ozone (90%). In this layer, ozone is formed through chemical reactions involving the decomposition of oxygen molecule (O_2) to two oxygen atoms (O). These reactions occur in the presence of radiation at a specific wavelength range ($\lambda < 242 \text{ nm}$).

Conversely, **tropospheric ozone** also known as ground-level ozone is considered as one of the most harmful atmospheric pollutants to human health. The latter is formed through a series of complex reactions involving different compounds, most importantly Volatile Organic compounds ($VOCs$) and nitrogen oxides (NO_x). These reactions occur under specific environmental conditions (presence of sunlight). The majority of ground-level ozone is the result of reactions between $VOCs$ and man-made NO_x only a small fraction comes from transported stratospheric ozone or from nature-induced NO_x .

2.1.1 Ozone precursors

As previously mentioned, ozone is the product of photochemical reactions of its precursors, the most important of them being: $VOCs$, NO_x , NH_4 and CO . These compounds are described in further detail below:

Volatile organic compounds:

Volatile organic compounds are a diverse group of organic chemicals that can easily evaporate at room temperature. They exclude carbon monoxide (CO) and carbon dioxide (CO_2) and are defined by the European directive 2004/42/CE (Parliament, 2004) as "any organic compound having an initial boiling point less than or equal to $250 \text{ }^\circ\text{C}$ measured at a standard pressure of $101,3 \text{ kPa}$ ".

$VOCs$ are primarily emitted from natural sources such as soils, oceans, and vegetation, with terrestrial vegetation accounting for approximately 90% of total global $VOCs$ emissions (Guenther et al., 2012). The remaining 10% of $VOCs$ emissions stem from anthropogenic sources, including the combustion of fossil fuels and biomass, compressed aerosol products, and solvents using.

As shown in Table 2.1, the lifetime of $VOCs$ in the atmosphere is highly variable, ranging from just a few hours to several days. This variability is due to the reactivity of $VOCs$ with hydroxyl radicals (OH), ozone (O_3), and nitrate radicals (NO_3). During the day, $VOCs$ are primarily eliminated through oxidation reactions with OH and O_3 , while at night, they react with NO_3 . The reactivity of $VOCs$ with these atmospheric constituents is the primary reason for their wide-ranging lifetimes.

Nitrogen oxides:

Compound	Atmospheric lifetime
Styrene	4.9 h
m-Xylene	11.8 h
p-Xylene	19.4 h
o-Xylene	20.3 h
Ethylbenzene	1.6 days
Toluene	1.9 days
Ethylene	4 days
Butane	5 days
Benzene	9.4 days
Propane	10 days
Ethane	60 days
Methane	9.6 years

Table 2.1: Atmospheric lifetime of some *VOCs* (adapted from Ragothaman and Anderson (2017)).

Nitrogen oxides include two main species: nitric oxide (NO) and nitrogen dioxide (NO_2). The majority of nitrogen oxides are emitted in the form of NO , which is rapidly transformed into NO_2 by chemical processes. Nitrogen oxides are formed when nitrogen (N_2) and oxygen (O_2) combine under high-temperature conditions, such as during combustion processes or lightning events.

Anthropogenic activities, including industrial effluents and automobile exhausts, account for approximately 50% of NO_x emissions. These sources release large concentrations of nitrogen oxides, particularly in urban areas where vehicle traffic and industrial processes are concentrated. At high altitudes, aircraft and lightning contribute to 20% of NO_x emissions. Finally biogenic activities, such as soil nitrification and denitrification, contribute to the remaining 30% of NO_x emissions

The lifetime of NO_x in the atmosphere varies depending on altitude. In high altitudes, its lifetime can extend up to 4 days, while in the lower layers, it lasts for only a few hours.

On a global scale, nitrogen oxides can be transported from a continent to another by NO_x reservoir species. The most important being peroxyacetyl nitrate (PAN, $CH_3COO_2NO_2$) and nitric acid (HNO_3). These reservoir species can be converted back into NO_x under certain conditions, allowing for the continued influence of NO_x on air quality and atmospheric chemistry even far from emission sources.

Carbon monoxide:

Carbon monoxide (CO) is a colorless, tasteless, and odorless trace gas primarily formed by the partial combustion of carbon-containing materials. It can also be produced through the oxidation of methane (CH_4) and other hydrocarbons in the atmosphere. CO is present

in the troposphere in very small concentrations, its major emission sources include solid waste disposal, industrial processes, fossil fuel burning for electricity and heat, and motor vehicles. The latter account for more than 60% of carbon monoxide emissions. The primary sink of CO is its oxidation by OH and its lifetime varies between two to four months in the atmosphere. Due to its relatively long lifetime in the troposphere, CO is considered as a useful tracer for hydrocarbon sources.

In the troposphere, the concentration of carbon monoxide is around 0.05 and 0.12 ppm . However, concentrations near emission sources can be 5 to 10 times higher, for instance, the concentrations in regions with dense smog, can reach values of 17 ppm .

Methane:

Methane (CH_4)¹ is the simplest hydrocarbon primarily released from natural sources. This natural gas originates from processes like anaerobic bacterial decomposition of organic matter, digestive processes in cows and termites, and volcanic eruptions. Additionally, human activities such as fossil fuel extraction, combustion, and waste management also contribute to methane production. With an atmospheric lifetime of about 8 years, methane is one of the most significant greenhouse gases, second only to CO_2 .

Although its concentration in the atmosphere is relatively low (around 1.8 ppm), methane is 25 times more powerful than CO_2 in trapping heat, making it a significant contributor to global warming.

The most important sink of methane is the hydroxyl radical (OH). The latter plays a significant role in reducing natural and man-made methane. However, due to the increasing anthropogenic methane emissions, there is a notable decline in OH levels in the atmosphere. This reduction in OH prolongs the atmospheric lifetime of CH_4 and indirectly intensifies the greenhouse effect.

2.1.2 Tropospheric ozone formation

In the stratosphere, O_3 is produced through chemical reactions of photodissociation of oxygen molecule (O_2) by UV radiation with wavelengths below 242 nm . Radiation below 290 nm are filtered in the upper atmospheric layers, making the only source of oxygen atom produced in the troposphere is via the photolysis of NO_2 . The production of tropospheric ozone follows the photochemical reaction 2.1.



¹Methane is also a VOC , however a distinction is made between methane and non-methane $VOCs$ ($NMVOCs$) because of methane's distinct characteristics e.g., lifetime (Table 2.1), air quality impacts, regulatory considerations.

ν is the frequency of the light which is equal to the speed of light divided by the wavelength λ .

The combining of O and O_2 is possible only in the presence of a third molecule M , as it absorbs the excess energy released during the formation of ozone. M can be trace gas molecules, particles, etc.

NO is converted back into NO_2 by reaction with ozone O_3 following reaction 2.2.

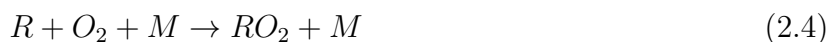


A photochemical equilibrium is established between reaction 2.1 and 2.2, implying a rapid conversion between NO and NO_2 leading to instantaneous destruction of the produced O_3 . These equations alone cannot explain the ozone concentrations observed in the troposphere. The net production of ozone is explained by the conversion of NO to NO_2 in the presence of peroxy radicals (HO_2 and RO_2) formed during VOC oxidation.

The oxidation of $VOCs$ (RH^2) process start by the reaction of $VOCs$ with OH radical following the reaction:



Oxygen is then used to form the peroxy radical (RO_2) following the reaction:



The conversion of NO to NO_2 is the critical reaction in the VOC oxidation cycle. This occurs as a result of the rapid radical transfer reaction with NO . Reaction 2.5 ensures a net production of ozone.



The radical RO reacts then with oxygen O_2 to produce an intermediary organic compound $R'CHO$ and radical HO_2 :

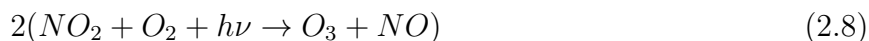


Radical HO_2 reacts with NO to form NO_2 :

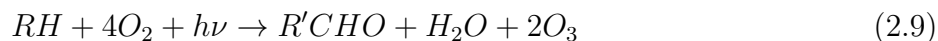


The conversion of NO to NO_2 in reactions 2.5 and 2.7 results in additional ozone production.

²More generally, RH refers to a hydrocarbon molecule.



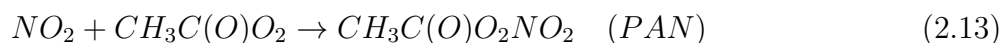
These chemical reactions result in the following balance:



The chain of reactions can be repeated indefinitely until the cycle is broken by the loss of one of the molecules. The reaction of peroxy radicals (RO_2 and HO_2) with HO_2 to form H_2O_2 (hydrogen peroxide) following reaction 2.10 and $ROOH$ (organic peroxide) following reaction 2.11 is one way of cycle breaking.



The reaction of NO_2 with a radical (OH or an organic radical) can also terminate the ozone production cycle by the formation of a sink species such as nitric acid (HNO_3) following reaction 2.12 or by the formation of a reservoir species such as PAN following reaction 2.13. Figure 2.2 displays a schematic representation of tropospheric ozone formation cycle.



2.1.3 Ozone chemical regimes

Ratio of $VOCs$ to nitrogen oxides NO_x at a specific location influences the concentration of ozone in that area. The latter varies non-linearly with NO_x and VOC_s concentrations. Figure 2.3 displays the variation of ozone concentration as a function of NO_x and $VOCs$ concentrations. As shown in Figure 2.3, there are two ozone production regimes:

NO_x limited regime:

When the $[VOC]/[NO_x]$ ratio is high, with $VOCs$ being more abundant than NO_x , the latter generally promotes ozone production. Here, the quantity of NO_x constrains ozone formation, making it " NO_x -limited". As shown in Figure 2.3, in NO_x -limited regime, where NO_x concentrations are below 40 *ppb*, an increase in $VOCs$ concentration will have nearly no effect

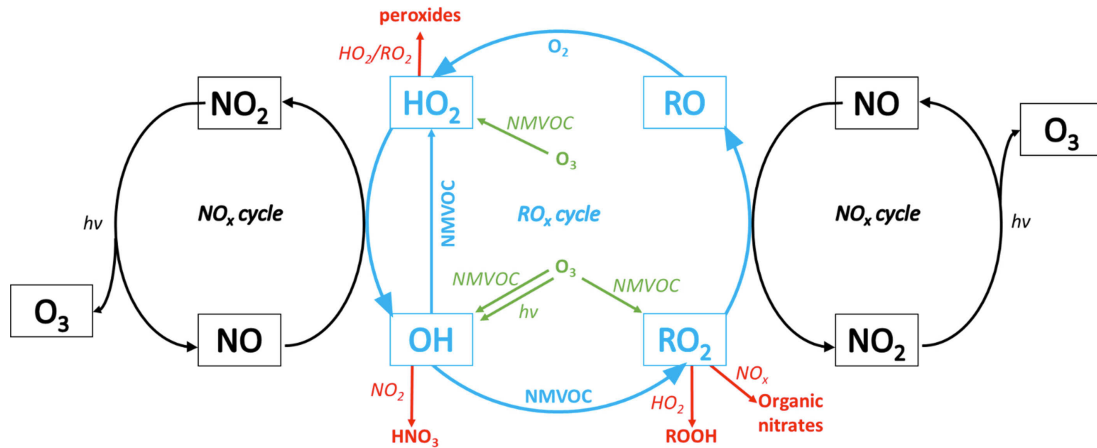


Figure 2.2: Ozone formation via the interactions between the RO_x - (blue) and NO_x -cycles (black). Interfering with the RO_x - NO_x cycle are ozone degrading reactions (green) via $NMVOC$ s (non-methane volatile organic compounds) as well as terminating reactions (red); $h\nu$, light. Methane and carbon monoxide are not displayed (adapted from Fitzky et al. (2019)).

on ozone production despite high RO_2 or HO_2 supply, reactions 2.5 and 2.7 limit ozone formation. This is called NO_x -limited regime because the availability of NO_x is the limiting factor in ozone formation.

VOC limited regime:

Conversely, when the ambient air has a low concentrations of VOC s, VOC s constrains ozone production as reaction 2.5 slows down. In this case an increase in NO_x concentrations has little effect on ozone production and may even decrease its concentration. In this situation, the amount of VOC s present restricts ozone formation, which is referred to as being "VOC-limited."

The O_3 concentration dependency on the ratio $[VOC]/[NO_x]$ can lead to significant ozone concentration variation during the week; this is known as **the week-end effect**. Heuss et al. (2003) observed a difference in ozone concentrations between weekdays and weekends in various locations across the United States. Figure 2.4 shows average hourly ozone concentration variation across the week for two sites: Los Angeles and Southeast desert. In most sites the average daily 1-hour ozone concentration increased on weekends compared to weekdays (by more than 10% in 138 sites and between 5% and 10% in 287 sites). This can be explained by the reduction in NO_x emissions on the week-end due to low traffic compared to weekdays. In a VOC -limited regime, the reduction of NO_x concentrations can lead to an increase in ozone production rate. Conversely, observed weekend ozone concentrations were lower than 5% in 29 monitoring sites, which is probably due NO_x reduction in a NO_x -limited regime.

Distinguishing the ozone regimes is crucial for understanding the spatial and temporal

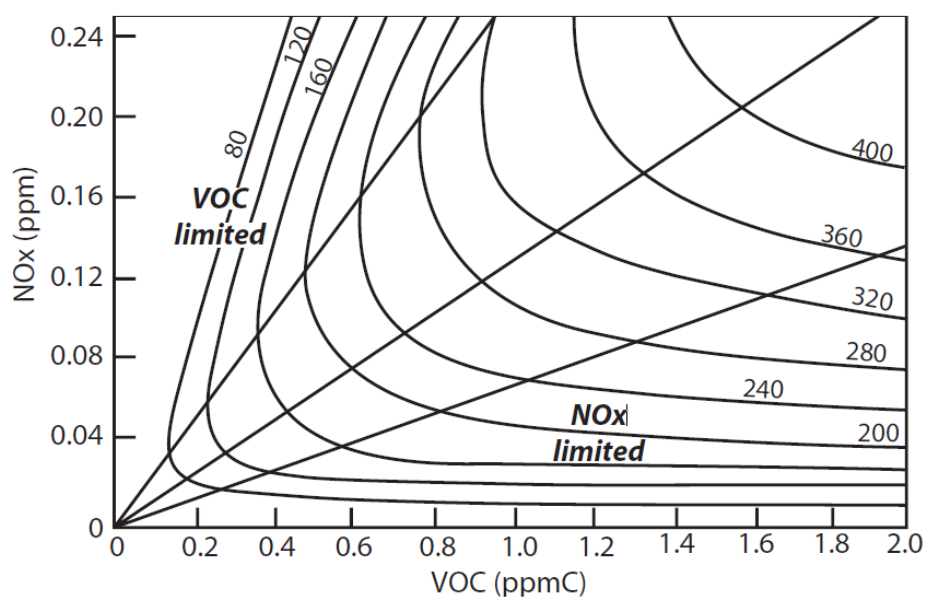


Figure 2.3: Ozone isopleth diagram. Isopleths show constant ozone concentrations, the ratio $[VOC]/[NO_x]$ is written at the end of isopleths. The unit of VOCs *ppmC* refers to Parts Per Million Carbon (adapted from Sillman (1999)).

variation of ozone concentrations. This knowledge is also important in developing effective emission control strategies that can help mitigate the adverse effects of ozone pollution on human health and the environment.

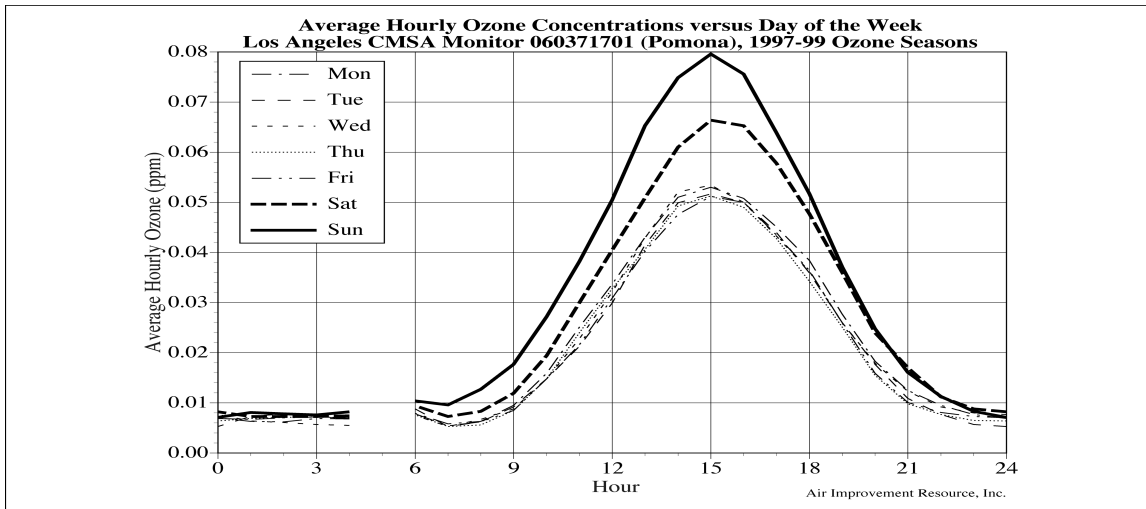
In **urban areas**, ozone production is generally *VOC*-limited. To reduce ground-level ozone concentrations in these areas, it is necessary to reduce *VOC* emissions. This can be achieved through various strategies such as implementing stricter regulations on industrial emissions, promoting the use of low-*VOC* products, and encouraging practices that reduce the release of *VOCs* into the atmosphere.

It is worth noting that reducing nitrogen oxides emissions in *VOC*-limited areas, will have a contrary effect on ozone formation. In fact, in these areas, NO_x destroys O_3 at night, a phenomenon known as ozone titration. Therefore, in these areas, reducing NO_x emissions may inadvertently lead to an increase in ozone concentrations due to the attenuated nocturnal ozone titration (Ren et al., 2022).

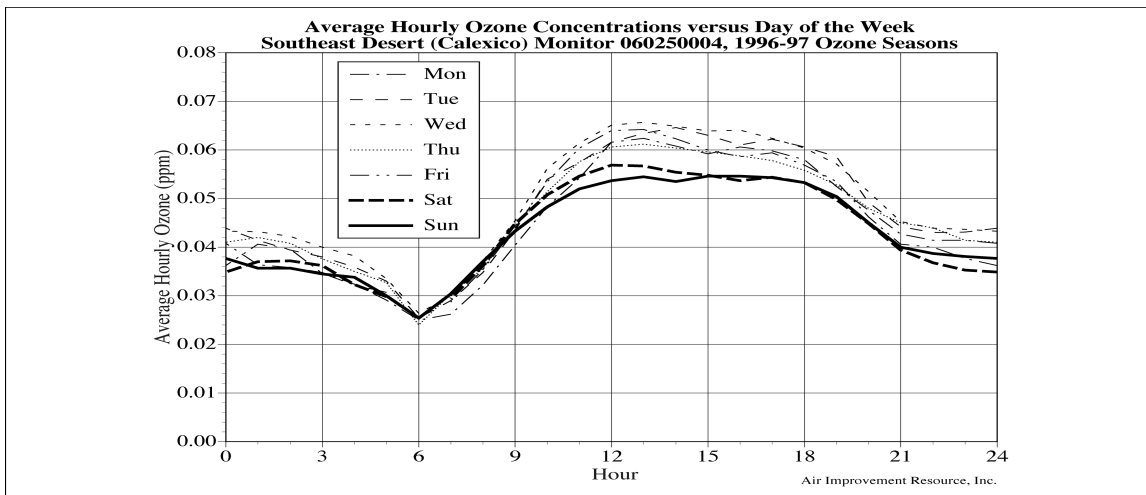
In **rural areas**, where ozone formation is NO_x -limited, reducing NO_x emissions can effectively lower ozone levels.

2.1.4 Ozone transport

Once formed, ozone can be transported both horizontally and vertically. Ozone transport mechanisms involve a variety of physical and chemical processes that enable ozone to be distributed throughout the atmosphere. Here are some of the main ozone transport mechanisms:



(a)



(b)

Figure 2.4: Average hourly O_3 concentrations in week days and week-end in Los Angeles (a) and in Southeast Desert (Calexico) (b) (adapted from Heuss et al. (2003)).

Advection: Advection refers to the horizontal movement of air masses carrying ozone. Wind patterns in the atmosphere can transport ozone-rich air masses from one region to another. This can occur on various scales, from local to global, and is influenced by large-scale atmospheric circulation patterns such as the jet streams and trade winds.

Vertical Mixing and Turbulence: Vertical mixing and turbulence help distribute ozone vertically within the atmosphere. Convective processes, such as those associated with thunderstorms and updrafts, can transport ozone-rich air from the lower troposphere to higher altitudes. This mixing is important for maintaining ozone concentrations at different altitudes.

Stratosphere-Troposphere Exchange (STE): The boundary between the stratosphere and the troposphere is not always well-defined. In some regions, there are processes that allow ozone-rich air from the stratosphere to mix with the troposphere and vice versa.

The transfer of ozone from the stratosphere to the troposphere can be due to a variety of atmospheric mechanisms. A notable example is the occurrence of strong updrafts in deep-convection systems, which can transport trace gases from the lower atmospheric boundary layer (ABL) to the upper troposphere and lower stratosphere (UTLS) such as ozone together with its precursors including *VOCs*, *NO_x* and *CO*. This in turn triggers significant changes in chemical composition, leading to considerable ozone formation in both the upper troposphere and lower stratosphere. Conversely, deep-convection can also cause air masses with high ozone concentrations to flow downwards from the stratosphere into the lower troposphere, according to Chen et al. (2022) an approximate 5-15% of tropospheric ozone origins are attributed to the transport of stratospheric ozone into the troposphere. Consequently, the role of deep convection in shaping ozone budgets in the stratosphere and troposphere is of paramount importance.

2.2 Aerosols

Aerosols are present in the atmosphere in the form of microscopic solid particles or liquid droplets. Carbon-containing aerosols can be divided into two groups: **Primary Organic Aerosols (POA)** and **Secondary Organic Aerosols (SOA)**.

In the context of air quality, aerosols contribute significantly to air pollution, causing multiple effects on both human health and the environment. According to the WHO, short- and long-term exposure to aerosols can cause respiratory and cardiovascular diseases and, in some cases, lung cancer. Furthermore, due to their distinctive characteristics of reflecting and absorbing solar radiation, aerosols are recognized as an important constituent of the climate system, playing a particularly crucial role in maintaining the Earth's radiative balance. These micro-particles also exert a considerable influence on cloud formation processes, serving as essential nuclei for the condensation of water vapor. As a consequence, aerosols exert a multi-faceted impact on radiative balance and cloud dynamics, underlining their integral role in the complex interplay of Earth's atmospheric processes.

2.2.1 Primary organic aerosols

POAs are particles that are directly emitted into the atmosphere characterized by a diameter ranging from 100 *nm* to a few micrometers, they account for 95% of the aerosols present in the atmosphere. These particles are directly released into the air from diverse origins. Roughly 90% of the yearly aggregate of primary organic aerosols suspended in the atmosphere emanates

Aerosol type	Emission flux (Mt/year)
Natural primary organic aerosol	
Desert dust	1000-3000
Sea salt	1000-6000
POAs from biomass combustion	20-35
POAs from biogenic sources	1000
Anthropogenic primary organic aerosol	
Industrial dust	40-130
POAs from biomass combustion	50-90
Carbon soot (fossil fuels)	6-10
Organic carbon (fossil fuels)	20-30

Table 2.2: Annual emission flux of primary organic aerosols from natural and anthropogenic sources in Mt= 10^{12} g (from Boucher (2012)).

from natural sources.

Generally, natural POAs result from the friction between the wind and the superficial layers of a given surface. For instance, desert dust and sea salt are instances of this phenomenon, originating from the mechanical interaction between wind and the surfaces of oceans or deserts. The effectiveness of this mechanism hinges on wind velocity, with notable friction-induced emissions occurring at wind speeds exceeding 8 m/s (Monahan, 1968). The Sahara Desert alone contributes an estimated 60-200 million tons of suspended primary aerosols annually (Goudie and Middleton, 2001). Other natural sources encompass aerosols generated from incomplete biomass combustion during droughts and emissions from vegetation such as pollen.

Moreover, anthropogenic sources like vehicle emissions, the combustion of fossil fuels, and human-induced biomass burning stand as significant contributors to POAs. Table 2.2 summarizes the primary sources of POAs and provides an approximate annual estimate of the emitted POA quantities.

2.2.2 Secondary organic aerosols

SOAs are not emitted directly into the atmosphere but are rather formed through the gas-phase oxidation of volatile or non-volatile organic compounds or through condensation on pre-existing particles.

Secondary organic aerosols result from the conversion of some compounds called precursors from gas phase to particles. This process happens essentially in three steps: **nucleation, condensation and coagulation**.

Durant the nucleation phase, the compound is transformed from gas phase to liquid or solid phase. The condensation step starts when the formed particle reaches a diameter of a few nanometers, at this stage the surrounding air starts to condensate on the formed particle. The

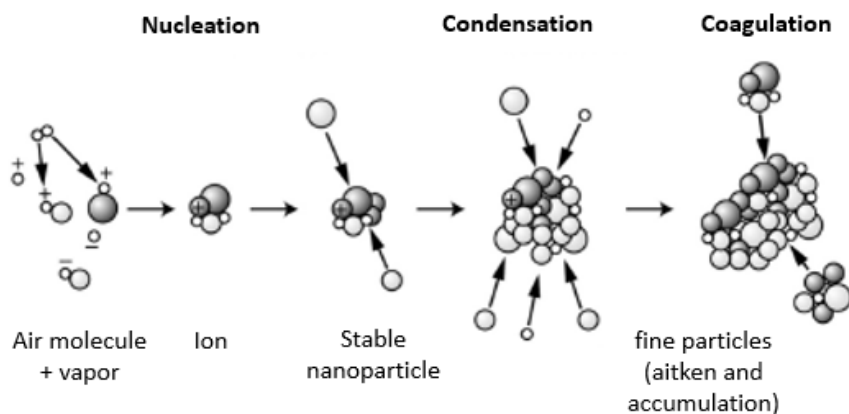


Figure 2.5: Secondary aerosol formation processes (adapted from Delmas and Mégie (2015)).

size of the particle increases further to reach a size of few micrometers in the third phase, where particles coagulate together as a result of turbulence and thermal agitation. The secondary organic aerosols emission processes are shown in Figure 2.5.

The precursors of SOAs are diverse, they include: sulfur dioxide SO_2 , ammonia NH_3 and volatile organic compounds $VOCs$ emitted from anthropogenic and biogenic sources. $VOCs$ from biogenic sources are considered as the most important precursor in SOA formation. In fact, according to Srivastava et al. (2022), the estimated annual fluxes of SOA by atmospheric models shows a predominance of SOA resulting from biogenic $VOCs$ with a total annual flux of 88 Tg, followed by SOA from biomass burning with an annual total of 17 Tg and SOA from anthropogenic $VOCs$ with an annual total of 10 Tg.

The production of SOA from $VOCs$ originates from the formation of low-volatility compounds. These compounds result from the oxidation of $VOCs$ with other atmospheric compounds including hydroxyl radical (OH), nitrate radical (NO_3) and ozone (O_3). After their formation, low-volatility compounds go through the three phases of nucleation, condensation and coagulation to form secondary organic aerosols.

2.2.3 Environmental impact of aerosols

Aerosols are not only essential players in atmospheric processes but also have a considerable influence on the planet's climate, air quality, ecosystems, and human health. The intricate relationship between aerosols and the environment stems from their diverse sources, chemical compositions, and physical properties.



Figure 2.6: A view of Paris taken from Saint-Germain-en-Laye, December 5, 2016 (from LeMonde.fr).

2.2.3.1 Visibility

According to the World Meteorological Organization (WMO), visibility is defined as "the greatest distance at which a black object of suitable dimensions (located on the ground) can be seen and recognized when observed against the horizon sky during daylight or could be seen and recognized during the night if the general illumination were raised to the normal daylight level" (WMO, 1966). Visibility can be reduced by a variety of environmental factors including, fog, rain, snow, etc. However, a common source of visibility impairment in high air pollution episodes is linked to the scattering of light by suspended aerosols.

As shown in Figure 2.6, in December 2016, Paris experienced a pollution episode with a peak concentration of $146 \mu\text{g m}^{-3}$ reached the 1st December 2016, attributed to a significant release of fine particles. This episode was both the longest-lasting and the most intense in the previous ten years.

Impaired visibility significantly affects transportation systems, including aviation, road traffic, and maritime activities. Pilots, drivers, and ship operators face increased risks due to decreased visibility, leading to potential accidents, travel disruptions, and even fatalities. Ensuring safe and efficient movement within these sectors becomes challenging under such conditions.

2.2.3.2 Climate

Aerosols can significantly effect the Earth's climate directly by impacting the Earth's radiative balance and indirectly by serving as a condensation nuclei for clouds formation:

Aerosols and solar radiation:

Aerosols have distinct reflective and absorptive characteristics, depending on their shape, size and composition. These characteristics have a direct influence on incoming solar radiation, given that aerosols scatter and absorb a significant proportion of solar energy. This results in an attenuation of the incident radiative flux, leading to a reduction in global surface temperatures. This effect, known as the **direct effect** of aerosols on climate, manifests itself as cooling. The 1991 Mount Pinatubo³ volcanic eruption, which caused a global atmospheric cooling of 0.4°C , is a perfect illustration of this phenomenon.

Aerosols have also a **semi-direct effect** on climate, this effect stems from the absorption of solar radiation by aerosols. The warming caused by absorbing aerosols can lead to changes in atmospheric stability and circulation patterns. It can potentially reduce the relative humidity in the boundary layer, affecting cloud formation and properties.

Aerosols and clouds:

Due to their hygroscopic characteristics, aerosols can serve as cloud condensation nuclei (CCN), which play an essential role in triggering cloud formation. Increasing aerosol concentrations in the atmosphere can disrupt the fundamental physical processes underlying cloud formation. This disruption stems from the high concentration of CNN, which leads to an increased abundance of smaller water droplets inside clouds. This phenomenon entails an augmentation in cloud reflectivity. Known as the **indirect effect** of aerosols, this process is triggered by aerosol-induced changes in cloud properties, leading to an amplified reflection of solar radiation by clouds, thus causing additional radiative cooling.

The secondary aspect of this indirect effect can be attributed to the decreased water droplet's size. This reduction contributes to the elongation of cloud lifespans, subsequently prolonging their reflective capabilities and, consequently, intensifying the cooling effect.

2.3 Influence of BVOCs on atmospheric chemistry and air quality

Biogenic volatile organic compounds play an instrumental role in shaping atmospheric chemistry and air quality. These compounds are significant contributors to the production of various atmospheric pollutants, particularly ground-level ozone (O_3) and secondary organic aerosols (SOAs). This impact arises from the multiple oxidation reactions undergone by highly reactive BVOCs like isoprene leading to the formation of peroxy radicals. In highly polluted areas, these peroxy radicals can induce the production of ground-level ozone O_3 and other oxidants.

³The 1991 eruption of Mount Pinatubo is one of the most powerful volcanic eruptions of the 20th century. It was a catastrophic event that had profound global effects. The eruption took place from June 15 to June 16, 1991.

Similarly, BVOCs oxidation by nitrate radical (NO_3), ozone (O_3) and hydroxyl radicals (OH) can lead to the formation of intermediate compounds that act as a condensation support for aerosols formation.

BVOCs can also influence atmospheric chemistry by long distance transport of atmospheric pollutant precursors. For instance, the oxidation of BVOCs in a polluted area (with high NO_x concentration) may induce the formation of organic nitrates mainly peroxyacetylnitric anhydrides (MPANs) and peroxyacetylnitrates (PANs) from BVOCs oxidation products. These two products act as a NO_x reservoir species and can be advected in a wider scale as their atmospheric lifetimes goes beyond months. Under favorable conditions, MPANs and PANs liberate the transported NO_x , leading to increased NO_x levels in unpolluted regions. As a result, the atmospheric chemical composition can be significantly changed leading to an alteration in the local air quality of distant regions.

The impact of BVOCs on atmospheric chemistry is not limited to their direct chemical reactions. They can also influence the concentrations and reactivity of other atmospheric species. For instance, BVOCs can scavenge and neutralize reactive radicals, such as hydroxyl radicals (OH), thereby affecting the overall oxidative capacity of the atmosphere.

Additionally, BVOCs are cable of influencing atmospheric chemistry on a global scale by influencing the atmospheric concentration of carbon monoxide (CO). In fact, when BVOCs are oxidized in the atmosphere, they can produce CO as a byproduct. Due to its relatively long lifetime reaching several months, carbon monoxide can be advected in a larger scale. The transported CO might be oxidized by OH leading to the formation of tropospheric ozone.

2.4 Conclusion of Chapter 2

Air quality holds a particular place in atmospheric science research, monitoring and controlling the levels of air pollutants is of paramount importance in preventing their impacts on human health and the surrounding environment.

Although our understanding of the dynamics governing air quality is extensive, some areas of atmospheric chemistry are still uncharted territory. As we already know, air quality will undergo significant changes in the future in response to climate change. This raises important questions: How will air quality adapt in the face of climate change, future anthropogenic emissions, and shifts in natural emissions induced by climate change? To address these questions, we will first examine, in the next chapter, how our climate is predicted to evolve in response to global warming.

Climate change

Since the pre-industrial era, climate change has had a significant impact on various aspects of human life and its surrounding environment. Since then, many efforts have been deployed to study the origins of climate change, predict its future evolution and develop various mitigation and adaptation strategies. For this purpose, in 1988, **the International Panel on Climate Change** (IPCC) was created by the World Meteorological Organization (WMO) in cooperation with the United Nations Environment Program (UNEP). The purpose of this organization, is to produce comprehensive assessments on the state of knowledge of climate change. Its area of activity focuses on 3 main topics: the assessment of human induced climate change, the assessment of climate change future impact and the last activity focuses on providing potential mitigation and adaptation strategies.

In the present Chapter we will provide a general representation of the current and future states of climate with a specific focus on the impact of climate change on the magnitude and frequency of all important elements of the climate system. The main objective of this chapter is to provide an overview of how climate change can impact air quality and the feedback loop in which biogenic emissions and the atmosphere influence each other. At the end of this chapter, the objectives of this thesis will be presented.

3.1 Current climate change: Evidence and impact

According the 5th assessment report (AR5) of the IPCC, climate change is defined as "a change in the state of the climate that can be identified (e.g., by using statistical tests) by changes in the mean and/or the variability of its properties and that persists for an extended period, typically decades or longer. Climate change may be due to natural internal processes or external forcings such as modulations of the solar cycles, volcanic eruptions and persistent anthropogenic changes in the composition of the atmosphere or in land use. Note that the Framework Convention on Climate Change (UNFCCC), in its Article 1, defines climate change as: 'a change of

climate which is attributed directly or indirectly to human activity that alters the composition of the global atmosphere and which is in addition to natural climate variability observed over comparable time periods'. The UNFCCC thus makes a distinction between climate change attributable to human activities altering the atmospheric composition and climate variability attributable to natural causes.”

The latest IPCC assessment report (AR6) was published in March 2023. This report uncovered a fundamental finding about the contribution of human activities to the climate change observed today. In fact, AR6 revealed that global warming was **unequivocally** caused by the emission of greenhouse gases (GHGs) from **human activities**, resulting in a $+1.1^{\circ}\text{C}$ increase in global surface temperature in 2011-2020 compared to pre-industrial temperature levels 1850-1900 (Arias et al., 2021). Human-induced global warming was caused mainly by the combustion of fossil fuels and industrial processes, land use changes, lifestyle choices, and patterns of consumption and production. Collectively, these factors have led to a notable increase in global surface temperature within a range of 0.8 to 2°C . In contrast, natural sources such as solar radiation and volcanic activity have played a relatively minor role in global surface temperature changes, contributing only around $\pm 0.1^{\circ}\text{C}$.

The consequences of this human-caused global warming are evident in the alarming rise in the atmospheric concentrations of three key greenhouse gases: carbon dioxide (CO_2), methane (CH_4), and nitrous oxide (N_2O). As shown in Figure 3.1, over the past century, the atmospheric concentrations of these gases have risen by substantial percentages. Carbon dioxide levels, primarily emitted through the burning of fossil fuels and deforestation, have increased by 47%. Methane, emitted from sources such as livestock, agriculture, and fossil fuel extraction, has experienced a staggering 156% increase. Nitrous oxide, stemming from industrial and agricultural activities, has risen by 23%. These escalating concentrations of GHGs significantly contribute to the greenhouse effect, trapping heat within the Earth’s atmosphere and intensifying the process of global warming.

The ongoing observable shifts in the climate have impacted several critical components of the Earth, including the biosphere, oceans, cryosphere, and atmosphere. This phenomenon has led to a notable increase in the frequency and intensity of extreme weather events. According to the findings of the AR6 report, these amplified occurrences of heatwaves, intense precipitation, and prolonged droughts can be attributed to the influence of human-induced climate change activities. These anthropogenic factors have not only spurred the increase in extreme heatwaves and heavy rainfall events but have also contributed to the heightened occurrence of tropical cyclones. It is thus becoming increasingly clear that human actions are having a major influence on the intensification of extreme weather events.

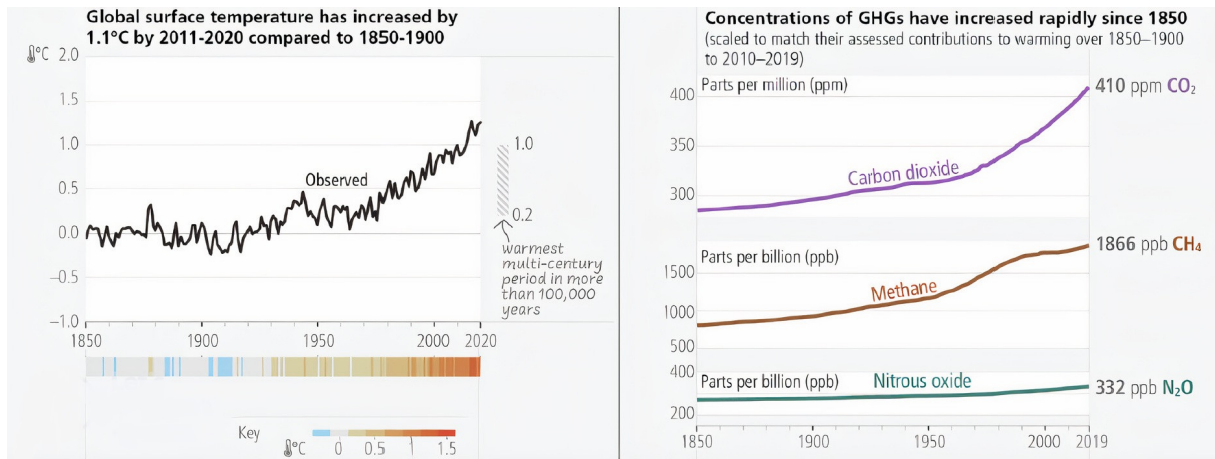


Figure 3.1: Global surface temperature and GHGs concentration evolution during the period 1850-2020 (adapted from Arias et al. (2021)).

3.2 Future climate: Description and impact

To simulate future weather patterns, IPCC employs a comprehensive hierarchy of climate models, with the goal of analyzing potential changes in the climate system. This hierarchy includes various types of models, starting from simple climate models and progressing to models of intermediate complexity, comprehensive climate models, and Earth System Models. Each model type offers different levels of detail and sophistication in representing the complex interactions within the Earth’s climate system.

In order to determine the impact of climate change in the future, an essential aspect is estimating the concentration of greenhouse gases and other pollutants in the atmosphere. These emissions can arise from both natural processes, such as volcanic activity and biogenic sources, and human activities, commonly referred to as anthropogenic sources. Accurate estimations of these emissions and concentrations are crucial for projecting future climate scenarios and assessing the potential impacts of climate change on various aspects of the Earth’s systems, including weather patterns, ecosystems, and human societies. By combining the insights from the hierarchy of climate models with estimations of greenhouse gas and pollutant concentrations, the IPCC can generate projections and scenarios that aid policymakers, scientists, and communities in understanding and preparing for potential changes in future weather patterns and the broader climate system.

Under the framework of the Coupled Model Intercomparison Project Phase 5 (CMIP5) of the World Climate Research Program, several pathways of pollutant emission called **RCPs** (Representative concentration pathways) were developed. These scenarios describe different possible futures of greenhouse gas emissions and concentrations, aerosol emissions, and land use changes. By covering a range of possibilities, these pathways aimed to capture the diverse outcomes that could arise from various socioeconomic and technological factors. In the fifth Assessment Report

(AR5) of the IPCC, four RCPs were specifically chosen for analysis: RCP2.6, RCP4.5, RCP6, and RCP8.5. The numeric value in each acronym indicates the radiative forcing level (watts per square meter), expected to be reached by the year 2100 under the given scenario. These RCPs provided a basis for evaluating the potential climate impacts and risks associated with different greenhouse gas emission trajectories. However, the deployment of these scenarios encountered a limitation in understanding and considering the socioeconomic factors causing GHGs future changes, as RCPs focus primarily on the physical aspects of climate change (greenhouse gas concentrations and radiative forcing) neglecting completely the underlying external factors driving these changes. The complexity of human behavior, economic development, and policy choices were critical elements that needed to be considered when assessing future greenhouse gas emissions and their consequences. Consequently, the IPCC recognized the need to incorporate a more comprehensive understanding of the interplay between socioeconomic factors and greenhouse gas emissions, this led the development of a new set of scenarios called **Shared Socioeconomic Pathways (SSPs)**. These scenarios were introduced to better understand the underlying drivers of greenhouse gas emissions and to explore the potential consequences of different mitigation and adaptation strategies.

3.2.1 Shared Socioeconomic Pathways

The impacts and risks related to climate change in the future are now assessed based on SSPs. These pathways aim to explore adaptation and mitigation strategies that can be used in the scope of climate change. SSPs scenarios are narratives, translated into sets of assumptions describing alternative evolution of future society based on changes in economy, technology, demographics, policies and institutions and environment and natural resources. Five narratives have been constructed by the IPCC, spanning a wide range of possible evolution of anthropogenic drivers of climate change:

- **SSP1 (Sustainability):**

This pathway envisions a world with low challenges to mitigation and adaptation. It is characterized by rapid economic growth, reduced inequality, and a focus on sustainable development. Technological advancements and global cooperation lead to a more sustainable and equitable world.

- **SSP2 (Middle of the road):**

This pathway represents a world with medium challenges to mitigation and adaptation. It is characterized by a continuation of historical trends, with moderate economic growth, slow technological advancements, and uneven progress in addressing environmental and social issues.

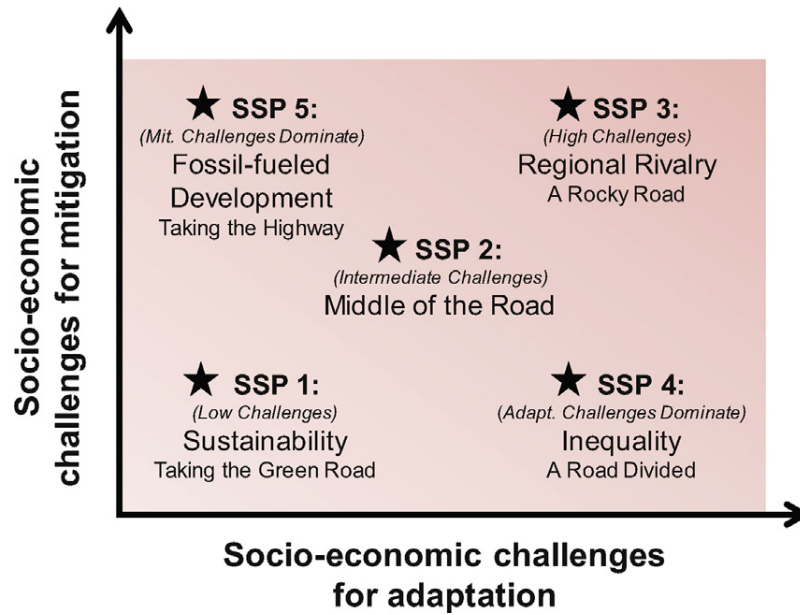


Figure 3.2: Description of the five SSPs each described by a specific level of socio-economic challenges for adaptation and mitigation (adapted from O'Neill et al. (2017)).

- **SSP3 (Regional rivalry):**

This pathway envisions a world with high challenges to mitigation and adaptation. It is characterized by a fragmented world with regional power blocs, slow economic growth, and limited cooperation on global issues. Environmental and social challenges are addressed primarily at the regional level, leading to uneven progress and increased inequality.

- **SSP4 (Inequality):**

This pathway represents a world with low challenges to mitigation but high challenges to adaptation. It is characterized by a highly unequal world, with a small, wealthy global elite and a large, impoverished majority. Technological advancements primarily benefit the elite, leading to limited progress in addressing environmental and social issues for the majority.

- **SSP5 (Fossil-fueled development):**

This pathway envisions a world with high challenges to mitigation and low challenges to adaptation. It is characterized by rapid economic growth driven by fossil fuel use, with a focus on individual well-being and material consumption. Technological advancements lead to increased resilience to climate change impacts, but efforts to reduce greenhouse gas emissions are limited.

Figure 3.2 represents socio-economic challenges for mitigation and adaptation for different SSPs.

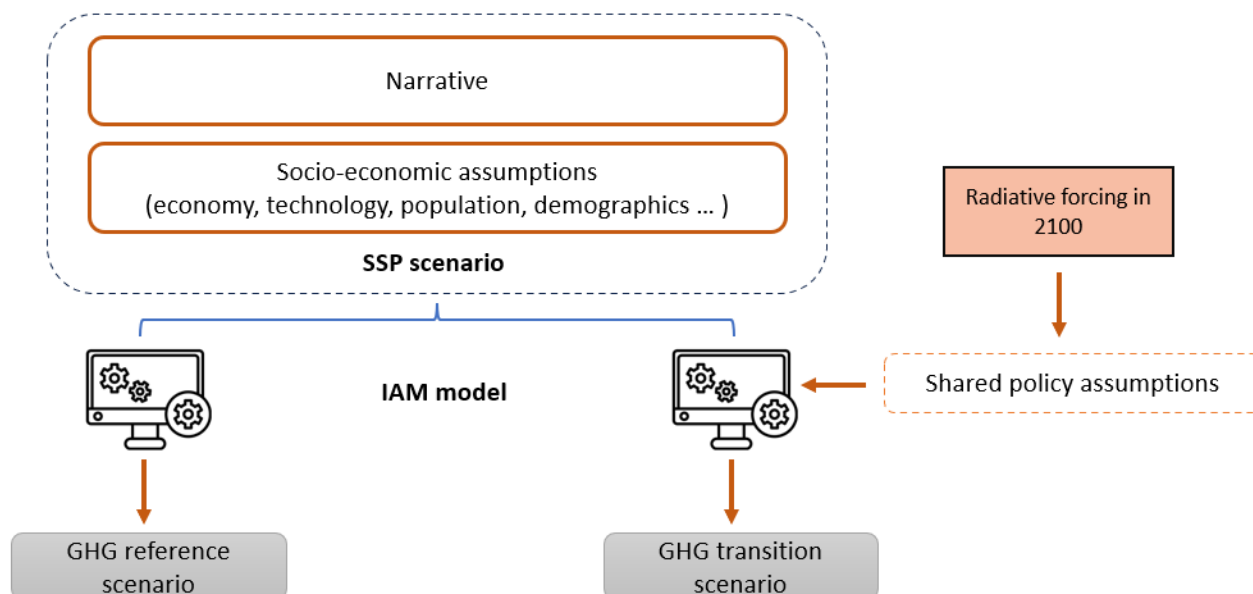


Figure 3.3: GHG reference and transition scenarios generation scheme for a given SSP scenario.

To build the SSP scenarios, scientists use the so-called IAM models (Integrated Assessment Models). These economic models receive as input the socio-economic assumptions underlying each SSP, and translate these socio-economic conditions into estimates of characteristics of future energy consumption and greenhouse gas emissions. These models are therefore economic rather than physical. IAMs produce two types of GHG emission scenarios: **reference scenarios** and **transition scenarios**. Reference scenarios are obtained by applying the socio-economic conditions of a SSP to an IAM model, without adding to the simulations any climate change mitigation policies additional to those already undertaken. These simulations do not incorporate either any feedback loops from the climate to the economy (e.g. the deterioration in Gross Domestic Product (GDP) due to the increased intensity and frequency of extreme events). Transition scenarios are obtained by adding another condition to the IAMs: the targeted radiative forcing in 2100. We then use SPAs (Shared Policy Assumptions), a set of assumptions to model policy measures and the speed of international collaboration on mitigation. Consequently, reference scenarios are used as counterfactual to assess the impact of a climate policy, by comparing emissions with a transition scenario, for a given SSP scenario. The different steps for generating a GHG emission scenario are schematized in Figure 3.3.

Finally, researchers use climate models, i.e. numerical representations of the planet and the interactions between its various climate-modulating reservoirs (atmosphere, oceans and continental surfaces), to convert greenhouse gas emissions (output from IAM models) into atmospheric greenhouse gas concentrations, and hence into future warming and associated climate parameters: **climate projections**. Many institutions produce global climate models. These models are therefore forced with greenhouse gas emission scenarios. The Coupled Model In-

SSP x - y scenario	Closest RCP scenario
SSP1-1.9	Not available. No equivalently low RCP scenario exists.
SSP1-2.6	RCP2.6, although RCP2.6 might be cooler for the same model settings.
SSP2-4.5	RCP4.5 and, until 2050, also RCP6.0. Forcing in the latter was even lower than RCP4.5 in the early decades of the 21st century.
SSP3-7.0	Between RCP6.0 and RCP8.5, although SSP3-7.0 non- CO_2 emissions and aerosols are higher than in any of the RCPs.
SSP5-8.5	RCP8.5, although CO_2 emissions under SSP5-8.5 are higher towards the end of the century. CH_4 emissions under SSP5-8.5 are lower than under RCP 8.5. When used with the same model settings, SSP5-8.5 may result in slightly higher temperatures than RCP8.5.

Table 3.1: Description of the correspondence between SSPs and RCPs (adapted from Arias et al. (2021)).

tercomparison Project coordinates the consolidation work and harmonizes the results between these different climate models (more than twenty). It is these climate projections that are assessed in the IPCC's 6th Assessment Report.

In the sixth Assessment Report of IPCC (AR6), 5 sub-scenarios derived from the 5 principal scenarios (SSP1, SSP2, SSP3, SSP4 and SSP5) were selected to assess the different risks related to climate change in the future, two scenarios with high and very high GHG emissions: **SSP5-8.5** and **SSP3-7.0**, one scenario with intermediate GHG emissions: **SSP2-4.5** and two scenarios with very low and low GHG emissions: **SSP1-1.9** and **SSP1-2.6** (SSP x - y , x denotes the number referring to the scenario used, y indicates the estimated radiative forcing reached by the end of the 21 century). These scenarios were selected so as to provide a degree of agreement with the scenarios used previously (RCPs). Table 3.1 shows the approximate correspondence between SSP and RCP scenarios. This mapping is important for our study, as many previous research studies on future air quality assessment have been carried out using RCP scenarios.

As shown in Figure 3.4, CO_2 emissions in the SSP5-8.5 scenario increase almost linearly until 2080, by 2050 CO_2 emissions double with regards to current levels. The high-GHG emissions scenario SSP3-7.0 is likewise distinguished by rising CO_2 emissions, with emissions almost doubling by 2100 from current levels. The low GHGs emission pathways: SSP1-2.6 and SSP1-1.9 show declining emissions of CO_2 , reaching zero around 2070 and 2050 respectively.

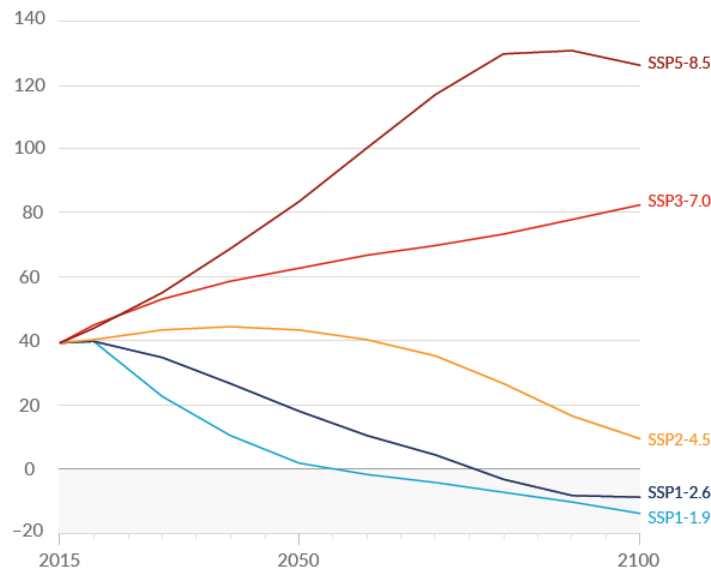


Figure 3.4: Future annual emissions of CO_2 in $GtCO_2/yr$ (adapted from Arias et al. (2021)).

According to the results of the application of climate models under the SSP scenarios shown in the AR6, ongoing GHG emissions would cause changes in the magnitude and frequency of all important elements and natural cycles of the climate system, particularly:

- **Temperature:**

As shown in Figure 3.5, in nearly all considered projected pathways, global temperature will rise further in the short term (2021-2040). Under the SSP5-8.5, (SSP2-4.5, SSP3-7.0) and (SSP1-2.6, SSP1-1.9), global temperature change is very likely, likely and more likely, than not, respectively, to exceed the $1.5^\circ C$ global warming level relative to 1850-1900.

In the long term (2081-2100), in the very high GHG emissions scenario (SSP5-8.5), temperature will reach $4.4^\circ C$, in the intermediate GHG emissions scenario (SS2-4.5) global warming will reach $2.7^\circ C$ and for low GHG emissions scenario (SSP1-1.9) temperature will reach $1.4^\circ C$.

Based on extended climate scenarios beyond 2100, predictions reveal a global warming of $1.0^\circ C - 2.2^\circ C$ and $6.6^\circ C - 14.1^\circ C$ in 2300 relative to 1850-1900 for SSP1-2.6 and SSP5-8.5 respectively.

- **Ocean warming:**

The global ocean will continue to warm through the 21st century. The CMIP6 models show a global ocean temperature increase by $0.6^\circ C$ and $3.4^\circ C$ following SSP1-1.9 and SSP5-8.5, respectively in 2081-2100 compared to 1995-2014.

- **Precipitation:**

Under all considered scenarios, global land precipitation will increase on long term (2081-

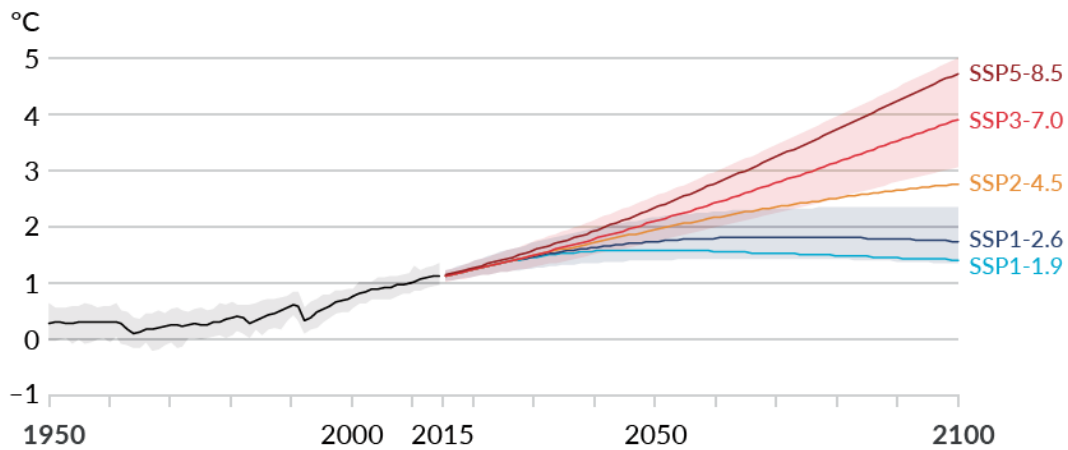


Figure 3.5: Global surface temperature change relative to 1850-1900 (adapted from Arias et al. (2021)).

2100) compared to 1995-2014. In low (SSP1-1.9) and high (SSP5-8.5) GHG emissions scenarios, land precipitation will change by 2.4% and 8.3% respectively. These changes are in line with the precipitation results assessed with the RCP projections in the AR5. As global surface air temperature rises in the 21st century, precipitation will alter significantly regionally and seasonally. Precipitations will increase over tropical oceans and high latitudes and decrease in subtropical regions.

- **Global mean sea level:**

Under all considered SSPs, the Global Mean Sea Level (GMSL) will continually increase until 2100. The SSP3-7.0 predicts a rise of 0.46-0.74m in GMSL on average for the period 2081-2100 compared with 1995-2014. The SSP1-2.6 scenario predicts a lower GMSL long-term change (0.3-0.54m).

- **Arctic sea ice area:**

As illustrated in Figure 3.6, under the medium emissions scenarios (SSP2-4.5) and high emissions scenarios (SSP5-8.5 and SSP3-7.0), **September** arctic will be ice-free by the end of this century (sea ice area less than 1 million km²). Similarly, **March** arctic sea ice area will decrease in the future but at much lower rate than in September.

- **Ocean carbon and ocean surface pH:**

Carbon absorption by land and oceans is set to increase through the 21st century. Under high-emission scenarios, the proportion of emissions captured by ocean and land sinks is likely to lower compared to low-emission pathways. Ocean acidification will increase though the 21st century (the ocean surface pH will decrease), except for SSP1-2.6 and SSP1-1.9, where ocean surface pH will decrease until around 2070.

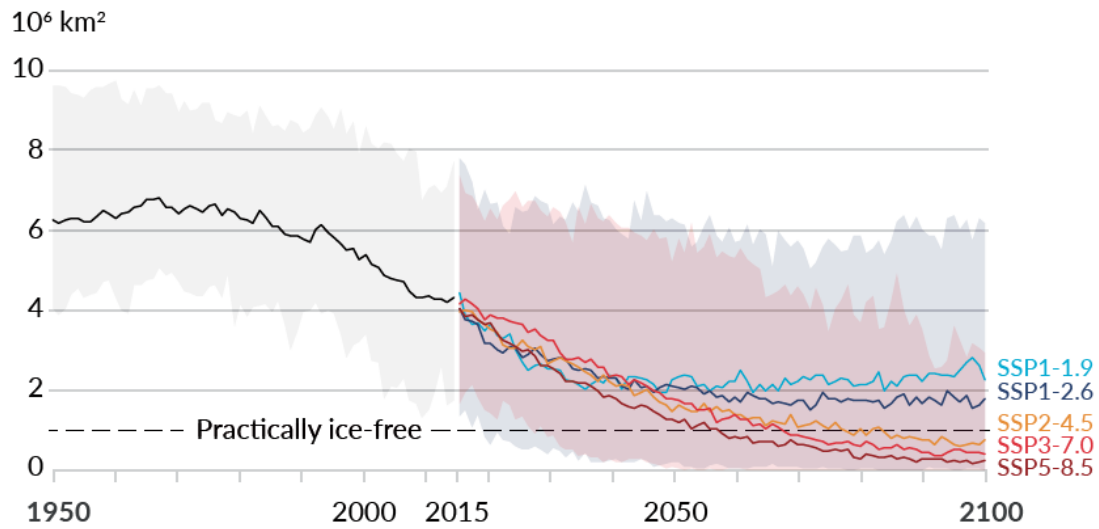


Figure 3.6: September Arctic sea ice area (adapted from Arias et al. (2021)).

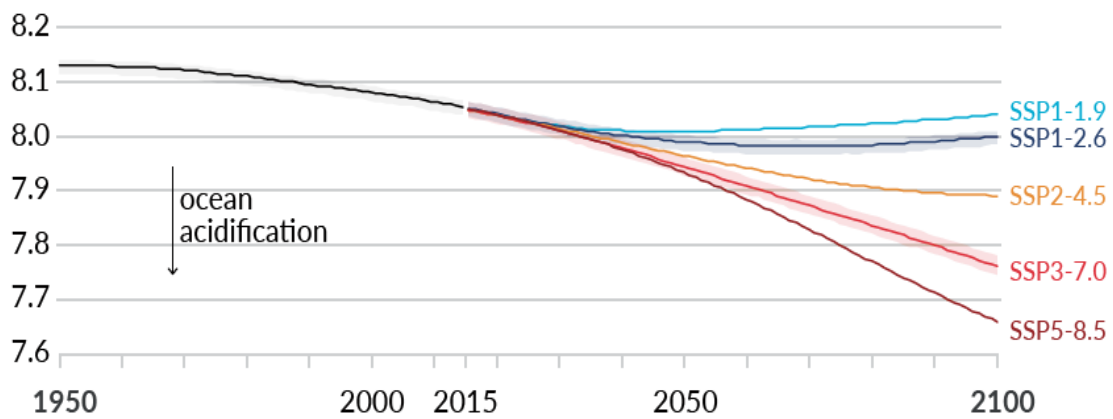


Figure 3.7: Global ocean surface pH (adapted from Arias et al. (2021)).

3.2.2 Future climate impacts and risks

Changes in temperature, precipitation, radiative energy and other climatological parameters patterns can alter many aspects of human and natural systems. The first aspect of climate change impacts in the future is the increasing occurrence of extreme events.

According to Arias et al. (2021), at a 2°C global warming level, extreme precipitation intensity and frequency will increase in most region of the globe, most importantly in Africa and Asia. The increasing occurrence in heavy precipitations will increase flooding events and the related human and natural risks. Similarly, aridity and drought events are likely to be more severe and frequent in multiple globe regions including America, Africa, Australia and Europe. Finally, heatwaves frequency and intensity will increase at a global scale.

Climate-related risks for every level of warming are expected to touch: economic growth, human

security, water supply, food security, livelihoods, health, biodiversity, etc. The risks related to the alteration of different aspects of human and natural systems will increase with every incremental rise in global warming. However, the impact of climate change does not only depend on global warming level but also in regional inequalities across the globe, for instance, in countries with limited income (e.g. sub-Saharan Africa), hundreds of millions of people will be affected by malnutrition and infectious diseases as a result of climate-induced alteration of food and freshwater availability. Additionally, the increasing climatic risks in those countries can induce a reduction in economic growth and thus increase inequalities and poverty rates.

3.3 Change at a $+2^{\circ}\text{C}$ global warming for SSP3-7.0

According to the IPCC's 6th assessment report, the global warming level of 2°C relative to 1850-1900 for SSP3-7.0 is expected to be reached by the period **2037-2056**. As shown in Figure 3.8, a warming of $+2^{\circ}\text{C}$ will affect the entire globe, with continental temperature change being significantly greater than ocean temperature change. The most severely affected areas are the northern hemisphere's high latitudes, where temperature trends are likely to exceed 6°C .

The land precipitation anomalies under a $+2^{\circ}\text{C}$ climate change level are estimated to $+2.4\%$ relative to 1995-2014. As shown in Figure 3.8, precipitations are expected to decrease in subtropical regions and increase particularly over northern and southern high latitudes.

As for soil moisture, the expected changes in a $+2^{\circ}\text{C}$ climate change level, follow the tendency of precipitation and evapotranspiration. The combined effect of these factors will lead to a notable decrease in South America, South Africa and Australia.

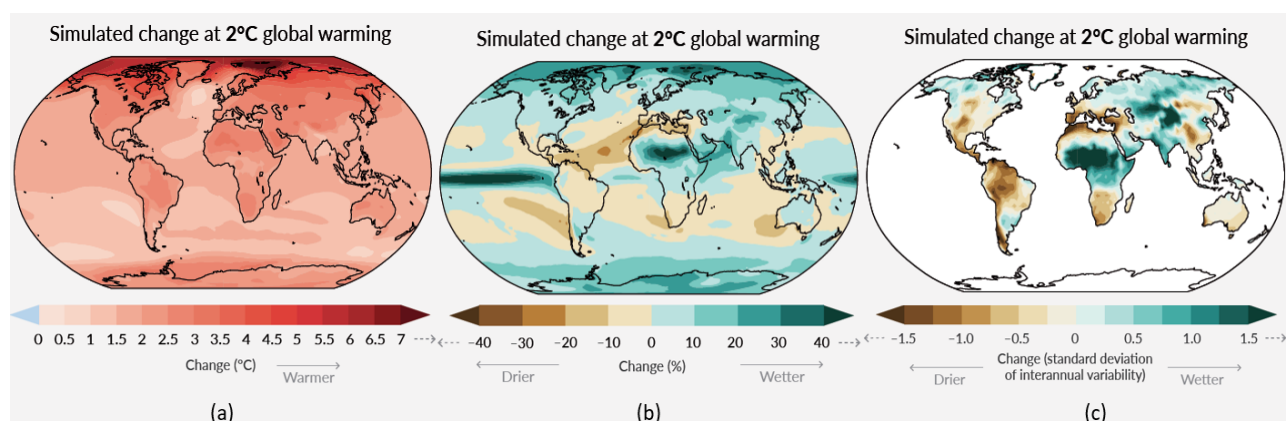


Figure 3.8: Simulated mean annual temperature change (in $^{\circ}\text{C}$) (a), precipitation absolute change (in %) (b), total column soil moisture change (as standard deviation) (c) relative to the period 1850-1900. Precipitation and soil moisture might have a false high change rate in dry regions (from Arias et al. (2021)).

3.4 Climate change and air quality

3.4.1 Pollution control in the SSP scenarios

As outlined in Table 3.2, in addition to the specified adaptation and mitigation assumptions associated with each emission scenario, additional assumptions concerning air pollution control related to O_3 and aerosols precursors are included for each SSP. These supplementary emission inventories for air pollution serve as integral components in studies focusing on the evaluation of air quality in the future. In this context, the IPCC presents a set of emissions of reactive gases and aerosol precursors (NH_3 , $NMVOCs$, NO_x , CH_4 , SO_x , CO) for each socio-economic pathway. These emissions include both human-made emissions and those stemming from biomass burning. Anthropogenic emissions are categorized into various sectors such as agriculture, residential sources, transportation, power generation, and industrial activities.

Emission scenario	Policy strength	Technological innovation	Key relevant characteristics of SSPs
SSP1-SSP5	Strong	Pollution control technology costs drop substantially with control performance increasing.	Sustainability driven; rapid development of human capital, economic growth and technological progress; prioritized health concerns.
SSP2	Medium	Continued modest technology advances.	Middle of the road scenario.
SSP3-SSP4	Weak	Lower levels of technological advance overall.	Fragmentation, inequalities.

Table 3.2: Qualitative framework for pollution control in the SSPs (adapted from Rao et al. (2017)).

The inventories of air pollutant precursors are determined for each SSP through the use of two primary sets of data: **activity data** and **emission factors** (Rao et al., 2017).

The determination of activity data involves determining quantitative information on the processes or activities resulting in pollutant emissions associated with each SSP. This covers a comprehensive range of parameters related to the level of activity (e.g., vehicle kilometers traveled, production levels, fuel and energy consumption) across various activities (e.g., industrial production, transportation via road, air, rail, and maritime routes, residential energy utilization, and agricultural practices). To illustrate, a specific SSP might project high levels of industrialization and urbanization, thereby leading to increased energy use and transportation needs.

The second pivotal parameter is the emission factor, which represents the quantity of a particular pollutant emitted per unit of a specific activity. These factors are instrumental in

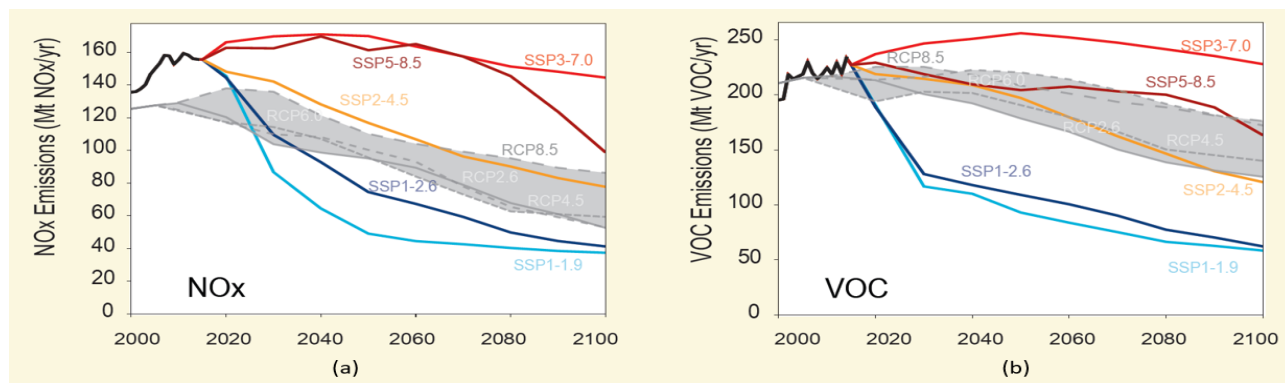


Figure 3.9: Representation of the atmospheric concentration of NO_x (a) and VOCs (b) over the period 2000-2100 for the different SSPs (from Arias et al. (2021)).

estimating emissions originating from diverse sources including energy combustion, industrial processes, transportation, and agriculture. The interplay between activity data and emission factors is subsequently employed within integrated assessment models (IAMs) to generate emissions across different scenarios and policy assumptions. Figure 3.9 illustrates the evolution of volatile organic compounds (VOCs) and nitrogen dioxides (NO_x) under distinct emission scenarios from 2000 to 2100. Under the SSP3-7.0 scenario, it is expected that the emissions of VOCs and NO_x will experience a substantial rise until 2050, followed by a decline extending toward the end of the 21st century.

3.4.2 The impact of climate change on air quality

Climate change can shape air quality trends in the future through many factors. First, climate change can have a direct impact on the atmospheric concentration of certain air pollutant precursors, mainly natural emissions. Additionally, meteorological variables like temperature and solar radiation can directly impact air quality by modifying the production rates of certain atmospheric pollutants. Indirectly, these meteorological shifts can also perturb the transport patterns of pollutants through changes in the frequency and intensity of atmospheric blocking episodes. Lastly, climate-driven chemical changes may further alter the atmospheric lifetime of pollutants, thereby affecting overall air quality dynamics. Numerous modeling assessments studies have examined future projected ozone and aerosols patterns, examining different assumptions to identify the driving forces behind the changing ozone and aerosols levels (meteorology, natural emissions, anthropogenic emissions, etc.).

In its latest report, the IPCC examined the impact of climate change on tropospheric ozone trends in isolation from changes in the ozone precursors emissions. This sensitivity study accounts for the changing frequency of meteorological conditions shaping air quality, including convection, high-pressure stagnation patterns, etc. As shown in Figure 3.10, in a +2°C warm-

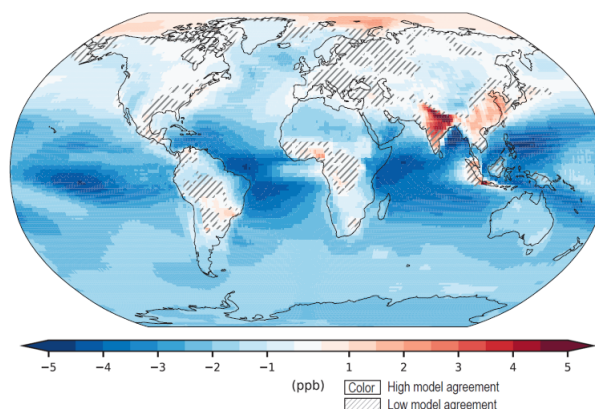


Figure 3.10: Annual mean change in surface ozone O_3 in ppb at a $+2^\circ C$ warming level. Ozone change is calculated as the difference between ozone with evolving future emissions and sea surface temperature under the SSP3-7.0 scenario and ozone with the same setup but with fixed present-day sea surface temperature (from Arias et al. (2021)).

ing level, global ground-level ozone decreased within a range of -1.7 ± 0.16 ppb , this decrease is particularly pronounced in unpolluted regions and over ocean tropical areas. According to the AR5, ozone decrease in unpolluted areas is primarily explained by enhanced ozone destruction processes driven by increased temperature levels and water vapor abundance resulting from climate change. Over polluted regions (e.g., South East Asia, India), climate change induced an increase of a few ppb in surface ozone levels. This effect is known as **ozone penalty due to climate change**. The same result applies to some regions of South America and South Africa, where increased ozone production is attributable to the substantial sources of biogenic emissions in these areas.

Future trends in air pollutant levels are controlled by the first-level impact of climate change on the net production rate of these pollutants, and the impact of anthropogenic emissions from the Shared Socioeconomic Pathways, particularly emissions of certain gases and aerosols precursors. In this context, the AR6 examined the combined effect of climate change and anthropogenic emissions on ozone and SOAs levels in the future. As illustrated in Figure 3.11, the results of this sensitivity study showed that the SSP3 scenario, which includes low climate change and air pollution mitigation strategies resulted in the most important increase in global $PM_{2.5}$ ¹ until 2050 and global surface ozone O_3 through 2100. High GHGs emission scenario SSP5 and low GHGs emission scenario SSP1, which assume effective global implementation of strict pollution control policies, resulted in the largest improvements in atmospheric pollutant concentrations (ozone and $PM_{2.5}$) in 2100. The middle of the road emission scenario SSP2 resulted in the lowest decrease in mid-century to reach the $PM_{2.5}$ reduction levels of SSP5 by 2100.

¹Particulate matter smaller than 2.5 microns in diameter.

The main finding of the air pollution sensitivity studies conducted by the IPCC in the AR6, is that the future trajectory of global and local air quality is predominantly driven by changes in emissions of air pollutant precursors rather than climate-related factors.

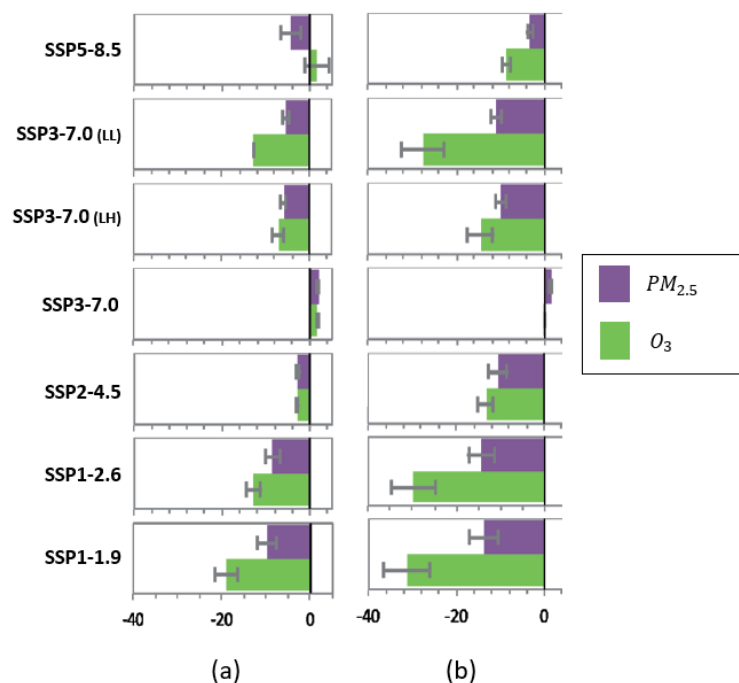


Figure 3.11: Percent change in global surface ozone O_3 and particulate matter $PM_{2.5}$ in 2040 (a) and in 2100 (b) relative to 2019. SSP-3.0 LL is SSP3-7.0 with low short-lived climate forcers (SLCFs) and CH_4 emissions, SSP-3.7.0 LH is SSP-3.7.0 with low SLF's emissions and high CH_4 emissions (from Arias et al. (2021)).

However, the analysis of future global and regional air quality in the AR6 report does not take into account the potential impact of climate change on BVOCs. It is anticipated that biogenic emissions will undergo substantial alterations due to the effects of global warming, as detailed in the following section. In this context, Lin et al. (2008) investigated the complex interaction between climate, biogenic emissions and air quality in the United States and China for the timeframes 2095-2099 and 1996-2000. The study's results indicated that the projected ozone levels in 2095-2099 were more strongly impacted by changes in biogenic emissions than by climatic factors. Specifically, the outcomes revealed that surface ozone concentrations increased by 1-15 *ppb* due to heightened isoprene emissions. In contrast, considering only the influence of climate change resulted in a mere 3 *ppb* increase in surface ozone concentrations. This underscores the high influence of biogenic emissions on surface ozone levels compared to climate-driven changes. Considering the prominent importance of biogenic emissions in determining future air quality trends, the following section explores how these emissions are expected to evolve in response to climate change, and the resulting feedback loop between emissions and climate.

3.5 The impact of a changing environment on BVOCs

The emission of BVOCs is profoundly influenced by a range of meteorological and environmental factors, such as light, temperature, soil moisture, atmospheric concentrations of air pollutants, land cover and land use, leaf area index (LAI²), etc. As a result, our focus in this section will be on examining how environmental changes in general and climate change in particular can affect biogenic emissions.

Land use change:

Land cover and land use (LCLU) change can result from natural sources such as CO_2 concentration changes, precipitation changes, temperature changes or from anthropogenic sources such as urbanization, afforestation, deforestation and agriculture expansion. Land-use surveys and studies estimate an overall increase in cultivated land of 455% over the last 3 centuries 1700-1990 and an increase in grazing land of more than a factor of six. These changes are altering the characteristics and distribution of vegetation species, and can have a significant effect on the emissions of biogenic emissions.

Fu and Liao (2014) conducted a study examining the impact of land cover changes on biogenic emissions in China. During the period from the late 1980s to the mid-2000s, China has experienced notable land use transformations, including a significant expansion of urban areas, which increased by a factor of four, leading to a 4% reduction in vegetation cover, particularly affecting cultivated land and grasslands. On the other hand, forested areas in south- and north-east China witnessed an increase of 10%-30% and 5%-15%, respectively. The combined influence of meteorological factors and land cover changes contributed to an overall 11.4% increase in biogenic volatile organic compounds emissions.

Various studies have also examined the potential influence of future land cover and land use changes on BVOCs. For instance, Hantson et al. (2017) investigated the evolution of isoprene and monoterpenes emissions in relation to climate change, CO_2 levels, and land use alterations. Their research highlighted a global shift in land use, characterized by increased croplands and pastures due to human activities, leading to reduced isoprene and monoterpenes emissions in tropical and mid-altitude regions, respectively. These results are in line with the findings of Chen et al. (2009), who predicted a decline in isoprene and monoterpenes emissions in the United States in 2045-2054 compared to 1990-1999, primarily due to a 52% expansion of croplands and a 31% expansion of pastures. The projected changes in emissions were found to be predominantly influenced by both meteorological factors and future land use changes.

Global warming:

²LAI is the ratio of the total leaf area of vegetation in a specific area to the ground area it covers, expressed in m^2/m^2 .

The escalating impact of climate change on global temperatures has significant repercussions on the emission of biogenic species. This effect is two-fold: direct, as the emission of biogenic species experiences an exponential rise with increasing temperatures, and indirect, as the lengthening of the growing season for plants is expected due to climate change. Accordingly, numerous efforts have been dedicated to assessing the impact of rising temperatures on the emission of biogenic species.

For instance, a study by Peñuelas and Llusà (2003) projected that BVOCs emissions could surge by 25-45% in response to a global warming of 2-3°C. On a regional scale, Bauwens et al. (2018) found that the combined effect of rising temperatures and decreasing solar radiation, resulting from climate change, led to a 1.1% annual increase in isoprene fluxes over Europe between 2070 and 2099 compared to the period from 1979 to 2014. This trend was particularly pronounced over European Russia and eastern Europe.

Similarly, a study investigating regional air quality in the United States examined the impact of climate change on four summers (2001, 2002, 2051, and 2052) and reported a considerable increase in isoprene and terpenes emissions in 2051/2052 by 20-92% and 20-56%, respectively (Zhang et al., 2008).

As for Subarctic regions, which are known as the most effected areas by global warming, are subject to important biogenic emissions changes due to increasing temperatures. Experiments conducted by Faubert et al. (2010) on subarctic tundra revealed that a temperature increase of 1.9–2.5°C resulted in a doubling of monoterpenes and sesquiterpenes emissions from the tundra. Another study measured an increase in emissions ranging from 56 to 83% in response to exposure of subarctic tundra to a temperature rise of 3 to 4°C (Tiiva et al., 2008).

Water stress and drought:

Precipitation as many other meteorological variables are predicted to change in the future as a result of increasing temperatures. Climate models indicate a global increase in precipitation under different climate change scenarios. However, the combined effect of changing precipitation and evapotranspiration patterns is expected to lead to a reduction in soil moisture levels, particularly in arid and semi-arid regions, notably in South America, South Africa, and the Middle East. This decline in soil moisture will directly impact the emission of biogenic species. Nevertheless, the impact of water stress can vary depending on the degree of damage or stress exerted on the plant. Extreme water stress can significantly reduce BVOC release, while moderate drought can enhance it.

Drought intensity is not the only factor that can influence the emission of biogenic compounds, drought duration plays also a significant role in shaping the emission of biogenic species. An important study conducted by Saunier et al. (2020) investigated the influence of climate change-induced drought on biogenic emissions and ozone concentration through two drought scenarios.

The first scenario involved a short drought lasting for one year with a 35% decrease in annual precipitation, while the second scenario was characterized by a long drought spanning three years with the same percentage reduction in annual precipitation. The results revealed that during the short drought scenario, isoprene emissions increased in June, July, and August. In contrast, under the long drought scenario, isoprene emissions decreased throughout the entire studied period.

CO_2 atmospheric concentration:

Atmospheric concentrations of CO_2 can exert various influences on the emission of BVOCs. Elevated CO_2 concentrations contribute to increased photosynthetic activity, which enhances the rate of assimilation, a phenomenon known as the carbon fertilization effect. As a result of this effect, vegetation productivity and plant growth are amplified, leading to a higher leaf area index.

However, the escalating biogenic emissions resulting from the CO_2 -induced increase in biomass are partially offset by the inhibitory effect of CO_2 . Researchers such as Possell and Hewitt (2011) and Wilkinson et al. (2009) have developed empirical parameterizations to model the direct impact of atmospheric CO_2 concentration changes on the emission of isoprene. These empirical models help to better understand and quantify the complex interactions between CO_2 concentrations and isoprene emissions.

$$\gamma_{CO_2} = I_{smax} \times (1 + (C_i/C_*)^h) \quad (3.1)$$

Equation 3.1 represents the CO_2 parameterization for isoprene emissions by Wilkinson et al. (2009), where $I_{smax} = 1.34$, $C_* = 585 \text{ ppm}$, $h = 1.46$ and C_i is the CO_2 leaf concentration under non water stress conditions (= 70% of the atmospheric CO_2 concentration). This empirical parameterization was derived from growth experiments with two types of aspen plants at various CO_2 concentrations.

$$\gamma_{CO_2} = m/(1 + b \times m \times C_{CO_2}) \quad (3.2)$$

Equation 3.2 represents the parametrization of Possell and Hewitt (2011), where, C_{CO_2} is the atmospheric concentration of carbon dioxide, m and b are model parameters having the values of 8.49 and 0.0024 ppm^{-1} respectively. This parametrization is achieved by a non-linear regression, using a laboratory and field combination of measurements derived from a selection of different research studies involving a variety of vegetation types.

In their study, Bauwens et al. (2018) investigated the inhibitory effect of CO_2 and its impact on future isoprene emission flux over Europe. The research revealed that, overall, there is a

global increase in isoprene emissions at a rate of 1.1% per year due to rising temperatures. However, it is essential to consider the inhibitory effect of CO_2 on isoprene emissions, which leads to a reduction in the emission trends to 0.76% per year. These results are in line with the findings of Pacifico et al. (2012), which predicted that the increase in isoprene emissions in 2100-2109 linked to global warming will be partially offset by the inhibition of isoprene emissions by CO_2 .

3.6 The impact of BVOCs on climate

The impact of biogenic emissions goes beyond their effects on atmospheric chemistry and the composition of the Earth's atmosphere. These emissions can indirectly influence climate by disturbing the Earth's radiative balance through greenhouse effect, aerosols cooling effect and cloud cover. This climate-vegetation feedback mechanism is shown in Figure 3.12.

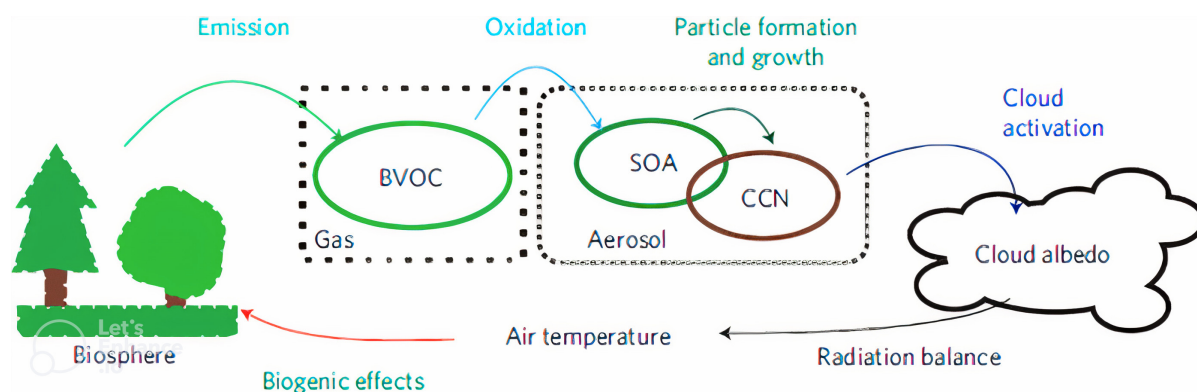


Figure 3.12: Schematic representation of the interaction between biogenic emissions, air chemistry and climate with the feedback mechanism between the three components (adapted from Paasonen et al. (2013)).

With changing environmental conditions, it is expected that biogenic emissions will increase in the near future. This increase in biogenic emissions will consequently lead to a rise in secondary organic aerosols concentrations, which can serve as cloud condensation nuclei. The augmented concentration of cloud condensation nuclei can, in return, influence the physical properties of clouds, particularly the optical thickness, leading to a significant increase in clouds albedo (Kurtén et al., 2003). As a result, the amplified concentrations of SOAs arising from BVOCs emissions directly impact the Earth's radiative balance, represented by a net **cooling effect**. Aerosols can also induce an indirect cooling effect by enhancing the assimilation of CO_2 by plants. This effect is due to the scattering of light by aerosols, providing an additional source of light for the canopy (Niyogi et al., 2004).

Similarly, the BVOCs-driven **warming effect** results from the increased concentration and lifetime of certain greenhouse gases, in particular the increased atmospheric lifetime of methane

CH_4 and the increased production rate of ozone O_3 .

According to Unger (2014a), the alterations in land cover between the 1850s and 2000s, driven by the expansion of global croplands, resulted in a global atmospheric cooling effect with a net global radiative impact of $-0.11 \pm 0.17 \text{ W/m}^{-2}$. These changes are primarily driven by the alteration of biogenic emissions triggered by the land cover change, which contributed to a disruption in the formation of various cooling and warming compounds, including aerosols, methane (CH_4), and ozone (O_3).

A broader study was undertaken to investigate the influence of BVOCs human-induced changes on global climate, including factors such as CO_2 inhibition, anthropogenic land cover change, climate change, etc. The results of this study revealed a significant decline in global biogenic flux estimation of approximately 22% from the 1850s (777 TgC/yr) to the 2000s (607 TgC/yr). This substantial reduction led to a net cooling effect on the global climate through changes of atmospheric chemistry. The estimated magnitude of this cooling effect is approximately -0.17 W/m^{-2} (Unger, 2014b). Figure 3.13 represents the contribution of each atmospheric pollutant to the difference in radiative forcing between the years 1850 and 2000, considering two scenarios: one taking into account the variability of both BVOCs and anthropogenic emissions, and the other considering only anthropogenic emissions.

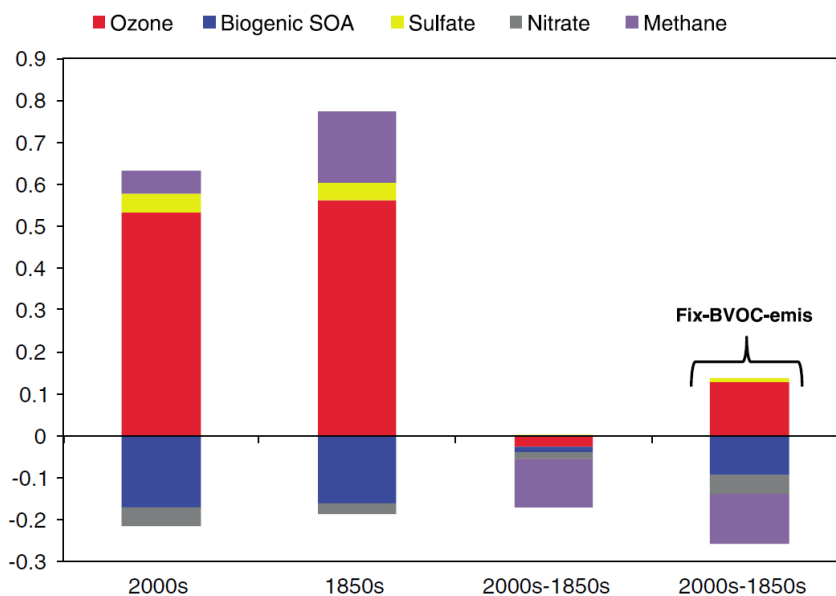


Figure 3.13: Radiative effect W/m^2 of BVOCs emission in the 1850s and the 2000s and the contribution of multiple warming and cooling climate pollutants. 2000s-1850s defines the global radiative forcing of BVOC emissions for this time period. Fix-BVOC-emis represents the radiative forcing considering the changes to anthropogenic emissions only (adapted from Unger (2014b))

3.7 Thesis objectives

Once volatile organic compounds are released into the atmosphere, they play a major role in altering its chemistry and composition, consequently impacting the global climate. BVOCs influence various atmospheric gases and aerosols chemistry. These alterations have far-reaching consequences on several key meteorological components, including incoming short-wave radiation, surface temperature, and precipitation, which in turn affect vegetation and biogenic emissions via global warming, land use and land cover change, increasing CO_2 concentrations and frequent drought events. These changes create a feedback loop where the atmosphere and biogenic emissions reciprocally influence each other. This feedback loop can either amplify or mitigate the response of vegetation to changing environmental conditions.

The complex interactions between biogenic emissions and the surrounding atmosphere underline the need for a comprehensive understanding of their role in shaping future air quality trends. In the present work, our objective is to investigate the impact of climate change on the emission of biogenic species under a $+2^\circ C$ climate change conditions. To achieve this, we have developed a coupled model named SURFEX-MEGAN specifically designed to simulate biogenic emissions. This model underwent rigorous testing and evaluation in Chapter 4. We aim to comprehensively understand the underlying processes driving isoprene change in the future, considering factors such as the influence of climate change itself, the inhibitory effect of CO_2 , and the fertilization effect of CO_2 in Chapter 5. Moving forward, in Chapter 6, we will analyze global and regional air quality under a $+2^\circ C$ climate change conditions, with a specific focus on ozone assessment. Our focus will be on understanding the specific contribution of biogenic emissions to the evolution of air quality. It is worth noting that our assessment will exclusively concentrate on ozone, as the aerosol scheme in the atmospheric-chemistry model used is not fully developed to account for biogenic emissions.

BVOCs modeling with SURFEX-MEGAN

The terrestrial BVOC model used in the present study is MEGANv2.1, which is one of the most used models within the biogenic emissions and atmospheric chemistry community to estimate the flux of biogenic organic compounds. It can be used in an offline mode but has also been coupled with other models. Several studies have been conducted implementing the MEGAN model within various canopy environment models or chemical-transport models, each model has a different version/implementation of the MEGAN algorithms and different weather and land cover driving variables. In the present work we have implemented the MEGANv2.1 in the surface model SURFEX. This coupled model will serve as a base to estimate the flux of biogenic emissions in the context of a +2°C climate change level. In this Chapter, we will first provide a detailed overview of the MEGAN and SURFEX models. These two models serve as the foundational components of our study. Subsequently, we will delve into the specific objectives, technical implementation details, and the assessment of present isoprene fluxes estimated with the coupled SURFEX-MEGAN model.

4.1 MEGAN

MEGAN (Model of Emission of Gases and Aerosols from Nature) is a modeling system used to estimate the flux of numerous biogenic species from vegetation to the atmosphere. The first version of MEGAN (MEGANv2.0) was developed by Guenther et al. (2006) and was designed for the estimation of net biosphere emission of isoprene into the atmosphere, later on, Sakulyanontvittaya et al. (2008) updated this version to include emissions of monoterpenes and sesquiterpenes. The last released version is MEGANv3, the latter is designed for local and regional simulations and incorporates advanced features and improved modeling techniques, however the most widely used version among the scientific community is MEGANv2.1 (Guenther et al., 2012). The latter is designed for global modeling and was tested with different model configuration, input data and was implemented in various canopy environment models

as well as chemistry transport models.

The MEGAN model includes algorithms that take into account the emission response to **light**, **temperature**, **LAI**, **soil moisture** and **CO₂ concentrations** variations. MEGAN uses these algorithms to estimate the flux of **147** biogenic species from terrestrial vegetation, these individual species can then be grouped under the appropriate class for a given chemical scheme. As schematized in Figure 4.1, MEGAN needs several input parameters to estimate the flux of biogenic species. First, MEGAN needs the **atmospheric meteorological state**: short-wave direct and diffused solar radiation, temperature, wind speed/direction, specific humidity; **Land cover data**: plant functional types (PFTs) distribution and LAI and lastly **atmospheric chemical composition**: CO₂ concentrations. As illustrated in Figure 4.2 MEGAN incorporates a canopy environment model that estimates the fraction, temperature and PPFD¹ of sun and shade leaves at different canopy levels. The incorporation of the canopy environment model in MEGAN stems from the high variation of temperature and light within a canopy. Considering that leaves temperature is equal to ambient air temperature can lead to an underestimation of biogenic fluxes by 5%. The resulting outputs from the canopy environment model are used by different algorithms which estimate the response of vegetation to driving variables: **leaf age algorithm**, **light and temperature algorithm**, **soil moisture algorithm** and **CO₂ algorithm**. These results, along with the emission potential data of different vegetation types, provide the basis for a final estimate of biogenic emission fluxes above canopy.

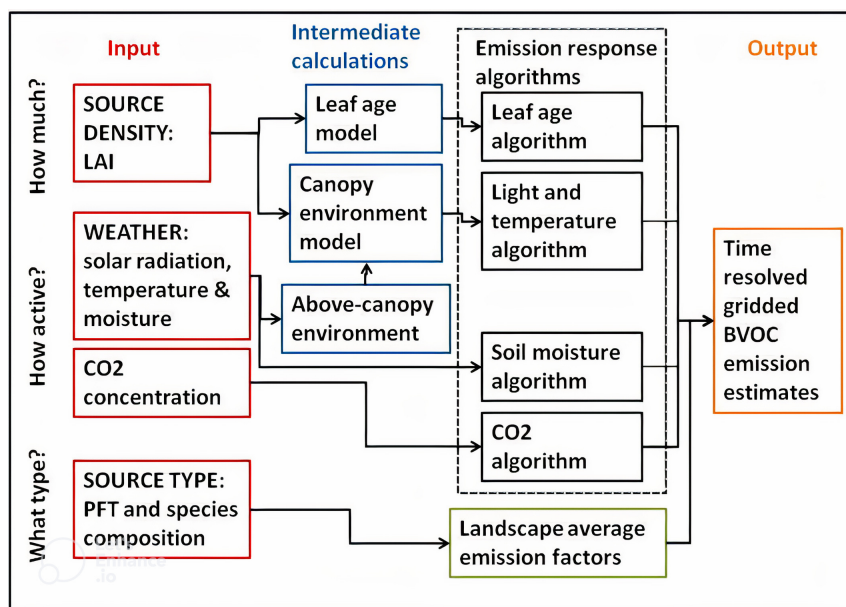


Figure 4.1: Schematic of MEGAN2.1 model components and driving variables. (adapted from Guenther et al. (2012))

¹Photosynthetic Photon Flux Density is the flux of photons that plants can use for photosynthesis, it is within the spectral range 400nm-700nm.

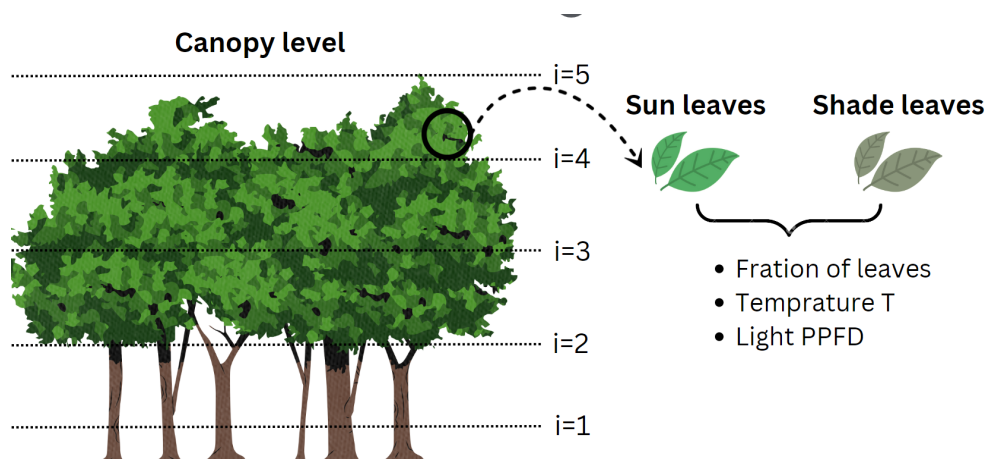


Figure 4.2: Representation of the canopy environment model used in MEGAN2.1.

4.1.1 Plant functional types

Plant cover is a key information required by MEGAN to estimate biogenic fluxes above the canopy. In the stand-alone version MEGANv2.1, plant functional types are extracted from the CLM4² PFT fraction database. The latter includes 16 vegetation types shown in Table 4.1, with cropland and tropical broadleaf trees having the highest spatial coverage.

CLM4 PFTs are believed to be generally valid for modeling biogenic emissions on a global scale, however, on a local and regional scale, the use of CLM4 PFTs may induce some uncertainties in the estimation of biogenic fluxes. This concern arises from the fact that some PFTs include both high BVOC emitters and low BVOC emitters, e.g., temperate deciduous tree class includes oaks with high isoprene emission rates and maples with low isoprene emission rates (Guenther et al., 2012).

A grid cell in MEGAN is represented by **16** vegetation types, the estimation of biogenic fluxes is done using as simple multiplication of the **activity factor** and the **emission factor** and summing over the 16 vegetation types following equation 4.1.

$$F_i = \gamma_i \times \sum_{j=1}^n (\varepsilon_{ij} \times \chi_j) \quad (4.1)$$

Where F_i is the above canopy flux of a compound class i in $\mu\text{g m}^{-2} \text{h}^{-1}$, γ_i is the dimensionless activity factor of a compound i (this factor is equal to 1 in standard conditions described below), ε_{ij} is the emission potential (also known as emission factor) of a compound i and vegetation type j at standard conditions and χ_j is the fractional grid box areal coverage.

²Community Land Model is a land surface model developed and maintained by the National Center for Atmospheric Research (NCAR).

Plant functional type	Surface coverage	Plant functional type	Surface coverage
Needleleaf Evergreen Temperate Tree	5.46	Broadleaf Evergreen Temperate Shrub	0.18
Needleleaf Evergreen Boreal Tree	10.6	Broadleaf Deciduous Temperate Shrub	4.15
Needleleaf Deciduous Boreal Tree	1.46	Broadleaf Deciduous Boreal Shrub	9.33
Broadleaf Evergreen Tropical Tree	15.6	Arctic C3 Grass	4.94
Broadleaf Evergreen Temperate Tree	2.64	Cool C3 Grass	14.3
Broadleaf Deciduous Tropical Tree	12.9	Warm C4 Grass	13.2
Broadleaf Deciduous Temperate Tree	5.33	Crop1	16.3
Broadleaf Deciduous Boreal Tree	2.14	Crop2	-

Table 4.1: Description of CLM4 plant functional types and the spatial coverage for each PFT (in $10^{12}km^2$) (adapted from Guenther et al. (2012)).

4.1.2 Emission factor

The emission factor, commonly referred to as the emission potential, represents the potential of a type of vegetation to release a given biogenic compound in standard conditions, defined as "LAI equal to $5 m^2 m^{-2}$ for a canopy consisting of 80% mature, 10% growing and 10% old leaves. Further standard canopy conditions include a solar angle equal to 60° , transmission of PPFD through the atmosphere (i.e. ratio between PPFD at the top of the canopy and at the top of the atmosphere) equal to 0.6, air temperature of $303 K$, air humidity equal to $14 g kg^{-1}$, wind speed equal to $3 m s^{-1}$ and soil moisture of $0.3 m^3 m^{-3}$ for current canopy environmental conditions; and for average canopy environmental conditions of the past 24 h leaf temperature of $297 K$, PPFD of 200 and $50 \mu mol m^{-2} s^{-1}$ for sunlit and shaded leaves respectively." in (Sindelarova et al., 2014).

In MEGAN, the estimation of the emission factor of a vegetation type can be achieved by two means, either by using the distribution of PFTs and the PFT-specific emission potential shown in Table 4.2, or by using a grid map of the emission potential data. This map has been developed on the basis of a land use map containing the detailed distribution of vegetation types and the PFT-specific emission potential, or flux measurements above the canopy if available. Figure 4.3 displays the gridded map of isoprene emission factor. As illustrated in this figure, regions with particularly high isoprene emissions are concentrated in the tropical band. In these regions, there are a number of plant functional types that are prolific isoprene emitters, particularly dense populations of tropical broadleaf trees. These are prominently found in the

Compound Class	EF ₁	EF ₂	EF ₃	EF ₄	EF ₅	EF ₆	EF ₇	EF ₈	EF ₉	EF ₁₀	EF ₁₁	EF ₁₂	EF ₁₃	EF ₁₄	EF ₁₅
Isoprene	600	3000	1	7000	10000	7000	10000	11000	2000	4000	4000	1600	800	200	1
Myrcene	70	70	60	80	30	80	30	30	30	50	30	0.3	0.3	0.3	0.3
Sabinene	70	70	40	80	50	80	50	50	50	70	50	0.7	0.7	0.7	0.7
Limonene	100	100	130	80	80	80	80	80	60	100	60	0.7	0.7	0.7	0.7
3-Carene	160	160	80	40	30	40	30	30	30	100	30	0.3	0.3	0.3	0.3
<i>t</i> - β -Ocimene	70	70	60	150	120	150	120	120	90	150	90	2	2	2	2
β -Pinene	300	300	200	120	130	120	130	130	100	150	100	1.5	1.5	1.5	1.5
α -Pinene	500	500	510	600	400	600	400	400	200	300	200	2	2	2	2
Other Monoterpenes	180	180	170	150	150	150	150	150	110	200	110	5	5	5	5
α -Farnesene	40	40	40	60	40	60	40	40	40	40	40	3	3	3	4
β -Caryophyllene	80	80	80	60	40	60	40	40	50	50	50	1	1	1	4
Other Sesquiterpenes	120	120	120	120	100	120	100	100	100	100	100	2	2	2	2
232-MBO	700	60	0.01	0.01	0.01	0.01	0.01	2	0.01	0.01	0.01	0.01	0.01	0.01	0.01
Methanol	900	900	900	500	900	500	900	900	900	900	900	500	500	500	900
Acetone	240	240	240	240	240	240	240	240	240	240	240	80	80	80	80
CO	600	600	600	600	600	600	600	600	600	600	600	600	600	600	600
Bidirectional VOC	500	500	500	500	500	500	500	500	500	500	500	80	80	80	80
Stress VOC	300	300	300	300	300	300	300	300	300	300	300	300	300	300	300
Other VOC	140	140	140	140	140	140	140	140	140	140	140	140	140	140	140

Table 4.2: MEGAN2.1 biogenic emission classes and emission factors ($\mu\text{g m}^{-2} \text{ h}^{-1}$) for each of the plant functional types (adapted from Guenther et al. (2012)).

Amazonian and Congo rainforests, as well as in the forests of Southeast Asia.

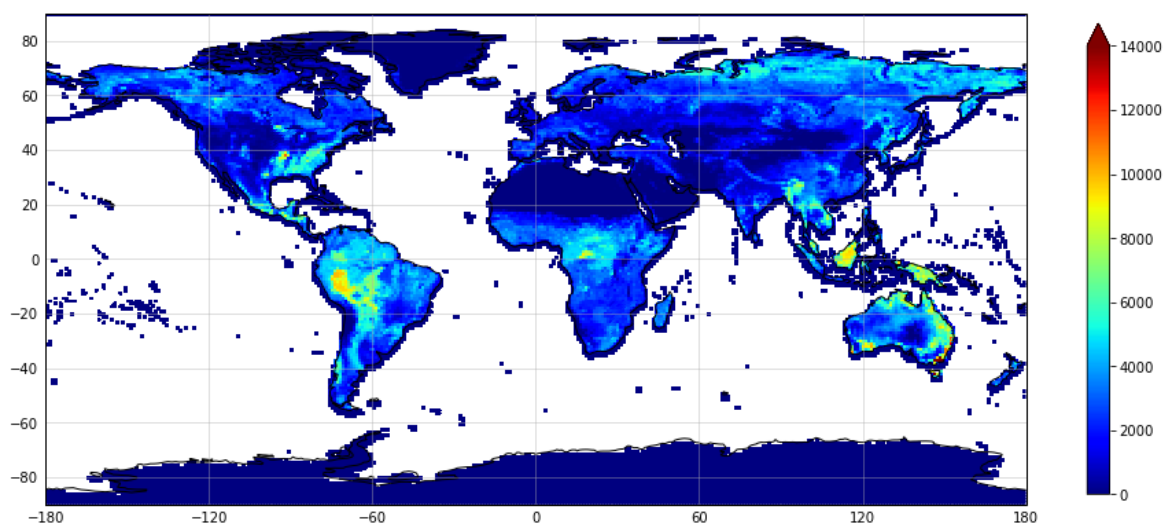


Figure 4.3: Isoprene emission factor map in $\mu\text{g m}^{-2} \text{ h}^{-1}$.

4.1.3 Activity factor

The activity factor describes the influence of key environmental conditions and meteorological factors on BVOCs emissions. This factor is unitless and varies across biogenic species.

The activity factor include many parametrizations accounting for the response of vegetation to a change in LAI, CO_2 concentrations, soil moisture, temperature, light and leaf age following equation 4.2.

$$\gamma_i = C_{CE} \times LAI \times \gamma_{PPFD,i} \times \gamma_{T,i} \times \gamma_{age,i} \times \gamma_{SM,i} \times \gamma_{CO_2} \quad (4.2)$$

Where γ_i is the activity factor of a compound i , C_{CE} is a canopy environment coefficient used to normalise γ_i (=0.57) at standard conditions listed above, $\gamma_{PPFD,i}$, $\gamma_{T,i}$, $\gamma_{age,i}$, $\gamma_{SM,i}$ and $\gamma_{CO_2,i}$ are factors accounting for the influence of light, temperature, leaf age, soil moisture and CO_2 concentrations respectively for a given compound i .

4.1.3.1 Light activity factor

The light activity factor γ_{PPFD} incorporates a light-independent fraction (LIF) and a light-dependent fraction (LDF) following equation 4.3.

$$\gamma_{PPFD} = LDF \times \gamma_{PPFD,LDF} + LIF \quad (4.3)$$

LDF represents the degree at which a compound emission is light-dependent ($0 < LDF < 1$), $LIF = 1 - LDF$. Isoprene for example has only the light-dependent response as its LDF is equal to 1. Accordingly, $\gamma_{PPFD,LDF}$ follows isoprene response to light estimated as:

$$\begin{aligned} \gamma_{PPFD,LDF} &= a \times ((b \times PPF D) / ((1 + b^2 \times PPF D^2))^{1/2}) \\ a &= 0.0468 \times \exp(0.0005 \times (PPFD_{24} - PPF D_*)) \times (PPFD_{240})^{0.6} \\ b &= 0.004 - 0.0005 \times \ln(PPFD_{240}) \end{aligned} \quad (4.4)$$

The isoprene light parametrization was originally developed by Guenther et al. (1999). $PPFD$ is the light received by leaves in $\mu mol m^{-2} s^{-1}$, $PPFD_*$ is equal to $50 \mu mol m^{-2} s^{-1}$ and $200 \mu mol m^{-2} s^{-1}$ for shade and sun leaves respectively. $PPFD_{24}$ and $PPFD_{240}$ is the average light received by leaves in the past 24h and 240h respectively.

Guenther et al. (2006) studied isoprene response to $PPFD$ using the light parametrization described above. As shown in Figure 4.4, isoprene emissions increase linearly with $PPFD$, similarly, the more light a plant received the preceding day, the more isoprene it will emit the following day.

4.1.3.2 Temperature activity factor

Temperature can influence biogenic emissions by a light-dependent fraction that follows isoprene response and a light-independent fraction that follows the monoterpenes response following:

$$\gamma_T = LDF \times \gamma_{T,LDF} + LIF \times \gamma_{T,LIF} \quad (4.5)$$

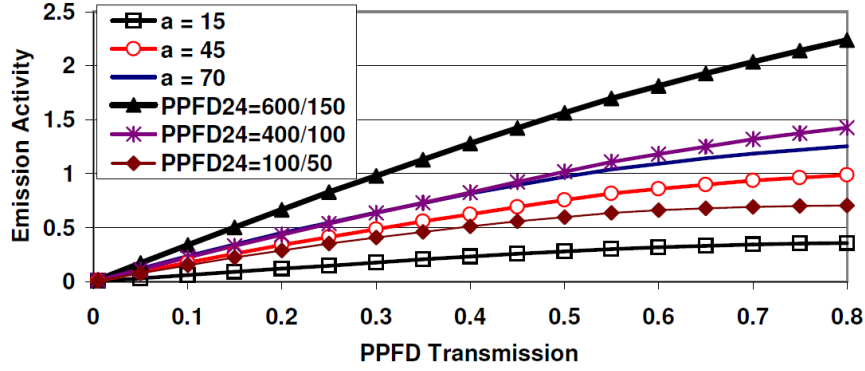


Figure 4.4: MEGAN estimates of isoprene emission response to PPFD transmission for leaves exposed to different solar angles (15, 45 and 70 degrees) and for average PPF24 levels for the past 24 to 240 h ($PPFD_{24} = PPFD_{240}$ in each case) that include 600 and 150 $\mu\text{mol m}^{-2} \text{s}^{-1}$ respectively, for sun leaves and shade leaves, 400 and 100 $\mu\text{mol m}^{-2} \text{s}^{-1}$ for sun and shade leaves, and 100 and 50 $\mu\text{mol m}^{-2} \text{s}^{-1}$ for sun and shade leaves, using MEGANv2.0 (adapted from Guenther et al. (2006)).

The light-dependent temperature activity factor is:

$$\begin{aligned}
 \gamma_{T,LDF} &= E_a \times ((C_2 \times \exp(C_1 \times x)) / (C_2 - C_1 \times (1 - \exp(C_2 \times x)))) \\
 E_a &= \alpha \times \exp(0.05 \times (T_{24} - T_*)) \times \exp(0.05 \times (T_{240} - T_*)) \\
 x &= ((1/T_a) - (1/T)) / 0.00831 \\
 T_a &= 313 + (0.6 \times (T_{240} - T_*))
 \end{aligned} \tag{4.6}$$

Where T_{24} and T_{240} represent the average leaf temperature in the past 24h and 240h respectively. T_* is leaf temperature at standard conditions (297K), T is leaf temperature, C_1 , C_2 and α are empirical parameters, C_1 and α depend on the biogenic compound and $C_2 = 230$ (Guenther et al., 2012).

The light-independent temperature activity factor is:

$$\gamma_{T,LIF} = \exp(\beta \times (T - T_*)) \tag{4.7}$$

As shown in Figure 4.5, isoprene emissions increase with temperature up to an optimum and then start to decrease gradually due to thermal stress. Plants exposed to higher temperatures in the previous day, tend to release higher isoprene emissions. The maximum emission also tend to occur at higher temperatures for scenarios with high T_{24} which is explained by the isoprene release mechanism triggered by plants being exposed to extremely high temperatures.

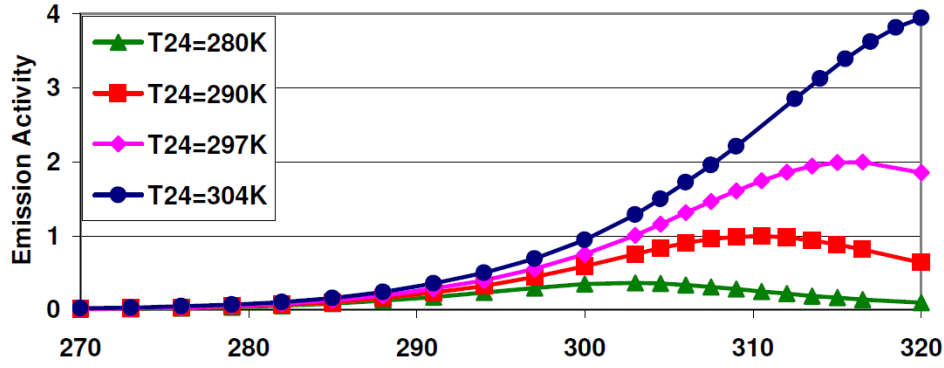


Figure 4.5: MEGAN estimates of isoprene emission response to temperature for leaves exposed to different average temperatures (280K, 290K, 297K and 305K) during the past 24 to 240 h ($T_{24} = T_{240}$ in each case) using MEGANv2.0 (adapted from Guenther et al. (2006)).

4.1.3.3 Soil moisture activity factor

MEGAN includes a soil moisture parametrization for isoprene only following Pegoraro et al. (2004) parametrization:

$$\begin{aligned} \gamma_{SM} &= 0 & \theta < \theta_w \\ \gamma_{SM} &= \frac{(\theta - \theta_w)}{\Delta\theta_1} & \theta_w < \theta < \theta_1 \\ \gamma_{SM} &= 1 & \theta > \theta_1 \end{aligned} \quad (4.8)$$

Where θ represents the soil water content in m^3/m^3 , θ_w is the wilting point³ in m^3/m^3 , $\Delta\theta_1$ is a parameter defined empirically = 0.04 in (Guenther et al., 2012) and = 0.06 in (Guenther et al., 2006) and $\theta_1 = \theta_w + \Delta\theta$.

Biogenic emission's sensitivity to soil moisture was investigated in several studies. Sindelarova et al. (2014) reported a global reduction of isoprene emissions by 50% after including soil moisture parametrization, this reduction is significant in arid and semi-arid regions (e.g. Australia, South-America and Africa). Henrot et al. (2017) and Guenther et al. (2006) reported a lower decrease rate of 15.2% and 7% respectively after introducing the soil moisture deficit algorithm.

4.1.3.4 Leaf age activity factor

The estimation of leaf age in MEGAN is done by dividing the plant cover into four categories depending on the state of growth of the foliage (new - growing - mature - senescing). Following this description, the leaf age activity factor is:

$$\gamma_{Age} = Fr_{new} \times E_{new} + Fr_{gro} \times E_{gro} + Fr_{mat} \times E_{mat} + Fr_{sen} \times E_{sen} \quad (4.9)$$

³The soil moisture threshold below which plants cannot extract water from the soil.

Fr_{new} , Fr_{gro} , Fr_{mat} and Fr_{sen} represent the fraction of new, growing, mature and senescing foliage respectively. These parameters are calculated based on current and previous month's leaf area index data.

E_{new} , E_{gro} , E_{mat} and E_{sen} are empirical parameters representing leaves emission potential at different growth stages. These coefficient are specified for each compound class. For isoprene, $E_{new} = 0.05$, $E_{gro} = 0.6$, $E_{mat} = 1$ and $E_{sen} = 0.9$, meaning that mature and senescing leaves have the highest isoprene emission rate.

4.1.3.5 CO_2 inhibition factor

CO_2 inhibition factor in MEGAN was designed specifically for isoprene following Heald et al. (2009) parametrization:

$$\gamma_{CO_2} = I_{max} - ((I_{max}(0.7 \times C_i))^h)/((C_*)^h + (0.7 \times C_i)^h) \quad (4.10)$$

C_i is the ambient air CO_2 concentration, $I_{max}=1.344$, $h=1.4614$ and $C_*=585$ are empirical parameters. γ_{CO_2} decreases with increasing ambient CO_2 concentrations and is equal to 1 for $C_i=400$ *ppmv*. The relevance of including this parameter is particularly important when attempting to model BVOCs in future climate, as CO_2 concentrations are expected to increase significantly in the future, thus, it is important to take into account the inhibition of isoprene emissions due to elevated CO_2 concentrations by integrating γ_{CO_2} factor.

Sindelarova et al. (2014) studied the model's sensitivity to integrating γ_{CO_2} inhibition factor on isoprene emissions for the year 2003. This sensitivity test resulted in an overall increase of isoprene emissions over the studied period by 2.7%. This increase can be explained by the low CO_2 concentrations in 2003 estimated to 373 *ppmv* (< 400 *ppmv*).

4.2 SURFEX

SURFEX is a surface modeling interface used to simulate surface-atmosphere exchanges. This platform was developed by Météo France in cooperation with the scientific community. The latest version of SURFEX (SURFEXv9.0) was released in late 2023. However, the present work was conducted using the version SURFEXv8.1 (Le Moigne, 2018).

SURFEX aims to model the interactions between the surface and the upper atmospheric layer by simulating sensible and surface heat fluxes, momentum fluxes, CO_2 fluxes, aerosol fluxes, etc. To achieve this, SURFEX requires detailed input data on the meteorological and radiative states of the atmospheric layer above the surface, e.g. pressure, wind speed and direction, temperature, specific humidity, convective and large-scale precipitation (rain and snow), long- and short-wave solar radiation (direct and diffuse components) and atmospheric CO_2 concentrations.

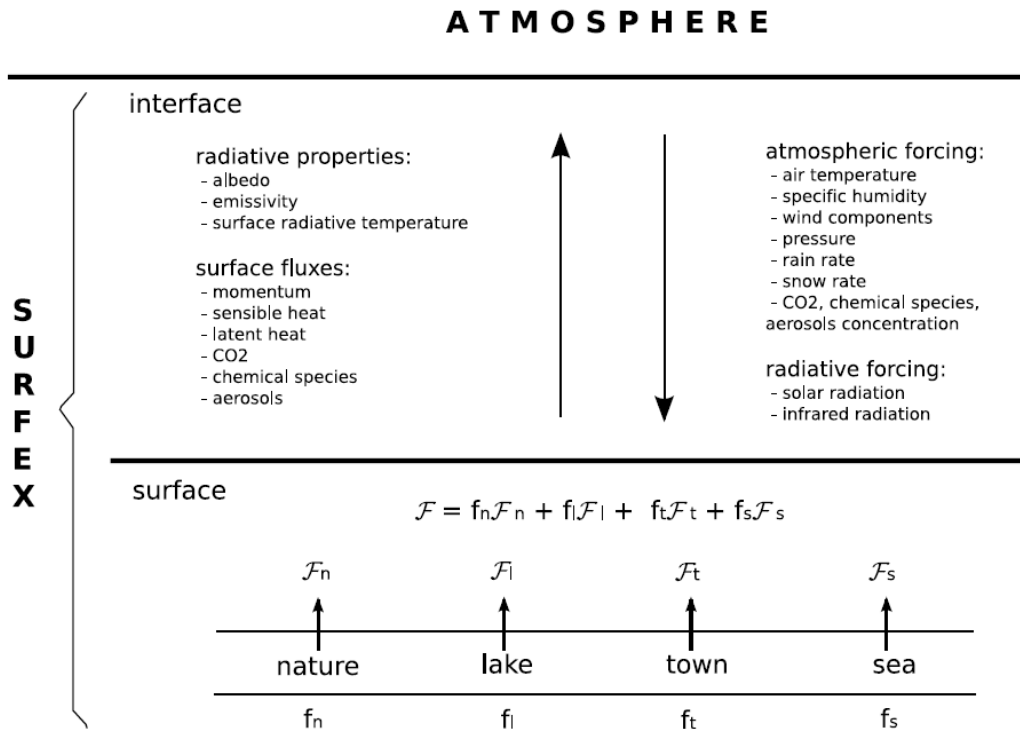


Figure 4.6: Description of the exchanges between an atmospheric model sending meteorological and radiative fields to the surface and Surfex composed of a set of physical models that compute tiled variables F_* covering a fraction f_* of a unitary grid box and an interface where the averaged variables F are sent back to the atmosphere (adapted from Le Moigne (2018)).

In SURFEX, a surface grid box is composed of four tiles representing: **nature**, **sea/ocean**, **town** and **lake**. Nature tile is composed of 16 living plant functional types and 3 non-living types (bare soil - snow - rocks). These land types are also known as patches. The land cover spatial distribution as well as the fraction of the four tiles and the 19 patches are provided by **ECOCLIMAP**. In SURFEX, the flux exchange between the surface and the upper atmospheric layer is estimated for the four different tiles using a specific scheme for each type of surface. The output flux represents the average flux for the four tiles as shown in Figure 4.6.

The surface processes governing the physics of each tile are represented by 4 physical schemes, **ISBA**⁴ for nature tile (Noilhan and Mahfouf, 1996), **TEB** for town tile (Masson, 2000), **SEA** for sea/ocean tile and **FLAKE** for lake tile (Mironov et al., 2010).

SURFEX requires various physiographic data to simulate flux exchanges between the surface and the atmosphere, such as land use, bathymetry⁵, soil texture, topography and lake depth. The databases used by SURFEX to extract the necessary data are described below.

⁴Interaction between Soil Biosphere and Atmosphere.

⁵The measurement of depth of water in oceans, seas, or lakes.

4.2.1 ECOCLIMAP

ECOCLIMAP is a surface cover database providing information about the global land cover map represented by covers⁶ at 1/120° spatial resolution and the corresponding land surface parameters at 1-km spatial resolution. ECOCLIMAP’s surface parameters are designed to initialize soil conditions.

ECOCLIMAP was developed by Météo France, there are currently 3 versions of ECOCLIMAP: ECOCLIMAP-I, ECOCLIMAP-II and ECOCLIMAP-SG⁷. ECOCLIMAP-SG is the latest version available at 300m spatial resolution. This version’s philosophy is different from the others. The most popular version among the scientific community is ECOCLIMAP-II (Faroux et al., 2013), as it has improved land use data over Europe.

Patch	Land type description	Patch	Land type description
1	No vegetation (smooth)	11	Tropical grassland (C4)
2	No vegetation (rocks)	12	Peat bogs, parks and gardens (irrigated grass)
3	Permanent snow and ice	13	Tropical broadleaf deciduous
4	Temperate broadleaf cold-deciduous summergreen	14	Temperate broadleaf evergreen
5	Boreal needleleaf evergreen	15	Temperate needleleaf evergreen
6	Tropical broadleaf evergreen	16	Boreal broadleaf cold-deciduous summergreen
7	C3 cultures types	17	Boreal needleleaf cold-deciduous summergreen
8	C4 cultures types	18	Boreal grass
9	Irrigated crops	19	Shrub
10	Grassland (C3)		

Table 4.3: Description of the SURFEX land types (Le Moigne, 2018).

SURFEX translates the covers from ECOCLIMAP as tiles (nature, sea/ocean, town and lake) and land types represented in Table 4.3. SURFEX extracts also from ECOCLIMAP the needed surface parameters for each tile and each land type. For the nature tile, each vegetation type is defined by various land cover data e.g. LAI, height of trees, soil and root depth, vegetation fraction, emissivity, near infrared, visible and UV albedo, minimum stomatal resistance. In ECOCLIMAP-I, LAI data are extracted from the satellite AVHRR⁸, whereas, in ECOCLIMAP-II, LAI data are derived from MODIS⁹ satellite, with a 10-day time step defi-

⁶A cover is defined as a homogeneous ecosystem.

⁷ECOCLIMAP -Second Generation.

⁸Advanced Very High Resolution Radiometer.

⁹MODerate resolution Imaging Spectroradiometer.

dition available for the period 2002-2006. Table 4.4 displays the important surface parameters extracted from ECOCLIMAP for nature and town tiles.

Tile	Surface parameters
Nature	<ul style="list-style-type: none"> - 3 Soil depths (root, soil, ice) - Height of trees (for vegetation) - Near infrared, visible and UV albedo - LAI - Vegetation fraction - Minimum stomatal resistance - Emissitivity - Dynamical vegetation roughness length - Water supply quantity - vegetation response type to water stress
Town	<ul style="list-style-type: none"> - Town roughness length - Albedo of roofs, roads and walls - Emissitivity of roofs, roads and walls - Heat capacity of roofs, roads and walls - Thermal conductivity of roofs, roads and walls - Building height - Building fraction - Building shape - Canyons shape

Table 4.4: Surface parameters defined in ECOCLIMAP (Le Moigne, 2018).

The remaining physiographic fields are extracted from other databases. Soil texture is extracted from sand and clay cover maps defined at 1km spatial resolution from the HWSD¹⁰ database. Bathymetry data are extracted from the ETOPO2¹¹ database with a horizontal resolution of approximately 4km. As for topography, different database are available: GTOPO30¹² with a spatial resolution of approximately 1km, SRTM-250m¹³ with a spatial resolution of approximately 250m and GMTED2010¹⁴, which is available at 250m and 1km horizontal reso-

¹⁰Harmonized World Soil Database is a global soil database developed by the Food and Agriculture Organization of the United Nations (FAO), the International Soil Reference and Information Centre (ISRIC), the International Institute for Applied Systems Analysis (IIASA), and other partners.

¹¹The ETOPO2 Global Relief Model is a digital elevation model (DEM) created by the National Geophysical Data Center (NGDC), a part of the National Oceanic and Atmospheric Administration (NOAA) in the United States.

¹²GTOPO30 is a digital elevation model dataset that was created by the United States Geological Survey (USGS).

¹³Shuttle Radar Topography Mission dataset was collected by the Space Shuttle Endeavour in the year 2000 and 2001, using radar technology to map the Earth's surface topography.

¹⁴Global Multi-resolution Terrain Elevation Data 2010 is a DEM dataset that provides elevation data for the Earth's land surfaces. It was developed by the USGS as part of an effort to create a consistent and high-quality DEM dataset for various applications.

lution.

4.2.2 Land surface model ISBA

As we are particularly interested in biogenic emissions, we will focus on the description of the natural tile as well as the physical processes simulated by SURFEX for vegetation land cover.

ISBA (Interaction between Soil Biosphere and Atmosphere) is a land surface parametrization scheme used in SURFEX. It is designed to simulate the interactions between the soil, vegetation and the atmosphere specifically the exchange of water and heat between these 3 different components, taking into consideration factors like soil physics, plant physiology, and meteorological conditions.

ISBA scheme incorporates the treatment of soil water and heat content using two different soil physics and discretization schemes, **force-restore** approach and **diffusive** approach, the treatment of snow using one- or multi-layer snow schemes and the treatment of the intercepted water. Most importantly, ISBA includes parametrizations to simulate vegetation photosynthesis and soil moisture stress, as well as LAI/biomass evolution, carbon cycle, respiration and evapotranspiration processes and CO_2 flux exchange between vegetation and the atmosphere with two different approaches **ISBA-A-gs** and **ISBA-CC**.

4.2.2.1 Treatment of the soil heat and water content

Force-restore:

This approach was initially designed for a soil discretization with 2 layers (2-L) (Noilhan and Mahfouf, 1996), but was later adapted to include 3 soil layers (3-L) (Boone et al., 1999). Figure 4.7 displays a schematic representation of the 2-L and 3-L force restore approach. The 2-L force-restore approach uses five prognostic equations to model surface and deep soil heat and water content.

$$\frac{\partial T_s}{\partial t} = C_T \times (R_n - H - LE) - \frac{2\pi}{\tau}(T_s - T_2) \quad (4.11)$$

$$\frac{\partial T_2}{\partial t} = \frac{1}{\tau} \times (T_s - T_2) \quad (4.12)$$

Where T_s is the surface temperature, T_2 is the deep soil temperature, R_n is the net radiation, H is the sensible heat flux, LE is latent heat flux and C_T is a coefficient calculated based on vegetation, snow fraction and heat capacity.

$$\frac{\partial w_g}{\partial t} = \frac{C_1}{\rho_w d_1} \times (P_g - E_g) - \frac{C_2}{\tau} \times (w_g - w_{geq}) \quad (0 < w_g < w_{sat}) \quad (4.13)$$

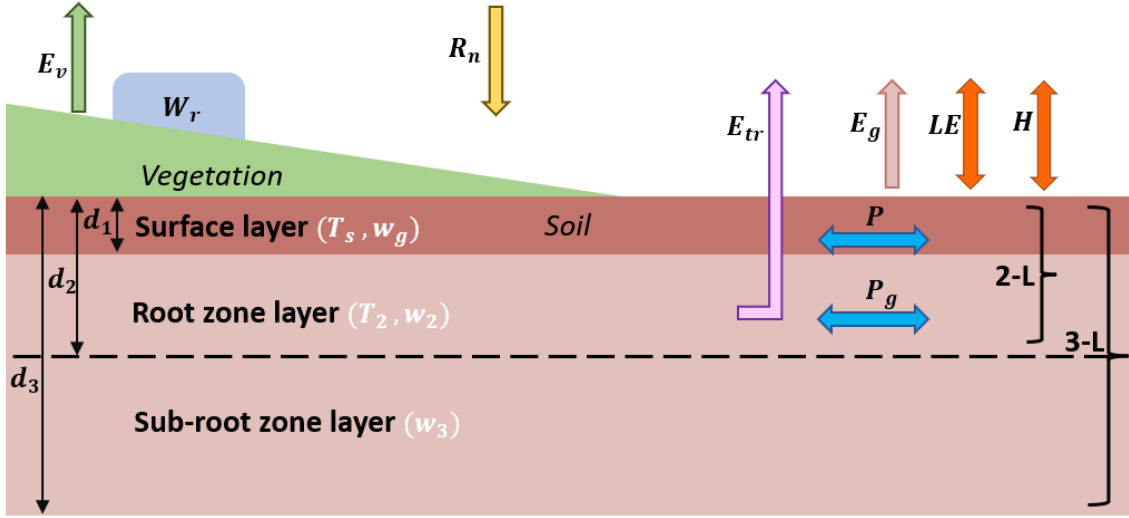


Figure 4.7: ISBA force-restore scheme.

$$\frac{\partial w_2}{\partial t} = \frac{1}{\rho_w d_2} \times (P_g - E_g - E_{tr}) - \frac{C_3}{d_2 \tau} \times \max[0, (w_2 - w_{fc})] \quad (0 < w_2 < w_{sat}) \quad (4.14)$$

$$\frac{\partial W_r}{\partial t} = veg \times P - (E_v - E_{tr}) - R_r \quad (0 < W_r < W_{rmax}) \quad (4.15)$$

Where w_g and w_2 are the top- and deep- soil volumetric water content respectively, w_{sat} is the saturated volumetric moisture content, W_r is the intercepted water by the canopy, w_{fc} is the field capacity volumetric moisture content, w_{geq} is the equilibrium surface volumetric moisture, C_1 and C_2 are force restore coefficients for soil moisture, C_3 is a dimensionless drainage coefficient that depend on the soil texture, P and P_g are the precipitation at screen and ground level, E_g is the evaporation at the soil surface, E_{tr} is the transpiration rate, E_v is the evaporation from the vegetation, d_1 and d_2 are the depths of the top and deep soil, ρ_w is the density of liquid water and veg is the fractional vegetation cover.

For the 3-L force restore approach, a distinction is made between the root zone layer and the sub-root zone layer, the soil water content in these layers is modeled as follows:

$$\frac{\partial w_2}{\partial t} = \frac{1}{\rho_w d_2} \times (P_g - E_g - E_{tr}) - \frac{C_3}{d_2 \tau} \times \max[0, (w_2 - w_{fc})] - \frac{C_4}{\tau} \times (w_2 - w_3) \quad (4.16)$$

$(0 < w_2 < w_{sat})$

$$\frac{\partial w_3}{\partial t} = \frac{d_2}{d_3 - d_2} \times \left[\frac{C_3}{\tau d_2} \times \max[0, (w_2 - w_{fc})] + \frac{C_4}{\tau} \times (w_2 - w_3) \right] - \frac{C_3}{(d_3 - d_2)\tau} \times \max[0, (w_3 - w_{fc})]$$

$(0 < w_3 < w_{sat})$

(4.17)

Where d_3 is the depth of the sub-root zone layer and C_4 is a dimensionless coefficient that represents the vertical diffusion.

Diffusion:

Multi-layer soil diffusion parametrization have been incorporated into land surface models to enable the heat and mass diffusion equations to be solved in an explicit way. By using multiple layers, the total depth of the soil is discretized, allowing for explicit computation of profiles for temperature and moisture as a function of the vertical characteristics of the soil, whether homogeneous or heterogeneous.

In theory, multi-layer soil diffusion schemes provide a more accurate description than the force-restore parametrization, as they explicitly parameterize a wide range of processes which are harder to represent in other simpler methods (e.g. the interplay between soil processes and cold processes, representation of the vertical root profile in the soil) (Decharme et al., 2011). The diffusion approach uses the following equations to model heat transfer between the surface and the soil layers:

$$\frac{\partial T_s}{\partial t} = C_T \times \left(G - \frac{\bar{\lambda}_1}{\Delta \bar{z}_1} \times (T_s - T_2) \right) \quad (4.18)$$

$$\frac{\partial T_i}{\partial t} = \frac{1}{C_{g_i} \times \Delta z_i} \times \left[\frac{\lambda_{i-1}}{\Delta \bar{z}_{i-1}} \times (T_{i-1} - T_i) - \frac{\bar{\lambda}_i}{\Delta \bar{z}_i} \times (T_i - T_{i+1}) \right] \quad \forall i \in [2, N] \quad (4.19)$$

Where, T_i is the temperature at the i^{th} soil layer, T_s is the surface temperature equal to T_1 , Δz_i is the thickness of the i^{th} layer, $\Delta \bar{z}_i = \Delta z_i + \Delta z_{i+1}$ and c_{g_i} is the total soil heat capacity. $\bar{\lambda}_i$ is calculated as following, with λ_i being the thermal conductivity at layer i .

$$\bar{\lambda}_i = \frac{\Delta z_i + \Delta z_{i+1}}{\frac{\Delta z_{i+1}}{\lambda_{i+1}} + \frac{\Delta z_i}{\lambda_i}} \quad (4.20)$$

The governing equations for water transfer within the soil are:

$$\frac{\partial w_1}{\partial t} = \frac{1}{\Delta z_1} \left[-\bar{k}_1 \times \left(\frac{\psi_1 + \psi_2}{\Delta \bar{z}_1} + 1 \right) - \bar{v}_1 \times \left(\frac{\psi_1 + \psi_2}{\Delta \bar{z}_1} \right) + \frac{S_1}{\rho_w} \right] \quad (4.21)$$

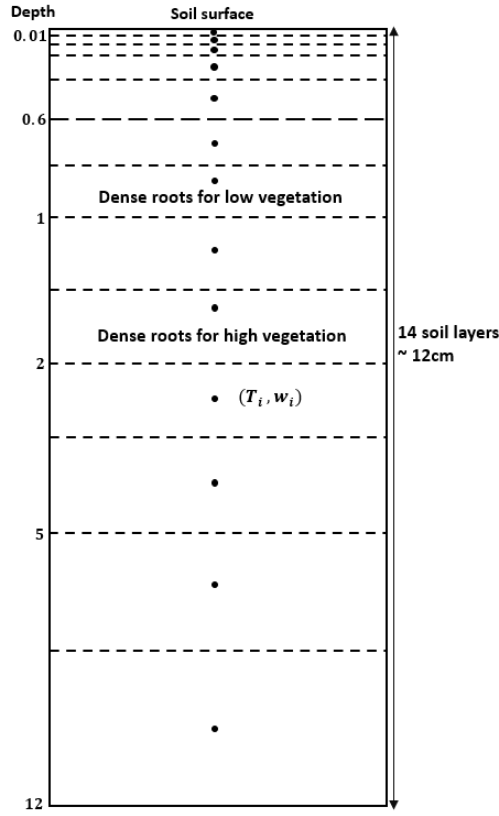


Figure 4.8: ISBA diffusion scheme.

$$\frac{\partial w_i}{\partial t} = \frac{1}{\Delta z_1} [F_{i-1} - F_i + \frac{S_i}{\rho_w}] \quad \text{with} \quad F_i = \bar{k}_i \times \left(\frac{\psi_i + \psi_{i+1}}{\Delta \bar{z}_i} + 1 \right) - \bar{v}_i \times \left(\frac{\psi_i + \psi_{i+1}}{\Delta \bar{z}_i} \right) \quad (4.22)$$

Where w_i is the soil moisture at the i^{th} layer, S_i is a source/sink term of soil water, $\bar{k}_i = \sqrt{k_i(\psi_i) \times k_{i+1}(\psi_{i+1})}$, k_i is the soil hydraulic conductivity, ψ_i is the soil matric potential, $\bar{v}_i = \sqrt{v_i(\psi_i) \times v_{i+1}(\psi_{i+1})}$ and v_i is the isothermal vapor conductivity.

In SURFEX, the diffusion scheme is used usually with 14 soil layers, the ISBA diffusion soil grid configurations with 14 layers is shown in Figure 4.8.

4.2.2.2 ISBA-A-gs

ISBA-A-gs is a photosynthesis model developed by Calvet et al. (1998) with the primary purpose of simulating the impact of varying environmental conditions, particularly changes in CO_2 concentrations, on stomatal conductance (g_s). Stomatal conductance represents a key parameter that governs the exchange rate of carbon dioxide and water vapor between leaves and the surrounding atmosphere. This exchange is derived by stomatal aperture which represents the degree to which stomata are open (i.e., open stomata enable the exchange of CO_2 and water

vapor).

The CO_2 responsive version of ISBA simulates the stomatal aperture based on a stomatal resistance parametrization developed by Jacobs (1994). This model aims to capture the complex physiological and biochemical processes taking place at leaf level (e.g., photosynthesis, transpiration and photo-respiration) by simulating two important parameters: leaf conductance to water vapour g_s and leaf net assimilation rate A_n . These parameters are estimated as a function of air specific humidity, solar radiation, leaf CO_2 concentrations and temperature.

The Jacob's model was designed specifically for vegetation under high soil moisture conditions, thus, Calvet et al. (1998) included a soil moisture parametrization to account for the vegetation response to soil water deficit by introducing the normalized soil moisture θ_2 in the calculation of A_n and g_s following equation 4.23:

$$\theta_2 = \frac{w_2 - w_{wilt}}{w_{fc} - w_{wilt}} \quad (4.23)$$

Where w_2 and w_{fc} are the soil volumetric moisture and the moisture content at the root zone, respectively. w_{wilt} represents the wilting point.

The ISBA-A-gs model also comprises a simple growth sub-model that simulates the LAI response to variation in the net assimilation rate A_n induced by CO_2 . This dynamic LAI is calculated on the basis of the biomass evolution (i.e. growth and mortality) driven by photosynthetic activity as follows:

$$dB = \frac{M_c}{P_c M_{CO_2}} \times A_{nI} \times dt - B \times d(t/\tau) \quad (4.24)$$

Where B is the bulk biomass kg/m^2 , M_{CO_2} and M_c are the molecular weights of carbon dioxide and carbon, respectively, A_{nI} is the integrated canopy net assimilation, P_c is the proportion of carbon in the dry plant biomass and τ is the effective life expectancy expressed as:

$$\tau(t) = \tau_{max} \times \frac{A_{nfm}(t)}{A_{n,max}} \quad (4.25)$$

Where τ_{max} is the maximum effective life expectancy, A_{nfm} is the maximum net assimilation of the past 24h and $A_{n,max}$ is the net assimilation found with an actual specific humidity deficit D_s of 0 g/kg , a PAR at height h of 500 W/m^2 and a leaf temperature of 25 and 35 $^\circ C$ for C_3 and C_4 plants, respectively.

The LAI is then calculated based on B and α_B which represents an empirical coefficient that depends on the vegetation type.

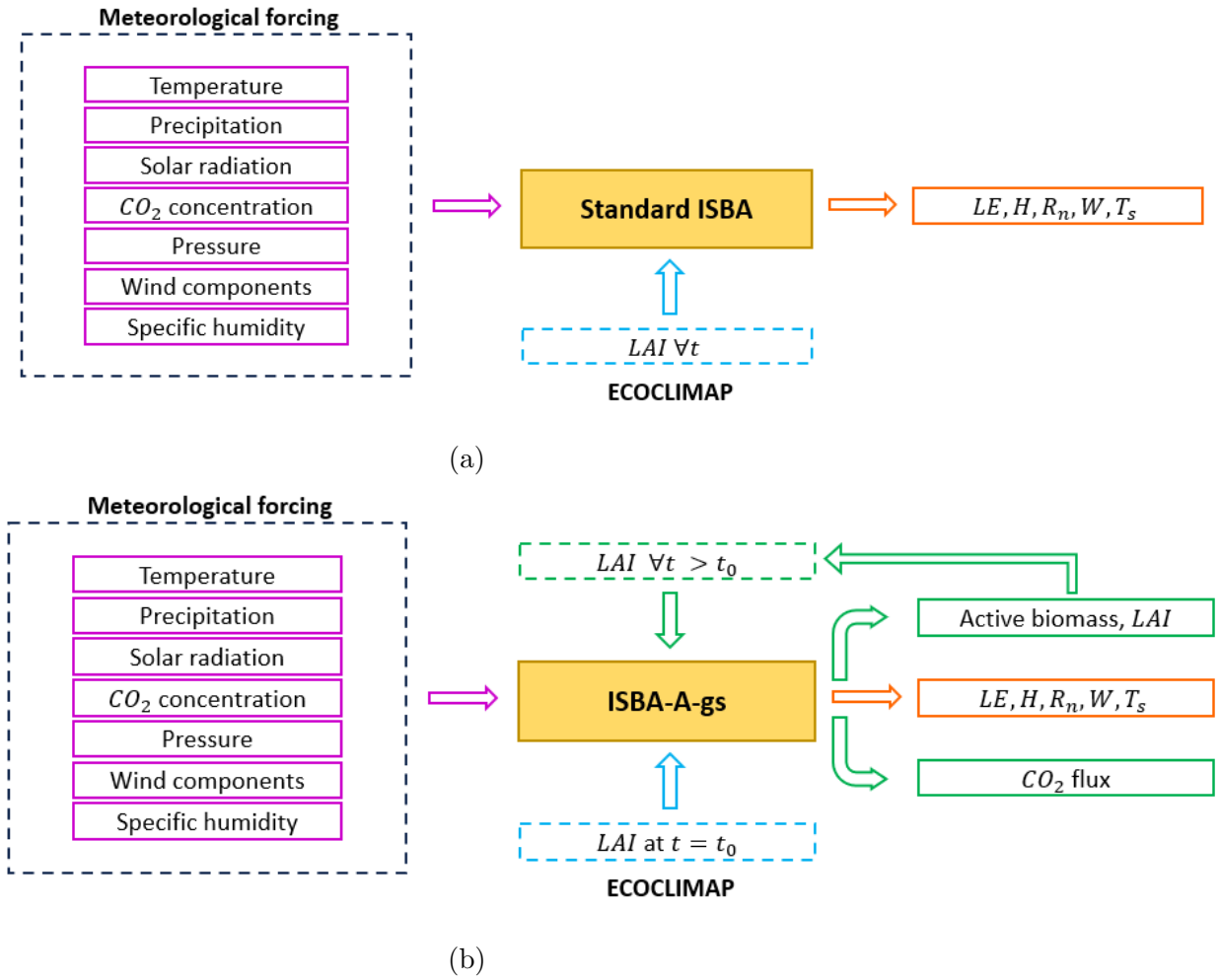


Figure 4.9: Differences between the standard ISBA model and the photosynthesis ISBA-A-gs model, LE is latent heat flux, R_n is the net radiation, H is sensible heat flux, T_s is the soil temperature and W is the moisture flux.

$$LAI = \frac{B}{\alpha_B} \quad (4.26)$$

Figure 4.9 shows a schematic representation of the two operating modes of the ISBA model. In the standard ISBA model, LAI is prescribed to the model and climatological values are extracted from ECOCLIMAP. Conversely, in the ISBA-A-gs photosynthesis model, the LAI is dynamically calculated from the evolution of biomass, the estimated LAI is looped back as model input, and the ECOCLIMAP LAI is only used during the first model time step.

The ISBA-A-gs CO_2 reactive model was tested on a global scale by running a global simulation over the period 1986-1995 and comparing the LAI simulation results with three satellite-

based LAI observations: ECOCLIMAP - MODIS and ISLSCP initiative II¹⁵ (Gibelin et al., 2006). The results of this study confirmed that ISBA-A-gs can simulate LAI realistically, as the spatial and temporal distribution of the models' LAI align well with satellite-based LAI observations. The seasonal cycle and the interannual variability are also well represented by the model. The ability of ISBA-A-gs to simulate leaf area index was also tested on a regional scale. Lafont et al. (2012) conducted a comparative study of the leaf area index produced by two land surface models ISBA-A-gs and ORCHIDEE¹⁶ (Krinner et al., 2005) and two satellite-derived leaf area index products MODIS and CYCLOPES¹⁷ over the period 1994-2007 in France. The results of the study showed that the ISBA-A-gs model captured interannual variability but did not represent seasonal variability well compared to satellite-based leaf area index observations, this has been explained by the absence of a phenology sub-model in ISBA-A-gs.

4.3 SURFEX-MEGAN coupling

To study the evolution of biogenic emissions in future climate, a coupling between the SURFEX model and the MEGAN model was implemented. This coupling aims to :

- Model biogenic emissions in present and future climates, as the SURFEX model can be used in an offline mode (i.e. using an external meteorological forcing file).
- Use the CO_2 -responsive ISBA-A-gs scheme to simulate leaf area index in future climate. In fact, using the stand-alone version of MEGAN to model biogenic emissions in the future together with LAI information derived from current satellite data is not accurate, as LAI is considered a crucial parameter in estimating biogenic emissions and this parameter is expected to undergo significant spatial and temporal changes resulting from climate change. Coupling the SURFEX and MEGAN models will enable us to use the dynamic LAI simulated by the ISBA-A-gs scheme driven by changes in atmospheric CO_2 concentrations, temperature, solar radiation and soil moisture as inputs to the MEGAN model, providing a more accurate representation of the vegetation density and distribution in a changing climate and thus improving the estimation of biogenic emissions in the future.
- Improve the estimation of biogenic fluxes. In fact, the ISBA land surface model in SURFEX provides precise vegetation-type-dependent parameters such as soil moisture, LAI, vegetation fraction, temperature and enables the estimation of biogenic emissions at patch

¹⁵The International Satellite Land-Surface Climatology Project initiative II is a scientific initiative that aims to collect different types of global data sets: vegetation, snow, radiation, meteorology, hydrology, etc.

¹⁶Organizing Carbon and Hydrology In Dynamic Ecosystems is a process-based terrestrial biosphere model designed to simulate energy, water and carbon fluxes of ecosystems.

¹⁷The CYCLOPES project aims to develop and produce global surface parameters, particularly leaf area index, fraction of green vegetation cover and photosynthetically active radiation.

level (i.e. the different activity factors are calculated for each vegetation type independently using PFT-specific meteorological and environmental parameters), thus, the calculation of fluxes on patch level improves the estimation of biogenic emissions fluxes.

The description of the SURFEX-MEGAN model coupling as well as the validation of the coupled model isoprene estimations was the subject of a scientific paper submitted to *Geoscientific Model Development* journal and in review (the preprint is available at <https://egusphere.copernicus.org/preprint/2023-2206/>), which is reported in full in the following:

Evaluation of isoprene emissions from the coupled model SURFEX-MEGANv2.1

Safae Oumami¹, Joaquim Arteta¹, Vincent Guidard¹, Pierre Tulet², and Paul D. Hamer³

¹CNRM, Université de Toulouse, Météo-France, CNRS, Toulouse, France

²Laboratoire d'Aérodologie, Université Paul Sabatier, CNRS, Toulouse, France

³NILU, Kjeller, Norway

Correspondence: Safae Oumami (safae.oumami@meteo.fr)

Abstract. Isoprene, a key biogenic volatile organic compound, plays a pivotal role in atmospheric chemistry. Due to its high reactivity, this compound contributes significantly to the production of tropospheric ozone in polluted areas, and to the formation of secondary organic aerosols.

The assessment of biogenic emissions is of great importance for regional and global air quality evaluation. In this study, we have implemented the biogenic emissions model MEGANv2.1 (Model of Emission of Gases and Aerosols from Nature, version 2.1) in the surface model SURFEXv8.1 (SURface EXternalisée in french, version 8.1). This coupling aims to improve the estimation of biogenic emissions using the detailed vegetation type-dependent treatment included in the SURFEX vegetation ISBA scheme. This scheme provides to MEGAN vegetation-dependent parameters allowing a more precise estimation of biogenic fluxes (e.g., leaf area index, soil moisture, wilting point data).

The present study focuses on the assessment of the SURFEX-MEGAN model isoprene emissions. The evaluation of the coupled SURFEX-MEGAN model results was carried out by conducting a global isoprene emissions simulation in 2019 and comparing the simulation results with other MEGAN-based isoprene inventories. The coupled model estimates a total global isoprene emission of 442Tg in 2019. The estimated isoprene is within the range of results obtained with other MEGAN-based isoprene inventories, ranging from 311Tg to 637Tg. The spatial distribution of SURFEX-MEGAN isoprene is consistent with other studies, with some differences located in low isoprene emission regions.

Several sensitivity tests were conducted to quantify the impact of different model inputs and configurations on isoprene emissions. Using different meteorological forcings resulted in a +/-5% change in isoprene emission using MERRA and IFS, respectively, compared with ERA5. The impact of using different emission factors data was also investigated. The use of PFT spatial coverage and PFT-dependent emission potential data resulted in a 14% reduction compared to using the isoprene emission potential gridded map. A significant reduction of around 38% in global isoprene emissions, was observed in the third sensitivity analysis, which applied a parameterization of soil moisture deficit, particularly in certain regions of Australia, Africa and South America.

The significance of coupling the SURFEX and MEGAN models lies particularly in the ability of the coupled model to be able to be forced with meteorological data from any time period. This means, for instance, that this system can be used to predict

25 biogenic emissions in the future. This aspect of this work is significant given the changes that biogenic organic compounds are expected to undergo as a result of changes in their climatic factors.

1 Introduction

30 Volatile Organic Compounds (VOCs) are a class of carbon-based chemicals known for their ability to evaporate easily at room temperature (Carroll and Kirschman, 2022). VOCs can be produced by human activities, with the primary anthropogenic sources being vehicle emissions, industrial processes, building materials, solvents, personal care products, the petroleum industry, and vehicular transport (Hester and Harrison (1995) - McDonald et al. (2018) - Rajabi et al. (2020)). VOCs are considered as one of the most important precursors in the formation of tropospheric ozone and secondary organic aerosols (Atkinson and Arey, 2003). These chemicals play a crucial role in ground-level photochemical ozone formation by controlling oxidant production rate in areas with sufficient NO_x (Nitrogen Oxides) concentrations (Hester and Harrison, 1995). On a global scale, VOCs are mainly emitted from natural sources: soils, oceans and vegetation. The VOC flux emitted from terrestrial vegetation accounts for 90% of the total emission (Guenther et al., 1995). Quantitatively, the most important biogenic volatile organic compound (BVOC) is isoprene (C_5H_8). According to MEGANv2.1 (Model of Emission of Gases and Aerosols from Nature version 2.1) (Guenther et al., 2012), isoprene accounts for about half of all the biogenic species emitted. Isoprene is also known for its high reactivity, as it contributes considerably to the formation of ground-level ozone (Chameides et al., 1988). 40 Monoterpenes and sesquiterpenes are also considered as important BVOCs due to their substantial impact on the generation of atmospheric organic aerosols on a global scale (Griffin et al. (1999) - Ervens et al. (2011) - Shrivastava et al. (2017)). The emission of ozone and the formation of atmospheric aerosols have effects that reach beyond air quality and human health concerns. They also exert a substantial influence on the current and future state of our climate. Consequently, achieving a precise estimation of BVOCs is of utmost importance. This precision is also crucial for making accurate forecasts of air pollutants using chemical-transport models on both regional and global scales. Such precise predictions are not only fundamental for 45 assessing air quality but also for quantifying the exact radiative forcing effects arising from ozone and aerosols under both present and future climate conditions. In this context, biogenic emissions are expected to alter in the future as a response to the changing patterns of temperature, solar radiation, land cover and use, and the increasing frequency and intensity of drought events. This creates a need for BVOC modelling tools that can be applied to study present and future climate and air quality modelling assessment. 50

The terrestrial BVOC model used in the present study is MEGANv2.1, which is one of the most used models within the biogenic emissions and atmospheric chemistry community to estimate the flux of biogenic organic compounds. It can be used in an offline mode but has also been coupled with other models. Several studies have been conducted implementing the MEGAN model within various canopy environment models or chemical-transport models, each model has a different version/implementation of the MEGAN algorithms and different weather and land cover driving variables. As a result, the estimated emissions can differ considerably (the annual global isoprene emission varies between 311Tg and 637Tg) (Messina et al. (2016) - Henrot et al. (2017) - Bauwens et al. (2018) - Zhang et al. (2021)).

Our scientific aim was to derive a method for estimating BVOC emissions for present and future climate scenarios that would be capable of considering both atmosphere and land surface processes as well as land-atmosphere interactions that impact vegetation. Our objective was to therefore develop a modelling system for BVOCs based on MEGANv2.1 that would be flexible enough to use a variety of meteorological forcing datasets, e.g., present day reanalyses and output from climate models for future scenarios. Furthermore, this modelling system would have to be capable of simulating impacts on vegetation arising from atmosphere-land interactions. In this study, we have therefore chosen to implement MEGANv2.1 within the SURFEXv8.1 (Surface Externalised) model, which is a land surface modelling platform developed by Météo-France in cooperation with the scientific community. While MEGANv2.1 has been coupled with SURFEX in previous work, this was done in the frame of the mesoscale atmospheric model MESO-NH (Lac et al., 2018) that includes online coupled chemistry. We have been motivated to develop this coupling further for the following reasons. First, SURFEX can be used in offline mode (i.e. using an external meteorological forcing file), this option enables simulations to be performed in present and future climates. Second, SURFEX includes a detailed canopy environment model called ISBA (Le Moigne, 2018). This scheme provides precise vegetation-type-dependent parameters such as soil moisture, Leaf Area Index (LAI), vegetation fraction, temperature, etc. Additionally, this scheme can simulate LAI, which varies in parallel with numerous environmental and meteorological variables. Based on this dynamic LAI, the coupled model can assess and predict the impact of climate change on the biosphere. This impact primarily include alterations in the density and distribution of vegetation, thereby exerting a direct influence on the release of biogenic compounds. In this respect, coupling the SURFEX and MEGAN models can create a feedback loop that takes into account both the impact of climate on vegetation and the impact of vegetation on climate.

The SURFEX and MEGAN2.1 models are presented in section 2, as well as a description of the models offline coupling. Section 3 is dedicated to the evaluation of the coupled model isoprene emissions in comparison with other isoprene inventories. The evaluation of the sensitivity tests results conducted on MEGAN's driving variables is discussed in section 4.

2 Models description

2.1 SURFEX model

SURFEX (Surface Externalisée, in French) (Le Moigne, 2018) is a surface modelling platform developed by Météo-France in cooperation with the scientific community. SURFEX simulates the interaction between the surface and the atmosphere by simulating the flux exchange between the soil and the upper atmospheric layer (e.g., latent heat flux, sensible heat flux, CO₂ flux, chemical species and aerosols). The most recent version of SURFEX (SURFEXv9.0) was released in January 2023; however, in this work, we have used SURFEXv8.1 which is widely used at present (Schoetter et al. (2020) - Zsebeházi and Szépszó (2020) - Schoetter et al. (2017)).

SURFEX can be run in an offline mode or coupled to an atmospheric model, e.g., the global numerical weather prediction model ARPEGE (Déqué et al., 1994). Used in an online mode, SURFEX extracts the necessary meteorological data from the global weather prediction model. In offline mode, a forcing file should be prescribed as input to the model. The forcing file should contain spatio-temporal gridded maps of atmospheric variables: air temperature, specific humidity, wind components,

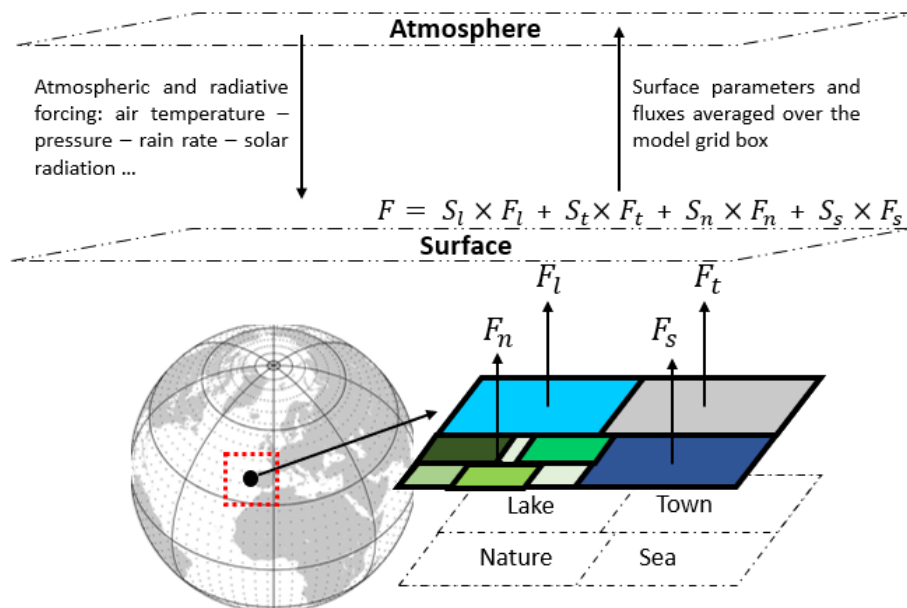


Figure 1. Grid cell representation in SURFEX and description of flux exchanges between the surface and atmospheric layer above.

pressure, rain rate, CO₂ and radiative variables: solar radiation and infrared radiation. During a model time step, each surface grid box receives the forcing variables listed above, in return SURFEX computes averaged fluxes for momentum, sensible and latent heat, chemical species and dust fluxes, etc, and then returns these quantities to the atmosphere by adding radiative terms such as surface temperature, direct and diffuse surface albedo, and surface emissivity (Le Moigne, 2018).

95 As shown in Figure 1, each grid box in SURFEX is represented by 4 adjacent tiles: nature, urban areas, sea or ocean and lakes. The final fluxes are the average of the fluxes calculated over nature, city, sea/ocean and lake, weighted by their respective fraction (S_l, S_t, S_n, S_s). SURFEX contains four principal surface schemes: ISBA for the nature tile (Calvet et al., 1998), TEB for urban areas (Masson, 2000), FLAKE Mironov et al. (2010) for lakes and SEA for sea and oceans. SURFEX can also simulate aerosol chemistry and surface processes, and can be used for assimilation of surface variables (Le Moigne, 2018).

100 To define the surface coverage, SURFEX uses ECOCLIMAP-II, which is a 1km global database of land covers made by CNRM (Centre National des Recherches Météorologiques, in French) (Faroux et al., 2013). It describes the types of surfaces covering the whole earth.

ECOCLIMAP-II provides the fraction data for the 19 patches (nature tile). In addition to that, it provides land surface parameters relative to each patch, i.e., each vegetation type has a defined soil depth, height of trees, LAI (Leaf Area Index) available at
 105 10 day time steps and vegetation fraction. LAI is represented by a 5-year averaged LAI climatology over the period 2002-2006. In ISBA, the calculation of surface parameters is based on an aggregation process at patch level (i.e., from the 19 land cover types down to the selected number of patches) for each point of the grid according to the horizontal resolution (Le Moigne, 2018).

2.2 MEGANv2.1 model

110 The MEGAN model is a global emission platform designed to estimate the net emission of gases and aerosols from terrestrial ecosystems into the atmosphere. It is an updated version of MEGANv2.0 developed by Guenther et al. (2006) to estimate isoprene flux and MEGAN2.02 which was described for monoterpene and sesquiterpene emissions by Sakulyanontvittaya et al. (2008).

MEGANv2.1 (the model's routines and input data can be found here <https://bai.ess.uci.edu/megan/data-and-code/megan21>,
115 last access: 8 September 2023) includes algorithms that take into account the main known processes controlling biogenic emissions, it allows to estimate the flux of 19 compound classes, which are decomposed into 147 individual species such as isoprene, monoterpenes, sesquiterpenes, carbon monoxide, alkanes, alkenes, aldehydes, acids, ketones, and other oxygenated VOCs (Guenther et al., 2012). Those species can then be lumped into the appropriate categories for the chemical scheme for use in chemical transport models. The stand-alone version of MEGANv2.1 requires as input weather data (temperature,
120 precipitation, solar radiation, wind, photosynthetic photon flux), atmospheric chemical composition (CO₂ concentration), land cover data (plant functional types distribution and LAI data) and emission factor data.

The estimation of biogenic fluxes in MEGANv2.1 is based on a simple equation (Equation 1) to calculate the net primary emission flux from terrestrial landscapes (F_i) into the above-canopy atmosphere ($\mu\text{m}^{-2}\text{s}^{-1}$). This equation comprises two significant components: firstly, the emission factor, which represents the emission potential of a specific compound associated
125 with a particular vegetation type, and secondly, the emission activity factor, which reflects how this emission potential responds to variations in environmental conditions and meteorological conditions.

$$F_i = \gamma_i \times \sum_{j=1}^n (\varepsilon_{ij} \times \chi_j) \quad (1)$$

Where γ_i is the dimensionless activity factor of a compound i (this factor is equal to 1 in standard conditions described below),
 ε_{ij} is the emission potential (also known as emission factor) of a compound i and vegetation type j at standard conditions and
130 χ_j is the fractional grid box areal coverage.

2.2.1 Vegetation and emission factor

A grid cell in MEGANv2.1 is represented by different types of vegetation also called Plant Functional Types (PFTs). A distribution of 16 PFTs is used to represent the vegetation cover, consistent with the vegetation categories used in the Community Land Model version 4 (CLM4) (Gent et al., 2011), which is a model used to simulate the interactions between the surface and
135 the atmosphere.

The emission factor represents the potential of a vegetation type to emit a specific chemical species under standard conditions. The list of standard conditions used in MEGANv2.1 is shown in Table 1. These conditions are relative to vegetation (e.g., LAI, growing and mature foliage fractions), meteorology (e.g., solar angle, PPFD transmission, temperature, humidity, wind speed), soil (e.g., soil moisture) and canopy (e.g., the past 24h and 240h temperature and PPDD for sun and shade leaves).

140 The estimation of BVOCs in MEGANv2.1, can be done by using global gridded high-resolution emission potential map pre-

Parameter	Standard value
LAI	$5 m^2 m^{-2}$
Canopy	80% mature, 10% growing and 10% old foliage.
Solar angle	60°
PPFD transmission	0.6
Air temperature	$303 K$
Humidity	$14 kg g^{-1}$
Wind speed	$3 m s^{-1}$
Soil moisture	$0.3 m^3 m^{-3}$
Temperature of the past 24 and 240h	$297 K$
PPFD of the past 24h and 240h	$200 \mu mol m^{-2} s^{-1}$ for sun leaves and $50 \mu mol m^{-2} s^{-1}$ for shade leaves.

Table 1. List of standard conditions used in MEGANv2.1 (Guenther et al., 2006).

scribed as input to the model (this map is provided with the MEGAN code for 10 predominant biogenic species) or by using PFTs spatial coverage and PFTs dependent emission potential data.

2.2.2 Emission activity factor

The emission activity factor represents the response of the vegetation to a change in environmental and meteorological conditions. The activity factor γ_i of a compound class i is calculated in the MEGANv2.1 fortran code as the multiplication of factors accounting for emission response to light $\gamma_{P,i}$, temperature $\gamma_{T,i}$, leaf age $\gamma_{A,i}$, soil moisture $\gamma_{SM,i}$, leaf area index (LAI) and CO₂ inhibition $\gamma_{CO_2,i}$ as follows:

$$\gamma_i = C_{CE} \times LAI \times \gamma_{P,i} \times \gamma_{T,i} \times \gamma_{A,i} \times \gamma_{SM,i} \times \gamma_{CO_2,i} \quad (2)$$

The canopy environment coefficient C_{CE} is used to normalise the activity factor at standard conditions listed above and is dependent on the canopy environment model being used. In MEGANv2.1 code, the equation used to calculate γ_i is:

$$\gamma_i = \gamma_{A,i} \times \gamma_{SM,i} \times \gamma_{CO_2} \times ((1 - LDF) \times \gamma_{TLI,i} \times \gamma_{LAI,i} + LDF \times \gamma_{TLD,i}) \quad (3)$$

Where $\gamma_{TLI,i}$ is the sum of temperature light-independent activity factor at 5 canopy levels and $\gamma_{TLD,i}$ is the sum of the product of light activity factor and temperature light-dependent activity factor at 5 canopy levels. In fact, in MEGANv2.1 the emission of each compound class includes a light-dependent fraction (LDF) and a light-independent fraction (LIF = 1 - LDF) that is not influenced by light. Each compound has a specific LDF (for isoprene LDF = 1). Light-dependent emissions are calculated following the isoprene response to temperature described by Guenther et al. (2006) and light-independent emissions follows the monoterpene exponential temperature response described by Guenther et al. (1993). The calculation of light-dependent and independent factors is based on a detailed canopy environment model that estimates light (PPFD), temperature (T), and fraction of sun and shade leaves at 5 canopy levels. The calculation of $\gamma_{TLI,i}$ and $\gamma_{TLD,i}$ is presented in equations 4, 5, 6

160 and 7, where γ_{TLI}^j and γ_{TLD}^j are calculated as the sum of temperature light-independent factor and light-dependent factor respectively weighted by the fraction of sun leaves f_{sun}^j and the fraction of shade leaves $(1 - f_{sun}^j)$ in each canopy level.

$$\gamma_{TLI} = \sum_{j=1}^5 \gamma_{TLI}^j \quad (4)$$

$$\gamma_{TLI}^j = \gamma_{TI,sun} \times f_{sun}^j + \gamma_{TI,shade} \times (1 - f_{sun}^j) \quad (5)$$

165
$$\gamma_{TLD} = C_{CE} \times LAI \times \sum_{j=1}^5 \gamma_{TLD}^j \quad (6)$$

$$\gamma_{TLD}^j = \gamma_{P,sun} \times \gamma_{TD,sun} \times f_{sun}^j + \gamma_{P,shade} \times \gamma_{TD,shade} \times (1 - f_{sun}^j) \quad (7)$$

The calculation of $\gamma_{TI,sun}$, $\gamma_{TI,shade}$, f_{sun}^j , $\gamma_{P,sun}$, $\gamma_{TD,sun}$, $\gamma_{P,shade}$ and $\gamma_{TD,shade}$ is detailed in Guenther et al. (2012).

2.3 SURFEX-MEGAN coupling

170 The coupling of MEGAN2.1 and SURFEXv8.1 is based on a previous implementation of MEGAN in MESO-NH5.4. MESO-NH5.4 is an atmospheric non-hydrostatic research model designed for studies of physics and chemistry (Lac et al., 2018). This coupling involved merging MEGAN routines and linking the required inputs of the biogenic model with SURFEX's parameters.

The present study focuses on the online integration of MEGAN in SURFEX. The ultimate aim of this coupling is to be able to
 175 force the coupled model through various climate change scenarios in order to assess climate change impact on the biosphere and to quantify the effect of these changes on biogenic emissions and therefore on global and local air quality. As well, this coupling aims to improve biogenic emission estimations by providing the MEGAN model with detailed vegetation-dependent inputs at patch level. This allows key land surface parameters used by MEGAN, i.e. leaf area index and soil moisture, to be calculated at a more precise scale. Thus, activity factors are individually calculated for each patch. This approach allows for a
 180 more accurate representation of biogenic emissions in the context of climate change and their impact on air quality.

In the coupled model the estimation of biogenic fluxes of various species was carried out based on 16 vegetation types extracted from the ECOCLIMAP-II database (Faroux et al., 2013). Each vegetation type from ECOCLIMAP-II was mapped to its corresponding defined in CLM4. Table 2 represents the mapping used in the coupled model. For most CLM4 PFTs, existing similar vegetation types are defined in ECOCLIMAP-II. However, when considering shrubs, CLM4 classifies them into
 185 three distinct categories: Evergreen temperate shrub, Deciduous temperate shrub, and Broadleaf deciduous shrub. Conversely, ECOCLIMAP-II does not provide separate classifications for these three distinct types of shrubs. To overcome this limitation,

CLM PFT number	Description	ECOCLIMAP patch number	Description	Type
1	Needleleaf Evergreen Temperate Tree	15	Temperate Needleleaf Evergreen	NT
2	Needleleaf Evergreen Boreal Tree	5	Boreal Needleleaf Evergreen	NT
3	Needleleaf Deciduous Boreal Tree	17	Boreal Needleleaf Cold-Deciduous Summergreen	NT
4	Broadleaf Evergreen Tropical Tree	6	Tropical Broadleaf Evergreen	BT
5	Broadleaf Evergreen Temperate Tree	14	Temperate Broadleaf Evergreen	BT
6	Broadleaf Deciduous Tropical Tree	13	Tropical Broadleaf Deciduous	BT
7	Broadleaf Deciduous Temperate Tree	4	Temperate Broadleaf Cold-Deciduous Summergreen	BT
8	Needleleaf Broadleaf Deciduous Boreal Tree	16	Boreal Broadleaf Cold-Deciduous Summergreen	NT
9	Broadleaf Evergreen Temperate Shrub	19	Shrub [-30° < lat < 30°]	SHRB
10	Broadleaf Deciduous Temperate Shrub	19	Shrub [-60° < lat < -30° or 30° < lat < 60°]	SHRB
11	Broadleaf Deciduous Boreal Shrub	19	Shrub [60° < lat]	SHRB
12	Arctic C3 Grass	18	Boreal Grass	GRLD
13	Cool C3 Grass	10	Grassland (C3)	GRLD
14	Warm C4 Grass	11	Tropical Grassland (C4)	GRLD
15	Crop1 (Wheat)	7	C3 Cultures Types	CROP
16	Crop2 (Corn)	8	C4 Cultures Types	CROP

Table 2. Description of the mapping between CLM4 and ECOCLIMAP vegetation types, the 16 PFTs are grouped into 6 vegetation types (NT: Needleleaf Trees, BT: Broadleaf Trees, SHRB: Shrubs, GRLD: Grassland, CROP: Crops) (5 ECOCLIMAP patches are not included in this list as they represent patch 1 = bare soil, patch 2 = rock, patch 3 = snow, patch 9 = irrigated crops and patch 12 = peat bogs, parks and gardens).

the three plant functional types corresponding to the different types of shrubs were introduced within ECOCLIMAP-II by assigning the shrub patch to a specific geographical area based on a given latitudinal range. The evergreen temperate shrub type is specified in the coupled model as the shrub patch in tropical regions ($-30^\circ < \text{latitude} < 30^\circ$), the deciduous temperate shrub in temperate regions ($-60^\circ < \text{latitude} < -30^\circ$ or $30^\circ < \text{latitude} < 60^\circ$), and the deciduous boreal shrub in boreal regions ($60^\circ < \text{latitude}$). This approach allows for a more accurate representation of shrubs in the coupled model.

Figure 2 represents a comparison between the vegetation types used in MEGAN stand-alone and the ones defined in ECOCLIMAP-II. For comparison, we have grouped the 16 PFTs into 6 main vegetation types: Broadleaf evergreen trees, Needleleaf evergreen trees, Deciduous trees, Shrubs, Grassland and Crops. The vegetation spatial distribution and intensity is similar for most vegetation types in ECOCLIMAP-II and CLM4. For shrubs, the substantial difference in vegetation distribution is due to the vegetation height threshold used in ECOCLIMAP-II (2m) and in CLM4 (10m). For vegetation-related input data, MEGAN can use climatological LAI from the ECOCLIMAP-II database, in this case, the LAI is defined for each vegetation type in a 10-day time step or the dynamic LAI estimated for each vegetation type with the vegetation scheme in SURFEX. LAI_v defined as the LAI in a grid cell divided by the vegetation fraction is considered equal to the current LAI and LAI_p (previous LAI) is

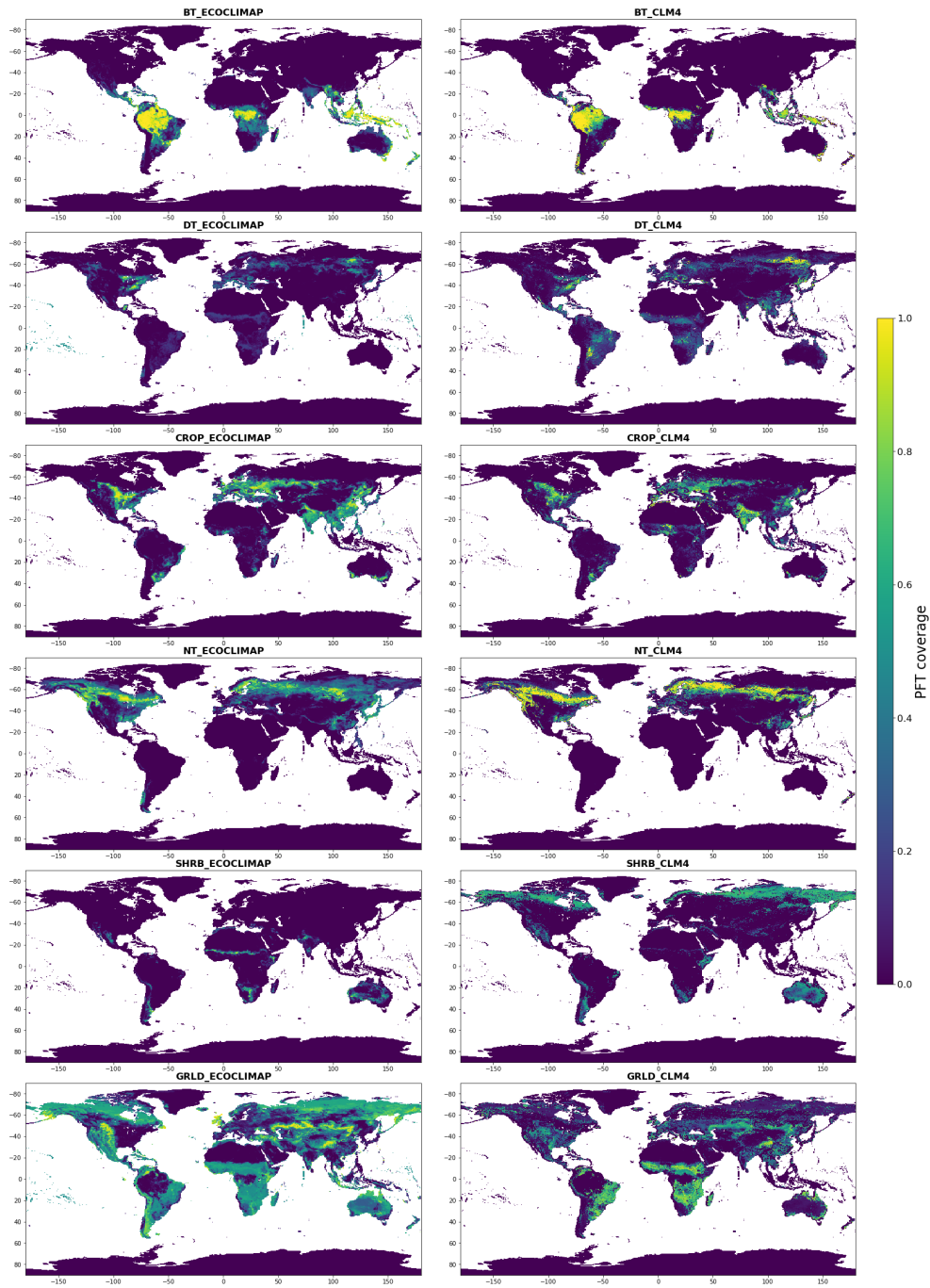


Figure 2. Spatial coverage of the 6 vegetation types defined in Table 2: BT (Broadleaf Trees), NT (Needleleaf Trees), DT (Deciduous Trees), GRLD (Grassland), SHRB (Shrubs) and CROP (Crops) in CLM4 (right) and in ECOCLIMAP-II (left).

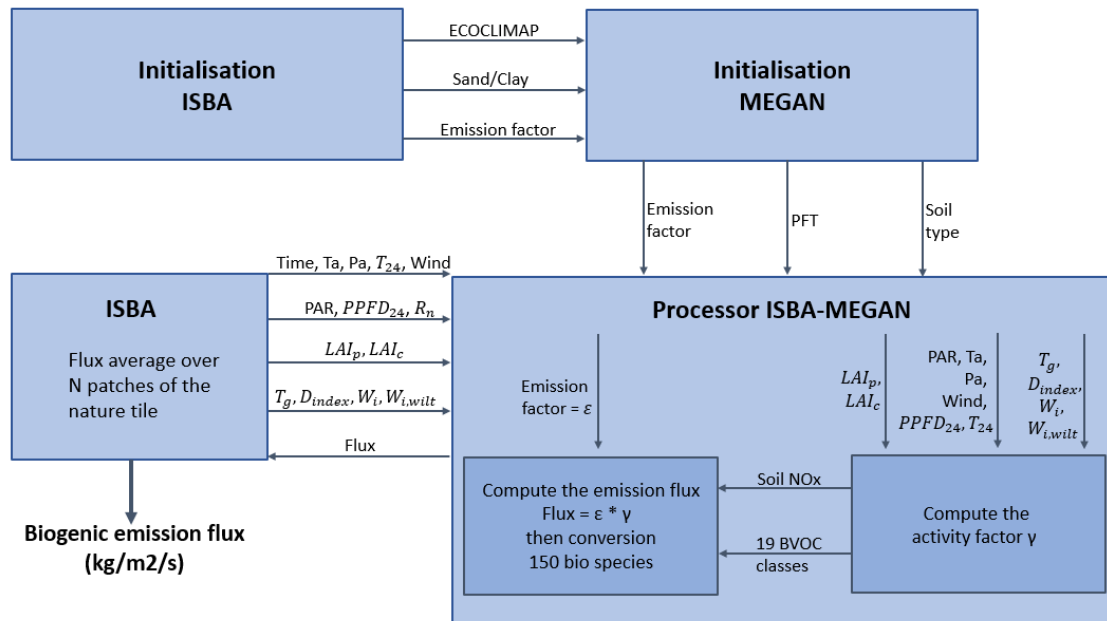


Figure 3. Schematic description of the SURFEX-MEGAN coupling. T_a is the temperature at 2m height, P_a is the surface pressure, T_{24} and $PPFD_{24}$ are the previous day mean temperature and PPFD, respectively, W_i and $W_{i,wilt}$ are the soil moisture and wilting point at different soil layers, respectively, T_g is the soil surface temperature, ϵ is the emission factor, γ is the activity factor, R_n is the incoming shortwave solar radiation flux, LAI_p and LAI_c are the LAI value of the previous and current day, respectively, D_{index} is the soil category.

200 defined as the LAI value of the past 10 days.

In the SURFEX model time step, all surface variables are interpolated and updated for each grid cell. Each tile is treated independently by using a specific scheme. For the Nature tile, the surface parameters are calculated following the vegetation-type aggregation process, which merges several vegetation types into a single patch (ranging from 1 to 19).

It is important to clarify that the coupling of SURFEX and MEGAN is online, which means that MEGAN's estimation of biogenic fluxes interact dynamically with the ISBA scheme (Interaction between Soil Biosphere and Atmosphere). ISBA is the scheme used for Nature tile to compute the exchanges of energy and water between the continuum soil-vegetation-snow and the atmosphere above.

The online implementation of MEGAN was done following the SURFEX's conceptual framework, which separates the initialisation phase from the temporal evolution phase. This involved setting up specific routines to initialise and interpolate MEGAN-related parameters (e.g., emission factors). The temporal estimation of biogenic emissions was carried out as an integral part of the ISBA scheme. This was achieved by integrating MEGAN routines that estimate the activity factor for each vegetation patch, using vegetation parameters estimated by ISBA, which encompass factors like soil moisture and wilting point at different layers (depending on the soil discretization method), leaf area index, photosynthetic active radiation (PAR), surface temperature, etc. Figure 3 shows a global representation of the online implementation of MEGAN in SURFEX.

3.1 Model setup

The coupled SURFEX-MEGAN model was utilised to conduct a global simulation of isoprene in 2019 using ERA5 meteorological forcing. This simulation is referred to as the reference simulation (abbreviated to REF).

ERA5 is a reanalysis based on the integrated forecasting system IFS (numerical weather forecasting model and data assimilation system, developed jointly by ECMWF and by Météo-France) (Hersbach et al., 2020). For the REF SURFEX-MEGAN simulation, the ERA5 forcing file includes hourly reanalysis meteorological fields defined on a $1^\circ \times 1^\circ$ spatial resolution grid (re-gridded from the native $31 \text{ km} \times 31 \text{ km}$ resolution). Temperature and specific humidity were extracted at 2m height; wind speed and wind direction were calculated based on zonal and meridian wind components at 10m height. As there are no available inputs for surface incident diffuse shortwave radiation and CO_2 rate, these parameters were assigned values of 0 Wm^{-2} and 410 ppm, respectively. The CO_2 concentration value corresponds to the 2019 annual mean of CO_2 observed at Mauna Loa (Keeling et al., 2000).

In this study, the calculation of PPFD and temperature for sun and shade leaves at different canopy heights was done using the canopy model integrated in MEGAN; the incoming PAR (Photosynthetically active radiation) at the top of the canopy was assumed to be 48% of the incoming shortwave radiation (Jacovides et al., 2003) (Nagaraja Rao, 1984); a conversion factor of 4.6 and $4.0 \mu_{mol} \text{ photons } J^{-1}$ was used to convert PAR to PPFD for diffused and direct radiation respectively (Guenther et al., 2012). Unless otherwise stated, in all coupled model simulations the estimation of isoprene flux was done based on isoprene potential map and the effect of soil moisture deficit and CO_2 on BVOC emissions was not taken into account (the γ_{sm} and γ_{CO_2} factors were assigned to 1). This choice allows a better comparison with other emission inventories.

For simplicity, we have used the ISBA 2-L scheme in the present study. In this scheme, the soil is represented with two layers, the heat and moisture exchanges between the layers and the atmosphere is modelled with the force-restore method (Le Moigne, 2018), this approach is described further in section 4.

3.2 Comparison of SURFEX-MEGAN isoprene emissions with other datasets**3.2.1 Isoprene inventories description**

The validation of the results obtained by the coupled model was evaluated by comparing the 2019 global and regional isoprene emission results with other isoprene inventories estimated with the MEGAN model. The data used for this comparison are presented in Table 3, additional information regarding the simulation setup used to generate the results is also provided. For inventories with unavailable 2019 isoprene emissions, the closest available year was used for comparison.

CAMS-GLOB-BIO is a high-resolution global emission inventory of the main biogenic species including isoprene, monoterpene, sesquiterpenes, methanol, acetone, and ethene (Sindelarova et al., 2022). It provides monthly average inventories and monthly average daily profiles of 3 different emission scenarios for the period 2000-2019. CAMS-GLOB-BIOv1.2 is a $0.5^\circ \times 0.5^\circ$ spatial resolution dataset obtained with ERA-interim meteorology, the vegetation cover is based on the CLM4 16 PFTs

and the emissions are calculated based on the emission potential map provided along with the MEGANv2.1 code. CAMS-GLOB-BIOv3.0 and CAMS-GLOB-BIOv3.1 have a higher spatial resolution of $0.25^\circ \times 0.25^\circ$ and are based on the ERA5 meteorology. The aim of the 3.0 scenario is to capture the impact of the land cover annual evolution on biogenic emissions by using the land cover data provided by the Climate Change Initiative of the European Space Agency (ESA-CCI). The 3.1 scenario uses the CLM4 vegetation cover and emission potential map for isoprene and main monoterpenes. The EP (Emission Potential) map was updated over Europe using high-resolution land cover maps and detailed information of tree species composition and emission factors from the EMEP MSC-W model system.

MEGAN-MACC is a biogenic emission inventory developed under the Monitoring Atmospheric Composition and Climate project (MACC) (Sindelarova et al., 2014). It includes monthly mean emissions of 22 biogenic species (isoprene, monoterpenes, sesquiterpenes, methanol and other oxygenated VOCs and carbon monoxide) estimated by the MEGANv2.1 model on a global $0.5^\circ \times 0.5^\circ$ grid for the time period 1980-2020, using meteorological fields of Modern-Era Retrospective Analysis for Research and Applications (MERRA).

The ALBERI dataset is a bottom-up inventory of isoprene emissions developed in the frame of the ALBERI project funded by the Belgian Science Policy Office (Opacka et al., 2021). Isoprene emissions are estimated by the MEGANv2.1 model, coupled with the canopy environment model MOHYCAN (Model for Hydrocarbon emissions by the CANopy) (Wallens, 2004) (Bauwens et al., 2018). The model was driven by the ERA-interim meteorological fields, vegetation description was provided from satellite-based Land Use/Land Cover (LULC) datasets at annual timesteps. The LULC datasets are based on the MODIS PFT dataset and are adjusted to match the tree cover distribution from the Global Forest Watch (GFW) database (Hansen et al., 2013).

3.2.2 Spatio-temporal distribution analysis

The global annual isoprene emission estimated with SURFEX-MEGAN simulation is 443Tg. The isoprene estimates of the coupled model falls within the range of previous reported values calculated with MEGANv2.1, varying between 311Tg and 637Tg. The discrepancies between isoprene totals obtained by different studies are due to many factors, including model assumptions and input data (e.g., meteorology, LAI, vegetation distribution). In fact, according to Messina et al. (2016), isoprene emissions are highly dependent on LAI, as they linearly increase up to a $LAI=2m^2/m^2$, then gradually decrease to become almost constant above $5m^2/m^2$. As shown by Sindelarova et al. (2014), the use of different LAI inputs (MERRA reanalysis data instead of MODIS LAI data) can lead to a 4% increase in annual isoprene emissions. The use of different data of photosynthetically active radiation (PAR) can also significantly impact the calculated isoprene emissions. Sindelarova et al. (2014) found that using PAR calculated from incoming shortwave radiation instead of PAR from the MERRA reanalysis led to a 17.5% increase in total isoprene emissions. Further in this section, we will examine other individual factors responsible for the total isoprene discrepancies and the differences in spatio-temporal distribution between isoprene estimates from SURFEX-MEGAN and other isoprene inventories.

Figure 4 displays the mean annual isoprene flux of the six inventories. As shown in Figure 4, the spatial distribution of isoprene shows similar general spatial patterns for the different datasets, with important isoprene emissions located in South America

Ref.	Dataset	Resolution	Weather	PAR	LAI	PFT	Emission potential	Data availability	Isoprene Tg/year
a	CAMS-GLOB-BIOv1.2	$0.5^\circ \times 0.5^\circ$	ERA Interim	α	MODIS	CLM4	EP map	2000-2018	385 (2018)
a	CAMS-GLOB-BIOv3.0	$0.25^\circ \times 0.25^\circ$	ERA5	α	MODIS	ESA-CCI	PFT dependent	2000-2019	311 (2019)
a	CAMS-GLOB-BIOv3.1	$0.25^\circ \times 0.25^\circ$	ERA5	α	MODIS	CLM4	EP map(updated in Europe)	2000-2020	471 (2019)
b	MEGAN-MACC	$0.5^\circ \times 0.5^\circ$	MERRA	MERRA	MODIS	CLM4	EP map	1980-2020	637 (2019)
c	ALBERI	$0.5^\circ \times 0.5^\circ$	ERA Interim	ERA Interim	MODIS	CLM4	PFT dependent	2001-2018	347 (2018)
This study	SURFEX-MEGAN	$1^\circ \times 1^\circ$	ERA5	α	ECOC-LIMAP	ECOC-LIMAP	EP map	2019	443 (2019)

Table 3. List of isoprene inventories used for the model validation and description of driving input data, α is the conversion factor used to approximate PAR from surface solar downward radiation = 0.45, (a) Sindelarova et al. (2022), (b) Sindelarova et al. (2014), (c) Opacka et al. (2021).

(the Amazon rainforest) and Africa (the Congo rainforest), however some differences can be discerned in Australia as well as in the maximum isoprene emission estimated by each inventory. These discrepancies, can be attributed to the emission potential data used in each simulation and the PFT cover present in the area, as the spatial distribution of isoprene can be highly impacted by both the model assumptions regarding emission capacity and the spatial distribution of the vegetation types considered.

285 The isoprene flux in the SURFEX-MEGAN simulation shows a comparable spatial pattern to CAMS-GLOB-BIOv3.1. This similarity can be attributed to the fact that both simulations use ERA5 meteorological forcing, the same isoprene emission potential gridded map and similar vegetation distributions (cf. section 2.3). The isoprene emissions in MEGAN-MACC shows also similar spatial pattern, with more significant emissions located in Australia and South America. In contrast, the spatial distribution of isoprene in CAMS-GLOB-BIOv3.0 and ALBERI differs significantly from that of the SURFEX-MEGAN sim-
290 ulation, as these two simulations were produced using the PFT dependent emission potential table from MEGAN.

In isoprene low emission regions, such as North America, Europe, and North Asia, isoprene emissions from SURFEX-MEGAN are particularly higher when compared to other isoprene inventories. This discrepancy can be attributed to variations in vegetation types and their intensity between CLM4 and ECOCLIMAP in these specific areas. As shown in Figure 2, needleleaf trees and grassland density in Asia and North America are notably greater in ECOCLIMAP, making the emissions in these regions
295 substantially higher in SURFEX-MEGAN compared to other CLM4 PFTs-based isoprene inventories.

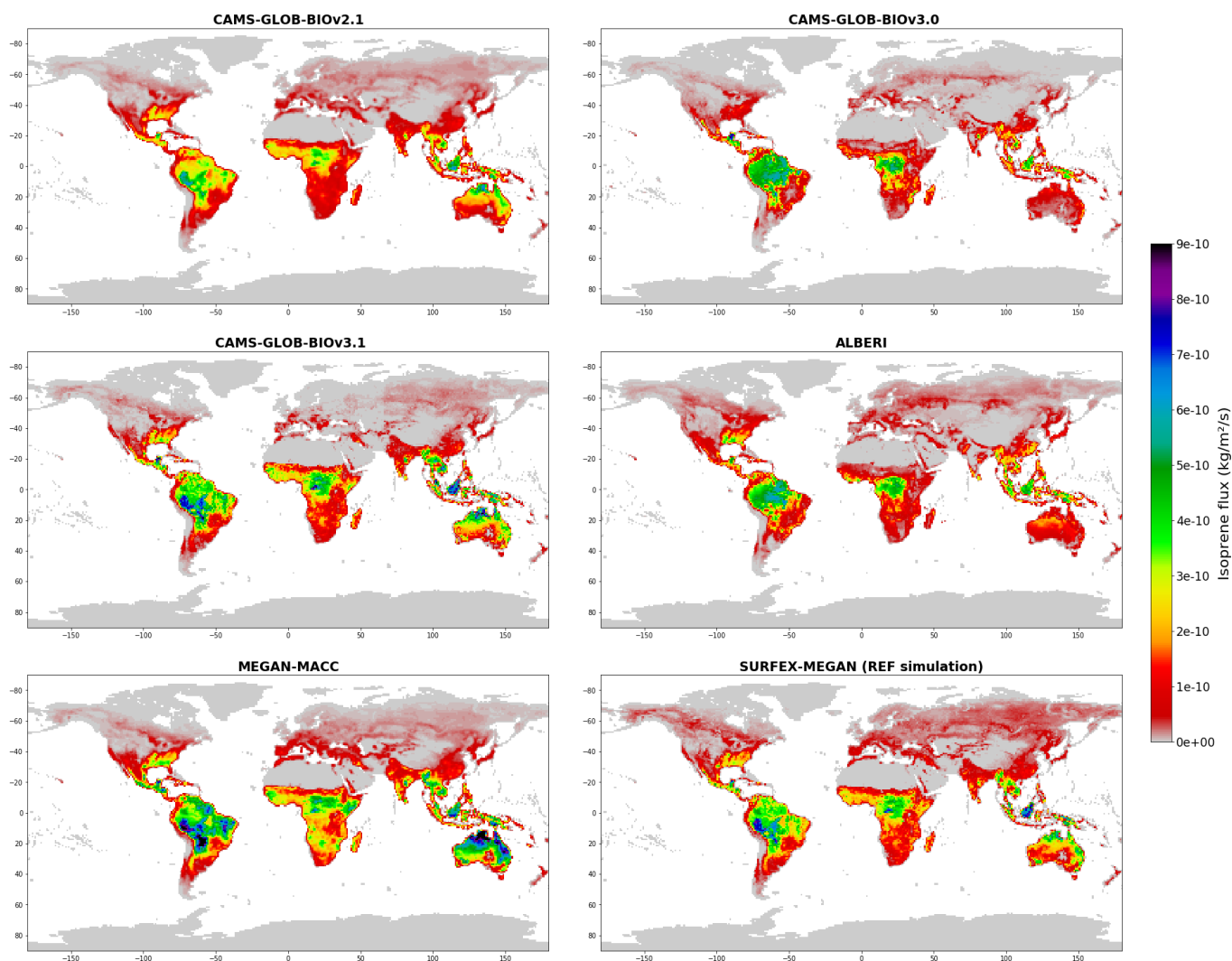


Figure 4. Spatial distribution of annual mean isoprene ($\text{kg/m}^2/\text{s}$) of CAMS-GLOB-BIOv2.1, CAMS-GLOB-BIOv3.0, CAMS-GLOB-BIOv3.1, MEGAN-MACC, ALBERI and SURFEX-MEGAN in 2019 (2018 for CAMS-GLOB-BIOv2.1 and ALBERI).

Figure 5 represents the time series of global monthly isoprene in 2019 of SURFEX-MEGAN compared to the five other inventories. The monthly variation of isoprene emissions in the SURFEX-MEGAN simulation is marked by small monthly fluctuations. The maximum isoprene emission occurs in boreal summer (July/August) with a total isoprene of 40Tg and the minimum in boreal winter (February) with a total isoprene of 33Tg. The annual cycle of SURFEX-MEGAN isoprene is in agreement with the ALBERI and CAMS-GLOB-BIOv1.2 datasets. A visible shift is noticed for MEGAN-MACC and CAMS-GLOB-BIOv(3.0 - 3.1) isoprene annual cycle with peak concentrations occurring in December/January and minimum in May/June.

Figure 6 and 7 represent respectively, monthly and yearly relative contribution of different zonal regions to isoprene emissions for the different datasets. In the SURFEX-MEGAN simulation, the annual cycle of isoprene follows the seasonal cycle: In Boreal summer (May – June – July - August), isoprene emissions are preponderant in the northern hemisphere (60% of total emission in this period) and in austral summer (October - November – December – January – February), isoprene emissions are preponderant in southern hemisphere (64% of total emission in this period). As shown in Figure 6, southern and northern tropical regions predominate throughout the year, their contribution to the total emission in the SURFEX-MEGAN simulation varies between 33% to 60% and 30% to 44% respectively, this is due to the meteorological conditions that are favourable all year-round (both in terms of temperature and solar radiation) and due to the high concentration of vegetation in these areas. Northern temperate regions are only active during boreal summer with a maximum contribution of 24% in July. The contribution of southern temperate regions follows a cyclical pattern, with a maximum in austral summer (6% in reference simulation). Finally, the Arctic is characterised by a very low activity, which is due to the unfavourable weather conditions and relatively low vegetation cover.

The monthly variation in isoprene emissions is strongly influenced by the emitting regions contribution throughout the year. As already mentioned, southern tropical regions are active throughout the year for all isoprene datasets, with particularly high contributions during November/December and lower contributions during June/July. As shown in Figure 7, southern tropical regions account for approximately 49% of annual isoprene emissions in SURFEX-MEGAN and CAMS-GLOB-BIOv2.1. However, their contribution to the annual isoprene is significantly higher in MEGAN-MACC (56%), CAMS-GLOB-BIOv(3.0 - 3.1) (54% - 52%), which can explain the peak in isoprene emissions observed during November/December. Conversely, isoprene emissions from northern temperate regions are relatively higher in SURFEX-MEGAN (10%), CAMS2.1 (9%) and ALBERI (11%), compared to MEGAN-MACC (7%) and CAMS3.0/3.1 (6%). These regions are active mainly during boreal summer, which can explain the isoprene peak observed during July for SURFEX-MEGAN/CAMS2.1/ALBERI.

The isoprene spatial and temporal distribution of the SURFEX-MEGAN coupled model are in agreement with other MEGAN-driven isoprene inventories. The evaluation of the total annual isoprene is however hard to assess, as the emissions are highly affected by both model input data and model assumptions.

4 SURFEX-MEGAN isoprene sensitivity tests

In order to analyse isoprene emission variation linked to MEGAN's driving parameters, 3 sensitivity tests were conducted. As stated in (Guenther et al., 2012) isoprene emissions depend on various meteorological and environmental parameters as well as the model assumptions. In this study, we have investigated isoprene emission sensitivity to meteorology using 2 different additional meteorological datasets (both IFS and MERRA) (S1), analysed isoprene emissions with a different set of emission potentials (S2), and studied the impact of soil moisture on isoprene emission (S3). Table 4 summarises the list of sensitivity tests performed in this study, along with a description of each test setup. The impact of each sensitivity test was examined on the global and regional scales by analysing the annual isoprene emission contribution from nine geographical regions defined in the GlobEmission project (www.globemission.eu). The spatial extent of the regions is given in Figure 8.

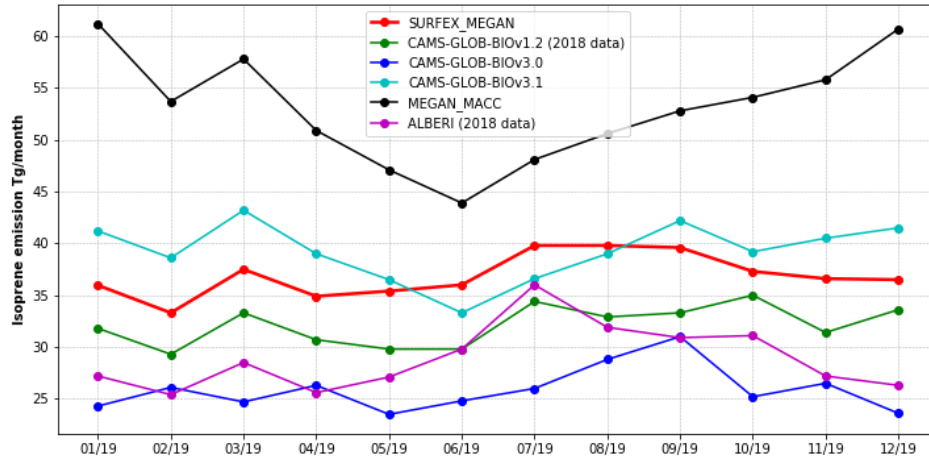


Figure 5. Global monthly isoprene (Tg/month) from different the six datasets in 2019. 2018 data was used for CAMS-GLOB-BIOv2.1 and ALBERI.

Simulation	Description	Meteorology	γ_{SM}	Emission potential
RS	reference simulation	ERA5	=1	ϵ_{map}
S1	use of MERRA meteorological forcing	MERRA	=1	ϵ_{map}
S1	use of IFS meteorological forcing	IFS	=1	ϵ_{map}
S2	use of isoprene emission potential	ERA5	=1	ϵ_{PFT}
S3	study the impact of soil moisture on isoprene	ERA5	variable	ϵ_{map}

Table 4. List of sensitivity runs performed.

4.1 Meteorology

The emission rate of isoprene can be influenced by a variety of meteorological factors, including temperature, solar radiation and atmospheric humidity. To illustrate the impact of these factors on isoprene emission estimated by SURFEX-MEGAN, two simulations were conducted using two different meteorological datasets: IFS forecast dataset (operational real-time weather forecast, forecast grid data) and MERRA. MERRA was undertaken by NASA’s Global Modelling and Assimilation Office. The data were generated with version 5.2.0 of the Goddard Earth Observing System (GEOS) atmospheric model and data assimilation system (DAS) and covers the period from 1979 to present (Rienecker et al., 2011). The MERRA data are defined on an hourly basis on a grid of 0.625° latitude and 0.5° longitude resolution. However to avoid considering the effect of spatial resolution on isoprene emission (Pugh et al., 2013), the MERRA reanalysis meteorological fields were interpolated to align with the reference simulation spatial resolution ($1^\circ \times 1^\circ$).

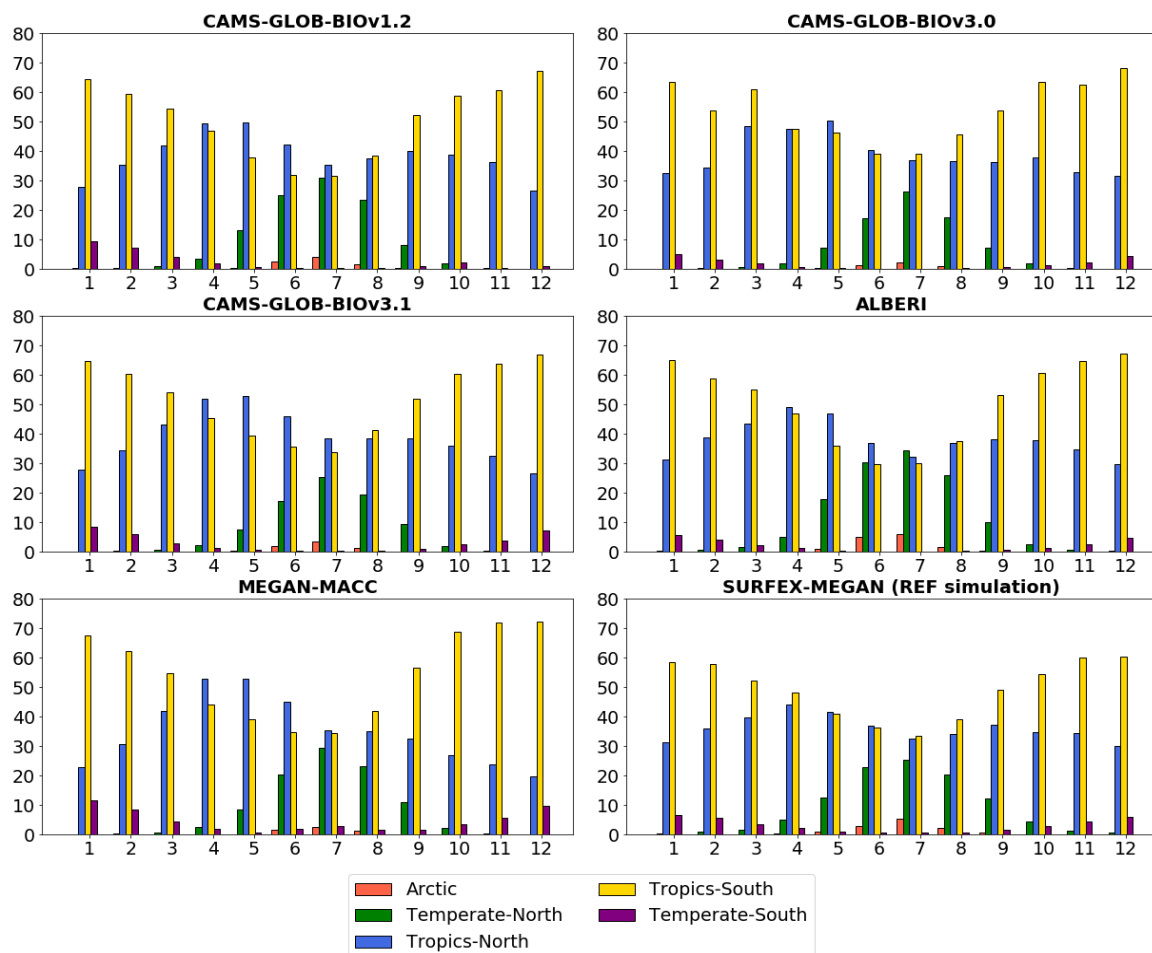


Figure 6. Contribution of zonal regions to monthly isoprene in CAMS-GLOB-BIOv2.1, CAMS-GLOB-BIOv3.0, CAMS-GLOB-BIOv3.1, MEGAN-MACC, ALBERI and SURFEX-MEGAN simulation in 2019 (2018 for CAMS-GLOB-BIOv2.1 and ALBERI). The zonal bands are defined as: Arctic ($90^{\circ}, 60^{\circ}$), Temperate-North($60^{\circ}, 30^{\circ}$), Tropics-North($30^{\circ}, 0^{\circ}$), Tropics-south($0^{\circ}, -30^{\circ}$), Temperate-south($-30^{\circ}, -60^{\circ}$).

The reference simulation uses ERA5 meteorological forcing, however, the version of IFS used in ERA5 is a newer and more advanced version of the IFS that was used in the near real time forecasts in 2019 for operations. This improved version of the IFS for ERA5 uses a numerical climatology model for modelling physical processes, while the version used for operational real-time forecasts uses process parameterization schemes that are optimised for fast and real-time execution. The IFS meteorological forcing was extracted from the IFS operational real-time forecasts model with a spatial resolution of $1^{\circ} \times 1^{\circ}$ and a temporal resolution of 3h.

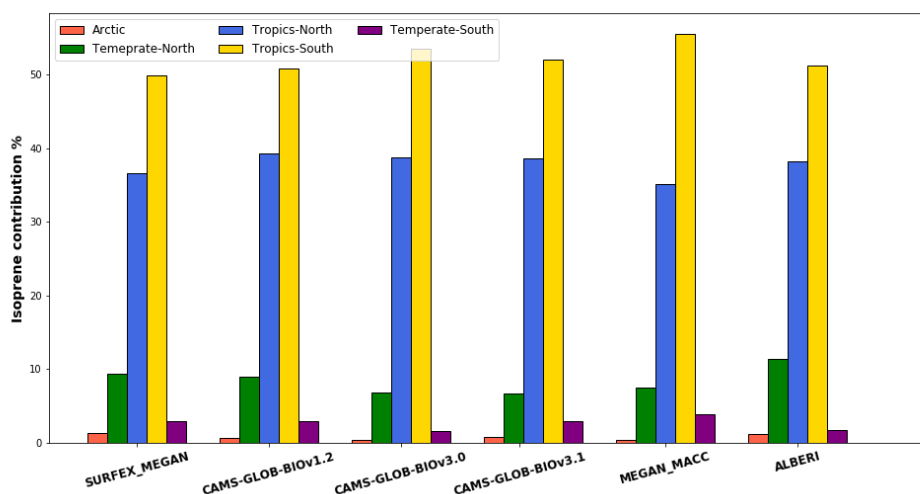


Figure 7. Contribution of zonal regions to annual isoprene for different emission datasets in 2019 (2018 for CAMS-GLOB-BIOv2.1 and ALBERI).

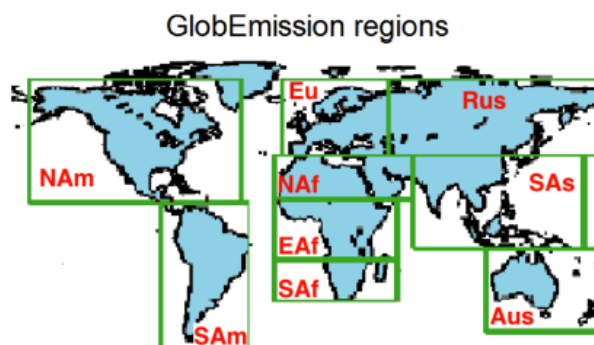


Figure 8. Geographical extent of the GlobEmission regions (NAm: North America, SAm: South America, Eu: Europe, NAf: North Africa and middle East, EAf: East Africa, SAf: South Africa, Rus: Russia, SAs: South East Asia, Aus: Australia), from Sindelarova et al. (2014).

The S1-MERRA simulation has the highest global annual isoprene in 2019 with a total of 462Tg, followed by reference simulation (ERA5) and S1-IFS with a total of 443Tg and 421Tg respectively. The mean annual isoprene flux difference in 2019
 355 between S1 simulations and reference simulation is shown in Figure 9. ERA5 isoprene emissions are higher in both the Amazon and Congo rainforests as well as over Indonesia compared to IFS isoprene estimates. On the other hand, ERA5-based isoprene emissions are lower than MERRA isoprene in eastern Australia but higher in Africa. To investigate the origin of these differences, an analysis of meteorological parameters that drive isoprene emission was performed focusing particularly

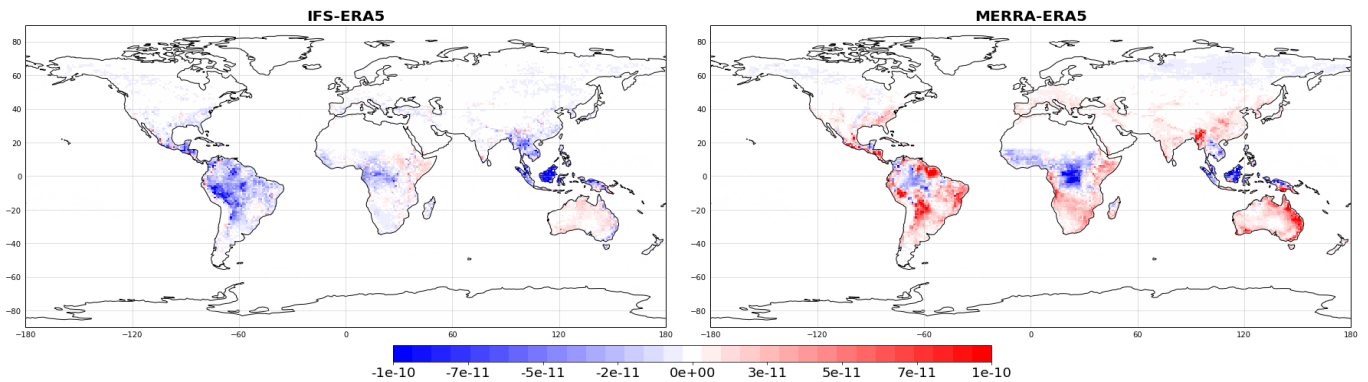


Figure 9. Annual mean isoprene difference (kg/m²/s) between S1-IFS and reference simulation (left) and between S1-MERRA and reference simulation (right).

on temperature and solar radiation. These parameters influence the emission of biogenic species via two factors γ_P and γ_T detailed by Guenther et al. (2012).
360

As shown by Guenther et al. (2006), the estimate of isoprene flux in MEGAN is temperature dependent, with emissions increasing exponentially with temperature to a maximum that depends on the average temperature of the last 24 hours. MEGAN emissions depend also on the amount of light received by vegetation. The isoprene estimate increases almost linearly with PPFD, the rate of increase depends on the average PPFD over the last 24 hours. To study the linear dependence between the isoprene flux estimates and PPFD, we examined the correlation between the difference in isoprene estimates, and the difference in light (PAR) between the reference (with the ERA5 meteorological forcing) and S1 simulations (with the IFS and MERRA meteorological forcings). Figure 10 displays the temporal correlation coefficient between isoprene flux differences and light differences for reference and S1-IFS simulations, as well as reference and S1-MERRA simulations. The PAR contributes strongly to the explanation of isoprene discrepancies between reference and S1 simulations, as the correlation coefficient exceeds 0.8 in regions where isoprene is emitted. Thus, the difference in isoprene emission flux across the three simulations is mainly due the different PAR input used in the simulation's meteorological forcing file. The correlation study was not conducted on other isoprene meteorological drivers, such as temperature, as the dependence of isoprene on this parameter is exponential.
365
370

Figure 11 and Figure 12 represent the isoprene distribution by region of all performed tests and the mean temperature/PAR relative difference between the MERRA and the ERA5 data inputs. On a regional scale, MERRA temperature and downward radiation received by vegetation are higher in Australia and South America compared to ERA5, resulting in higher isoprene estimates in those regions (+10% in Australia and +7% in South America). Conversely, MERRA temperature and radiation inputs are lower in East Africa, resulting in lower isoprene estimates for that region (-3%).
375

Several studies have been conducted to quantify the MEGAN model sensitivity to meteorology. For example, Arneth et al. (2011) showed that using different meteorological forcings can lead to different emission estimates where the use of CRU
380

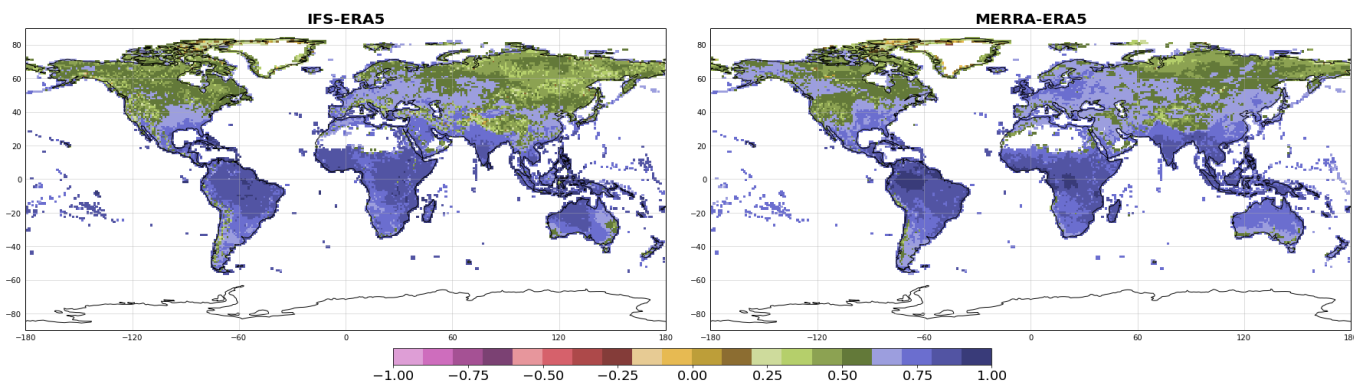


Figure 10. Pearson correlation coefficient of PAR and isoprene difference between reference and S1 simulations (S1-IFS (left) and S1-MERRA (right)).

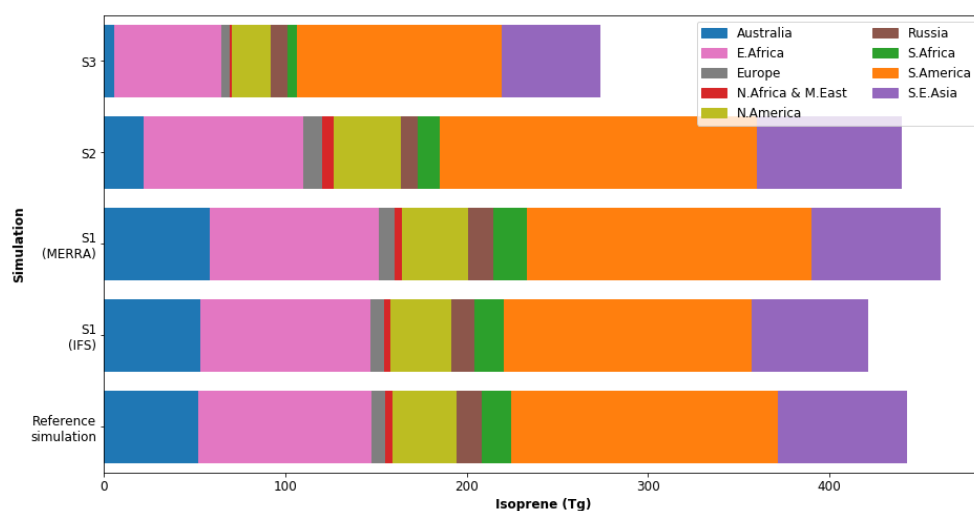


Figure 11. Isoprene total emission by region (defined in Figure 8) of the reference simulation, S1 simulation (IFS/MERRA), S2 simulation (emission potential) and S3 simulation (soil moisture).

(Climatic research Unit) meteorology instead of the NCEP (National Center for Environmental Prediction) reanalysis product led to a 10% decrease with MEGANv2. Sindelarova et al. (2022) also detected a difference of the total BVOC MEGANv2.1 estimations between CAMS-GLOB-BIOv2.1 and CAMS-GLOB-BIOv3.1 and explained that the discrepancies are mainly due the use of different meteorological inputs.

385 On a global scale the use of different meteorological forcing has been observed to have an impact on the amount of isoprene emissions estimated with the SURFEX-MEGAN model. The use of MERRA meteorology led to a 5% increase in isoprene emissions, while the use of IFS meteorology resulted in a decrease of 4.8% in comparison with the reference simulation.

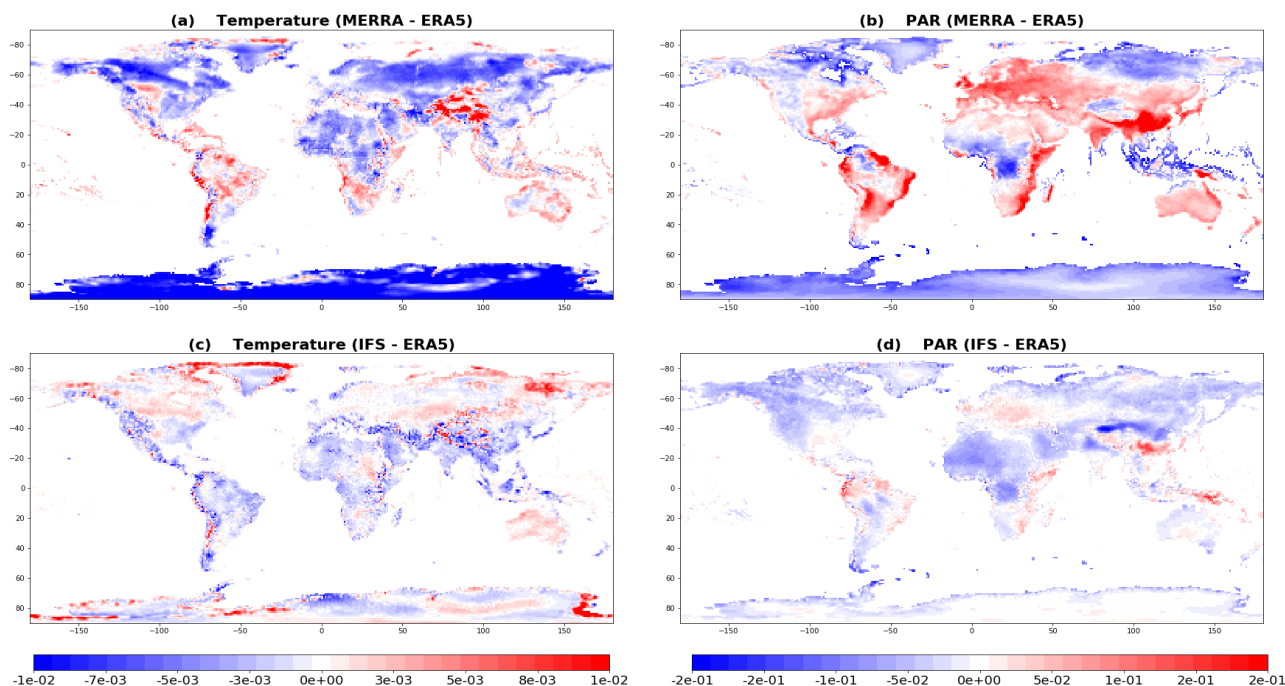


Figure 12. Mean temperature relative difference between MERRA and ERA5 (a), mean PAR relative difference between MERRA and ERA5 (b), mean temperature relative difference between IFS and ERA5 (c) and mean PAR relative difference between IFS and ERA5 (d). Red represents areas where the difference between temperature/PAR is positive and blue areas where the difference is negative.

4.2 Emission potential of isoprene

MEGANv2.1 defines two approaches to estimate biogenic fluxes, the first one is based on the use of the biogenic species emission potential maps ϵ_{map} these gridded maps are made based on a land cover including more than 2000 eco regions each with specific emission factors (Guenther et al., 2012). The compilation of these maps was done to cover the large differences in emission potential between species belonging to the same generalised PFT (e.g., temperate deciduous tree). For other PFTs, including only low isoprene emitters, the use of the PFT-specific emission factor is sufficient (e.g., boreal deciduous and needle trees). The second approach consists of using the 16 generalised plant functional type distribution ϵ_{PFT} along with their specific emission factor (Guenther et al., 2012).

To compare between the two approaches, we have estimated global isoprene fluxes during 2019 using emission potential values ϵ_{PFT} instead of the emission potential data from the gridded maps ϵ_{map} used in the reference simulation. Figure 13 shows mean difference in isoprene emissions between the S2 simulation using ϵ_{PFT} and the reference simulation using ϵ_{map} . The total annual isoprene of simulation S2 is 390Tg, the data indicates that on a global scale, the isoprene emissions have decreased by 12%. As shown in Figure 11, this decrease is particularly pronounced in Australia (-58%) and South Africa (-25%). A notable increase is observed in Europe (+32%) and in South America (+19%), particularly in the northern Amazon.

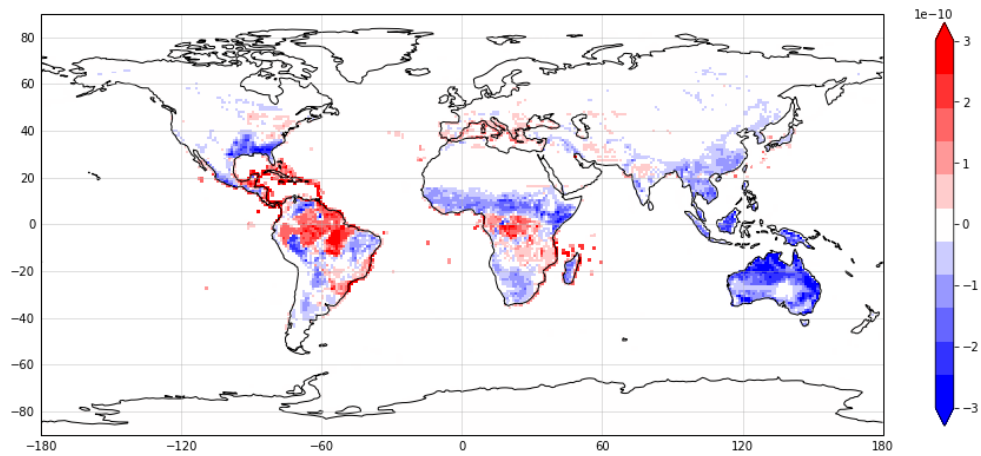


Figure 13. Annual mean isoprene difference (kg/m²/s) between sensitivity test S2 and reference simulation.

The results of this sensitivity test are aligned with the findings of Sindelarova et al. (2014). The MEGAN-MACC average annual isoprene emissions dropped by 14% when using the emission potential values ϵ_{PFT} instead of the emission potential map ϵ_{map} . The decrease concerns Australia (-47%) and South Africa (-28%) and the increase concerns South America (+10%) and Europe (+18%).

The results of this sensitivity test explains partially the differences observed in section 3. CAMS-GLOB-BIOv3.0 and ALBERI inventories used ϵ_{PFT} data to estimate isoprene flux, resulting in a lower isoprene emissions compared to other datasets, as annual isoprene flux dropped by 29% and 21% respectively compared to reference simulation. Sindelarova et al. (2022) reported a similar decrease rate in isoprene emissions estimated at 30% of CAMS-GLOB-BIOv3.0, which uses PFT-specific emission potential data and PFT distribution, compared to CAMS-GLOB-BIOv3.1, which uses isoprene emission potential gridded map.

4.3 Soil moisture

Prior research has investigated the association between soil moisture and isoprene emissions. Results indicate that isoprene emissions exhibit a three-phased response to drought and declining soil water. In the initial days of drought, plants tend to retain a stable isoprene emission rate, in some instances, the emission rate may even slightly increase (Pegoraro et al., 2007). The second stage starts when soil moisture falls below a specific threshold, at which point the rate of isoprene emission begins to decrease. Extended exposure to severe drought leads to a gradual decrease in isoprene emissions, eventually, the emissions became insignificant over time (Tingey et al. (1981) - Pegoraro et al. (2004b) - Wang et al. (2021) - Wang et al. (2022) - Trimmel et al. (2023)).

The response of isoprene emission to drought is simulated in MEGAN indirectly by the MEGAN canopy environment model by incorporating the leaf temperature estimate, which is affected by soil moisture. MEGAN also includes a γ_{SM} factor which

directly simulates the response of isoprene emission to drought. This factor is derived from soil moisture parameterization experiments conducted by Pegoraro et al. (2004a). The γ_{SM} is defined as follows:

$$\gamma_{SM} = 1 \quad \theta > \theta_1 \quad \gamma_{SM} = \frac{(\theta - \theta_w)}{\Delta\theta_1} \quad \theta_w < \theta < \theta_1 \quad \gamma_{SM} = 0 \quad \theta < \theta_w \quad (8)$$

425 where θ is soil moisture (volumetric water content, m³ m⁻³), θ_w (m³ m⁻³) is wilting point (the soil moisture level below which plants cannot absorb water from soil) and $\Delta\theta_1$ (=0.04) is an empirical parameter and $\theta_1 = \theta_w + \Delta\theta_1$ (Guenther et al., 2012). The third sensitivity test (S3) was conducted to examine the effect of soil moisture on isoprene emissions. To estimate γ_{SM} , MEGAN uses wilting point data calculated in SURFEX from the sand and clay covers given as input to the coupled model following Clapp and Hornberger (1978) and Lepistö et al. (1988) approaches. The sand and clay data are extracted from HWSD
430 (The Harmonised World Soil Database), which is a global soil database developed by the FAO (Food and Agriculture Organisation of the United Nations) in collaboration with IIASA (International Institute for Applied Systems Analysis) in order to provide information on the physical and chemical properties of soils across the world.

In order to accurately estimate soil moisture, a four-year spin-up period was required to stabilise the soil water content with the ISBA force-restore 2-L scheme. This approach is used to simulate the exchange of energy and water between the surface
435 and the atmosphere and is based on the balance between the forces that drive the exchange of energy and water (radiation, temperature, and precipitation) and the restoring forces that return the system to equilibrium (evaporation, transpiration, and runoff) (Boone et al., 1999) (Hu and Islam, 1995). The wilting point and soil water content are calculated at different soil layers, depending on the ISBA scheme model used. In ISBA force-restore 2-L scheme, the soil is represented with two layers. In the present study, to evaluate soil moisture impact on isoprene emissions, we have used soil moisture and wilting point data
440 from the second layer, as it most accurately represents the root depth of the vegetation.

The integration of the soil moisture algorithms led to a total isoprene emissions of 273Tg, with a global decrease of 38% compared to the reference simulation. Figure 14, 15 and 16 show the mean annual isoprene difference between S3 simulation and reference simulation, the spatial distribution of average γ_{SM} over 2019 and the mean annual soil liquid water content estimated at the second ISBA-2L layer as well as the relative wilting point data used in the S3 simulation respectively. The
445 decrease concerns mainly arid and semi-arid regions, the largest decrease can be observed in Australia (-89%), followed by North Africa and Middle East (-82%), South Africa (-67%) and East Africa (-38%). In South America, emissions are lower by 23% and the decrease is mainly located in Brazil.

Previous studies have studied the impact of soil moisture on isoprene emissions and have reported varying decrease rates. Guenther et al. (2006) obtained the lowest decrease rate of 7%, Müller et al. (2008) found a decrease rate of 21% and Sindelarova et al. (2014) reported the highest decrease rate of 50%. The discrepancies in the reported values of isoprene decrease
450 rate can be attributed to the use of different soil moisture and wilting point data. The latter, is a critical parameter, as it defines the limit below which, the soil moisture activity factor is set to 0, consequently, Guenther et al. (2012) stressed the importance of using consistent wilting point data with the soil moisture input. In this context, SURFEX-MEGAN model enhances the

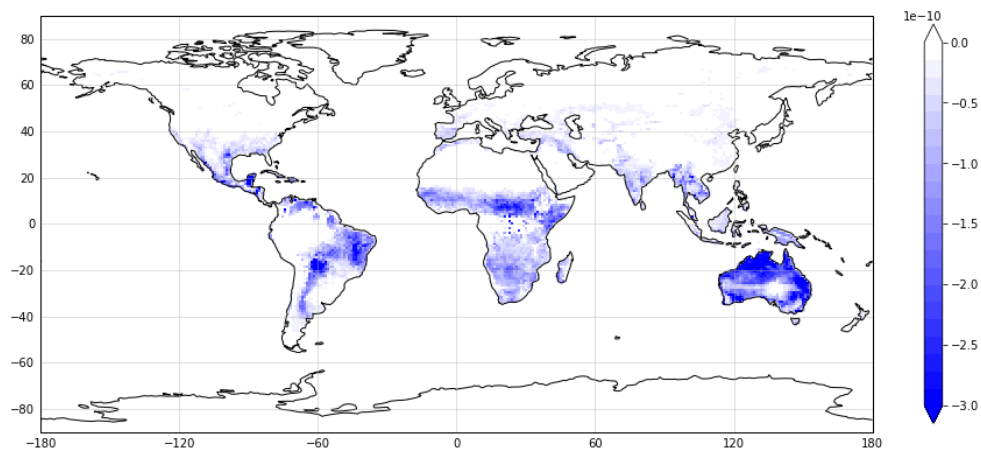


Figure 14. Annual mean isoprene difference (kg/m²/s) between sensitivity test S3 and reference simulation.

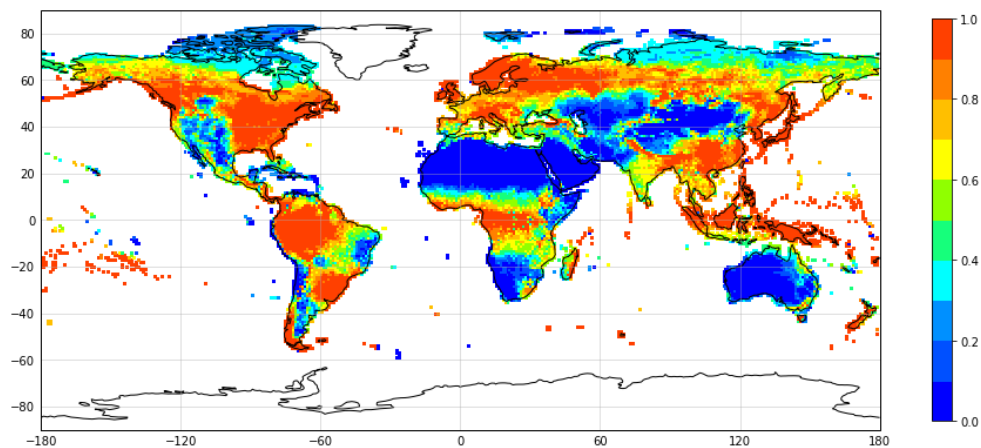


Figure 15. Spatial distribution of the mean annual soil moisture dependence factor γ_{SM} in S3 simulation.

precision of γ_{SM} calculation by using vegetation type-dependent soil moisture at a given layer and wilting point data at the
 455 same soil layer.

5 Conclusions

The presented paper describes the implementation of the biogenic model MEGANv2.1 (Guenther et al., 2012) in the surface
 model SURFEX (Le Moigne, 2018). The aim of this coupling is to improve the accuracy of vegetation type-specific param-
 eters for MEGAN2.1 by leveraging the detailed canopy environment model built into SURFEX. This improved accuracy, should
 460 lead to better estimates of BVOCs.

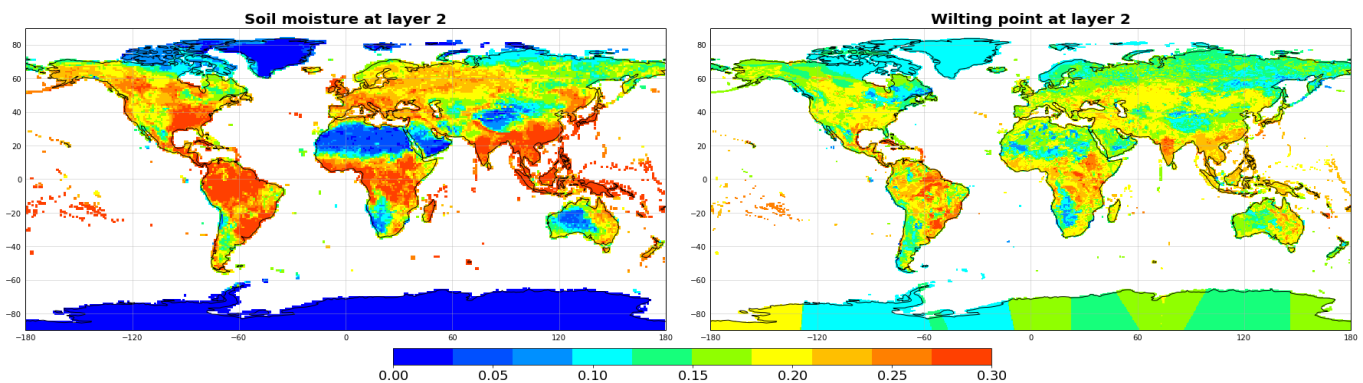


Figure 16. Annual average soil liquid water content (m³/m³) (left) and wilting point data (m³/m³) (right) of the ISBA-2L second layer.

The coupling validation was done by running a global simulation (1°, hourly) in 2019 using ERA5 meteorological data inputs. The total annual isoprene is estimated to be 443Tg. The SURFEX-MEGAN total annual isoprene is within the range of isoprene estimates reported in previous studies. To validate the coupled model, the 2019 isoprene simulation results were compared to isoprene estimates of 3 previous published studies. A spatial and temporal analysis were conducted to compare the different results. The SURFEX-MEGAN emission estimates were shown to have a comparable spatial distribution to the other inventories, especially to the ones using similar setup (e.g., meteorology, emission potential data). As for the monthly variation of isoprene emissions, SURFEX-MEGAN follows the same temporal pattern as some of the inventories, the shift in the annual isoprene cycle was explained by the difference in the contribution of the emitting regions to the global isoprene for each inventory.

A list of sensitivity tests was performed to investigate the impact of key MEGAN variables on isoprene emissions. To highlight the difference between the coupled SURFEX-MEGAN model and other MEGAN-based models, the results of the sensitivity tests were compared with the findings of other studies. The use of different meteorological forcings resulted in isoprene estimates varying up to +/- 5% of the reference run results, with Australia, South America and Africa being the most affected regions. The use of different input of emission potential data led to a decrease of 14% globally. The activation of the soil moisture parametrization was shown to have the greatest impact on isoprene emissions. On a global scale, the emission have decreased by 38%, the largest decrease was observed in Australia (-89%) and in Africa. The decrease rate related to the activation of the soil moisture activity factor varies across different studies, which has been attributed to inconsistencies in the soil moisture and wilting point data employed. The SURFEX-MEGAN model offers an advantage in this regard, as it can compute the wilting point and soil moisture at the same soil layer for different vegetation types, leading to a more precise estimation of the gamma soil moisture. This high sensitivity to soil moisture emphasises the importance of conducting further studies in this area in order to reduce uncertainties, in particular by refining the estimation of the empirical parameter $\Delta\theta_1$.

The potential perspectives to be explored from this study concern the assessment of biogenic emissions in future climates as BVOCs are expected to undergo significant changes resulting from the alteration of biogenic emission climate drivers. This

assessment is particularly relevant to air quality forecasting in the context of ongoing global warming and predicted future
485 climate change. In this respect, the particularity of SURFEX lies in its ability to be used in offline mode as it can be forced with
future climate meteorology. SURFEX also includes a biomass evolution sub-model, allowing the evolution of vegetation den-
sity (leaf area index) as a function of changing meteorological and environmental variables. This feature would be of particular
use for predicting biogenic emissions under future climate scenarios whereby the evolution in vegetation could be simulated in
SURFEX using the dynamic LAI vegetation scheme.

490 *Code availability.* The SURFEX code is available at: <https://www.umr-cnrm.fr/surfex/spip.php?rubrique8>. The MEGAN code is available
at: <https://bai.ess.uci.edu/megan/data-and-code/megan21>. The code for the coupled model SURFEX-MEGAN can be made available upon
request from Safae Oumami (safae.oumami@meteo.fr).

Author contributions. PT contributed to the implementation of MEGAN in MesoNH, to editing and revision of the paper. SO implemented
and developed the updates of the online SURFEX-MEGAN coupling, performed the simulations and complementary analyses, and drafted
495 the paper. VG and JA contributed to the design of the simulations, provision of the data, analysis and interpretation of the results, and editing
and revision of the paper. PH contributed to the editing and revision of the paper.

Competing interests. The authors declare that they have no competing interests.

Acknowledgements. We thank Alex Guenther and the University of California, Irvine (UCI) for providing the MEGANv2.1 code and the
necessary data. We thank the SURFEX team at CNRM for their invaluable assistance in facilitating the online coupling of SURFEX-
500 MEGAN, as well as for the provided access to the SURFEXv8.1 code and physiographic fields data. The ERA5 and IFS meteorological data
were provided by the European Centre for Medium-Range Weather Forecasts (ECMWF). The MERRA meteorological data was provided
by the NASA's Global Modelling and Assimilation Office (GMAO). The MEGAN-MACC and CAMS-GLOB-BIO isoprene emissions were
extracted from the Emissions of atmospheric Compounds and Compilation of Ancillary Data (ECCAD) database. The ALBERI isoprene
dataset was made available by the Tropospheric Modelling team of the Royal Belgian Institute for Space Aeronomy (BIRA-IASB).

505 **References**

- Arnth, A., Schurgers, G., Lathiere, J., Duhl, T., Beerling, D., Hewitt, C., Martin, M., and Guenther, A.: Global terrestrial isoprene emission models: sensitivity to variability in climate and vegetation, *Atmospheric Chemistry and Physics*, 11, 8037–8052, 2011.
- Atkinson, R. and Arey, J.: Atmospheric degradation of volatile organic compounds, *Chemical reviews*, 103, 4605–4638, 2003.
- Bauwens, M., Stavrakou, T., Müller, J.-F., Van Schaeybroeck, B., De Cruz, L., De Troch, R., Giot, O., Hamdi, R., Termonia, P., Laffineur, Q.,
510 et al.: Recent past (1979–2014) and future (2070–2099) isoprene fluxes over Europe simulated with the MEGAN–MOHYCAN model, *Biogeosciences*, 15, 3673–3690, 2018.
- Boone, A., Calvet, J.-C., and Noilhan, J.: Inclusion of a third soil layer in a land surface scheme using the force–restore method, *Journal of Applied Meteorology*, 38, 1611–1630, 1999.
- Calvet, J.-C., Noilhan, J., Roujean, J.-L., Bessemoulin, P., Cabelguenne, M., Olioso, A., and Wigneron, J.-P.: An interactive vegetation SVAT
515 model tested against data from six contrasting sites, *Agricultural and Forest Meteorology*, 92, 73–95, 1998.
- Carroll, G. T. and Kirschman, D. L.: A peripherally located air recirculation device containing an activated carbon filter reduces VOC levels in a simulated operating room, *ACS omega*, 2022.
- Chameides, W., Lindsay, R., Richardson, J., and Kiang, C.: The role of biogenic hydrocarbons in urban photochemical smog: Atlanta as a case study, *Science*, 241, 1473–1475, 1988.
- 520 Clapp, R. B. and Hornberger, G. M.: Empirical equations for some soil hydraulic properties, *Water resources research*, 14, 601–604, 1978.
- Déqué, M., Drevet, C., Braun, A., and Cariolle, D.: The ARPEGE/IFS atmosphere model: a contribution to the French community climate modelling, *Climate Dynamics*, 10, 249–266, 1994.
- Ervens, B., Turpin, B., and Weber, R.: Secondary organic aerosol formation in cloud droplets and aqueous particles (aqSOA): a review of laboratory, field and model studies, *Atmospheric Chemistry and Physics*, 11, 11 069–11 102, 2011.
- 525 Faroux, S., Kaptué Tchuenté, A., Roujean, J.-L., Masson, V., Martin, E., and Le Moigne, P.: ECOCLIMAP-II/Europe: A twofold database of ecosystems and surface parameters at 1 km resolution based on satellite information for use in land surface, meteorological and climate models, *Geoscientific Model Development*, 6, 563–582, 2013.
- Gent, P. R., Danabasoglu, G., Donner, L. J., Holland, M. M., Hunke, E. C., Jayne, S. R., Lawrence, D. M., Neale, R. B., Rasch, P. J., Vertenstein, M., et al.: The community climate system model version 4, *Journal of climate*, 24, 4973–4991, 2011.
- 530 Griffin, R. J., Cocker III, D. R., Seinfeld, J. H., and Dabdub, D.: Estimate of global atmospheric organic aerosol from oxidation of biogenic hydrocarbons, *Geophysical research letters*, 26, 2721–2724, 1999.
- Guenther, A., Hewitt, C. N., Erickson, D., Fall, R., Geron, C., Graedel, T., Harley, P., Klinger, L., Lerdau, M., McKay, W., et al.: A global model of natural volatile organic compound emissions, *Journal of Geophysical Research: Atmospheres*, 100, 8873–8892, 1995.
- Guenther, A., Karl, T., Harley, P., Wiedinmyer, C., Palmer, P. I., and Geron, C.: Estimates of global terrestrial isoprene emissions using
535 MEGAN (Model of Emissions of Gases and Aerosols from Nature), *Atmospheric Chemistry and Physics*, 6, 3181–3210, 2006.
- Guenther, A., Jiang, X., Heald, C. L., Sakulyanontvittaya, T., Duhl, T. a., Emmons, L., and Wang, X.: The Model of Emissions of Gases and Aerosols from Nature version 2.1 (MEGAN2. 1): an extended and updated framework for modeling biogenic emissions, *Geoscientific Model Development*, 5, 1471–1492, 2012.
- Guenther, A. B., Zimmerman, P. R., Harley, P. C., Monson, R. K., and Fall, R.: Isoprene and monoterpene emission rate variability: model
540 evaluations and sensitivity analyses, *Journal of Geophysical Research: Atmospheres*, 98, 12 609–12 617, 1993.

- Hansen, M. C., Potapov, P. V., Moore, R., Hancher, M., Turubanova, S. A., Tyukavina, A., Thau, D., Stehman, S. V., Goetz, S. J., Loveland, T. R., et al.: High-resolution global maps of 21st-century forest cover change, *science*, 342, 850–853, 2013.
- Henrot, A.-J., Stanelle, T., Schröder, S., Siegenthaler, C., Taraborrelli, D., and Schultz, M. G.: Implementation of the MEGAN (v2. 1) biogenic emission model in the ECHAM6-HAMMOZ chemistry climate model, *Geoscientific model development*, 10, 903–926, 2017.
- 545 Hersbach, H., Bell, B., Berrisford, P., Hirahara, S., Horányi, A., Muñoz-Sabater, J., Nicolas, J., Peubey, C., Radu, R., Schepers, D., et al.: The ERA5 global reanalysis, *Quarterly Journal of the Royal Meteorological Society*, 146, 1999–2049, 2020.
- Hester, R. E. and Harrison, R. M.: *Volatile organic compounds in the atmosphere*, vol. 4, Royal Society of Chemistry, 1995.
- Hu, Z. and Islam, S.: Prediction of ground surface temperature and soil moisture content by the force-restore method, *Water Resources Research*, 31, 2531–2539, 1995.
- 550 Jacovides, C., Tymvios, F., Asimakopoulos, D., Theofilou, K., and Pashiardes, S.: Global photosynthetically active radiation and its relationship with global solar radiation in the Eastern Mediterranean basin, *Theoretical and Applied Climatology*, 74, 227–233, 2003.
- Keeling, C., Piper, S., Bacatow, R., Wahlen, M., Whorf, T., Heimann, P., and Meijer, H.: 2005. Atmospheric CO₂ and 13CO₂ exchange with the terrestrial biosphere and oceans from 1978 to, 2000.
- Lac, C., Chaboureaud, J.-P., Masson, V., Pinty, J.-P., Tulet, P., Escobar, J., Leriche, M., Barthe, C., Aouizerats, B., Augros, C., et al.: Overview
555 of the Meso-NH model version 5.4 and its applications, *Geoscientific Model Development*, 11, 1929–1969, 2018.
- Le Moigne, P.: SURFEX scientific documentation, V8. 1, 2018.
- Lepistö, A., Whitehead, P., Neal, C., and Cosby, B.: Modelling the effects of acid deposition: Estimation of long-term water quality responses in forested catchments in Finland, *Hydrology Research*, 19, 99–120, 1988.
- Masson, V.: A physically-based scheme for the urban energy budget in atmospheric models, *Boundary-layer meteorology*, 94, 357–397,
560 2000.
- McDonald, B. C., De Gouw, J. A., Gilman, J. B., Jathar, S. H., Akherati, A., Cappa, C. D., Jimenez, J. L., Lee-Taylor, J., Hayes, P. L., McKeen, S. A., et al.: Volatile chemical products emerging as largest petrochemical source of urban organic emissions, *Science*, 359, 760–764, 2018.
- Messina, P., Lathière, J., Sindelarova, K., Vuichard, N., Granier, C., Ghattas, J., Cozic, A., and Hauglustaine, D. A.: Global biogenic volatile
565 organic compound emissions in the ORCHIDEE and MEGAN models and sensitivity to key parameters, *Atmospheric Chemistry and Physics*, 16, 14 169–14 202, 2016.
- Mironov, D., Heise, E., Kourzeneva, E., Ritter, B., Schneider, N., and Terzhevik, A.: Implementation of the lake parameterisation scheme FLake into the numerical weather prediction model COSMO, 2010.
- Müller, J.-F., Stavrakou, T., Wallens, S., De Smedt, I., Van Roozendaal, M., Potosnak, M., Rinne, J., Munger, B., Goldstein, A., and Guenther, A.:
570 A.: Global isoprene emissions estimated using MEGAN, ECMWF analyses and a detailed canopy environment model, *Atmospheric Chemistry and Physics*, 8, 1329–1341, 2008.
- Nagaraja Rao, C.: Photosynthetically active components of global solar radiation: measurements and model computations, *Archives for meteorology, geophysics, and bioclimatology, Series B*, 34, 353–364, 1984.
- Opacka, B., Müller, J.-F., Stavrakou, T., Bauwens, M., Sindelarova, K., Markova, J., and Guenther, A. B.: Global and regional impacts of
575 land cover changes on isoprene emissions derived from spaceborne data and the MEGAN model, *Atmospheric Chemistry and Physics*, 21, 8413–8436, 2021.

- Pegoraro, E., Rey, A., Bobich, E. G., Barron-Gafford, G., Grieve, K. A., Malhi, Y., and Murthy, R.: Effect of elevated CO₂ concentration and vapour pressure deficit on isoprene emission from leaves of *Populus deltoides* during drought, *Functional Plant Biology*, 31, 1137–1147, 2004a.
- 580 Pegoraro, E., Rey, A., Greenberg, J., Harley, P., Grace, J., Malhi, Y., and Guenther, A.: Effect of drought on isoprene emission rates from leaves of *Quercus virginiana* Mill., *Atmospheric Environment*, 38, 6149–6156, 2004b.
- Pegoraro, E., Potosnak, M. J., Monson, R. K., Rey, A., Barron-Gafford, G., and Osmond, C. B.: The effect of elevated CO₂, soil and atmospheric water deficit and seasonal phenology on leaf and ecosystem isoprene emission, *Functional Plant Biology*, 34, 774–784, 2007.
- Pugh, T., Ashworth, K., Wild, O., and Hewitt, C.: Effects of the spatial resolution of climate data on estimates of biogenic isoprene emissions, 585 *Atmospheric Environment*, 70, 1–6, 2013.
- Rajabi, H., Mosleh, M. H., Mandal, P., Lea-Langton, A., and Sedighi, M.: Emissions of volatile organic compounds from crude oil processing—Global emission inventory and environmental release, *Science of The Total Environment*, 727, 138 654, 2020.
- Rienecker, M. M., Suarez, M. J., Gelaro, R., Todling, R., Bacmeister, J., Liu, E., Bosilovich, M. G., Schubert, S. D., Takacs, L., Kim, G.-K., et al.: MERRA: NASA’s modern-era retrospective analysis for research and applications, *Journal of climate*, 24, 3624–3648, 2011.
- 590 Sakulyanontvittaya, T., Duhl, T., Wiedinmyer, C., Helmig, D., Matsunaga, S., Potosnak, M., Milford, J., and Guenther, A.: Monoterpene and sesquiterpene emission estimates for the United States, *Environmental science & technology*, 42, 1623–1629, 2008.
- Schoetter, R., Masson, V., Bourgeois, A., Pellegrino, M., and Lévy, J.-P.: Parametrisation of the variety of human behaviour related to building energy consumption in the Town Energy Balance (SURFEX-TEB v. 8.2), *Geoscientific Model Development*, 10, 2801–2831, 2017.
- Schoetter, R., Kwok, Y. T., de Munck, C., Lau, K. K. L., Wong, W. K., and Masson, V.: Multi-layer coupling between SURFEX-TEB-v9. 0 595 and Meso-NH-v5. 3 for modelling the urban climate of high-rise cities, *Geoscientific Model Development*, 13, 5609–5643, 2020.
- Shrivastava, M., Cappa, C. D., Fan, J., Goldstein, A. H., Guenther, A. B., Jimenez, J. L., Kuang, C., Laskin, A., Martin, S. T., Ng, N. L., et al.: Recent advances in understanding secondary organic aerosol: Implications for global climate forcing, *Reviews of Geophysics*, 55, 509–559, 2017.
- Sindelarova, K., Granier, C., Bouarar, I., Guenther, A., Tilmes, S., Stavrakou, T., Müller, J.-F., Kuhn, U., Stefani, P., and Knorr, W.: Global 600 data set of biogenic VOC emissions calculated by the MEGAN model over the last 30 years, *Atmospheric Chemistry and Physics*, 14, 9317–9341, 2014.
- Sindelarova, K., Markova, J., Simpson, D., Huszar, P., Karlicky, J., Darras, S., and Granier, C.: High-resolution biogenic global emission inventory for the time period 2000–2019 for air quality modelling, *Earth System Science Data*, 14, 251–270, 2022.
- Tingey, D. T., Evans, R., and Gumpertz, M.: Effects of environmental conditions on isoprene emission from live oak, *Planta*, 152, 565–570, 605 1981.
- Trimmel, H., Hamer, P., Mayer, M., Schreier, S. F., Weihs, P., Eitzinger, J., Sandén, H., Fitzky, A. C., Richter, A., Calvet, J.-C., et al.: The influence of vegetation drought stress on formaldehyde and ozone distributions over a central European city, *Atmospheric Environment*, 304, 119 768, 2023.
- Wallens, S.: Modélisation des émissions de composés organiques volatils par la végétation, 2004.
- 610 Wang, P., Liu, Y., Dai, J., Fu, X., Wang, X., Guenther, A., and Wang, T.: Isoprene emissions response to drought and the impacts on ozone and SOA in China, *Journal of Geophysical Research: Atmospheres*, 126, e2020JD033 263, 2021.
- Wang, Y., Lin, N., Li, W., Guenther, A., Lam, J. C., Tai, A. P., Potosnak, M. J., and Seco, R.: Satellite-derived constraints on the effect of drought stress on biogenic isoprene emissions in the southeastern US, *Atmospheric Chemistry and Physics*, 22, 14 189–14 208, 2022.

Zhang, M., Zhao, C., Yang, Y., Du, Q., Shen, Y., Lin, S., Gu, D., Su, W., and Liu, C.: Modeling sensitivities of BVOCs to different versions of MEGAN emission schemes in WRF-Chem (v3. 6) and its impacts over eastern China, *Geoscientific Model Development*, 14, 6155–6175, 2021.

Zsebeházi, G. and Szépszó, G.: Modeling the urban climate of Budapest using the SURFEX land surface model driven by the ALADIN-Climate regional climate model results, *IDŐJÁRÁS/QUARTERLY JOURNAL OF THE HUNGARIAN METEOROLOGICAL SERVICE*, 124, 191–207, 2020.

4.4 Conclusion of Chapter 4

To examine the evolution of biogenic emissions under future climate conditions, a coupling between the SURFEX model and the MEGAN model was implemented.

The primary objective of this coupling is to simulate biogenic emissions within present and future climate conditions, as the SURFEX model can be used in an offline model (i.e. using an external meteorological forcing file). Furthermore, the CO_2 -responsive scheme incorporated within SURFEX allows the estimation of leaf area index. This parameter is predicted to undergo significant alterations in response to climate change. The incorporation of this scheme contributes significantly to providing a more accurate representation of the vegetation density and distribution in a changing climate. Consequently, it improves the precision of biogenic emission estimations in future scenarios.

The coupled model was validated by comparing the 2019 total annual isoprene emissions with other MEGAN-based inventories. The SURFEX-MEGAN total annual isoprene is estimated to be 443Tg. This value is within the range of isoprene estimates reported in previous studies. In the following chapter, we will explore the effects of climate change on isoprene emissions, particularly within the context of a $+2^\circ C$ global temperature increase. Additionally, we will conduct an in-depth investigation to determine the key driving factors controlling future trends in isoprene emissions.

Impact of a +2°C climate on isoprene emissions

As detailed in the preceding chapters, biogenic organic compounds represent a key element in conditioning the current and future states of atmospheric chemistry and climate. Their interactions with the atmosphere lead to the formation of ozone and SOAs, both of which are recognized as substantial air pollutants. These components exert distinct impacts on climate. SOAs contribute to a cooling effect, whereas ozone and methane have a warming influence. Hence, it is of paramount importance to anticipate the future evolution of biogenic emissions, given their high sensitivity to temperature, which is projected to rise as a consequence of climate change. This assessment is crucial for predicting future air quality and understanding the feedback mechanisms introduced by BVOCs into the climate system. This includes their significant contribution to radiative forcing through aerosols, ozone and methane, all of which are directly influenced by BVOC emissions.

In this Chapter, we will explore the effect of climate change on biogenic emissions using the coupled SURFEX-MEGAN model. Our primary emphasis will be on evaluating the future changes in isoprene levels according to a warming level of +2°C relative to 1850-1900.

5.1 Methodology

Isoprene simulations were conducted using the SURFEX-MEGAN model, at a spatial grid resolution of $1.4^\circ \times 1.4^\circ$. To conduct a comparative analysis of current and future isoprene emissions, two distinct simulations were performed: one representing the present climate over **2010-2014** and another reflecting future isoprene emissions covering **2046-2050**.

The meteorological data used for the future-climate simulation was derived from the outputs of the **CNRM-ESM2-1** Earth System Model¹ (ESM) (S  f  rian et al., 2019), applied to the SSP3-

¹Earth System Models are used to simulate the interactions and processes that occur within the Earth's various interconnected systems: atmosphere, oceans, land surface, ice sheets and biogeochemical cycles. These models are designed to provide a comprehensive representation of the Earth's climate system and its underlying

7.0 GHG emission scenario at a spatial resolution of 1.4°. The CNRM-ESM2-1 ESM model, jointly developed by CNRM and CERFACS (Centre Européen de Recherche et de Formation Avancée en Calcul Scientifique, in French), is one of the ESM models used in the CMIP6 project, its findings were integrated into the IPCC’s sixth assessment report. The present-climate simulation was also carried out using the CNRM-ESM2-1 ESM historical outputs representing the industrial-era climate (1850-2014).

The historical ($HIST_{2010-2014}$) and the future-climate ($FUT_{2046-2050}$) simulations of SURFEX-MEGAN were performed using the ISBA-A-gs photosynthesis scheme. This scheme incorporates the NCB prognostic biomass option, enabling the dynamic evolution of leaf area index as a function of weather and soil conditions. The NCB option includes six biomass pools: leaves, twigs, stems, wood, roots (fines and woody roots) and a storage of nonstructural carbohydrates. To ensure a comprehensive representation of soil processes, we adopted the ISBA diffusion scheme with 14 layers to model soil heat and water exchange. The land coverage distribution and associated parameters were derived from the ECOCLIMAP-II dataset (Faroux et al., 2013).

Importantly, for both the present and future climate simulations, we assumed that the vegetation distribution remains static only vegetation density varies. We acquired land cover and land use data from ECOCLIMAP-II for both simulation scenarios. It is worth noting that changes in vegetation distribution occur only when the LAI of a specific plant functional type reaches zero, implying the extinction of that vegetation type. However, for example, if a location contains crops, these cannot transform into shrub vegetation in the future. The assumption adopted, that land cover and land use remain unchanged, is consistent with the results of Ward et al. (2014) and Hurtt et al. (2011), suggesting that predicted changes in land use and land cover in the future are less significant than what has occurred in the past.

Unless explicitly mentioned, we excluded the influence of soil moisture on biogenic emissions ($\gamma_{sm} = 1$). Additionally, we accounted for the inhibitory effect of CO_2 on isoprene emissions in both simulation cases. The inclusion of the CO_2 effect was done following the Heald et al. (2009) parametrization (Chapter 4). The detail of historical and future-climate simulations setup is represented in Table 5.1.

Simulation	Description	Period	γ_{CO_2}	γ_{SM}	LAI
$HIST_{2010-2014}$	Present-climate simulation	2010-2014	On	Off	Prognostic
$FUT_{2046-2050}$	Future-climate simulation	2046-2050	On	Off	Prognostic

Table 5.1: Description of the present- and future-climate simulations setup.

physical, chemical and biological processes.

5.2 SSP3-7.0 fields analysis

According to the IPCC's Sixth Assessment Report, the SSP3-7.0 scenario is expected to result in a temperature rise of approximately +2°C by 2037-2056. The primary objective of this chapter is to assess biogenic emission fluxes under a +2°C climate change scenario. However, due to computational limitations, running the SURFEX-MEGAN model for all biogenic species throughout the 2037-2056 period proved unfeasible within the computational resources available for our study. Consequently, the focus shifted to conducting simulations for a shorter timeframe, solely considering the most prevalent biogenic compound, isoprene. The selection of the 2046-2050 period for the future climate simulation was determined by the point at which the SSP3-7.0 scenario achieves a +2°C increase compared to the pre-industrial period of 1850-1900, as illustrated in Figure 5.1. Within this interval, the temperature deviation from the 1850-1900 baseline is approximately 2°C (= 1.94°C).

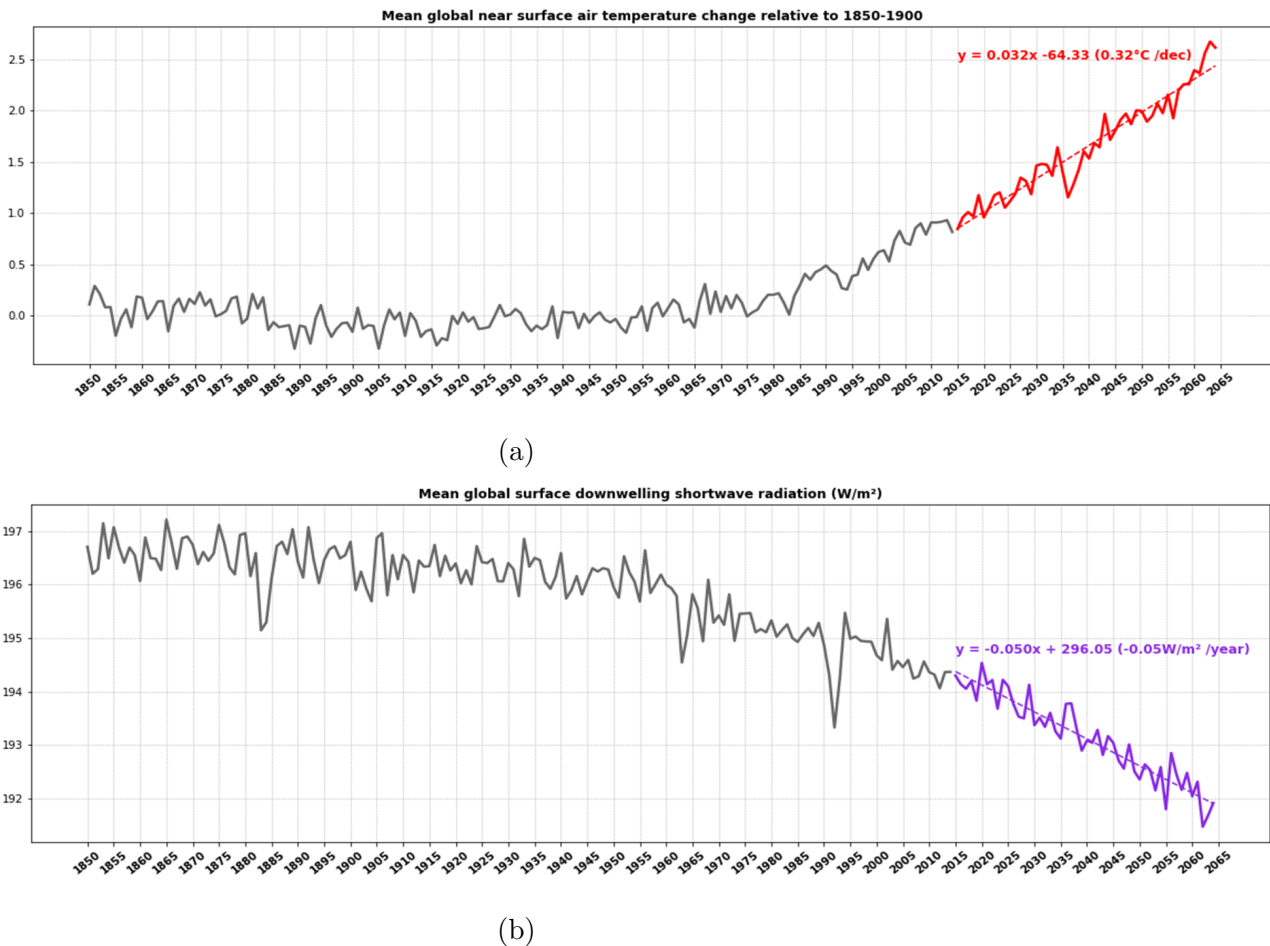


Figure 5.1: Mean annual global near surface air temperature change relative to 1850-1900 (a) and mean annual global surface downwelling shortwave radiation (W/m^2) (b). SSP3-7.0 temperature and shortwave radiation data are represented in red and blueviolet, respectively. The temperature and solar radiation linear regression plot is represented in dashed line.

Furthermore, we have investigated alterations in global surface downwelling shortwave radiation for the SSP3-7.0 scenario. This specific factor holds paramount importance in assessing the anticipated evolution of biogenic emissions under future climate conditions. As illustrated in Figure 5.1b, a notable decrease in incoming solar radiation is observed for the SSP3-7.0 scenario, persisting until 2065. This decline can be attributed to various intricately interacting components within the atmosphere, which are influenced by trends in water vapor, aerosols and cloud dynamics.

As outlined in Chapter 4, the influence of climate change on the release of biogenic emissions is multifaceted. It arises not only from the direct effects of temperature and solar radiation on emission mechanisms, but also from shifts in vegetation density due to changing precipitation and evapotranspiration patterns. These alterations can also impact the emission of biogenic compounds through drought and soil water unavailability. Additionally, the concentration of atmospheric CO_2 plays a significant role in influencing the emission of BVOCs, both directly through its inhibitory effect and indirectly by affecting biomass density. In this context, CO_2 is a critical factor in modeling photosynthetic processes that enhance plant growth.

Figure 5.2 illustrates the changes in mean annual leaf area index, precipitation flux and CO_2 volume mixing ratio simulated using the SSP3-7.0 scenario from 2015 to 2050. As depicted in Figure 5.2, the mean annual global precipitation is projected to increase with global warming, in line with findings from the 6th assessment report by the IPCC. This increase can be attributed to the combined influence of two key factors: fast atmospheric adjustments and slow-temperature driven responses.

The term "fast atmospheric adjustments" refers to properties of the atmosphere that exhibit near-instantaneous responses to radiative forcing, including air temperature, water vapor and clouds. These properties impact the frequency of precipitation events. In contrast, "slow-temperature driven responses" refer to atmospheric reactions occurring over more extended periods, which influence the intensity of precipitation.

The observed rise in atmospheric CO_2 concentration, coupled with changes in soil water availability and other relevant parameters, contributes to the overall upward trend in the modeled leaf area index using the ISBA-A-gs model, a phenomenon commonly referred to as the " **CO_2 fertilization effect**". It is important to note that the unusually high LAI values observed in 2015 are not generated by the ISBA model; instead, they are derived from ECOCLIMAP-II data and used as initial conditions for the SURFEX model.

5.3 Isoprene in present and future climate

Figure 5.3 illustrates the evolution of annual isoprene levels in present- and future-climate conditions. The present-climate total annual isoprene varies between 303 Tg and 313 Tg.

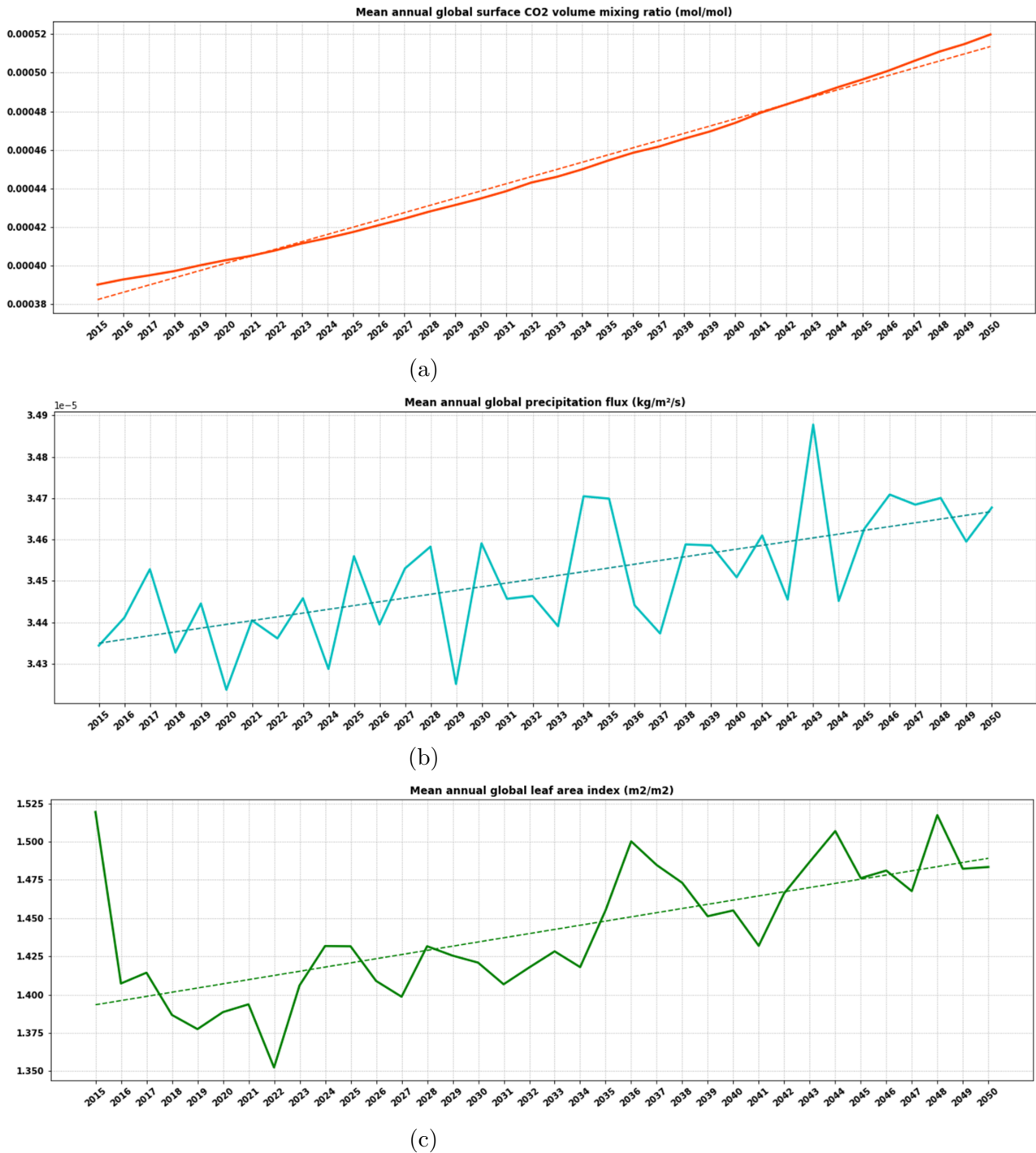


Figure 5.2: Mean annual global surface CO_2 volume mixing ratio in mol/mol (a), mean annual global precipitation flux in $kg/m^2/s$ (b) and mean annual global leaf area index in m^2/m^2 (c) over the period 2015-2050. The linear regression line for the three parameters is represented in dashed line.

The highest and lowest values were observed in 2010 and 2013, respectively, with an average annual isoprene estimate of approximately **307 Tg**. The SURFEX-MEGAN historical isoprene estimates are in agreement with other MEGAN-based isoprene inventories. CAMS-GLOB-BIOv3.0 estimated a similar total annual isoprene average of 298 Tg over the period 2010-2014. The SURFEX-MEGAN future-climate isoprene estimates indicate a **13%** increase compared to 2010-2014. The mean total annual isoprene averaged over 2046-2050 is estimated to **347 Tg**, exhibiting slight interannual variability, with isoprene levels ranging from a minimum of 318 Tg to a peak of 363 Tg, projected for 2046.

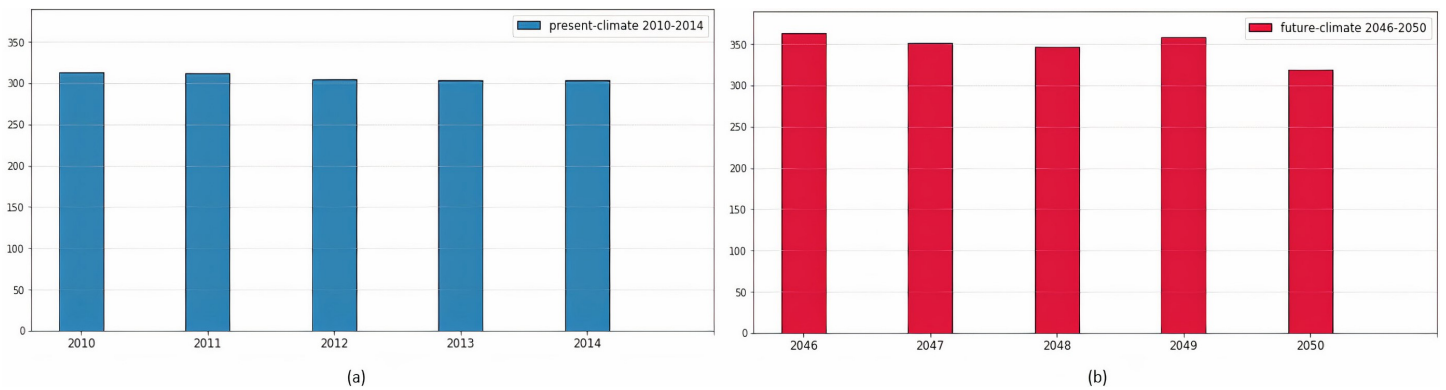


Figure 5.3: Total annual isoprene estimated with SURFEX-MEGAN over 2010-2014 (a) and 2046-2050 (b) in Tg.

As shown in Figure 5.4, isoprene emissions are expected to increase in a $+2^{\circ}\text{C}$ climate change level by 40 Tg. It is worth noting that this warming level is relative to the pre-industrial era and it corresponds only to a $+1^{\circ}\text{C}$ increase compared to present climate conditions. The increase in isoprene emissions is observed at a global scale. Regions like South America, Southern Africa and Southeast Asia, experienced the highest increase rates of 16%, 20% and 12%, respectively. In other low-isoprene emission regions such as Europe, Australia, North Africa and Russia, the isoprene increase rate is estimated to 10%, 7%, 14% and 9%, respectively.

To understand the origin of this rise, we conducted an in-depth examination of various factors influencing isoprene emissions, namely temperature, solar radiation, leaf area index and atmospheric concentration of carbon dioxide (CO_2).

As shown in Figure 5.5, according to the ISBA-A-gs estimates, LAI is expected to increase at global scale by 8% in 2046-2050 compared to 2010-2014. This rise is most prominent in high latitudes and in some areas in subtropical regions including North America, Europe, Russia and Southeast Asia, where vegetation density increased by 15%, 13%, 12% and 7%, respectively. However, in other regions particularly Southern Africa and some parts of South America, with projected high temperatures and low precipitations, LAI is expected to decline as a response to the soil moisture decreasing availability. These patterns in leaf area index can be explained by atmospheric CO_2 concentrations and soil moisture trends, the latter is

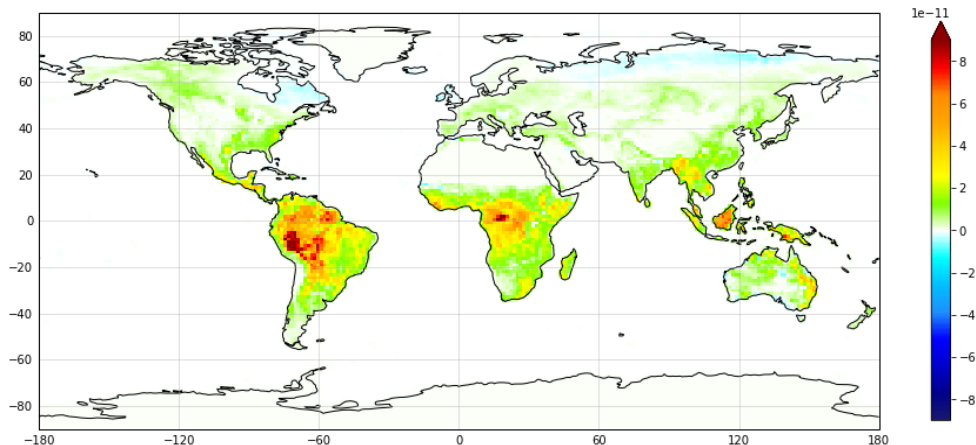


Figure 5.4: Absolute difference of SURFEX-MEGAN isoprene mean emission flux between 2046-2055 and 2010-2014 in $\text{kg}/\text{m}^2/\text{s}$.

influenced by precipitation and evapotranspiration. The projected shifts in leaf area index in 2046-2050 relative to 2010-2014 are consistent with the findings of Mahowald et al. (2016), who analyzed LAI projections of several CMIP5 earth system models under RCP4.5 and RCP8.5 scenarios. The results of this study highlight that by 2040 throughout the end of the century, the LAI will increase over most regions of the globe mainly over mountains and high latitudes and will decrease in some parts of the tropics including parts of Southern Africa and some parts of Central and South America.

The projected rise in isoprene emissions, can also be attributed to the increasing near-surface temperature levels resulting from the increase in greenhouse gases concentrations in the future. According to the SSP3-7.0 scenario, there is an anticipated increase of $1.3\text{ }^\circ\text{C}$ in near-surface temperature in 2046-2050 relative to 2010-2014. The most substantial temperature rise is anticipated in North Africa, with a temperature difference exceeding $1.5\text{ }^\circ\text{C}$. In South America, Southeast Asia, Southern Africa and Russia, the temperature rise is expected to exceed $1.1\text{ }^\circ\text{C}$. Meanwhile, in other global regions such as Australia, North America and Europe, the temperature is projected to rise by only $0.9\text{ }^\circ\text{C}$, $0.7\text{ }^\circ\text{C}$ and $0.4\text{ }^\circ\text{C}$ respectively.

Similarly, the amount of incoming solar radiation will shift in future climate as a result of trends in water vapor, aerosols and cloud dynamics. As shown in Figure 5.5, incoming short-wave radiation flux will decrease at a global scale by $1.5\text{ W}/\text{m}^2$ under the SSP3-7.0 scenario in 2046-2050 relative to 2010-2014. This decrease is particularly pronounced in Russia, Southeast Asia, Europe and North America. In high-isoprene emitting tropical regions including the Amazonian rainforest and some regions in Southern Africa, a significant increase in incoming solar flux is noted.

The increasing concentrations of CO_2 in future climate have two fold impact on isoprene emission. A positive impact, through the increase of vegetation density (LAI) resulting from the CO_2 fertilization effect and a negative impact represented by the inhibitory effect of atmospheric

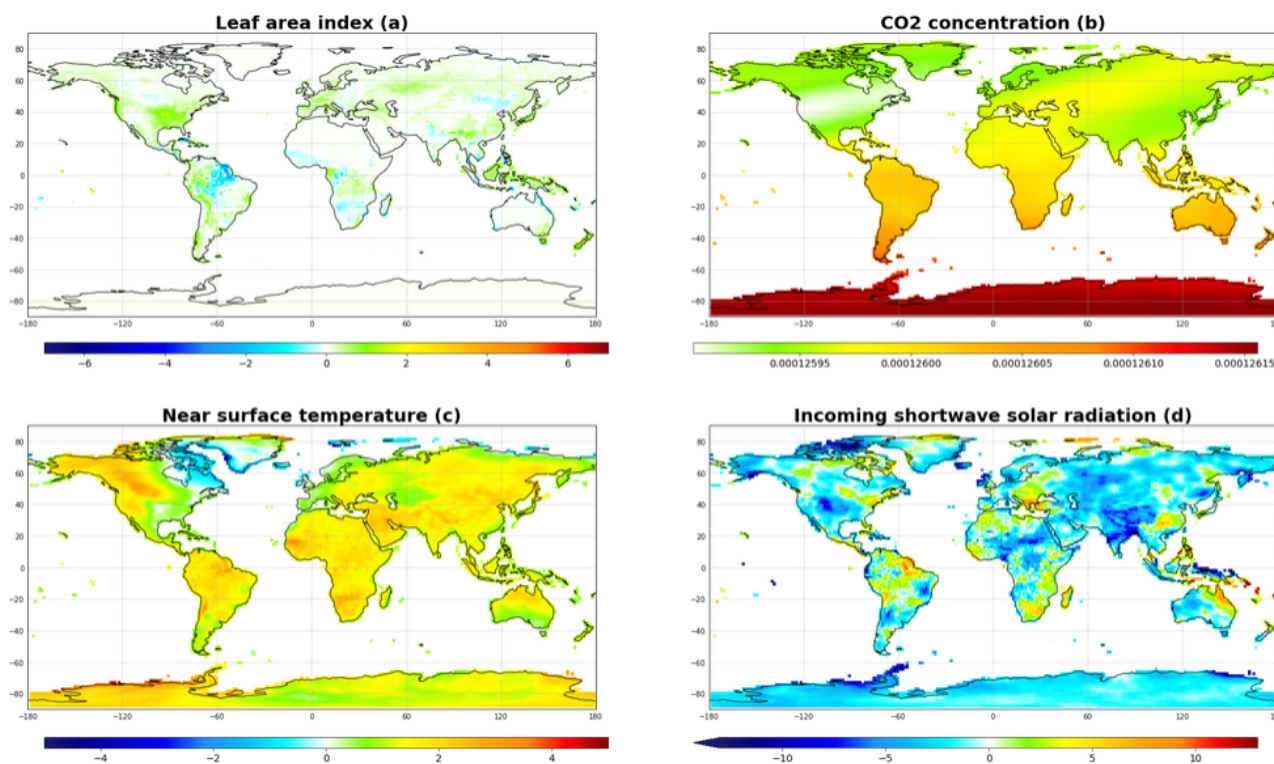


Figure 5.5: Absolute difference of SURFEX-MEGAN simulated leaf area index in m^2/m^2 (a), CO_2 volume mixing ratio in mol/mol (b), near surface air temperature in $^\circ\text{C}$ (c) and incoming shortwave radiation in W/m^2 (d) between (2046-2055) and (2010-2014).

CO_2 concentrations on isoprene emissions as detailed in Chapter 4. The SURFEX-MEGAN inhibition factor adopts the Heald et al. (2009) parametrization which penalizes isoprene emissions under atmospheric CO_2 concentrations exceeding 400ppm Sindelarova et al. (2014). At a global scale atmospheric CO_2 concentrations increased by 32% under SSP3-7.0 scenario over the period 2046-2050 compared to 2010-2014. In most isoprene emitting regions, atmospheric CO_2 concentrations exceeded 600ppm , leading to a substantial reduction in isoprene emissions trends through the inhibitory effect of carbon dioxide.

5.4 Attribution of isoprene changes

In the preceding section, we outlined the anticipated shifts in isoprene emissions under future-climate conditions, considering a comprehensive range of meteorological (e.g., temperature, solar radiation) and environmental factors (e.g., leaf area index, CO_2 concentrations) that influence the emission of biogenic species. However, this analysis lacks a detailed breakdown of the individual contribution of each of these factors to the projected trends in isoprene emissions. Therefore, in this section, we will attempt to assess the variations in isoprene emissions between the present and the future through four distinct scenarios: considering solely the **impact of**

Simulation	Description	γ_{CO_2}	LAI	Isoprene
Present-climate simulations (2014)				
<i>HIST</i>	Present-climate with prescribed LAI	Off	ECOCLIMAP	364 Tg
<i>HIST_{LAI}</i>	Present-climate with 2014 prognostic LAI	Off	ISBA-A-gs(2014)	299 Tg
Future-climate simulations (2050)				
<i>FUT</i>	Future-climate with prescribed LAI	Off	ECOCLIMAP	427 Tg
<i>FUT_{LAI}</i>	Future-climate with 2050 prognostic LAI	Off	ISBA-A-gs	349 Tg
<i>FUT_{CO₂}</i>	Future-climate with prescribed LAI and CO_2 inhibition	On	ECOCLIMAP	395 Tg
<i>FUT_{LAI,CO₂}</i>	Future-climate with 2050 prognostic LAI and CO_2 inhibition	On	ISBA-A-gs	323 Tg

Table 5.2: Description of the simulations used in the sensitivity analysis along with the total annual isoprene emission in Tg estimated with SURFEX-MEGAN.

climate change, considering both **climate change and the evolution of vegetation density**, considering the **impact of climate change and the inhibitory effect of CO_2** and finally, considering the combined **impact of climate change, alterations in vegetation density and the inhibitory effect of CO_2** .

In this sensitivity analysis, we conducted simulations using the SURFEX-MEGAN model for a brief period of one year: 2014 and 2050 to represent current and future climate conditions, respectively. Table 5.2 provides a concise summary of the setup used in this sensitivity analysis.

HIST represents the simulation depicting the current climate conditions (2014). The AST CPHOTO option is applied, deactivating the biomass evolution sub-model in ISBA. Consequently, the LAI data utilized in this simulation are derived from the climatological LAI dataset extracted from the ECOCLIMAP database. *HIST_{LAI}* is also a present-climate simulation, but the LAI data was not prescribed but rather simulated with the ISBA scheme. *FUT* is the simulation for future climate conditions (2050), where the biomass evolution sub-model was disabled and the LAI was prescribed based on the climatology database ECOCLIMAP. *FUT_{LAI}* is also a future-climate simulation, with the CO_2 inhibition factor deactivated and the LAI determined through the ISBA-A-gs biomass evolution sub-model. *FUT_{CO₂}* employs prescribed ECOCLIMAP LAI data while accounting for the CO_2 inhibitory effect. *FUT_{LAI,CO₂}* employs the ISBA-A-gs diagnosed LAI while factoring in the CO_2 inhibition effect.

5.4.1 Climate change

The isolated impact of climate change on isoprene emissions is assessed by comparing the present-climate *HIST* simulation and the future-climate *FUT* simulation. Both simulations were run using a horizontal resolution of 1.4° and a 10-day time step LAI extracted from the ECOCLIMAP database. In this study, the impact of climate change refers only to the effect of meteorological factors (e.g., temperature, PAR) on isoprene release.

The total annual isoprene emissions were estimated at 364 Tg and 427Tg for *HIST* and *FUT* simulations, respectively. When considering only the impact of meteorological factors, which include both temperature and incoming solar flux, isoprene emissions experienced a notable increase of **17%** with a difference of **63 Tg**.

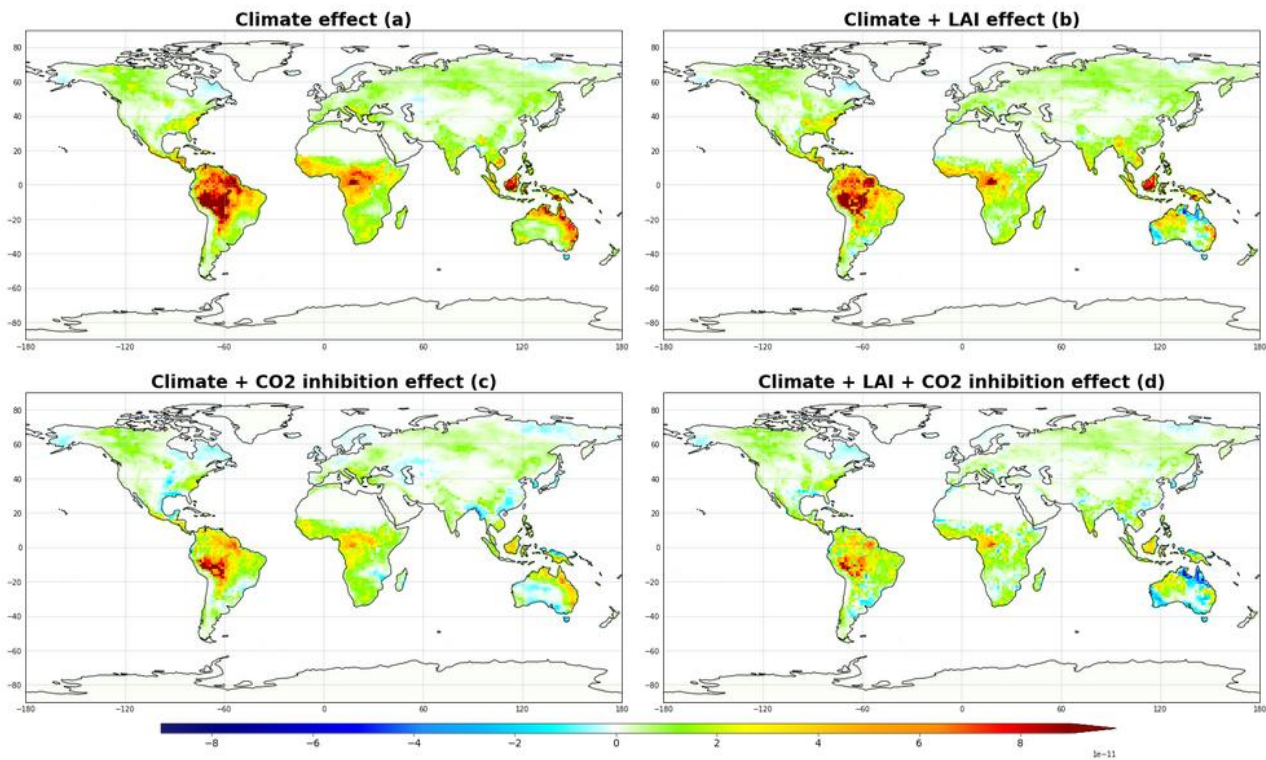


Figure 5.6: Impact of climate change (a), climate change and LAI (b), climate change and CO_2 inhibition factor (c) and climate change, LAI and CO_2 inhibition factor (d) on isoprene emissions between 2050 and 2014 for the SSP3-7.0 scenario.

As depicted in Figure 5.6, when accounting only for meteorological effects, isoprene emissions experienced a global increase, particularly in subtropical regions known for their dense vegetation, such as South America and Southern Africa. In these regions, isoprene emissions increased by 21% and 16%, respectively. As illustrated in Figure 5.7, in South America, there was a temperature rise of 2°C alongside a decrease in incoming solar radiation flux of 0.9 W/m^2 . This indicates that the observed increase in South America was primarily driven by temperature. In other regions across the globe, specifically Europe, Southeast Asia, North Africa,

North America and Australia, the estimated rates of isoprene increase are approximately 19%, 13%, 17%, 17% and 12%, respectively. The rise in isoprene levels in these regions exhibits a strong correlation with the temperature shift, as isoprene emissions increase exponentially with temperature. Notably, in Australia, the spatial pattern of isoprene alteration follows the distribution of temperature, which has experienced an increase of nearly 1° in this area.

These findings align with the conclusions drawn by Cao et al. (2021), who conducted a regression analysis on isoprene emissions predicted by the CMIP6 models to explore the individual contribution of temperature, solar radiation and CO_2 in explaining future isoprene trends. This study demonstrated that, for SSP3.7-0, temperature plays the dominant role in explaining future isoprene projections compared to other factors. Although solar radiation exhibits a negative impact due to its decline in high isoprene-emitting regions, its influence remains relatively limited in comparison to temperature.

Tai et al. (2013) have also investigated isoprene evolution with the MEGANv2.1 model in 2050 compared to 2010 under the IPCC SRES² A1B scenario. This scenario projects a +2.8°C temperature increase by the end of the 21st century compared to 1980-1999. The results of this study show that considering only the impact of climate change, isoprene emissions have increased by 29% ($\sim 112 \text{ Tg C yr}^{-1}$).

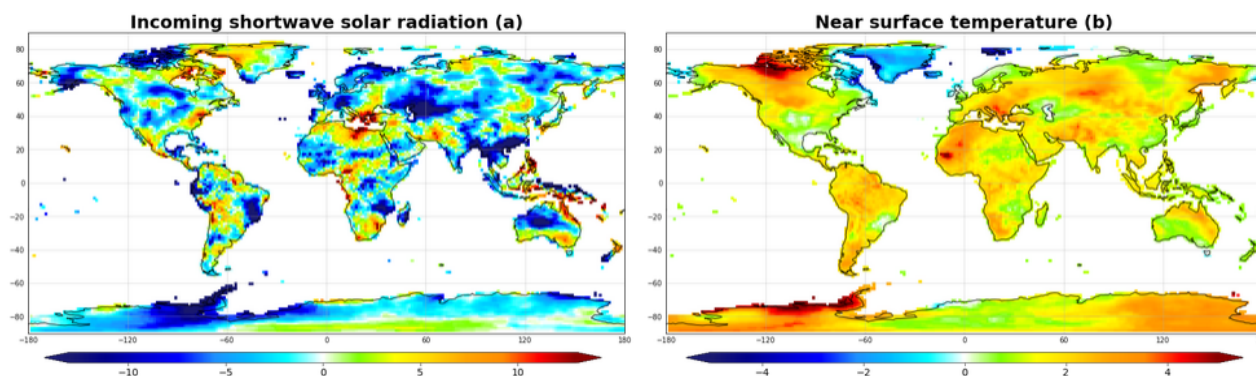


Figure 5.7: Absolute difference of near surface air temperature in °C (a) and incoming shortwave radiation in W/m^2 (c) between 2050 and 2014.

Similar studies were conducted in a regional scale. In their research, Bauwens et al. (2018) examined the impact of various isoprene drivers in Europe, under RCP2.6, RCP4.5 and RCP8.5 scenarios using the MOHYCAN (Model of HYdrocarbon emissions by the CANopy) model coupled to MEGAN. The findings of this study predict significant regional isoprene increase rates ranging between 7% to 110% in 2070-2099 relative to 1979-2014. In this regard, the SURFEX-MEGAN model projected an increase of 20% in Europe by 2050 compared to 2014 under the SSP3-7.0 scenario. As seen in Chapter 3, SSP3-7.0 is the scenario between RCP6.0 and RCP8.5.

²The SRES scenarios are from the IPCC's fourth assessment report.

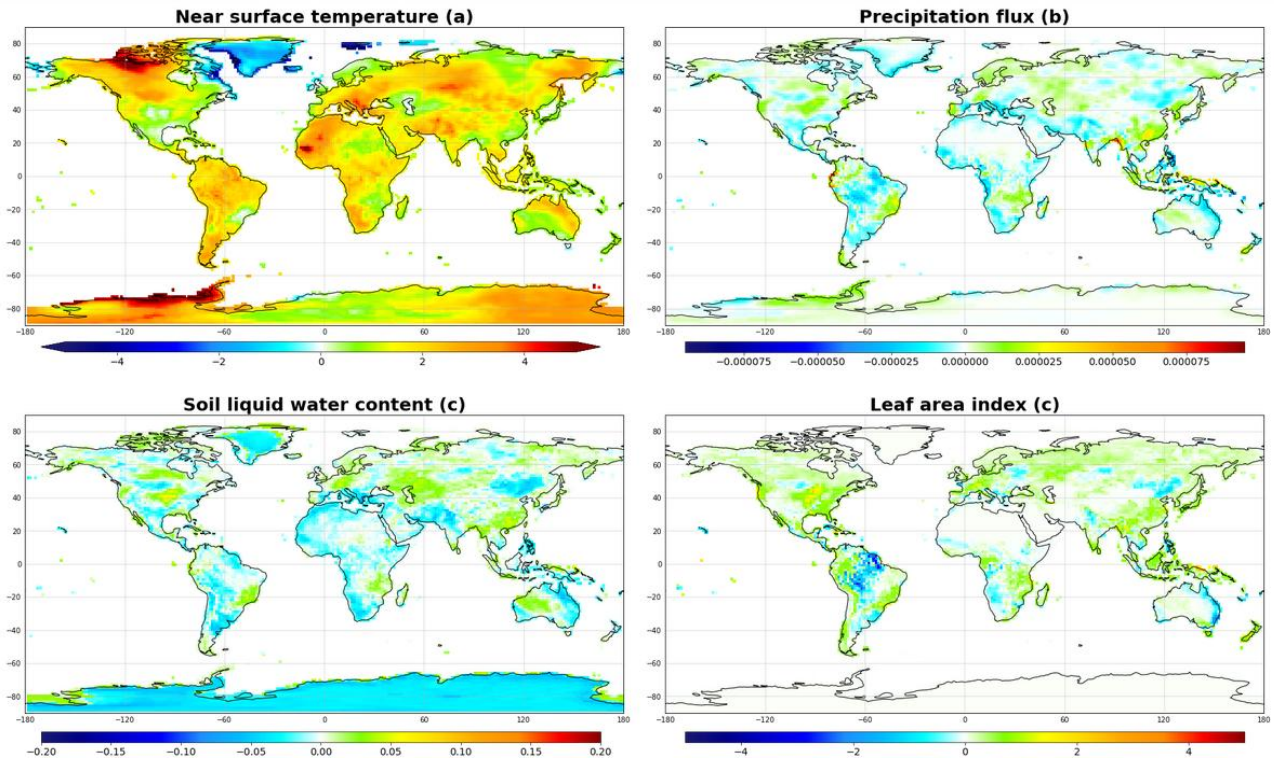


Figure 5.8: Absolute difference of temperature (a) in $^{\circ}\text{C}$, precipitation flux (b) in $\text{kg}/\text{m}^2/\text{s}$, soil liquid water content at the first DIFF layer (c) in m^3/m^3 and SURFEX-MEGAN simulated leaf area index in m^2/m^2 (d) between FUT_{LAI} and $HIST_{LAI}$.

The discrepancies in isoprene change attributed solely to the impact of climate change across the different studies can be linked to several factors. The latter include the specific climate change scenario selected, the scale at which the study is conducted and the historical as well as future climate periods chosen for comparison.

5.4.2 Climate change and Leaf Area Index

The significance of accounting for changes in vegetation density is evaluated by comparing $HIST_{LAI}$ and FUT_{LAI} . These simulations represent present and future climate conditions, incorporating the ISBA-A-gs dynamic LAI model to simulate vegetation density characteristic of 2014 and 2050, respectively.

The total annual isoprene emissions were estimated at 299 Tg and 349 Tg for $HIST_{LAI}$ and FUT_{LAI} simulations, respectively. When considering the combined effect of climate change with fixed vegetation and dynamic LAI, isoprene emissions increased by **16% \sim 50 Tg** under the SSP3-7.0 scenario in 2050 relative to 2014.

As illustrated in Figure 5.8, leaf area index experienced a global increase of 8% in 2050 compared to 2014. This augmentation is a direct consequence of the anticipated rise in CO_2 concentrations associated with the SSP3-7.0 scenario, leading to heightened photosynthesis and

subsequent biomass growth. Nevertheless, it is imperative to note that CO_2 concentrations alone cannot fully account for the observed LAI trends in the future. In fact, LAI variations are closely linked to other meteorological variables, mainly precipitation and temperature. As shown in Figure 5.8, the evolution of leaf area index is primarily influenced by precipitation and soil moisture patterns. However, in some regions, temperature also plays a significant role alongside precipitation. For instance, the substantial decrease observed in South America can be attributed to both soil moisture inefficiency and the heat stress resulting from high temperature rise.

The leaf density projections estimated by SURFEX are consistent with the outcomes anticipated by other dynamic vegetation models. These models predict a substantial foliage density decrease in the Amazonian forest, alongside an increase in high-latitude regions ((Lathiere et al., 2005) - (Gerber et al., 2004) - (Mahowald et al., 2016)).

The introduction of a combined approach involving fixed vegetation and dynamic leaf area index in the analysis of climate change’s influence on isoprene emissions led to a 50 Tg surge in emissions by 2050 compared to 2014. This stands in contrast to a 63 Tg increase observed when solely considering the effect of climate change. As illustrated in Figure 5.9, this reduction can be attributed to the decrease in isoprene emissions in high-isoprene emitting regions such as South America and Australia, where LAI has declined by 3% and 2% respectively. In contrast, Russia and North America have experienced a respective surge of 27% and 19% in isoprene emissions due to the CO_2 fertilization effect. Nevertheless, this uptick has a marginal impact on the overall global isoprene change, given the limited contribution of these regions to the total global isoprene flux, mainly due to the specific type of vegetation present in these areas.

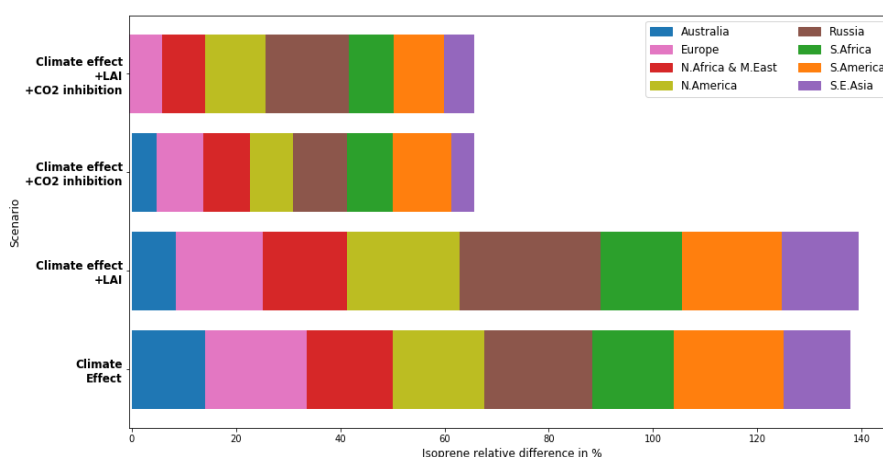


Figure 5.9: Isoprene relative difference between 2050 and 2014 for the four scenarios for different globe regions.

Squire et al. (2014) studied the sensitivity of future isoprene emissions to the CO_2 fertilization. Their findings indicate a projected rise of 17% ($\sim 78 \text{ Tg C yr}^{-1}$) under the SRES B2 scenario by 2095 relative to 2000. Similarly, Bauwens et al. (2018) predicted an increase in

isoprene emissions in Europe of 15%, 52% and 141% under the RCP2.6, RCP4.5 and RCP8.5 scenarios, respectively, by 2070–2099 relative to 1979–2014.

Few studies investigated the impact of vegetation density with fixed plant functional types distribution on isoprene emission trends as most incorporated the impact of changes in land use and/or land cover on biogenic emissions. In their study, Heald et al. (2009) examined the relative sensitivity of isoprene emission to alterations in nature-induced vegetation distribution and density, excluding the influence of croplands expansion and urbanization. The results of their study, show a widespread foliar expansion attributed to the CO_2 fertilization effect, specifically in northern high latitudes, resulting in a more than twofold increase in global isoprene production by 2100 (reaching 1240 Tg C yr⁻¹) compared to current levels under the A1B scenario. Divergences between the outcomes of Heald et al. (2009) and the present study can be attributed to the incorporation of land cover changes in future scenarios, leading to the regrowth of broadleaf forests in high latitudes, known to be significant isoprene emitters. Additionally, the dynamic vegetation model used in Heald et al. (2009) lacked consideration for nutrient limitations. This omission resulted in an overestimation of the biosphere’s capacity to absorb CO_2 by 74%. Consequently, future LAI increases may be notably lower than initially projected.

5.4.3 Climate change and CO₂ inhibition factor

CO_2 can influence isoprene emissions in two distinct ways: indirectly, through the CO_2 fertilization effect elucidated in the preceding section and directly, via the inhibitory effect that atmospheric CO_2 can exert on isoprene emission. Accounting for this factor in present-climate simulations has a marginal impact on isoprene emissions. Its significance becomes particularly pronounced when atmospheric carbon dioxide levels exceed 400 *ppmv* (Sindelarova et al., 2014). Various parametrizations exist to model the inhibitory effect of CO_2 on isoprene emissions (Wilkinson et al. (2009) - Possell and Hewitt (2011)). In the SURFEX-MEGAN model, we have adopted the Heald et al. (2009) parametrization, which models the CO_2 inhibition factor as follows:

$$\gamma_{CO_2} = I_{max} - ((I_{max}(0.7 \times C_i))^h) / ((C_*)^h + (0.7 \times C_i)^h) \quad (5.1)$$

Where C_i is the ambient air CO_2 concentration, $I_{max}=1.344$, $h=1.4614$ and $C_*=585$ are empirical parameters. As shown in Figure 5.10 γ_{CO_2} decreases non-linearly with increasing ambient CO_2 concentrations and is equal to 1 for $C_i=400$ *ppmv*.

To quantify the extent of this effect on future isoprene emissions, we conducted two experiments: *FUT_{CO₂}* and *HIST*. In the latter, we simulated the 2014 climate with the γ_{CO_2} factor deactivated (i.e., this factor was assigned a value of 1) and in the former we simulated the 2050

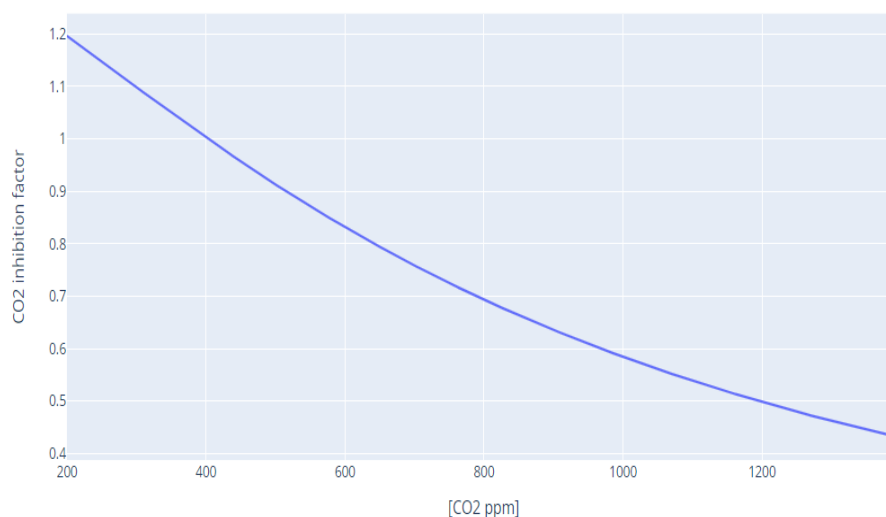


Figure 5.10: CO_2 inhibition factor following Heald et al. (2009) parametrization.

climate with a variable γ_{CO_2} .

The total annual isoprene emissions were estimated at 364 Tg and 395 Tg for *HIST* and *FUT_{CO₂}* simulations, respectively. The increase in atmospheric CO_2 concentrations in 2050 estimated to 610 ppm resulted in a γ_{CO_2} mean value of 0.8.

The combined impact of climate change and the inhibitory effect of CO_2 led to an increase of **9%** or approximately **31 Tg**. The inclusion of γ_{CO_2} led to a reduction of nearly half of the estimated increase observed when only considering the impact of climate change. As shown in Figure 5.9, the increase observed due to temperature rise was significantly compensated by the inhibitory effect of CO_2 . This effect was most prominent in South America, Southern Africa, Southeast Asia and Australia.

Heald et al. (2009) conducted a comprehensive study on isoprene response to changes in CO_2 levels. They projected a substantial drop of 217 Tg C yr⁻¹ in global isoprene emissions in 2100 under the A1B IPCC SRES scenario after integrating γ_{CO_2} . Compared to 2000 emissions, future isoprene decreased by 8%.

Building on Heald et al. (2009)'s work, Tai et al. (2013) extended the investigation by employing the parametrization framework proposed by Possell and Hewitt (2011). Their analysis underscored the critical role of CO_2 concentrations in shaping future isoprene emissions. They found that by considering the γ_{CO_2} effect, 2050 isoprene emissions dropped by 132 Tg C yr⁻¹ under the A1B IPCC SRES scenario, indicating a 5% reduction relative to 2000 emissions.

In a subsequent study, Bauwens et al. (2018) conducted a comparative analysis of the parametrizations for CO_2 inhibition proposed by Possell and Hewitt (2011) and Wilkinson et al. (2009). This analysis yielded valuable insights into the regional variations in isoprene emissions. In Europe, under the RCP8.5 scenario, they observed an 11% decrease and a 26% increase in isoprene emissions over 2070-2099 relative to 1979-2014 when applying the Possell and Hewitt

(2011) and Wilkinson et al. (2009) parametrizations, respectively. This highlights the nuanced and contrasting impacts of different parametrizations on projected isoprene emissions.

The potential of CO_2 -related processes to offset the rise in biogenic emissions induced by climate change is acknowledged. Nevertheless, these mechanisms remain largely uncharted territory. The incorporation of CO_2 effects relies heavily on experiments conducted on particular vegetation types and the outcomes of these studies are limited by a fundamental gap in comprehending the underlying mechanisms of CO_2 inhibition.

5.4.4 Climate change, Leaf Area Index and CO_2 inhibition factor

The examination of future isoprene emissions reveals a complex interplay of various factors. Initially, the dominant driver of increased emissions is temperature, resulting in a substantial rise of 63 Tg under a +2°C scenario. Incorporating the influence of CO_2 fertilization on leaf density contributed to partially offset this increase, as isoprene emissions in this scenario increased by only 50 Tg. This decrease is explained by the extensive decrease in biomass density observed in high isoprene-emitting regions, tempering the overall increase. Incorporating the CO_2 inhibition factor led to a rise in future emissions by 31 Tg, meaning that the increase predicted in the future by the first scenario dropped approximately by half. When considering all these factors, the net effect yielded a relatively modest uptick of 24 Tg in isoprene emissions by 2050, compared to 2014, under the SSP3-7.0 scenario.

As illustrated in Figures 5.6 and 5.9, this intricate balance between temperature, leaf density and CO_2 inhibition manifests differently across regions. In Australia, for instance, the initial temperature-driven surge was entirely offset by the decrease in leaf density and the inhibitory effects of CO_2 . Meanwhile, in South America and Southern Africa, the temperature-induced increase was only partially countered by the climate-induced deforestation in the Amazonian and Congo rainforests, as well as the inhibitory impact of CO_2 .

5.5 Comparison with CMIP6 models isoprene projections

5.5.1 Models description

In its latest phase, the coupled model intercomparison project (CMIP6) marked a significant advancement by incorporating isoprene projections for the first time. These projections include future isoprene estimations following the SSP scenarios alongside historical isoprene estimations. It is important to mention that the sixth IPCC assessment report did not include the multi-

Model	Isoprene scheme	Scenario	Resolution	γ_{CO_2}	Dynamic LAI	Change
SURFEX	G2012	SSP3-7.0	$1.4^\circ \times 1.4^\circ$	On ^(a)	Yes	+40
UKESM1-0-LL	P2011	SSP3-7.0	$1.25^\circ \times 1.88^\circ$	On ^(b)	Yes	-50
GISS-E2-1-G	G1995	SSP3-7.0	$2^\circ \times 2.5^\circ$	Off	Yes	+29
GFDL-ESM4	G2006	SSP3-7.0	$1^\circ \times 1.25^\circ$	Off	Yes	+50
		SST				
CESM2-WACCM	G2012	SSP3-7.0	$0.9^\circ \times 1.25^\circ$	On ^(a)	Yes	+92
		SST				

Table 5.3: List of CMIP6 isoprene emission projections and the emission total difference between 2045-2050 and 2010-2014. G1995 refers to the Guenther et al. (1995) isoprene emission model, G2006 is a newer version developed by Guenther et al. (2006), G2012 is the algorithm used currently in the MEGANv2.1 model by Guenther et al. (2012) and P2011 is the interactive BVOC model developed by Pacifico et al. (2011). (a) The estimation of γ_{CO_2} follows the Heald et al. (2009) parametrization and (b) follows the Niinemets et al. (1999) parametrization.

model biogenic emission projections analysis. However, addressing this gap, Cao et al. (2021) conducted a thorough ensemble multi-model isoprene analysis of seven CMIP6 models and considering four distinct SSP scenarios (SSP1-2.6, SSP2-4.5, SSP3-7.0 and SSP5-8.5).

In this section, we will try to evaluate the simulated isoprene evolution between the future-climate period 2046-2050 and the present-climate period 2010-2014 by comparing the SURFEX isoprene projections with 4 CMIP6 models: CESM2-WACCM, GFDL-ESM4, GISS-E2-1-G and lastly UKESM1-0-LL. The historical and future isoprene estimations of the different CMIP6 models were extracted from the Earth System Grid Federation server available at <https://esgf-index1.ceda.ac.uk/search/cmip6-ceda/>. Table 5.3 provides an overview of the studied CMIP6 models, with relevant specifications about the employed climate change scenario, the biogenic modeling framework used, the inclusion or exclusion of the inhibitory effect of CO_2 and whether the study incorporates anticipated vegetation density change.

The UK Met Office Hadley Centre, in conjunction with the Natural Environment Research Council (NERC), developed the English Earth system model UKESM1-0-LL (Sellar et al., 2020). Within this model, the iBVOC scheme is employed for the interactive calculation of biogenic emissions, specifically isoprene and monoterpenes. This scheme utilizes the isoprene emission model proposed by Pacifico et al. (2011) and incorporates the terpene emission parametrization described in Guenther et al. (1995). The isoprene emission scheme used in this model include the atmospheric CO_2 responsive parametrization by Niinemets et al. (1999). GISS-E2-1-G is a fully coupled Earth system model developed by the Goddard Institute for Space Studies (GISS), which is part of NASA (the National Aeronautics and Space Administration) in the United States (Kelley et al., 2020). This model uses also the Guenther et al. (1995) isoprene emission scheme. GFDL-ESM4 is a chemistry-carbon-climate Earth system model that

was developed by the Geophysical Fluid Dynamics Laboratory (GFDL) Dunne et al. (2020), this Earth system model estimates BVOCs based on the Guenther et al. (2006) MEGAN version. CESM2-WACCM, an American model, is the product of extensive development by the National Center for Atmospheric Research (NCAR). This model represents the latest version of the Community Earth System Model, as detailed by Danabasoglu et al. (2020). Within this framework, the land component is represented by CLM5 and the estimation of biogenic emissions is done based on MEGANv2.1. However this version uses the PCEEEA canopy environment approach described in Henrot et al. (2017) to estimate the different activity factors. The inclusion of the inhibitory effect of atmospheric CO_2 is based on the Heald et al. (2009) parametrization.

5.5.2 Isoprene change analysis

The CESM2-WACCM model exhibited the most pronounced change in isoprene emissions between the periods 2046-2050 and 2010-2014, followed sequentially by GFDL-ESM4, SURFEX GISS-E2-1-G and, lastly, by UKESM1-0-LL, with alterations of +92 Tg, +50 Tg, +40 Tg, +29 Tg and -50 Tg, respectively. All models projected a future increase in isoprene emissions, except for the UKESM1-0-LL model. The disparities in the anticipated shifts in isoprene emissions can be attributed to the use of different emission schemes, including the consideration or not of the inhibitory impact of CO_2 , as well as differences in projected shifts in leaf density. Furthermore, although all earth system models were driven by the SSP3-7.0 scenario, the predicted changes in multiple meteorological variables can vary significantly from one model to another (e.g., temperature, solar radiation, precipitation). These parameters exert a significant influence on the estimation of isoprene emissions. As noted by Fan et al. (2020), considerable variability in temperature trends exists among CMIP6 models. This variability is illustrated in Figure 5.11, which depicts the temperature difference between the studied CMIP6 models and CNRM-ESM2-1³ for the period 2046-2050. The substantial disparities in temperature outputs among CMIP6 models, which can exceed 4° in high-isoprene emitting regions, can lead to notable discrepancies in isoprene estimations across different models, given that the latter increases exponentially with temperature.

Figure 5.12 illustrates the mean isoprene difference between future and present estimations for the five models. Most models predicted a significant increase in isoprene emissions in tropical regions, particularly in South America, Southern Africa, Australia and Southeast Asia and a slight increase in high latitudes regions mainly Russia and Europe. However, UKESM1-0-LL showed a global decrease in isoprene emissions. This decrease is particularly pronounced in Northern South America, Southern Africa and Southeast Asia.

³SURFEX-MEGAN simulations were performed using the CNRM-ESM2-2 outputs.

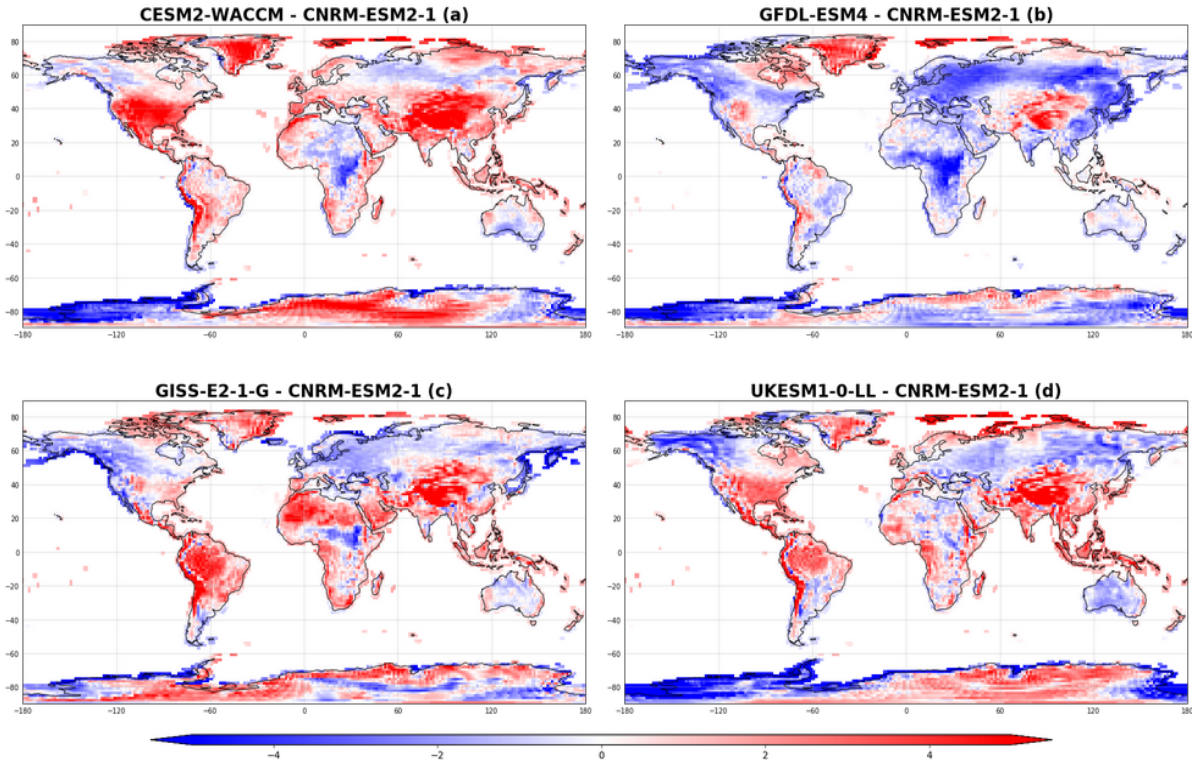


Figure 5.11: Mean absolute temperature difference in 2046-2050 between CESM2-WACCM (a), GFDL-ESM4 (b), GISS-E2-1-G (c), UKESM1-0-LL (d) and CNRM-ESM2-1 temperature output.

Despite using the same isoprene scheme (Guenther et al., 2012) and γ_{CO_2} parametrization (Heald et al., 2009), CESM2-WACCM exhibited a significant isoprene increase in the Amazonian and Congo rainforests compared to SURFEX, which showed a marginal increase in these regions. This discrepancy may be attributed to CESM2-WACCM’s predicted increase in vegetation density and subsequently, enhanced emissions, across most regions of the globe (see Appendix B, Figure B.1).

While UKESM1-0-LL anticipated the highest temperature and solar radiation increase in high-isoprene emitting regions compared to the other models (see Appendix B, Figure B.2 and B.3), it was the only model to predict a negative evolution in isoprene emissions of -50 Tg. This outcome can be attributed to the inhibitory factor used in this model, which follows the Ninemets et al. (1999) parametrization shown in Table 5.4. As depicted in Figure 5.13, this parametrization imposes a stronger penalty on isoprene emissions compared to the method proposed by Heald et al. (2009).

GISS-E2-1-G and GFDL-ESM4 exhibited increases in isoprene emissions of 29 Tg and 50 Tg, respectively. These models did not incorporate the inhibitory effect of atmospheric CO_2 .

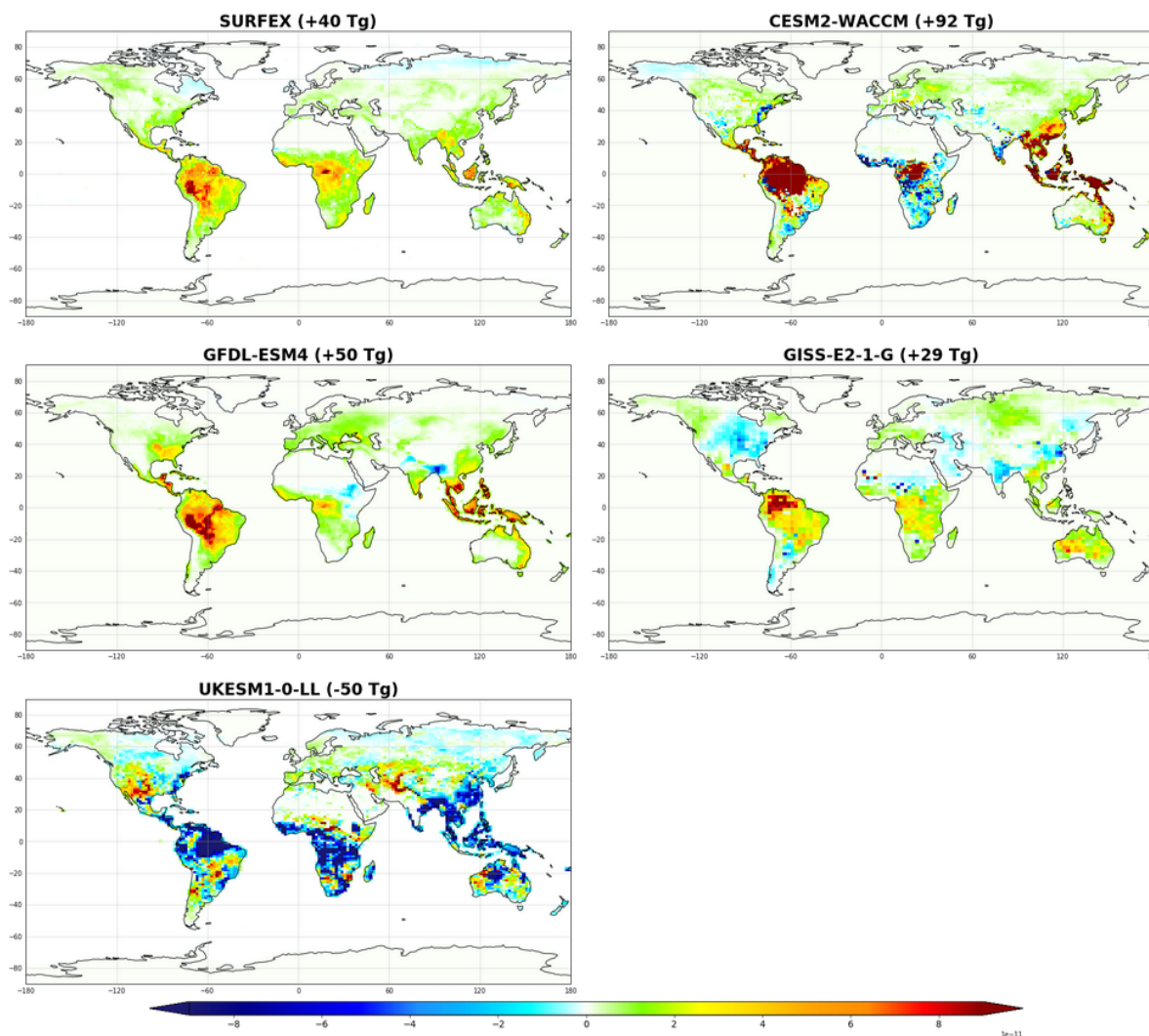


Figure 5.12: Isoprene flux difference between 2046-2050 and 2010-2014 for the coupled model SURFEX-MEGAN and the 4 CMIP6 models: CESM2-WACCM, GFDL-ESM4, GISS-E2-1-G and UKESM1-0-LL.

However, the change predicted by SURFEX and CESM2-WACCM which accounted for this effect, is comparable or even higher to the isoprene change predicted by GISS-E2-1-G and GFDL-ESM4. Therefore, these models should have projected higher isoprene changes since they have neglected the negative effect of CO_2 . This discrepancy can be attributed to the utilization of different isoprene schemes, with GISS-E2-1-G employing the scheme proposed by Guenther et al. (1995), GFDL-ESM4 adopting that of Guenther et al. (2006) and SURFEX and CESM2-WACCM employing the isoprene scheme of Guenther et al. (2012). According to Cao et al. (2021), the use of the Guenther et al. (2006) isoprene scheme, as opposed to Guenther et al. (2012), may lead to projections lower by up to 150 Tg. This further highlights the impact of the choice of isoprene scheme on emission projections.

As previously noted, the SURFEX-MEGAN isoprene simulations overlooked the influence of

Study	γ_{CO_2}
Heald et al. (2009)	$I_{max} - \frac{I_{max}(0.7 \times C_i)^h}{(C_*)^h + (0.7 \times C_i)^h}$
Niinemets et al. (1999)	$\frac{C_{st}}{0.7 \times C_i}$

Table 5.4: Atmospheric CO_2 activity factor. C_i is the ambient air CO_2 concentration, $I_{max}=1.344$, $h=1.4614$, $C_*=585$ and C_{st} is the atmospheric CO_2 concentration at standard conditions =370ppm.

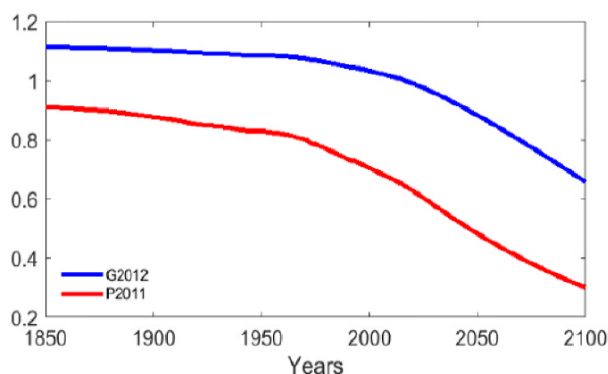


Figure 5.13: Inhibition factor γ_{CO_2} over the period 1850-2100 using the SSP3-7.0 CO_2 concentrations. G2012 (Guenther et al., 2012) uses the Heald et al. (2009) CO_2 parametrization and P2011 (Pacifico et al., 2011) the (Niinemets et al., 1999) CO_2 parametrization (adapted from Cao et al. (2021)).

anthropogenic-driven shifts in land use and land cover. While the CMIP6 models did incorporate dynamic vegetation models, it remains uncertain whether these models factored in anticipated human-induced alterations in land use and land cover when projecting isoprene emissions in a future-climate context. This particular consideration bears notable significance in forecasting future isoprene emissions, as highlighted by Cao et al. (2021), accounting for land cover change in future-climate simulations could result in a 34–67 Tg reduction in isoprene emissions.

5.6 Conclusion of Chapter 5

The assessment of future trends in BVOCs is of crucial importance, not only for predicting future air quality, but also for evaluating the radiative forcing effects of secondary organic aerosols and ozone, both of which originate from VOCs. In this context, the estimation of isoprene emissions, constituting 50% of total BVOCs, was conducted under a +2°C climate scenario. It is anticipated that isoprene emissions will experience a 40 Tg increase in a +2°C climate relative to the period 2010-2014. This rise is primarily attributed to projected future temperature increases, with solar radiation playing a minor role. The latter is projected to decline in accordance with the SSP3-7.0 scenario. The CO_2 fertilization effect led to a reduction in LAI in tropical regions and an augmentation in high latitudes. This resulted in a

net negative impact at a global scale, given that high-isoprene emitting regions are primarily located in the tropics. The inhibitory effect of CO_2 also demonstrated a substantial negative influence on future isoprene emissions, particularly pronounced at elevated CO_2 concentrations (exceeding $400ppm$). The isoprene projections from the SURFEX model were compared to those of other CMIP6 models. The majority of models projected a positive change ranging between 29 Tg and 92 Tg. The SURFEX model, driven by CNRM-ESM2-1 outputs, indicated a 40 Tg increase in 2046-2050 relative to 2010-2014. The UKESM1-0-LL model was the only model to predict a negative change. This discrepancy was attributed to the stronger penalization on isoprene emissions due to the CO_2 inhibition parameterization utilized in this model. The disparities in model results were attributed to variations in isoprene schemes, resolution, vegetation distribution and density, but most importantly, each model's output of temperature and solar radiation differed, despite employing the same SSP scenario.

Impact of isoprene in a +2°C climate on air quality

It is widely acknowledged that atmospheric pollutants such as ozone (O_3), present significant threats to human health when concentrations exceed defined thresholds (Sanhueza et al., 2003). In this context, climate change can potentially enhance ground-level ozone concentrations, the so-called "ozone-climate penalty"¹, but its impact is different when considering other factors mainly changes in emissions, atmospheric chemistry and transport and dry deposition patterns. In this chapter, we will attempt to study the impact of climate change on future global air quality, particularly on tropospheric ozone concentrations, by considering all factors that can impact ozone concentrations (e.g., meteorology, anthropogenic/biogenic/biomass burning emissions).

6.1 MOCAGE

MOCAGE (Modèle de Chimie Atmosphérique de Grande Échelle in French) is a 3-dimensional chemistry-transport model developed by CNRM (Josse et al., 2004). It is designed to simulate the tropospheric and stratospheric atmospheric composition by incorporating the physical and chemical processes associated with both gases and aerosols. MOCAGE serves both research and operational purposes, enabling real-time air quality evaluation as well as the assessment of how climate change might impact future air quality trends. Depending on the application, MOCAGE can be run on a global scale with nested regional scales defined at finer resolution, with several horizontal resolutions available. In the operational setting of MOCAGE at Météo-France, simulations are run on a global scale of $1^\circ \times 1^\circ$ ($0.5^\circ \times 0.5^\circ$ from end of November 2023), with a regional zoom on Europe where the spatial resolution is refined to $0.1^\circ \times 0.1^\circ$. In terms

¹Ozone-climate penalty, refers to the increase in ground-level ozone concentrations in the future resulting only from warmer temperatures.

of vertical representation, MOCAGE defines the atmospheric profile with a maximum of 47 levels (60 in the latest version), where level 1 is situated at the upper stratosphere (4 hPa, and 0.1 hpa in the latest version), and the lowermost level just above the surface (Figure 6.1). To address the challenge of representing reliefs, MOCAGE employs hybrid σ -pressure coordinates. The system represents a surface parallel to the Earth’s topography. At higher altitudes, where pressure gradients are greater, the coordinates behave like pressure coordinates, which are better suited to modeling large-scale atmospheric phenomena. This operational configuration of MOCAGE provides information to the regional CAMS (Copernicus Atmosphere Monitoring Service) multi-model ensemble and the French national air quality platform Prev’Air, among others.

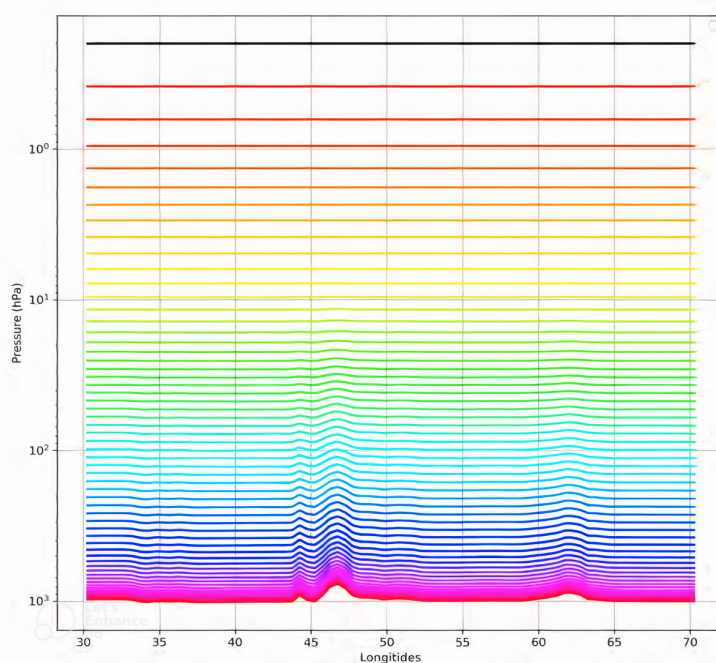


Figure 6.1: Representation of vertical level configuration of MOCAGE with 60 levels (adapted from El Aabaribaoune (2022)).

MOCAGE is a chemical-transport model, meaning that it simultaneously simulates the chemical transformations that compounds undergo along with their horizontal and vertical transport mechanisms. This offline model, relies on meteorological data sourced from either climate models (e.g., ARPEGE-climat), or weather forecast models (e.g., AROME, ALADIN, ARPEGE). Additionally, it requires inputs for biogenic and anthropogenic emissions, as well as deposition velocity data.

In MOCAGE, the transport of chemical compounds is modeled using a range of numerical schemes. These include schemes for both large-scale and sub-mesh transport. The former addresses advection, while the latter deals with convection and diffusion processes. For gaseous chemistry, a thorough chemical model named RACMOBUS is employed. This model com-

bines the tropospheric Regional Atmospheric Chemistry Mechanism (RACM) scheme (Stockwell et al., 1997) with the stratospheric REactive Processes Ruling the Ozone BUdget in the Stratosphere (REPROBUS) scheme (Lefevre et al., 1994). This comprehensive model includes 118 distinct species and 434 chemical reactions. Consequently, it enables the depiction of various scenarios, including near-surface urban pollution as well as the evolution of the ozone layer.

6.2 Methodology

For this study, MOCAGE was used to conduct two global simulations at a resolution of $1^\circ \times 1^\circ$: one for the present climate covering 2013, and another for the future climate representing 2050. Meteorological data inputs were derived from the SSP3-7.0 scenario operational analyses of CNRM-ESM2-1, with a temporal resolution of 3 hours and a spatial resolution of $1.4^\circ \times 1.4^\circ$. These inputs were interpolated onto a grid compatible with MOCAGE (1°).

Simulation	year	Isoprene	Other BVOCs	ANT/BB & VOCs	NO_x
<i>CTRL</i>	2013	<i>HIST</i> _{2010–2014} [*]	CAMS-GLOB-BIOv3.1 (2015)	Historical (2015)	
<i>Sim</i> _{LAI,CO₂}	2050	<i>FUT</i> _{LAI,CO₂} [*]	CAMS-GLOB-BIOv3.1 2015	SSP3-7.0 (2050)	
<i>Sim</i> _{ISO–CTRL}	2050	<i>HIST</i> _{2010–2014} [*]	CAMS-GLOB-BIOv3.1 (2015)	SSP3-7.0 (2050)	
<i>Sim</i> _{LAI}	2050	<i>FUT</i> _{LAI} [*]	CAMS-GLOB-BIOv3.1 (2015)	SSP3-7.0 (2050)	

Table 6.1: Description of the simulations used to model atmospheric composition with MOCAGE. (*) The details of the isoprene inventories used in each simulation are given in Chapter 5, Tables 5.1 and 5.2. ANT and BB represent emissions from anthropogenic and biomass burning sources, respectively.

Present- and future-climate biogenic emissions data were obtained from isoprene emissions of the simulations described in Chapter 5. As the SURFEX-MEGAN model did not account for the modeling of other BVOCs yet, emissions data for BVOCs (except for isoprene) in both present and future climate simulations were extracted from the CAMS-GLOB-BIOv3.1 inventory of 2015, (accessible here <https://atmosphere.copernicus.eu/data>). These BVOCs inventories were available at a spatial resolution of $0.25^\circ \times 0.25^\circ$ on a monthly time step. Anthropogenic emissions and biomass burning data were extracted from Input4MIPs (<https://esgf-node.llnl.gov/search/input4mips/>), using two sets of emissions data representing 2013 and 2050 under the SSP3-7.0 scenario. These emissions are defined at a spatial resolution of $0.5^\circ \times 0.5^\circ$ on a monthly basis. In this study, we incorporated a 6-year reanalysis of deposition velocity

input data for both present and future climate simulations. This parameter co-varies with LAI, vegetation distribution, and vegetation height; however, in this study we will neglect the impact of climate change on deposition velocity as the surface variables needed to estimate this parameter under future-climate conditions were unavailable.

To assess the evolution of ozone concentrations we have performed with the MOCAGE model four simulations listed in Table 6.1. To assess the impact of climate change which includes only meteorology and anthropogenic emissions on ozone concentrations we will compare *CTRL* and *Sim_{ISO-CTRL}* simulations. The contribution of varying isoprene emissions will be evaluated afterwards by comparing *Sim_{ISO-CTRL}* and *Sim_{LAI,CO₂}*. Finally, we will evaluate the impact of the inhibition effect of atmospheric CO_2 by comparing *Sim_{LAI}* and *Sim_{LAI,CO₂}*. The total annual anthropogenic and biomass burning NO_x and *VOCs* emissions, as well as biogenic *VOCs* emissions is listed for each simulation in Table 6.2.

Emission (Tg/yr)		<i>CTRL</i>	<i>Sim_{LAI,CO₂}</i>	<i>Sim_{ISO-CTRL}</i>	<i>Sim_{LAI}</i>
NO_x	ANT	138.7	151.8	151.8	151.8
	BB	13.7	12.3	12.3	12.3
	Total	152.4	164.1	164.1	164.1
VOC	ANT	164.1	198.2	198.2	198.2
	BB	63.2	57.9	57.9	57.9
	ISO	304	323	304	349
	OBVOC	333	333	333	333
	Total	864.3	912.1	893.1	938.1

Table 6.2: Total annual NO_x and VOC emissions from anthropogenic (ANT), biomass burning (BB) sources for historical (*CTRL*) and SSP3.7-0 simulations (*Sim_{LAI,CO₂}*, *Sim_{ISO-CTRL}* and *Sim_{LAI}*). For biogenic VOCs emissions, ISO and OBVOC represent the total emissions of isoprene and other biogenic species, respectively.

6.3 Emission changes

Figure 6.2 represents the difference in anthropogenic and biomass burning NO_x and VOCs emissions as well as biogenic VOCs emissions between 2050 and 2013. The SSP3-7.0 scenario is characterized by a fragmented world with high regional emission control policies discrepancy. In some parts of the world such as North America, Europe and Southern Africa, the SSP3-7.0 pathway predicts strong NO_x emission control policies. However, these emission controls are weaker in Southeast Asia, Central and South America, the Middle East and some parts of Africa. The same observations hold for anthropogenic and biomass burning VOCs emissions. Isoprene emissions are simulated with the SURFEX-MEGAN model for present (2013) and future-climate (2050) simulations. The selected years offer a focused examination of how tro-

ospheric ozone responds to even marginal shifts in isoprene emissions. In 2013, estimated isoprene emissions amounted to 304 Tg, while in the 2050 future-climate projection, they are expected to reach 323 Tg. As outlined in Chapter 5, this increase is influenced by shifts in temperature, leaf density, and elevated atmospheric CO_2 concentrations, which exert an inhibitory effect on isoprene emissions.

Given that we did not model the emissions of other BVOC species using the SURFEX-MEGAN model, we assumed that these emissions remain constant in the future. Consequently, alterations in biogenic VOCs emission are solely attributed to the changes in isoprene emissions. The latter's increase is particularly pronounced in densely vegetated areas mainly South America and Central Africa. The decrease observed in anthropogenic and biomass burning VOCs emissions in North America and Europe is partially offset by the increase in biogenic VOCs in these areas.

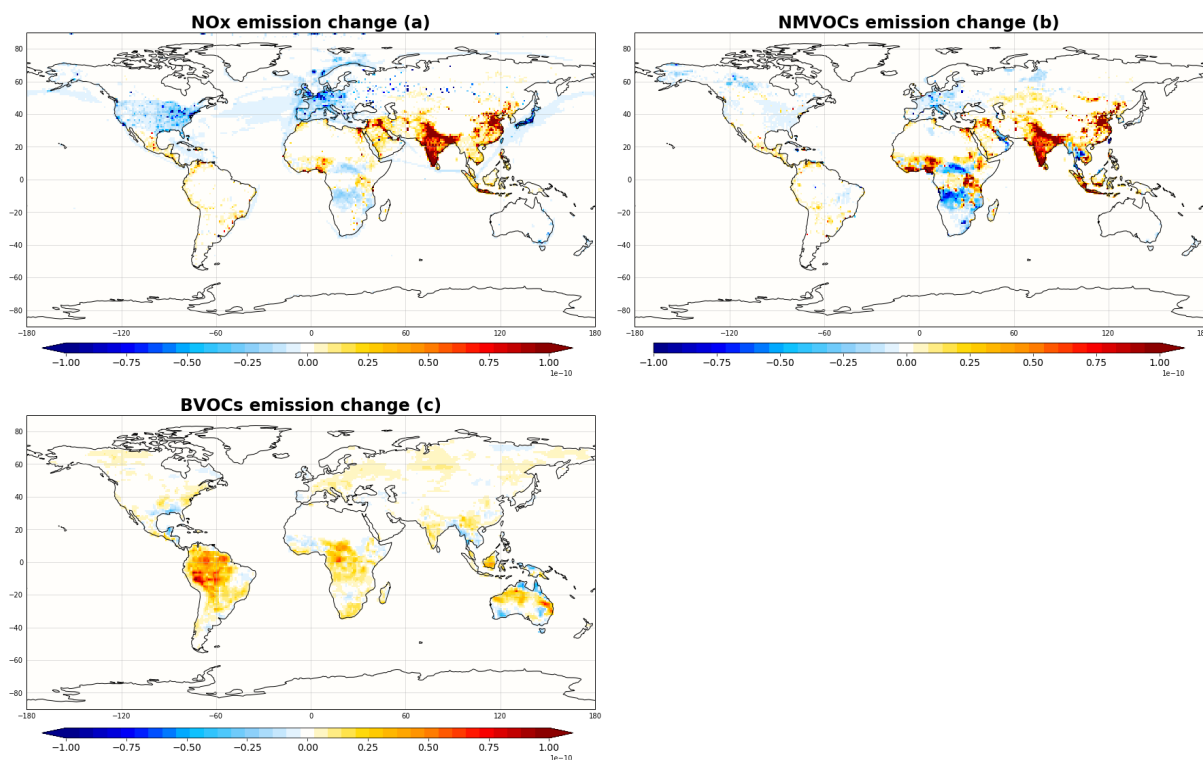


Figure 6.2: Difference in mean annual anthropogenic and biomass burning NO_x (a) and $NMVOCs$ (b) emissions in $kg/m^2/s$ and biogenic $NMVOCs$ in $kg/m^2/s$ (c) of SSP3-7.0 (2050) emissions and present day emissions (2013).

6.4 Ozone change

In the atmosphere, ozone is formed through chemical reactions involving nitrogen oxides (NO_x), volatile organic compounds (VOCs), carbon monoxide (CO) and hydroxyl radicals (OH). How-

ever, tropospheric ozone can be eliminated from the atmosphere through many chemical and physical processes. The chemical removal processes depend on the concentrations of NO_x , VOCs, and OH . The physical processes involve wet and dry depositions. The latter is considered a significant method of O_3 removal from the lower atmosphere.

The future assessment of ozone change will be undertaken in two phases. The first phase involves the analysis of ozone variation resulting exclusively from climate change impact, along with the evolution of NO_x levels, as well as emissions of anthropogenic and biomass burning VOCs. Subsequently, we will explore the supplementary impact of changes in BVOC emissions in general and isoprene emissions in particular.

Under the SSP3-7.0 scenario, the tropospheric ozone burden increased from 336 Tg in 2013 to 353 Tg in 2050, indicating an increase rate of 5%. The mean annual surface ozone concentration also increased by 12 ppb. The evolution of future air quality will be assessed by analyzing seasonal changes in surface ozone and NO_x concentrations between *Sim_{ISO-CTRL}* and *CTRL* simulations represented in Figure 6.3.

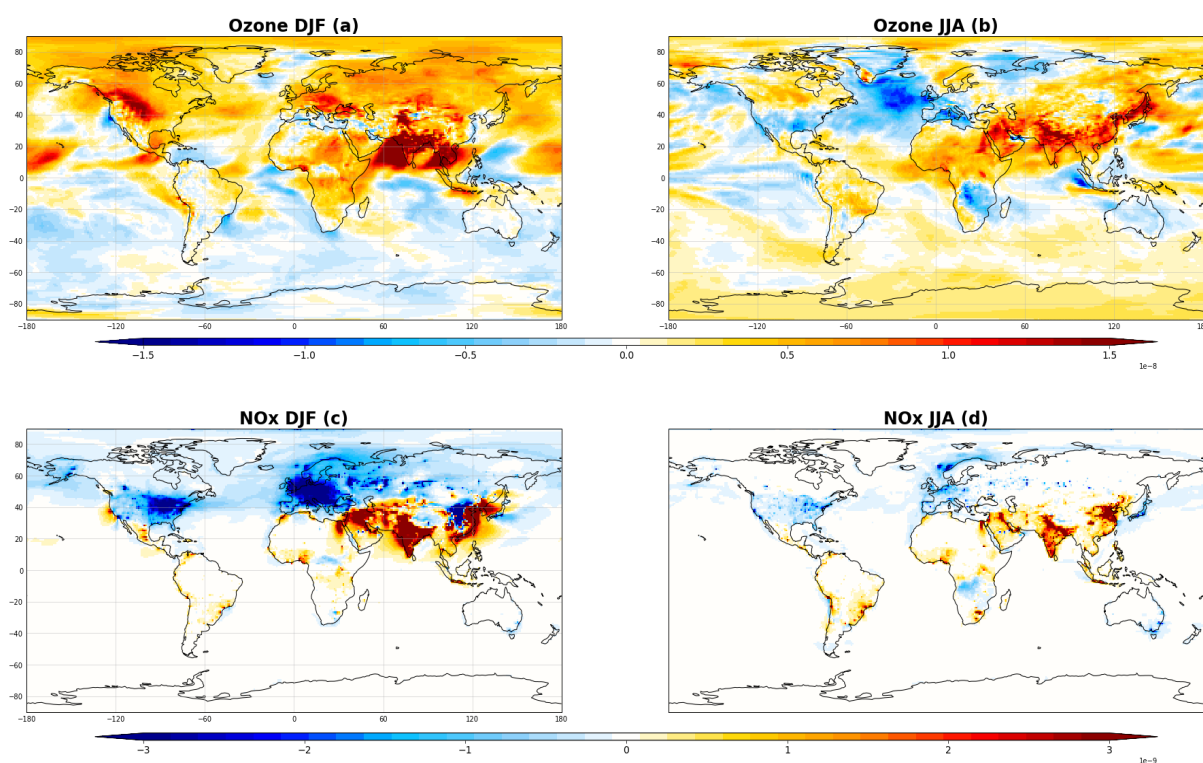


Figure 6.3: Difference in mean ozone (a,b) and NO_x concentrations (c,d) in ppv between *Sim_{ISO-CTRL}* and *CTRL* simulations in boreal winter (DJF: December-January-February) and boreal summer (JJA: June-July-August).

In boreal winter, the ozone regime dominating some continental regions such as North America, Europe and Russia is suggested to be *VOC*-limited (Liu et al., 2022), in this case the ambient air contains a low concentration of VOCs. Under the SSP3-7.0 scenario, it is projected

that the levels of Nitrogen Oxides will decrease in these regions. This reduction in NO_x results in less removal of hydroxyl radicals (OH) (reaction $NO_2 + OH \rightarrow HNO_3$), which are crucial for ozone formation, which explains why surface ozone will increase in these areas. Conversely, in other regions of the globe such as Southeast Asia, NO_x and VOCs from anthropogenic and biomass sources will both increase which will enhance ozone production in these regions (Figure 6.2). As for South America and Africa, the O_3 regime is suggested to be NO_x limited (Brown et al., 2022), as the emission of NO_x is limited compared to biogenic VOCs in these areas. In this context, since the VOCs emission from anthropogenic and biomass burning sources did not significantly change, the increase in ozone observed in Africa is likely due to temperature increase, this was confirmed by Brown et al. (2022), which attributed to temperature the increase in the ozone production rate in tropical regions where NO_x and isoprene emissions did not change significantly.

In Boreal summer, a shift is observed in the ozone chemical regime in North America and Europe. These regions experienced a notable increase in biogenic VOCs during summer, leading to a chemical regime of ozone that is primarily constrained by the availability of Nitrogen Oxides. Consequently, reducing NO_x emissions will limit ozone production in Europe and Southern North America. In Southeast Asia, the increase in both NO_x and VOCs emissions resulted in an increase in surface ozone in 2050. Lastly, Africa and South America are suggested to be NO_x limited throughout the year as confirmed by Brown et al. (2022), the decrease observed in Southern Africa can be explained by the reduction in NO_x emissions in this area. In NO_x -limited regimes, a decrease in NO_x emissions will lead to a decrease in ozone, as O_3 concentrations are proportional to NO_x emissions.

Overall, ozone burden increased by 5% in the future under the SSP3-7.0 emission assumptions. However this change is dominated by seasons, as the surface ozone increase is more pronounced globally in winter and less significant in summer. Additionally, the reduction in emissions of ozone precursors as implemented in SSP3-7.0 to improve future air quality in specific regions can yield contrasting outcomes depending on the season, potentially influencing the ozone chemical regime. For instance, the decrease in NO_x emissions in North America and Europe proves beneficial only during the summer season, but it may worsen air quality conditions in winter. Our study's findings are in agreement with those of Liu et al. (2022), who investigated changes in tropospheric ozone using the United Kingdom Earth System Model UKESM1, under the SSP3-7.0 scenario, comparing the periods of 2004-2014 and 2045-2055. Both studies indicate a similar projected increase of approximately 4% in the ozone burden. Consistently, our results show that surface ozone will increase in Europe and North America during winter and decrease during summer. However, the projected winter decrease in Southeast Asia, which contradicts our findings, can be attributed to differences in the inputs of anthropogenic VOCs emissions. In our study, the SSP3-7.0 emission inputs anticipate an increase in anthropogenic VOCs in

this region. This increase is not significant in the Liu et al. (2022) study, which explains the observed VOC-limited ozone regime in Southeast Asia and thus the decreased winter ozone emissions in this area.

6.5 Ozone sensitivity to isoprene emissions

Incorporating the evolution of biogenic emissions in simulating future air quality is of great importance. This stems from the fact that BVOCs account for about 90% of the total emitted VOCs, which are recognized as crucial precursors to tropospheric ozone. Among all BVOCs, isoprene is the most important biogenic compound, accounting for roughly half of the total emitted BVOCs. In this regard, to assess the importance of including future changes in biogenic emissions in modeling future air quality, we will compare the surface ozone levels of two simulations $Sim_{ISO-CTRL}$ and Sim_{LAI,CO_2} . The former represents future ozone simulated with present-day isoprene emissions with an annual total of 304 Tg and the latter represents projected 2050 ozone levels with simulated SURFEX-MEGAN isoprene emissions considering the impact of changing temperatures, leaf area index as well as the inhibitory effect of atmospheric CO_2 concentrations. With all these factors combined, the projected future isoprene emissions are estimated at 323 Tg (See Chapter 5).

The incorporation of isoprene emissions led to a minor rise in the total ozone burden, increasing from 353 Tg in the $Sim_{ISO-CTRL}$ scenario to 354 Tg in the Sim_{LAI,CO_2} scenario. Mean annual ozone concentrations also increased by 1 ppb when incorporating isoprene changes. Although there was not a significant shift in global ozone concentrations, the sensitivity of ozone to isoprene emissions can be detected on regional and local scales, as depicted in Figure 6.4. The net production of ozone, defined as the difference between ozone chemical production and destruction, decreased in numerous regions worldwide, particularly in South America, South Africa, and specific regions in Southeast Asia. The increase was only evident in specific locations, primarily in certain regions in Southeast South America, Europe, Southern Africa, and India.

Variations in ozone net production are closely correlated with fluctuations in isoprene flux. This correlation demonstrated either a positive or negative trend depending on the NO_x concentrations. In regions with elevated NO_x emissions, the correlation was positive, whereas in areas with low NO_x emissions, it was negative. In heavily polluted areas like India, Southeast China and some cities in Europe and North America, surface ozone levels followed the trends of isoprene emissions. For instance, during the boreal winter in India and Southeast China, air quality worsened due to increased isoprene emissions, as ozone concentrations increased by more than 1 ppb, but it improved in summer when isoprene emissions decreased, as ozone concentrations decreased by more than 1 ppb. In contrast, in NO_x limited areas, such as South

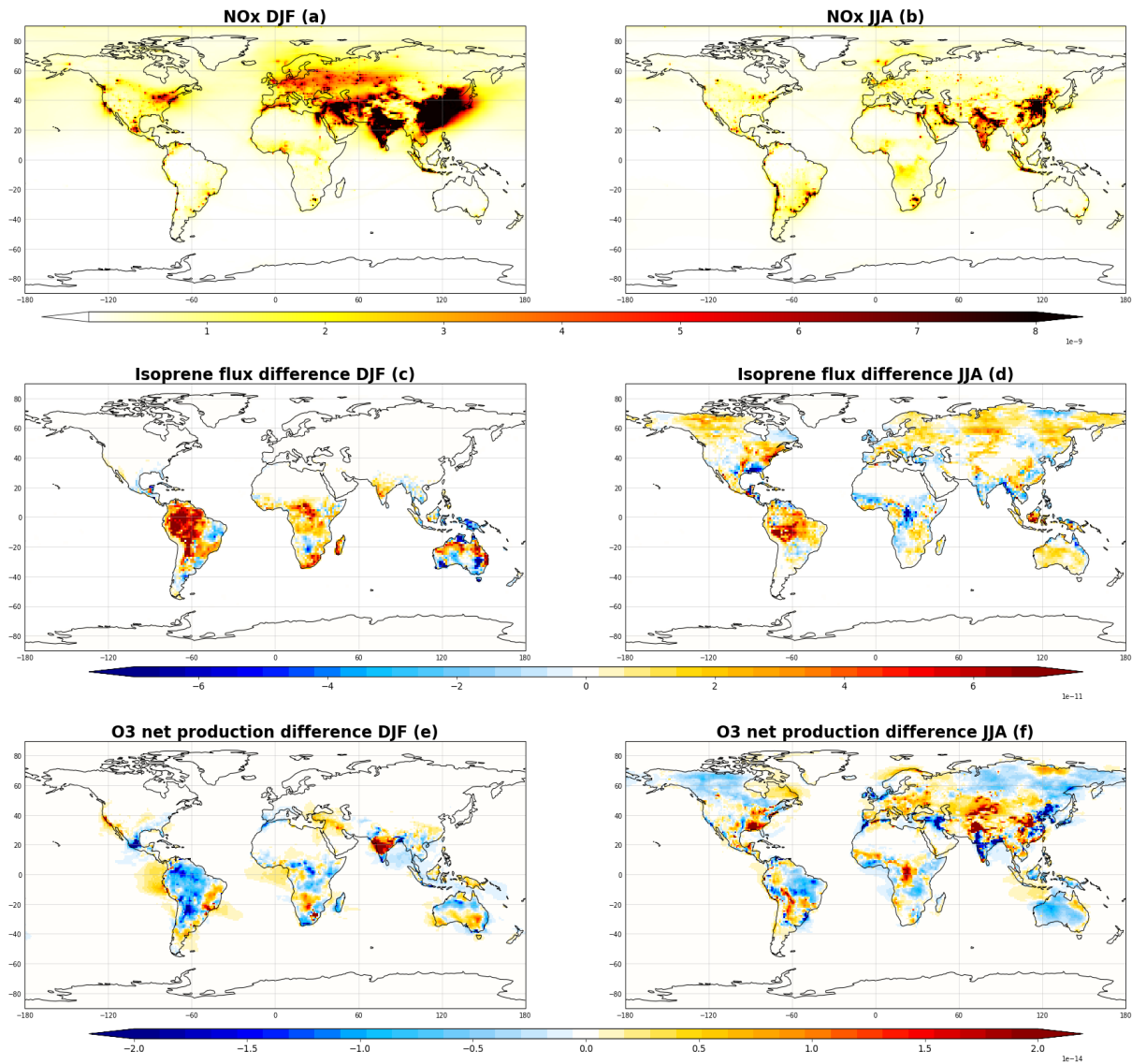


Figure 6.4: Distribution of mean NO_x concentrations (a,b) in ppv, difference in mean isoprene flux (c,d) in $kg/m^{-2}/s$ and in ozone net production rate in ppv/s (e,f) between Sim_{LAI,CO_2} and Sim_{ISO_CTRL} in boreal winter (DJF: December-January-February) and boreal summer (JJA: June-July-August).

America and Southern Africa, where future projections suggest an increase in isoprene emissions, both summer and winter experienced a reduction in net chemical production of ozone, which led to improved air quality throughout the year.

The sensitivity of ozone to isoprene emissions was previously discussed in Dunker et al. (2016), who found that isoprene might act to reduce ozone concentrations in NO_x limited areas. This can be explained by the direct reaction of ozone with isoprene and its oxidation products. Additionally, isoprene has pathways that can potentially lead to a decrease in NO_x levels, which indirectly have a negative impact on ozone production particularly in areas where NO_x concentrations are limited. Conversely, in regions characterized by high NO_x emissions, there is a positive correlation between isoprene emissions and net ozone production. This is because isoprene have an important role in reducing the destruction of ozone through its reaction with NO (See Chapter 2).

6.6 Impact of the CO_2 inhibition effect on air quality

As previously explained in Chapter 5, future isoprene projections vary in parallel with temperature, solar radiation, leaf density but most importantly, atmospheric CO_2 concentrations. The latter exerts a pronounced influence on shaping future isoprene trends, as elevated CO_2 levels can lead to a substantial reduction in isoprene emissions due to the inhibitory effect it imposes.

To assess the significance of accounting for the impact of γ_{CO_2} , we will conduct a comparative analysis between Sim_{LAI} where this factor was held constant at 1 and Sim_{LAI,CO_2} where the factor is variable.

The estimated annual isoprene emissions decreased from 350 Tg when neglecting the inhibition factor γ_{CO_2} in Sim_{LAI} to 323 Tg when accounting for this effect. Accordingly, the ozone burden and the global mean surface ozone concentrations experienced a decrease of approximately 5% and 4%, respectively, when neglecting this effect. The increase in isoprene emissions in Sim_{LAI} is observed at a global scale and most importantly in high isoprene emission regions (e.g., South America, Africa). As shown in Figure 6.5, in these regions the net production of surface ozone decreased and ozone concentrations dropped by more than 10 ppb. As explained in the previous chapter, the decrease in ozone levels is explained by the increase in isoprene emissions in areas with limited emission of NO_x . Conversely, in heavily polluted regions such as India and Southeast China ozone concentrations increased by approximately 2 ppb.

To assess the impact of considering future isoprene emissions with a deactivated CO_2 inhibition factor on future ozone levels in comparison to present ozone levels, we will conduct a comparative analysis between the $CTRL$ and Sim_{LAI} simulations.

The ozone burden remained consistent between the present and future scenarios, maintain-

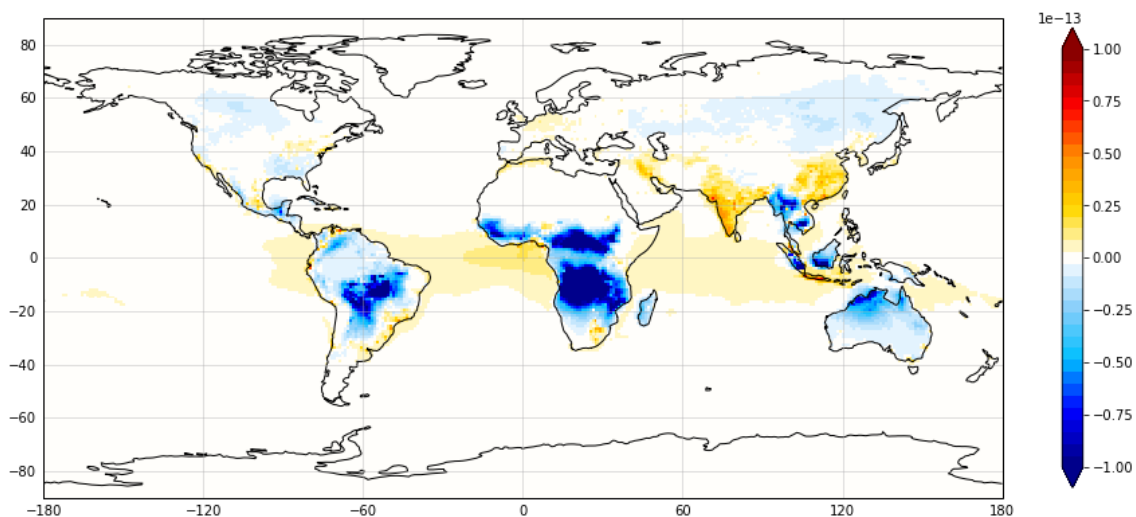


Figure 6.5: Difference in surface mean annual ozone net production rate in ppv/s between Sim_{LAI} and Sim_{LAI,CO_2} .

ing a similar value of 336 Tg. Nevertheless, notable variations in surface ozone levels were observed both seasonally and spatially. As shown in Figure 6.6, in boreal winter, the predicted increase in ozone levels in North America and Europe with fixed isoprene emissions (Figure 6.3) is also depicted when accounting for isoprene emission evolution. In winter, isoprene emissions are very low in these regions and therefore have no impact on ozone chemistry. Conversely, substantial changes in ozone production patterns were noted in South America and South Africa, where a significant increase in isoprene emissions was observed. The inclusion of interactive isoprene emissions has improved air quality in South America and South Africa (Figure 6.6 and Figure 6.3). As previously explained, this decrease in ozone levels can be explained by the increase in isoprene emissions in these regions.

In boreal summer, the differences in ozone production between the future and present scenarios in the northern hemisphere remained unchanged, regardless of the inclusion or not of future isoprene emissions. However, in South America and Africa, the increase in ozone concentrations depicted in Figure 6.3 was entirely counteracted when accounting for changes in isoprene emissions. In these regions, the increased isoprene emission levels led to a decrease in ozone concentrations and thus improved air quality.

6.7 Conclusion of Chapter 6

In a +2°C climate change level, ozone burden is projected to increase by 5% under the SSP3-7.0 scenario. The policy targeting emissions control, which involves reducing nitrogen oxide (NO_x) concentrations in North America and Europe, proves effective only in the summer months. This is because during this period, the emission of biogenic volatile organic compounds will shift the

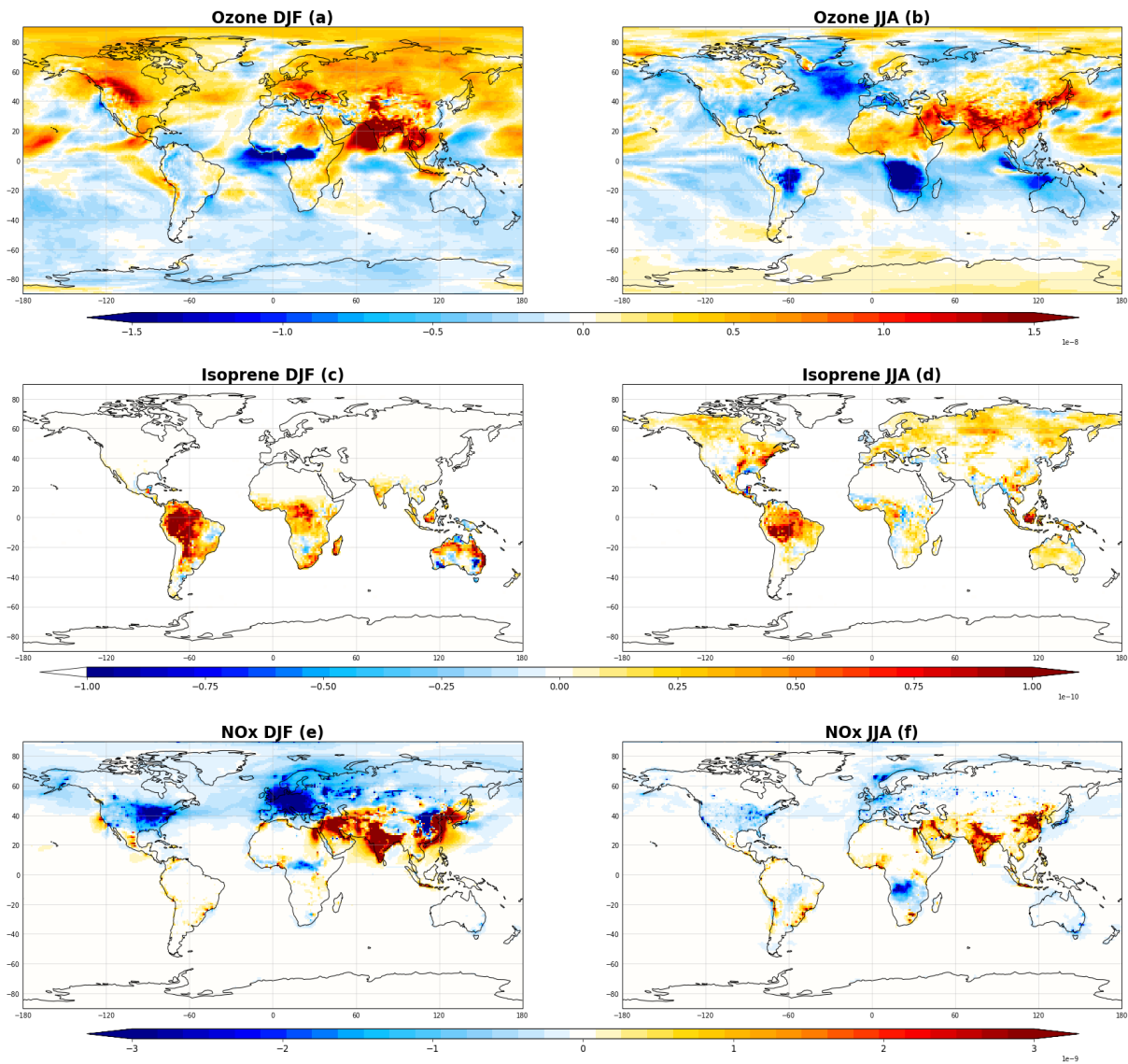


Figure 6.6: Difference in mean ozone (a,b) and NO_x concentrations (e,f) in ppv and in isoprene flux (c,d) in $kg/m^{-2}/s$ between *Sim_{LAI}* and *CTRL* simulations in boreal winter (DJF: December-January-February) and boreal summer (JJA: June-July-August).

ozone regime towards being limited by NO_x availability. However, in heavily polluted regions like Southeast Asia, where the SSP3-7.0 scenario assumes an increase in human-made emissions of NO_x and VOCs, air quality is anticipated to deteriorate throughout the year.

Although ozone sensitivity to isoprene emissions is high, the change in surface ozone concentrations between present and future-climate with fixed isoprene emissions and present and future-climate with evolving isoprene emissions is low. This is due to the expected rise in isoprene emissions driven by higher temperatures being offset by the inhibitory effect of CO_2 , resulting in only minor changes in isoprene emissions, of approximately 17 Tg. Consequently, the projected future changes in ozone levels are primarily driven by temperature and NO_x emissions, and only partially by isoprene changes. However, the impact of the latter becomes particularly significant locally, as it can improve or worsen air quality depending on NO_x concentrations level in this area.

Excluding the inhibitory effect of atmospheric CO_2 had a significant impact on ozone trends. While the overall global ozone burden stayed the same, there were notable improvements in future air quality in tropical regions, particularly in South America and South Africa, throughout the year when interactive isoprene emissions were considered with a deactivated γ_{CO_2} , as opposed to a scenario with fixed isoprene emissions. However, this effect was only marginal in the northern hemisphere, as the difference in ozone concentrations between the future and present scenarios remained unchanged in both cases, whether with fixed or interactive isoprene emissions.

Conclusions and perspectives

Reminder of the scientific questions

The present study aimed to answer the following two fundamental questions:

- How will biogenic emissions evolve in the future, particularly in the context of $+2^{\circ}\text{C}$ climate change level ?
- What impact will future variations in biogenic emissions have on air quality ?

Coupling and evaluation of the model SURFEX-MEGAN

To examine the evolution of biogenic emissions under future climate conditions, a coupling between the SURFEX and MEGAN models was implemented.

The primary objective of this coupling is to simulate biogenic emissions under present and future climate conditions. This is made possible by the adaptability of the SURFEX model, which can operate in an offline model (i.e. using an external meteorological forcing file). Furthermore, SURFEX includes a CO_2 -responsive scheme allowing the estimation of Leaf Area Index (LAI). This parameter is predicted to undergo significant alterations in response to climate change. The incorporation of this scheme contributes significantly to providing a more accurate representation of vegetation density in a changing climate, consequently improving the precision of biogenic emission estimations in future scenarios.

The coupling validation was done by running a global simulation (1° , hourly) in 2019 using ERA5 meteorological data inputs. The SURFEX-MEGAN total annual isoprene is estimated to 443Tg. This value is within the range of isoprene estimates reported in previous studies. To validate the coupled model, the 2019 isoprene simulation results were compared to isoprene estimates of 3 previous published studies. A spatial and temporal analysis were conducted to compare the different results. The SURFEX-MEGAN emission estimates were shown to have a comparable spatial distribution to the other inventories. As for the monthly variation of

isoprene emissions, SURFEX-MEGAN follows the same temporal pattern as some of the inventories, the shift in the annual isoprene cycle was explained by the difference in the contribution of the emitting regions to the global isoprene for each inventory.

A list of sensitivity tests was performed to investigate the impact of key MEGAN variables on isoprene emissions. To highlight the difference between the coupled SURFEX-MEGAN model and other MEGAN-based models, the results of the sensitivity tests were compared with the findings of other studies. The use of different meteorological forcings resulted in isoprene estimates varying up to +/- 5% of the reference run results, with Australia, South America and Africa being the most affected regions. The use of different input of emission potential data led to a decrease of 14% globally. The activation of the soil moisture parametrization was shown to have the greatest impact on isoprene emissions. On a global scale, the emission have decreased by 38%, the largest decrease was observed in Australia (-89%) and in Africa. The decrease rate related to the activation of the soil moisture activity factor varies across different studies, which has been attributed to inconsistencies in the soil moisture and wilting point data employed. The SURFEX-MEGAN model offers an advantage in this regard, as it can compute the wilting point and soil moisture at the same soil layer for different vegetation types, leading to a more precise estimation of the gamma soil moisture. This high sensitivity to soil moisture emphasizes the importance of conducting further studies in this area in order to reduce uncertainties, in particular by refining the estimation of the empirical parameter $\Delta\theta_1$.

Impact of a +2°C climate on isoprene emissions

To answer the first scientific question, present- and future-climate isoprene emissions were estimated using SURFEX-MEGAN. The coupled model was prescribed inputs from the CNRM-ESM2-1 Earth System Model under the SSP3-7.0 scenario. The future climate study period was set at 5 years and determined according to the temperature difference relative to the pre-industrial era 1850-1900, when an increase of 2°C was reached.

The projected mean isoprene emissions in 2046-2050 were estimated at 347 Tg, which indicates a 13% (+40 Tg) increase compared to isoprene levels in 2010-2014. The temperature rise level in 2046-2050 is estimated to +1.3°C relative to 2010-2014. The interannual variability in future isoprene emissions was relatively small, with values ranging between 318 and 363 Tg. Spatially, The increase in isoprene emissions affects the entire globe, with particular emphasis on South America, Southern Africa and Southeast Asia, where isoprene emissions have increased by 16%, 20% and 12%, respectively. In other low-isoprene emission regions such as Europe, Australia, North Africa and Russia, the isoprene increase rate was estimated to 10%, 7%, 14% and 9%, respectively.

The observed shifts in future isoprene emissions were attributable mainly to temperature, solar

radiation, leaf area index and atmospheric CO_2 concentrations. Temperature and leaf area index have a positive impact on isoprene emissions as they both are predicted to increase. Conversely, the decreasing levels of incoming solar radiation and the increasing concentrations of CO_2 have both a negative effect. The impact of the latter is known as the inhibitory effect of CO_2 .

A sensitivity analysis was conducted to determine the individual contribution of each of the factors mentioned above. This study demonstrated that the rise in future isoprene emissions was primarily attributed to projected future temperature increases, with solar radiation playing a minor role. The latter parameter is projected to decline in accordance with the SSP3-7.0 scenario. The CO_2 fertilization effect led to a reduction in LAI in tropical regions and an augmentation in high latitudes. This resulted in a net negative impact at a global scale, given that regions with high isoprene emissions are primarily located in the tropics. The inhibitory effect of CO_2 also demonstrated a substantial negative influence on future isoprene emissions, particularly pronounced at elevated CO_2 concentrations (exceeding 400 ppm).

The isoprene projections from the SURFEX-MEGAN model were compared to those of other CMIP6 models. The majority of models projected a positive change ranging between 29Tg and 92Tg. The SURFEX model, driven by CNRM-ESM2-1 outputs, indicated a 40Tg increase in 2046-2050 relative to 2010-2014. The UKESM1-0-LL model was the only model to predict a negative change. This discrepancy was attributed to the stronger penalization on isoprene emissions due to the CO_2 inhibition parameterization utilized in this model. The disparities in model results were attributed to variations in isoprene schemes, resolution, vegetation distribution, and density, but most importantly, each model's output of temperature and solar radiation differed, despite employing the same SSP scenario.

Impact of isoprene emissions in a +2°C climate on air quality

To answer the second scientific question, future air quality was simulated using the atmospheric-chemistry MOCAGE model. This study focused on the evaluation of surface ozone levels in 2050 compared to 2013 under the SSP3-7.0 scenario. Under the hypothesis of fixed isoprene emissions, the ozone burden increased by 5% and the mean surface global ozone concentrations by 12 ppb. The change in surface ozone levels varied with seasons. In boreal winter, ozone levels increased in North America, Europe, Southeast Asia and in boreal summer they decreased in North America and Europe but remained high in Southeast Asia. The policy targeting emissions control, which involves reducing nitrogen oxide (NO_x) concentrations in North America and Europe, proves effective only in the summer months. This is because during this period,

the emission of biogenic volatile organic compounds will shift the ozone regime towards being limited by NO_x availability. However, in heavily polluted regions like Southeast Asia, where the SSP3-7.0 scenario assumes an increase in human-made emissions of NO_x and VOCs, air quality is anticipated to deteriorate throughout the year.

A sensitivity analysis was conducted to determine the role of including interactive isoprene emissions in studying future air quality trends. This study proved that variations in ozone net production are closely correlated with fluctuations in isoprene flux. In regions with high NO_x emissions, ozone net production was positively correlated with isoprene emissions. In other regions, a negative correlation was detected. Although ozone sensitivity to isoprene emissions was proven to be high, the change in surface ozone concentrations between present and future-climate with fixed isoprene emissions and present and future-climate with evolving isoprene emissions was insignificant. This was explained by the expected rise in isoprene emissions driven by higher temperatures being offset by the inhibitory effect of CO_2 , resulting in only minor changes in isoprene emissions, of approximately 17 Tg. Consequently, the projected future changes in ozone levels are primarily driven by temperature and NO_x emissions, and only partially by isoprene changes. However, the impact of the latter becomes particularly significant locally, as it can improve or worsen air quality depending on NO_x concentrations level in this area.

To examine the impact of excluding the inhibitory effect of CO_2 on future ozone levels, another sensitivity study was conducted. Excluding the inhibitory effect of atmospheric CO_2 had a significant impact on ozone trends. While the overall global ozone burden stayed the same, there were notable improvements in future air quality in tropical regions, particularly in South America and South Africa throughout the year when interactive isoprene emissions were considered with a deactivated γ_{CO_2} , as opposed to a scenario with fixed isoprene emissions. However, this effect was only marginal in the northern hemisphere, as the difference in ozone concentrations between the future and present scenarios remained unchanged in both cases, whether with fixed or interactive isoprene emissions.

Perspectives

The current study suggests many potential perspectives for follow-up research.

Soil moisture

Soil moisture can affect the emission of biogenic species in two ways. Directly, through the soil moisture activity factor (Chapter 4), which regulates the emission of isoprene based on soil water availability. And indirectly through the influence it has on the vegetation photosynthetic activity and thus on vegetation density and LAI. This parameter controls also the emission rate

of BVOCs.

As demonstrated in the sensitivity studies presented in Chapter 4, the inclusion of the soil moisture activity factor led to a reduction of around 38% in global isoprene emissions estimated by the coupled model SURFEX-MEGAN. However, the impact of soil moisture deficit on isoprene emissions remains highly uncertain, with the MEGAN soil moisture parameterization being reported to significantly overestimate this effect in arid and semi-arid regions (Bauwens et al., 2018). This behavior was also observed in the SURFEX-MEGAN model.

Although many uncertainties surround this parameter, it is of high importance to consider the impact of soil moisture stress on projected isoprene emissions. In this context, the SURFEX model include the DIFF scheme which simulates soil water content at 14 soil layers. According to SURFEX simulations, soil moisture is expected to undergo significant changes in the context of a +2°C climate change. As shown in Figure A.1, the soil moisture at the fifth layer, representing the vegetation roots, is projected to decrease in the future in high isoprene emitting regions mainly in South America, South Africa and Southeast Asia. This reduction is expected to partially offset the observed increase in future isoprene emissions.

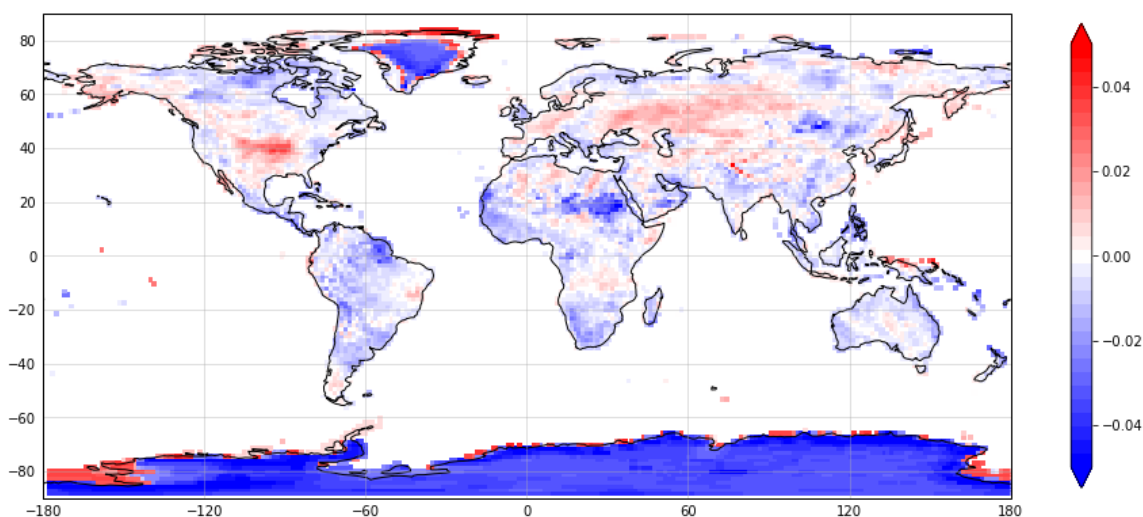


Figure A.1: Mean absolute difference in soil liquid water content at the fifth DIFF layer in m^3/m^3 between 2046-2050 and 2010-2014.

Land cover and land use

Although SURFEX incorporates a dynamic vegetation scheme that simulates the nature-induced changes in vegetation density, the prediction of future isoprene emissions was based on the hypothesis that land cover and land use remain unchanged. This hypothesis is clearly unrealistic, given that the vegetation distribution is expected to undergo significant nature- and human-induced changes in the future.

Hantson et al. (2017) found that future isoprene and monoterpenes emissions depend equitably on the land use and climate scenario considered. This study demonstrated that future isoprene emissions will relatively decrease by 33% as a response to anthropogenic land use change consisting of an increase in crop and pasture land-use. This study showed also that the nature-induced vegetation distribution have a marginal impact on the projections of future isoprene emissions as compared to human-induced land use changes.

Therefore, it is of utmost importance to take into account changes in land cover and land use in future projections of isoprene emissions with the SURFEX-MEGAN model. To this end, land use changes can be derived from the harmonized land use dataset (available at <https://luh.umd.edu/data.shtml>) and prescribed to SURFEX.

Implementation of SURFEX-MEGAN in the CNRM-ESM2-1 Earth System Model

CNRM-ESM2-1, a collaborative development by CNRM and CERFACS, is an Earth system model that employs SURFEX to simulate interactions between the Earth's surface and the atmosphere. As a potential avenue for further research, we could incorporate the updated version of SURFEX, which integrates the online implementation of MEGAN, into this ESM.

This integration will help providing interactive estimations of biogenic fluxes in the future based on various climate change scenarios. These estimations play a significant role in assessing the influence of climate on biogenic emissions, while also accounting for the feedback loop involving biogenic organic compounds and the Earth's radiative forcing. This feedback encompasses the cooling effect induced by aerosols and the warming effect induced by the formation of greenhouse gases such as ozone and methane.

Consequently, this research will enable us to determine the radiative forcing attributed to BVOCs in a climate change scenario with a temperature increase of +2°C considering a range of BVOCs-induced warming and cooling climate pollutants, mainly ozone, biogenic secondary organic aerosols, sulfate, Nitrate and Methane.

Air quality study

In the air quality analysis conducted in this study, our attention has been exclusively directed towards evaluating the effect of isoprene emissions on ozone trends. However, we have not accounted for the influence of other biogenic species. As a potential avenue for further research, we could broaden our scope to incorporate the impact of other biogenic species over an extended period. Conducting this study over a period of 10-20 years will improve the statistical significance of the conclusions driven from this analysis.

Additionally, as seen in Chapter 6, biogenic emissions will profoundly alter ozone levels in the

future and thus global and regional air quality trends. However, this assessment lacks the evaluation of secondary organic aerosols levels in the future as well as the impact of biogenic emissions on the formation processes of these compounds. In fact the chemistry-transport model MOCAGE employed in this air quality investigation incorporates a primitive scheme for simulating secondary organic aerosols. However, it is important to note that this scheme is not yet fully refined to accurately represent the influence of biogenic emissions on the processes governing SOA formation. Following additional refinement of this scheme, we can undertake a sensitivity analysis to assess how SOAs respond to changes in isoprene emissions under conditions of a +2°C climate change scenario.

Conclusions et perspectives

Rappel des questions scientifiques de la thèse

Cette étude avait pour but de répondre à deux questions fondamentales :

- *Comment les émissions biogéniques évolueront-elles dans le futur, en particulier dans le contexte d'un changement climatique de +2°C ?*
- *Quel sera l'impact des changements futurs des émissions biogéniques sur la qualité de l'air ?*

Couplage et évaluation du modèle SURFEX-MEGAN

Pour examiner l'évolution des émissions biogéniques dans les conditions climatiques futures, un couplage entre le modèle SURFEX et le modèle MEGAN a été mis en place.

L'objectif principal de ce couplage est de simuler les émissions biogéniques dans les conditions climatiques actuelles et futures. En effet, le modèle SURFEX peut être utilisé en mode hors ligne (en utilisant un fichier de forçage météorologique externe). De plus, le schéma de végétation tenant en compte les variations de CO₂ incorporé dans SURFEX permet d'estimer l'Indice de Surface Foliaire (LAI). Ce paramètre va de subir des altérations significatives en réponse au changement climatique. L'intégration de ce schéma contribue de manière significative à fournir une représentation plus précise de la densité et de la distribution de la végétation dans un contexte de conditions climatiques futures. Par conséquent, ce couplage permettra d'améliorer la précision des estimations des émissions biogéniques dans le futur.

La validation du couplage a été effectuée à partir d'une simulation globale des flux d'isoprène en 2019 avec le modèle couplé SURFEX-MEGAN. Le total annuel d'isoprène est estimé à 443 Tg. Cette valeur se situe dans la fourchette des estimations d'isoprène rapportées dans des études antérieures. Afin de valider le modèle couplé, les résultats de la simulation d'isoprène de 2019

ont été comparés aux estimations d'isoprène de trois études précédemment publiées. Une analyse spatiale et temporelle a été réalisée pour comparer les différents résultats. Les estimations d'émissions de SURFEX-MEGAN ont montré une distribution spatiale comparable aux autres inventaires. En ce qui concerne la variation mensuelle des émissions d'isoprène, SURFEX-MEGAN suit le même schéma temporel que certains des inventaires. Le décalage dans le cycle annuel de l'isoprène a été expliqué par la différence dans la contribution des régions émettrices à l'isoprène global pour chaque inventaire.

Une liste de tests de sensibilité a été réalisée pour examiner l'impact des variables clés de MEGAN sur l'émission d'isoprène. Pour souligner la différence entre le modèle couplé SURFEX-MEGAN et les autres modèles basés sur MEGAN, les résultats des tests de sensibilité ont été comparés aux conclusions d'autres études. L'utilisation de différents forçages météorologiques a entraîné une variation des estimations d'isoprène allant jusqu'à +/- 5% par rapport aux résultats de la simulation de référence, avec l'Australie, l'Amérique du Sud et l'Afrique étant les régions les plus touchées. L'utilisation de différentes données de potentielle d'émission a entraîné une diminution de 14% à l'échelle mondiale. L'activation de la paramétrisation de l'humidité du sol a montré avoir le plus grand impact sur les émissions d'isoprène. À l'échelle mondiale, les émissions ont diminué de 38%, la plus grande baisse ayant été observée en Australie (-89%) et en Afrique. Le taux de diminution lié à l'activation du facteur d'activité de l'humidité du sol varie d'une étude à l'autre, ce qui a été attribué à des incohérences dans les données d'humidité du sol et de point de flétrissement utilisées. Le modèle SURFEX-MEGAN présente un avantage à cet égard, car il peut calculer le point de flétrissement et l'humidité du sol dans la même couche de sol pour différents types de végétation, conduisant à une estimation plus précise du facteur d'humidité du sol γ_{SM} . Cette forte sensibilité à l'humidité du sol souligne l'importance de mener des études complémentaires afin de réduire les incertitudes, en particulier en affinant l'estimation du paramètre empirique $\Delta\theta_1$.

Impact d'un climat à +2°C sur les émissions d'isoprène

Pour répondre à la première question scientifique, les émissions d'isoprène dans le climat actuel et futur ont été estimées à l'aide de SURFEX-MEGAN. Les données d'entrée du modèle couplé ont été prescrites par le modèle Terre CNRM-ESM2-1 sous le scénario SSP3-7.0. La période d'étude du climat futur a été fixée à 5 ans et déterminée en fonction de la différence de température par rapport à l'ère préindustrielle 1850-1900, lorsqu'une augmentation de 2°C a été atteinte.

Les émissions moyennes d'isoprène en 2046-2050 ont été estimées à 347 Tg, ce qui représente une augmentation de 13% (+40 Tg) par rapport aux niveaux d'isoprène observés sur la période 2010-2014. Le niveau d'augmentation de la température en 2046-2050 est estimé à +1°C

par rapport à 2010-2014. La variabilité interannuelle des émissions futures d'isoprène était relativement faible, avec des valeurs comprises entre 318 et 363 Tg. Sur le plan spatial, l'augmentation des émissions d'isoprène affecte l'ensemble du globe, en particulier l'Amérique du Sud, l'Afrique du Sud et l'Asie du Sud-Est, où les émissions d'isoprène ont augmenté de 16%, 20% et 12%, respectivement. Dans d'autres régions à faibles émissions d'isoprène telles que l'Europe, l'Australie, l'Afrique du Nord et la Russie, le taux d'augmentation de l'isoprène a été estimé à 10%, 7%, 14% et 9%, respectivement.

Les changements observés dans les émissions futures d'isoprène étaient principalement attribuables à la température, au rayonnement solaire, à l'indice de surface foliaire (leaf area index, LAI) et aux concentrations atmosphériques de CO₂. La température et l'indice de surface foliaire ont un impact positif sur les émissions d'isoprène. Inversement, la diminution du rayonnement solaire incident et l'augmentation des concentrations de CO₂ ont tous deux un effet négatif. L'impact de ce dernier est connu sous le nom d'effet inhibiteur du CO₂.

Une analyse de sensibilité a été menée pour déterminer la contribution individuelle de chacun des facteurs mentionnés ci-dessus. Cette étude a démontré que l'augmentation future des émissions d'isoprène était principalement attribuée aux augmentations projetées de température, le rayonnement solaire jouant un rôle mineur. Conformément au scénario SSP3-7.0, ce paramètre va subir une diminution importante dans le futur. L'effet de fertilisation par le CO₂ a entraîné une réduction de l'indice de surface foliaire (LAI) dans les régions tropicales et une augmentation aux hautes latitudes. Cela a résulté en un impact net négatif à l'échelle mondiale, étant donné que les régions avec des émissions élevées d'isoprène se trouvent principalement dans les tropiques. L'effet inhibiteur du CO₂ a également démontré une influence négative substantielle sur les émissions futures d'isoprène, particulièrement prononcée à des concentrations élevées de CO₂ (dépassant 400 ppm).

Les projections d'isoprène du modèle SURFEX-MEGAN ont été comparées à celles d'autres modèles CMIP6. La majorité des modèles ont projeté un changement positif allant de 29Tg à 92Tg. Le modèle SURFEX, piloté par les sorties du CNRM-ESM2-1, indique une augmentation de 40Tg en 2046-2050 par rapport à 2010-2014. Le modèle UKESM1-0-LL est le seul à prévoir un changement négatif. Cette divergence a été attribuée à la pénalisation plus forte des émissions d'isoprène due à la paramétrisation de l'inhibition du CO₂ utilisée dans ce modèle. Les disparités dans les résultats des modèles ont été attribuées aux différences dans les schémas d'isoprène, la résolution, la distribution et la densité de la végétation, mais surtout, les sorties de température et de rayonnement solaire de chaque modèle différaient, malgré l'utilisation du même scénario SSP.

Impact des émissions d'isoprène dans un climat à +2°C sur la qualité de l'air

Pour répondre à la deuxième question scientifique, la qualité de l'air future a été simulée grâce au modèle de chimie-transport MOCAGE. Cette étude s'est concentrée sur l'évolution des niveaux d'ozone en 2050 par rapport à 2013, sur la base des émissions anthropiques et de combustion de biomasse du scénario SSP3-7.0. Sous l'hypothèse d'émissions fixes d'isoprène, la charge d'ozone a augmenté de 5% et les concentrations mondiales moyennes d'ozone à la surface de 12 ppb. L'évolution des niveaux d'ozone varie en fonction des saisons. En hiver boréal, les niveaux d'ozone ont augmenté en Amérique du Nord, en Europe et en Asie du Sud-Est, et en été boréal, ils ont diminué en Amérique du Nord et en Europe, mais sont restés élevés en Asie du Sud-Est. La politique de contrôle des émissions, qui consiste à réduire les concentrations d'oxyde d'azote (NO_x) en Amérique du Nord et en Europe, ne s'avère efficace que pendant les mois d'été. En effet, durant cette période, l'émission de composés organiques biogéniques fait basculer le régime d'ozone vers une limitation par la disponibilité des NO_x . Toutefois, dans les régions fortement polluées comme l'Asie du Sud-Est, où le scénario SSP3-7.0 prévoit une augmentation des émissions anthropiques de NO_x et de COV, la qualité de l'air devrait se détériorer tout au long de l'année.

Une analyse de sensibilité a été réalisée pour déterminer le rôle de l'inclusion des émissions d'isoprène dans l'étude des tendances futures de la qualité de l'air. Cette étude a prouvé que les variations de la production nette d'ozone sont étroitement corrélées aux fluctuations du flux d'isoprène. Dans les régions à fortes émissions de NO_x , la production nette d'ozone est positivement corrélée aux émissions d'isoprène. Dans d'autres régions, une corrélation négative a été détectée. Bien que la sensibilité de l'ozone aux émissions d'isoprène se soit avérée élevée, la variation des concentrations d'ozone à la surface entre le climat actuel et le climat futur avec des émissions d'isoprène fixes et le climat actuel et le climat futur avec des émissions d'isoprène évolutives était insignifiante. Cela s'explique par le fait que l'augmentation attendue des émissions d'isoprène due à des températures plus élevées est compensée par l'effet inhibiteur du CO_2 , ce qui n'entraîne que des changements mineurs dans les émissions d'isoprène, d'environ 17 Tg. Par conséquent, les changements futurs prévus dans les niveaux d'ozone sont principalement dus à la température et aux émissions de NO_x , et seulement partiellement aux changements dans l'isoprène. Cependant, l'impact de ce dernier devient particulièrement significatif au niveau local, car il peut améliorer ou détériorer la qualité de l'air en fonction du niveau des concentrations de NO_x dans cette zone.

Pour examiner l'impact de l'exclusion de l'effet inhibiteur du CO_2 sur les niveaux futurs d'ozone, une autre étude de sensibilité a été réalisée. L'exclusion de l'effet inhibiteur du CO_2 a eu un impact significatif sur les tendances de l'ozone. Alors que la charge globale d'ozone est restée

la même, il y a eu des améliorations notables de la qualité de l'air dans les régions tropicales, en particulier en Amérique du Sud et en Afrique du Sud, tout au long de l'année lorsque les émissions interactives d'isoprène ont été considérées avec un γ_{CO_2} désactivé, par opposition à un scénario avec des émissions d'isoprène fixes. Toutefois, cet effet n'était que marginal dans l'hémisphère nord, la différence de concentrations d'ozone entre les scénarios futurs et actuels restant inchangée dans les deux cas, que les émissions d'isoprène soient fixes ou interactives.

Perspectives

L'étude actuelle suggère de nombreuses perspectives potentielles pour des recherches complémentaires.

Humidité du sol

L'humidité du sol peut affecter l'émission d'espèces biogéniques de deux manières. Directement, par le biais du facteur d'activité de l'humidité du sol (Chapitre 4), qui régule l'émission d'isoprène en fonction de la disponibilité de l'eau dans le sol. Et indirectement, par l'influence qu'il a sur l'activité photosynthétique de la végétation et donc sur la densité de la végétation et le LAI. Ce paramètre contrôle également le taux d'émission des BVOCs.

Comme le montrent les études de sensibilité présentées au Chapitre 4, l'inclusion du facteur d'activité de l'humidité du sol a entraîné une réduction d'environ 38% des émissions d'isoprène estimées par le modèle couplé SURFEX-MEGAN. Cependant, l'impact du déficit d'humidité du sol sur les émissions d'isoprène reste très incertain, la paramétrisation de l'humidité du sol de MEGAN étant signalée comme surestimant de manière significative cet effet dans les régions arides et semi-arides (Bauwens et al., 2018). Ce comportement a également été observé dans le modèle SURFEX-MEGAN.

Bien que de nombreuses incertitudes entourent ce paramètre, il est très important de prendre en compte l'impact du stress hydrique du sol sur les émissions d'isoprène projetées. Dans ce contexte, le modèle SURFEX inclut le schéma DIFF qui simule la teneur en eau du sol dans 14 couches. Selon les simulations de SURFEX, l'humidité du sol devrait subir des changements significatifs dans le contexte d'un changement climatique de +2°C. Comme le montre la figure A.2, l'humidité du sol à la 5ème couche, qui représente les racines de la végétation, devrait diminuer dans le futur dans les régions à fortes émissions d'isoprène, principalement en Amérique du Sud, en Afrique du Sud et en Asie du Sud-Est. Cette réduction devrait partiellement compenser l'augmentation observée des émissions futures d'isoprène.

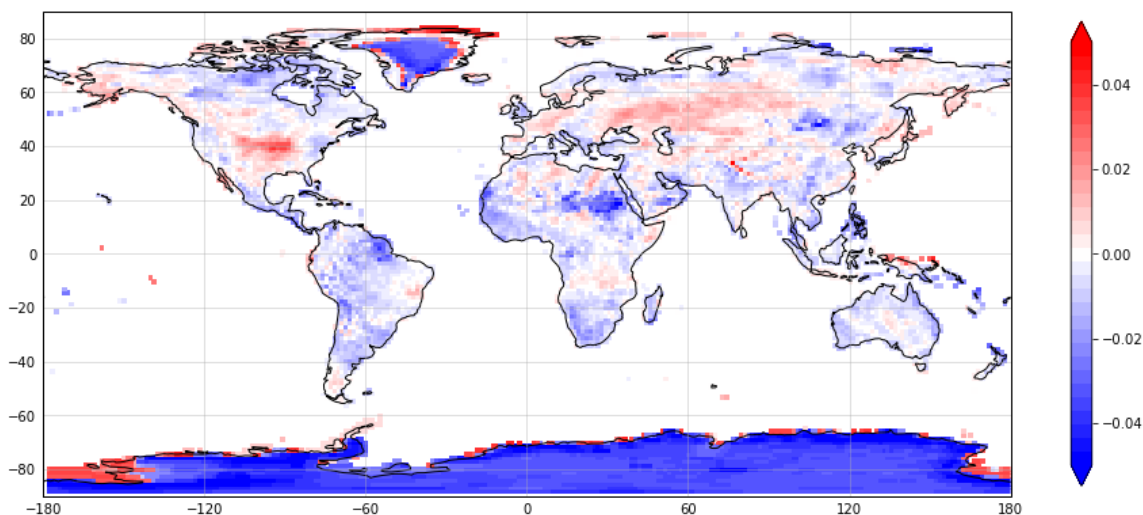


Figure A.2: Différence absolue moyenne de la teneur en eau liquide du sol à la 5ème couche DIFF en m^3/m^3 entre 2046-2050 et 2010-2014.

Occupation et utilisation des sols

Bien que SURFEX intègre un schéma de végétation dynamique qui simule les changements de densité de végétation induits par le climat, la prédiction des émissions futures d'isoprène était basée sur l'hypothèse que la couverture et l'utilisation des sols restaient inchangées. Cette hypothèse est manifestement irréaliste, étant donné que la distribution de la végétation devrait subir d'importants changements naturels et anthropiques.

Hantson et al. (2017) a constaté que les émissions futures d'isoprène et de monoterpènes dépendent équitablement du scénario d'utilisation des sols et du scénario climatique considérés. Cette étude a démontré que les émissions futures d'isoprène diminueront relativement de 33% en réponse au changement anthropique d'utilisation des sols, qui consiste en une augmentation de l'utilisation des terres cultivées et des pâturages. Cette étude a également montré que le changement de la distribution de la végétation due au changement climatique a un impact marginal sur les projections des futures émissions d'isoprène par rapport aux changements d'utilisation des sols anthropiques.

Par conséquent, il est de la plus haute importance de prendre en compte les changements dans l'occupation et l'utilisation des sols dans les projections futures des émissions d'isoprène à l'aide du modèle SURFEX-MEGAN. À cette fin, les changements d'utilisation des sols peuvent être dérivés de l'ensemble de données harmonisées sur l'utilisation des sols (disponible à <https://luh.umd.edu/data.shtml>) et prescrits à SURFEX.

Implémentation de SURFEX-MEGAN dans le modèle CNRM-ESM2-1

CNRM-ESM2-1, fruit d'une collaboration entre le CNRM et le CERFACS, est un modèle du système Terre qui utilise SURFEX pour simuler les interactions entre la surface et l'atmosphère. Il est essentiel donc d'incorporer la version actualisée de SURFEX, qui intègre l'implémentation en ligne de MEGAN, dans cet ESM.

Cette intégration permettra de fournir des estimations interactives des flux biogéniques dans le futur sur la base de différents scénarios de changement climatique. Ces estimations jouent un rôle important dans l'évaluation de l'influence du climat sur les émissions biogéniques, tout en tenant compte de la rétroaction entre les composés organiques volatils biogéniques et le forçage radiatif de la Terre. Cette rétroaction englobe l'effet de refroidissement induit par les aérosols et l'effet de réchauffement induit par la formation de gaz à effet de serre tels que l'ozone et le méthane.

Par conséquent, cette étude nous permettra de déterminer le forçage radiatif attribué aux BVOC dans un scénario de changement climatique à +2°C en considérant une gamme de polluants climatiques réchauffants et refroidissants, principalement l'ozone, les aérosols organiques secondaires, le sulfate, le nitrate et le méthane.

L'étude de la qualité de l'air

Dans l'analyse de la qualité de l'air réalisée dans cette étude, notre attention s'est portée exclusivement sur l'évaluation de l'effet des émissions d'isoprène sur les tendances de l'ozone. Cependant, nous n'avons pas tenu compte de l'influence d'autres espèces biogéniques. Comme piste de recherche potentielle, nous pourrions élargir notre champ d'investigation pour incorporer l'impact d'autres espèces biogéniques sur une période étendue. La réalisation de cette étude sur une période de 10 à 20 ans améliorera la validité statistique des conclusions tirées de cette analyse.

En outre, comme nous l'avons vu au Chapitre 6, les émissions biogéniques modifieront profondément les niveaux d'ozone dans le futur et donc les tendances mondiales et régionales de qualité de l'air. Toutefois, la présente étude ne comporte pas l'évaluation des niveaux d'aérosols organiques secondaires dans le futur, ni l'impact des émissions biogéniques sur les processus de formation de ces composés. En fait, le modèle de chimie-transport MOCAGE utilisé dans l'étude de qualité de l'air intègre un schéma primitif pour simuler les aérosols organiques secondaires. Cependant, il est important de noter que ce schéma n'est pas encore totalement affiné pour représenter avec précision l'influence des émissions biogéniques sur les processus régissant la formation des AOS. Après avoir affiné ce schéma, nous pourrions entreprendre une analyse de sensibilité pour évaluer comment les SOA répondront aux changements dans les émissions

d'isoprène dans les conditions d'un scénario de changement climatique de +2°C.

Acronyms

ABL Atmospheric Boundary Layer. 35

AR Assessment Report. 41, 54

BVOCs Biogenic Volatile Organic Compounds. 13

CCN Cloud Condensation Nuclei. 39

CMIP Coupled Model Intercomparison Project. 43

ESM Earth System Model. 115

GDP Gross Domestic Product. 46

GHGs Greenhouse gases. 42, 44, 54

GMSL Global Mean Sea Level. 49

IAM Integrated Assessment Models. 46

IPCC International Panel on Climate Change. 41, 43, 44

LAI Leaf Area Index. 56

LCLU Land Cover and Land Use. 56

MEGAN Model of Emission of Gases and Aerosols from Nature. 63

MOCAGE Modèle de Chimie Atmosphérique de Grande Échelle. 137

PFT Plant Functional Type. 64

PM Particulate Matter. 54

- POA** Primary Organic Aerosols. 35
- PPFD** Photosynthetic Photon Flux Density. 20
- RACM** Regional Atmospheric Chemistry Mechanism. 139
- RCP** Representative Concentration Pathway. xix, 43, 44, 47, 49
- REPROBUS** REactive Processes Ruling the Ozone BUdget in the Stratosphere. 139
- SLCFs** Short-Lived Climate Forcers. xiv, 55
- SOA** Secondary Organic Aerosols. 35, 39
- SPA** Shared Policy Assumptions. 46
- SSP** Shared Socioeconomic Pathway. xiv, 44–49
- STE** Stratosphere-Troposphere Exchange. 35
- UNEP** United Nations Environment Program. 41
- UNFCCC** United Nations Framework Convention on Climate Change. 41, 42
- UTLS** Upper Troposphere and Lower Stratosphere. 35
- UV** Ultraviolet. 26
- VOC** Volatile Organic Compound. 2, 8, 27
- WHO** World Health Organization. 25
- WMO** World Meteorological Organization. 38, 41

Bibliography

Arias, P., Bellouin, N., Coppola, E., Jones, R., Krinner, G., Marotzke, J., Naik, V., Palmer, M., Plattner, G.-K., Rogelj, J., Rojas, M., Sillmann, J., Storelvmo, T., Thorne, P., Trewin, B., Achuta Rao, K., Adhikary, B., Allan, R., Armour, K., Bala, G., Barimalala, R., Berger, S., Canadell, J., Cassou, C., Cherchi, A., Collins, W., Collins, W., Connors, S., Corti, S., Cruz, F., Dentener, F., Dereczynski, C., Di Luca, A., Diongue Niang, A., Doblus-Reyes, F., Dosio, A., Douville, H., Engelbrecht, F., Eyring, V., Fischer, E., Forster, P., Fox-Kemper, B., Fuglestvedt, J., Fyfe, J., Gillett, N., Goldfarb, L., Gorodetskaya, I., Gutierrez, J., Hamdi, R., Hawkins, E., Hewitt, H., Hope, P., Islam, A., Jones, C., Kaufman, D., Kopp, R., Kosaka, Y., Kossin, J., Krakovska, S., Lee, J.-Y., Li, J., Mauritsen, T., Maycock, T., Meinshausen, M., Min, S.-K., Monteiro, P., Ngo-Duc, T., Otto, F., Pinto, I., Pirani, A., Raghavan, K., Ranasinghe, R., Ruane, A., Ruiz, L., Sallée, J.-B., Samset, B., Sathyendranath, S., Seneviratne, S., Sörensson, A., Szopa, S., Takayabu, I., Tréguier, A.-M., van den Hurk, B., Vautard, R., von Schuckmann, K., Zaehle, S., Zhang, X., and Zickfeld, K.: Technical Summary, p. 33144, Cambridge University Press, Cambridge, United Kingdom and New York, NY, USA, <https://doi.org/10.1017/9781009157896.002>, 2021.

Baghi, R., Helmig, D., Guenther, A., Duhl, T., and Daly, R.: Contribution of flowering trees to urban atmospheric biogenic volatile organic compound emissions, *Biogeosciences*, 9, 3777–3785, 2012.

Bauwens, M., Stavrakou, T., Müller, J.-F., Van Schaeybroeck, B., De Cruz, L., De Troch, R., Giot, O., Hamdi, R., Termonia, P., Laffineur, Q., et al.: Recent past (1979–2014) and future (2070–2099) isoprene fluxes over Europe simulated with the MEGAN–MOHYCAN model, *Biogeosciences*, 15, 3673–3690, 2018.

Behnke, K., Ehrling, B., Teuber, M., Bauerfeind, M., Louis, S., Hänsch, R., Polle, A., Bohlmann, J., and Schnitzler, J.-P.: Transgenic, non-isoprene emitting poplars don't like it hot, *The Plant Journal*, 51, 485–499, 2007.

BIBLIOGRAPHY

- Bertin, N. and Staudt, M.: Effect of water stress on monoterpene emissions from young potted holm oak (*Quercus ilex* L.) trees, *Oecologia*, 107, 456–462, 1996.
- Boone, A., Calvet, J.-C., and Noilhan, J.: Inclusion of a third soil layer in a land surface scheme using the force–restore method, *Journal of Applied Meteorology*, 38, 1611–1630, 1999.
- Boucher, O.: *Aérosols atmosphériques: Propriétés et impacts climatiques*, Springer, 2012.
- Brown, F., Folberth, G. A., Sitch, S., Bauer, S., Bauters, M., Boeckx, P., Cheesman, A. W., Deushi, M., Dos Santos Vieira, I., Galy-Lacaux, C., et al.: The ozone–climate penalty over South America and Africa by 2100, *Atmospheric Chemistry and Physics*, 22, 12 331–12 352, 2022.
- Bucher, J.: SO₂-induced ethylene evolution of forest tree foliage, and its potential use as stress-indicator, *European Journal of Forest Pathology*, 11, 369–373, 1981.
- Calvet, J.-C., Noilhan, J., Roujean, J.-L., Bessemoulin, P., Cabelguenne, M., Olios, A., and Wigneron, J.-P.: An interactive vegetation SVAT model tested against data from six contrasting sites, *Agricultural and Forest Meteorology*, 92, 73–95, 1998.
- Cao, Y., Yue, X., Liao, H., Yang, Y., Zhu, J., Chen, L., Tian, C., Lei, Y., Zhou, H., and Ma, Y.: Ensemble projection of global isoprene emissions by the end of 21st century using CMIP6 models, *Atmospheric Environment*, 267, 118 766, 2021.
- Chen, J., Avise, J., Guenther, A., Wiedinmyer, C., Salathe, E., Jackson, R. B., and Lamb, B.: Future land use and land cover influences on regional biogenic emissions and air quality in the United States, *Atmospheric Environment*, 43, 5771–5780, 2009.
- Chen, Z., Liu, J., Qie, X., Cheng, X., Shen, Y., Yang, M., Jiang, R., and Liu, X.: Transport of substantial stratospheric ozone to the surface by a dying typhoon and shallow convection, *Atmospheric Chemistry and Physics*, 22, 8221–8240, 2022.
- Danabasoglu, G., Lamarque, J.-F., Bacmeister, J., Bailey, D., DuVivier, A., Edwards, J., Emmons, L., Fasullo, J., Garcia, R., Gettelman, A., et al.: The community earth system model version 2 (CESM2), *Journal of Advances in Modeling Earth Systems*, 12, e2019MS001 916, 2020.
- Decharme, B., Boone, A., Delire, C., and Noilhan, J.: Local evaluation of the Interaction between Soil Biosphere Atmosphere soil multilayer diffusion scheme using four pedotransfer functions, *Journal of Geophysical Research: Atmospheres*, 116, 2011.
- Delmas, R. and Mégie, G.: *Physique et chimie de l’atmosphère: 2e édition*, Belin, 2015.

BIBLIOGRAPHY

- Dement, W. A., Tyson, B. J., and Mooney, H. A.: Mechanism of monoterpene volatilization in *Salvia mellifera*, *Phytochemistry*, 14, 2555–2557, 1975.
- Dobson, H. E.: Floral volatiles in insect biology, *Insect-Plant Interactions* (1993), pp. 47–82, 2017.
- Dueck, T. A., De Visser, R., Poorter, H., Persijn, S., Gorissen, A., De Visser, W., Schapendonk, A., Verhagen, J., Snel, J., Harren, F. J., et al.: No evidence for substantial aerobic methane emission by terrestrial plants: a ^{13}C -labelling approach, *New Phytologist*, 175, 29–35, 2007.
- Dunker, A. M., Koo, B., and Yarwood, G.: Ozone sensitivity to isoprene chemistry and emissions and anthropogenic emissions in central California, *Atmospheric environment*, 145, 326–337, 2016.
- Dunne, J. P., Horowitz, L., Adcroft, A., Ginoux, P., Held, I., John, J., Krasting, J. P., Malyshev, S., Naik, V., Paulot, F., et al.: The GFDL Earth System Model version 4.1 (GFDL-ESM 4.1): Overall coupled model description and simulation characteristics, *Journal of Advances in Modeling Earth Systems*, 12, e2019MS002015, 2020.
- El Aabaribaoune, M.: Assimilation des luminances IASI dans un modèle de chimie transport pour la surveillance de l’ozone et des poussières désertiques, Ph.D. thesis, Université Paul Sabatier-Toulouse III, 2022.
- Fan, X., Duan, Q., Shen, C., Wu, Y., and Xing, C.: Global surface air temperatures in CMIP6: historical performance and future changes, *Environmental Research Letters*, 15, 104056, 2020.
- Faroux, S., Kaptué Tchuenté, A., Roujean, J.-L., Masson, V., Martin, E., and Le Moigne, P.: ECOCLIMAP-II/Europe: A twofold database of ecosystems and surface parameters at 1 km resolution based on satellite information for use in land surface, meteorological and climate models, *Geoscientific Model Development*, 6, 563–582, 2013.
- Faubert, P., Tiiva, P., Rinnan, Å., Michelsen, A., Holopainen, J. K., and Rinnan, R.: Doubled volatile organic compound emissions from subarctic tundra under simulated climate warming, *New Phytologist*, 187, 199–208, 2010.
- Fischer, N. H.: *Plant terpenoids as allelopathic agents*, 1991.
- Fitzky, A. C., Sandén, H., Karl, T., Fares, S., Calfapietra, C., Grote, R., Saunier, A., and Rewald, B.: The interplay between ozone and urban vegetation—BVOC emissions, ozone deposition, and tree ecophysiology, *Frontiers in Forests and Global Change*, 2, 50, 2019.

- Fu, Y. and Liao, H.: Impacts of land use and land cover changes on biogenic emissions of volatile organic compounds in China from the late 1980s to the mid-2000s: implications for tropospheric ozone and secondary organic aerosol, *Tellus B: Chemical and Physical Meteorology*, 66, 24987, 2014.
- Fuentes, J. D., Lerdau, M., Atkinson, R., Baldocchi, D., Bottenheim, J., Ciccioli, P., Lamb, B., Geron, C., Gu, L., Guenther, A., et al.: Biogenic hydrocarbons in the atmospheric boundary layer: a review, *Bulletin of the American Meteorological Society*, 81, 1537–1575, 2000.
- Gerber, S., Joos, F., and Prentice, I. C.: Sensitivity of a dynamic global vegetation model to climate and atmospheric CO₂, *Global Change Biology*, 10, 1223–1239, 2004.
- Gibelin, A.-L., Calvet, J.-C., Roujean, J.-L., Jarlan, L., and Los, S. O.: Ability of the land surface model ISBA-A-gs to simulate leaf area index at the global scale: Comparison with satellites products, *Journal of Geophysical Research: Atmospheres*, 111, 2006.
- Goudie, A. S. and Middleton, N. J.: Saharan dust storms: nature and consequences, *Earth-science reviews*, 56, 179–204, 2001.
- Greenberg, J., Asensio, D., Turnipseed, A., Guenther, A., Karl, T., and Gochis, D.: Contribution of leaf and needle litter to whole ecosystem BVOC fluxes, *Atmospheric Environment*, 59, 302–311, 2012.
- Guenther, A.: Biological and chemical diversity of biogenic volatile organic emissions into the atmosphere, *International Scholarly Research Notices*, 2013, 2013.
- Guenther, A., Hewitt, C. N., Erickson, D., Fall, R., Geron, C., Graedel, T., Harley, P., Klinger, L., Lerdau, M., McKay, W., et al.: A global model of natural volatile organic compound emissions, *Journal of Geophysical Research: Atmospheres*, 100, 8873–8892, 1995.
- Guenther, A., Baugh, B., Brasseur, G., Greenberg, J., Harley, P., Klinger, L., Serça, D., and Vierling, L.: Isoprene emission estimates and uncertainties for the Central African EXPRESSO study domain, *Journal of Geophysical Research: Atmospheres*, 104, 30 625–30 639, 1999.
- Guenther, A., Karl, T., Harley, P., Wiedinmyer, C., Palmer, P. I., and Geron, C.: Estimates of global terrestrial isoprene emissions using MEGAN (Model of Emissions of Gases and Aerosols from Nature), *Atmospheric Chemistry and Physics*, 6, 3181–3210, 2006.
- Guenther, A., Jiang, X., Heald, C. L., Sakulyanontvittaya, T., Duhl, T. a., Emmons, L., and Wang, X.: The Model of Emissions of Gases and Aerosols from Nature version 2.1 (MEGAN2.1): an extended and updated framework for modeling biogenic emissions, *Geoscientific Model Development*, 5, 1471–1492, 2012.

BIBLIOGRAPHY

- Guenther, A. B., Monson, R. K., and Fall, R.: Isoprene and monoterpene emission rate variability: observations with eucalyptus and emission rate algorithm development, *Journal of Geophysical Research: Atmospheres*, 96, 10 799–10 808, 1991.
- Hantson, S., Knorr, W., Schurgers, G., Pugh, T. A., and Arneth, A.: Global isoprene and monoterpene emissions under changing climate, vegetation, CO₂ and land use, *Atmospheric Environment*, 155, 35–45, 2017.
- Heald, C. L., Wilkinson, M. J., Monson, R. K., Alo, C. A., Wang, G., and Guenther, A.: Response of isoprene emission to ambient CO₂ changes and implications for global budgets, *Global Change Biology*, 15, 1127–1140, 2009.
- Henrot, A.-J., Stanelle, T., Schröder, S., Siegenthaler, C., Taraborrelli, D., and Schultz, M. G.: Implementation of the MEGAN (v2. 1) biogenic emission model in the ECHAM6-HAMMOZ chemistry climate model, *Geoscientific model development*, 10, 903–926, 2017.
- Heuss, J. M., Kahlbaum, D. F., and Wolff, G. T.: Weekday/weekend ozone differences: what can we learn from them?, *Journal of the Air & Waste Management Association*, 53, 772–788, 2003.
- Hurtt, G. C., Chini, L. P., Frohling, S., Betts, R., Feddema, J., Fischer, G., Fisk, J., Hibbard, K., Houghton, R., Janetos, A., et al.: Harmonization of land-use scenarios for the period 1500–2100: 600 years of global gridded annual land-use transitions, wood harvest, and resulting secondary lands, *Climatic change*, 109, 117–161, 2011.
- Jacobs, C., Van den Hurk, B., and De Bruin, H.: Stomatal behaviour and photosynthetic rate of unstressed grapevines in semi-arid conditions, *Agricultural and Forest Meteorology*, 80, 111–134, 1996.
- Jacobs, C. M. J.: Direct impact of atmospheric CO₂ enrichment on regional transpiration, Wageningen University and Research, 1994.
- Janson, R. W.: Monoterpene emissions from Scots pine and Norwegian spruce, *Journal of geophysical research: atmospheres*, 98, 2839–2850, 1993.
- Josse, B., Simon, P., and Peuch, V.-H.: Radon global simulations with the multiscale chemistry and transport model MOCAGE, *Tellus B: Chemical and Physical Meteorology*, 56, 339–356, 2004.
- Juuti, S., Arey, J., and Atkinson, R.: Monoterpene emission rate measurements from a Monterey pine, *Journal of Geophysical Research: Atmospheres*, 95, 7515–7519, 1990.

BIBLIOGRAPHY

- Kelley, M., Schmidt, G. A., Nazarenko, L. S., Bauer, S. E., Ruedy, R., Russell, G. L., Ackerman, A. S., Aleinov, I., Bauer, M., Bleck, R., et al.: GISS-E2. 1: Configurations and climatology, *Journal of Advances in Modeling Earth Systems*, 12, e2019MS002025, 2020.
- Keppler, F., Hamilton, J. T., Braß, M., and Röckmann, T.: Methane emissions from terrestrial plants under aerobic conditions, *Nature*, 439, 187–191, 2006.
- Kesselmeier, J. and Staudt, M.: Biogenic volatile organic compounds (VOC): an overview on emission, physiology and ecology, *Journal of atmospheric chemistry*, 33, 23–88, 1999.
- Krinner, G., Viovy, N., de Noblet-Ducoudré, N., Ogée, J., Polcher, J., Friedlingstein, P., Ciais, P., Sitch, S., and Prentice, I. C.: A dynamic global vegetation model for studies of the coupled atmosphere-biosphere system, *Global Biogeochemical Cycles*, 19, 2005.
- Kurtén, T., Kulmala, M., Dal Maso, M., Suni, T., Reissell, A., Vehkamäki, H., Hari, P., Laaksonen, A., Viisanen, Y., and Vesala, T.: Estimation of different forest-related contributions to the radiative balance using observations in southern Finland, *Boreal environment research*, 8, 275, 2003.
- Lafont, S., Zhao, Y., Calvet, J.-C., Peylin, P., Ciais, P., Maignan, F., and Weiss, M.: Modelling LAI, surface water and carbon fluxes at high-resolution over France: comparison of ISBA-Ags and ORCHIDEE, *Biogeosciences*, 9, 439–456, 2012.
- Lathiere, J., Hauglustaine, D., De Noblet-Ducoudré, N., Krinner, G., and Folberth, G.: Past and future changes in biogenic volatile organic compound emissions simulated with a global dynamic vegetation model, *Geophysical Research Letters*, 32, 2005.
- Le Moigne, P.: SURFEX scientific documentation, V8. 1, 2018.
- Lefevre, F., Brasseur, G., Folkins, I., Smith, A., and Simon, P.: Chemistry of the 1991–1992 stratospheric winter: Three-dimensional model simulations, *Journal of Geophysical Research: Atmospheres*, 99, 8183–8195, 1994.
- Lerdau, M., Guenther, A., and Monson, R.: Plant production and emission of volatile organic compounds, *Bioscience*, 47, 373–383, 1997.
- Lin, J.-T., Patten, K. O., Hayhoe, K., Liang, X.-Z., and Wuebbles, D. J.: Effects of future climate and biogenic emissions changes on surface ozone over the United States and China, *Journal of Applied Meteorology and Climatology*, 47, 1888–1909, 2008.
- Lindskog, A. and Potter, A.: Terpene emission and ozone stress, *Chemosphere*, 30, 1171–1181, 1995.

BIBLIOGRAPHY

- Liu, Z., Doherty, R. M., Wild, O., O’connor, F. M., and Turnock, S. T.: Tropospheric ozone changes and ozone sensitivity from the present day to the future under shared socio-economic pathways, *Atmospheric Chemistry and Physics*, 22, 1209–1227, 2022.
- Loreto, F. and Sharkey, T.: Isoprene emission by plants is affected by transmissible wound signals, *Plant, Cell & Environment*, 16, 563–570, 1993.
- Loreto, F., Ciccioli, P., Cecinato, A., Brancaleoni, E., Frattoni, M., and Tricoli, D.: Influence of environmental factors and air composition on the emission of [alpha]-pinene from *Quercus ilex* leaves, *Plant Physiology*, 110, 267–275, 1996.
- Mahowald, N., Lo, F., Zheng, Y., Harrison, L., Funk, C., Lombardozzi, D., and Goodale, C.: Projections of leaf area index in earth system models, *Earth System Dynamics*, 7, 211–229, 2016.
- Masson, V.: A physically-based scheme for the urban energy budget in atmospheric models, *Boundary-layer meteorology*, 94, 357–397, 2000.
- Mihaliak, C. A., Gershenzon, J., and Croteau, R.: Lack of rapid monoterpene turnover in rooted plants: implications for theories of plant chemical defense, *Oecologia*, 87, 373–376, 1991.
- Mironov, D., Heise, E., Kourzeneva, E., Ritter, B., Schneider, N., and Terzhevik, A.: Implementation of the lake parameterisation scheme FLake into the numerical weather prediction model COSMO, 2010.
- Monahan, E. C.: Sea spray as a function of low elevation wind speed, *Journal of Geophysical research*, 73, 1127–1137, 1968.
- Monson, R., Harley, P., Litvak, M., Wildermuth, M., Guenther, A., Zimmerman, P., and Fall, R.: Environmental and developmental controls over the seasonal pattern of isoprene emission from aspen leaves, *Oecologia*, 99, 260–270, 1994.
- Niinemets, Ü., Tenhunen, J., Harley, P. C., and Steinbrecher, R.: A model of isoprene emission based on energetic requirements for isoprene synthesis and leaf photosynthetic properties for *Liquidambar* and *Quercus*, *Plant, Cell & Environment*, 22, 1319–1335, 1999.
- Niyogi, D., Chang, H.-I., Saxena, V., Holt, T., Alapaty, K., Booker, F., Chen, F., Davis, K. J., Holben, B., Matsui, T., et al.: Direct observations of the effects of aerosol loading on net ecosystem CO₂ exchanges over different landscapes, *Geophysical Research Letters*, 31, 2004.
- Noilhan, J. and Mahfouf, J.-F.: The ISBA land surface parameterisation scheme, *Global and planetary Change*, 13, 145–159, 1996.

BIBLIOGRAPHY

- Opacka, B., Müller, J.-F., Stavrou, T., Bauwens, M., Sindelarova, K., Markova, J., and Guenther, A. B.: Global and regional impacts of land cover changes on isoprene emissions derived from spaceborne data and the MEGAN model, *Atmospheric Chemistry and Physics*, 21, 8413–8436, 2021.
- O’Neill, B. C., Kriegler, E., Ebi, K. L., Kemp-Benedict, E., Riahi, K., Rothman, D. S., Van Ruijven, B. J., Van Vuuren, D. P., Birkmann, J., Kok, K., et al.: The roads ahead: Narratives for shared socioeconomic pathways describing world futures in the 21st century, *Global environmental change*, 42, 169–180, 2017.
- Paasonen, P., Asmi, A., Petäjä, T., Kajos, M., Äijälä, M., Junninen, H., Holst, T., Abbatt, J., Arneth, A., Birmili, W., et al.: Warming-induced increase in aerosol number concentration likely to moderate climate change, *Nat. Geosci.*, 6, 438–442, 2013.
- Pacifico, F., Harrison, S., Jones, C., Arneth, A., Sitch, S., Weedon, G., Barkley, M., Palmer, P., Serça, D., Potosnak, M., et al.: Evaluation of a photosynthesis-based biogenic isoprene emission scheme in JULES and simulation of isoprene emissions under present-day climate conditions, *Atmospheric Chemistry and Physics*, 11, 4371–4389, 2011.
- Pacifico, F., Folberth, G., Jones, C., Harrison, S., and Collins, W.: Sensitivity of biogenic isoprene emissions to past, present, and future environmental conditions and implications for atmospheric chemistry, *Journal of Geophysical Research: Atmospheres*, 117, 2012.
- Parliament, E.: DIRECTIVE 2004/42/CE OF THE EUROPEAN PARLIAMENT AND OF THE COUNCIL of 21 april 2004 on the limitation of emissions of volatile organic compounds due to the use of organic solvents in certain paints and varnishes and vehicle refinishing products and amending directive 1999/13/EC, 2004.
- Pegoraro, E., Rey, A., Greenberg, J., Harley, P., Grace, J., Malhi, Y., and Guenther, A.: Effect of drought on isoprene emission rates from leaves of *Quercus virginiana* Mill., *Atmospheric Environment*, 38, 6149–6156, 2004.
- Peñuelas, J. and Llusà, J.: The complexity of factors driving volatile organic compound emissions by plants, *Biologia plantarum*, 44, 481–487, 2001.
- Peñuelas, J. and Llusà, J.: BVOCs: plant defense against climate warming?, *Trends in plant science*, 8, 105–109, 2003.
- Possell, M. and Hewitt, C. N.: Isoprene emissions from plants are mediated by atmospheric CO₂ concentrations, *Global Change Biology*, 17, 1595–1610, 2011.
- Ragothaman, A. and Anderson, W. A.: Air quality impacts of petroleum refining and petrochemical industries, *Environments*, 4, 66, 2017.

BIBLIOGRAPHY

- Rao, S., Klimont, Z., Smith, S. J., Van Dingenen, R., Dentener, F., Bouwman, L., Riahi, K., Amann, M., Bodirsky, B. L., van Vuuren, D. P., et al.: Future air pollution in the Shared Socio-economic Pathways, *Global Environmental Change*, 42, 346–358, 2017.
- Ren, J., Guo, F., and Xie, S.: Diagnosing ozone–NO_x–VOC sensitivity and revealing causes of ozone increases in China based on 2013–2021 satellite retrievals, *Atmospheric Chemistry and Physics*, 22, 15 035–15 047, 2022.
- Renwick, J. and Potter, J.: Effects of sulfur dioxide on volatile terpene emission from balsam fir, *Journal of the Air Pollution Control Association*, 31, 65–66, 1981.
- Sakulyanontvittaya, T., Duhl, T., Wiedinmyer, C., Helmig, D., Matsunaga, S., Potosnak, M., Milford, J., and Guenther, A.: Monoterpene and sesquiterpene emission estimates for the United States, *Environmental science & technology*, 42, 1623–1629, 2008.
- Sanhueza, P. A., Reed, G. D., Davis, W. T., and Miller, T. L.: An environmental decision-making tool for evaluating ground-level ozone-related health effects, *Journal of the Air & Waste Management Association*, 53, 1448–1459, 2003.
- Saunier, A., Ormeño, E., Piga, D., Armengaud, A., Boissard, C., Lathière, J., Szopa, S., Genard-Zielinski, A.-C., and Fernandez, C.: Isoprene contribution to ozone production under climate change conditions in the French Mediterranean area, *Regional Environmental Change*, 20, 1–8, 2020.
- Séférian, R., Nabat, P., Michou, M., Saint-Martin, D., Voldoire, A., Colin, J., Decharme, B., Delire, C., Berthet, S., Chevallier, M., et al.: Evaluation of CNRM Earth System Model, CNRM-ESM2-1: Role of Earth system processes in present-day and future climate, *Journal of Advances in Modeling Earth Systems*, 11, 4182–4227, 2019.
- Sellar, A. A., Walton, J., Jones, C. G., Wood, R., Abraham, N. L., Andrejczuk, M., Andrews, M. B., Andrews, T., Archibald, A. T., de Mora, L., et al.: Implementation of UK Earth system models for CMIP6, *Journal of Advances in Modeling Earth Systems*, 12, e2019MS001 946, 2020.
- Sharkey, T. D. and Loreto, F.: Water stress, temperature, and light effects on the capacity for isoprene emission and photosynthesis of kudzu leaves, *Oecologia*, 95, 328–333, 1993.
- Sharkey, T. D. and Singaas, E. L.: Why plants emit isoprene, *Nature*, 374, 769–769, 1995.
- Shulaev, V., Silverman, P., and Raskin, I.: Airborne signalling by methyl salicylate in plant pathogen resistance, *Nature*, 385, 718–721, 1997.

- Sillman, S.: The relation between ozone, NO_x and hydrocarbons in urban and polluted rural environments, *Atmospheric Environment*, 33, 1821–1845, 1999.
- Sindelarova, K., Granier, C., Bouarar, I., Guenther, A., Tilmes, S., Stavrakou, T., Müller, J.-F., Kuhn, U., Stefani, P., and Knorr, W.: Global data set of biogenic VOC emissions calculated by the MEGAN model over the last 30 years, *Atmospheric Chemistry and Physics*, 14, 9317–9341, 2014.
- Sindelarova, K., Markova, J., Simpson, D., Huszar, P., Karlicky, J., Darras, S., and Granier, C.: High-resolution biogenic global emission inventory for the time period 2000–2019 for air quality modelling, *Earth System Science Data*, 14, 251–270, 2022.
- Squire, O., Archibald, A., Abraham, N., Beerling, D., Hewitt, C., Lathièrè, J., Pike, R., Telford, P., and Pyle, J.: Influence of future climate and cropland expansion on isoprene emissions and tropospheric ozone, *Atmospheric Chemistry and Physics*, 14, 1011–1024, 2014.
- Srivastava, D., Vu, T. V., Tong, S., Shi, Z., and Harrison, R. M.: Formation of secondary organic aerosols from anthropogenic precursors in laboratory studies, *npj Climate and Atmospheric Science*, 5, 22, 2022.
- Stockwell, W. R., Kirchner, F., Kuhn, M., and Seefeld, S.: A new mechanism for regional atmospheric chemistry modeling, *Journal of Geophysical Research: Atmospheres*, 102, 25 847–25 879, 1997.
- Street, R., Owen, S., Duckham, S., Boissard, C., and Hewitt, C.: Effect of habitat and age on variations in volatile organic compound (VOC) emissions from *Quercus ilex* and *Pinus pinea*, *Atmospheric Environment*, 31, 89–100, 1997.
- Tai, A. P., Mickley, L. J., Heald, C. L., and Wu, S.: Effect of CO₂ inhibition on biogenic isoprene emission: Implications for air quality under 2000 to 2050 changes in climate, vegetation, and land use, *Geophysical Research Letters*, 40, 3479–3483, 2013.
- Tarayre, M., Thompson, J. D., Escarré, J., and Linhart, Y. B.: Intra-specific variation in the inhibitory effects of *Thymus vulgaris* (Labiatae) monoterpenes on seed germination, *Oecologia*, 101, 110–118, 1995.
- Tiiva, P., Faubert, P., Michelsen, A., Holopainen, T., Holopainen, J. K., and Rinnan, R.: Climatic warming increases isoprene emission from a subarctic heath, *New Phytologist*, 180, 853–863, 2008.
- Tingey, D. T., Manning, M., Grothaus, L. C., and Burns, W. F.: Influence of light and temperature on monoterpene emission rates from slash pine, *Plant Physiology*, 65, 797–801, 1980.

BIBLIOGRAPHY

- Turlings, T. C., Tumlinson, J. H., and Lewis, W. J.: Exploitation of herbivore-induced plant odors by host-seeking parasitic wasps, *Science*, 250, 1251–1253, 1990.
- Unger, N.: Human land-use-driven reduction of forest volatiles cools global climate, *Nature Climate Change*, 4, 907–910, 2014a.
- Unger, N.: On the role of plant volatiles in anthropogenic global climate change, *Geophysical Research Letters*, 41, 8563–8569, 2014b.
- Wang, C., Wang, Z., Qiao, X., Li, Z., Li, F., Chen, M., Wang, Y., Huang, Y., and Cui, H.: Antifungal activity of volatile organic compounds from *Streptomyces alboflavus* TD-1, *FEMS microbiology letters*, 341, 45–51, 2013.
- Ward, D., Mahowald, N., and Kloster, S.: Potential climate forcing of land use and land cover change, *Atmospheric Chemistry and Physics*, 14, 12 701–12 724, 2014.
- Wilkinson, M. J., Monson, R. K., Trahan, N., Lee, S., Brown, E., Jackson, R. B., Polley, H. W., Fay, P. A., and Fall, R.: Leaf isoprene emission rate as a function of atmospheric CO₂ concentration, *Global Change Biology*, 15, 1189–1200, 2009.
- WMO, G.: International meteorological vocabulary, 1966.
- Wright, G. A. and Schiestl, F. P.: The evolution of floral scent: the influence of olfactory learning by insect pollinators on the honest signalling of floral rewards, *Functional Ecology*, 23, 841–851, 2009.
- Zhang, Y., Hu, X.-M., Leung, L. R., and Gustafson Jr, W. I.: Impacts of regional climate change on biogenic emissions and air quality, *Journal of Geophysical Research: Atmospheres*, 113, 2008.

BIBLIOGRAPHY

Appendix A: The Jacobs A-gs model

The photosynthesis ISBA-A-gs model is based on the A-gs model described in Jacobs (1994) and Jacobs et al. (1996).

The net CO_2 assimilation rate at limiting CO_2 and saturated light conditions A_m is:

$$A_m = A_{m,max} \times (1 - \exp(\frac{-g_m^* \times (C_i - \Gamma)}{A_{m,max}})) \quad (6.1)$$

Where $A_{m,max}$ is the maximum net assimilation rate, g_m^* is the unstressed mesophyll conductance parameter, C_i is the leaf internal CO_2 concentration and Γ is the CO_2 compensation concentration. $A_{m,max}$ and Γ

The CO_2 leaf internal concentration C_i is expressed as:

$$C_i = C_s \times (f + (1 - f) \times \frac{\Gamma}{C_s}) \quad (6.2)$$

With

$$f = f_0 \times (1 - \frac{D_s}{D_{max}}) + f_{min} \times \frac{D_s}{D_{max}} \quad (6.3)$$

$$f_{min} = \frac{g_c}{g_c + g_m} \quad (6.4)$$

Where C_s is the CO_2 concentration at the leaf surface, D_s is the saturation deficit at the leaf surface, D_{max} is the maximum saturation deficit, f_0 is the value of for $D_s = 0$ $g \text{ kg}^{-1}$, g_c is the cuticular conductance and g_m is the mesophyll conductance.

The net CO_2 assimilation rate at limiting light and saturated CO_2 conditions A_n is:

$$A_n = (A_m + R_d) \times (1 - \exp(\frac{-\epsilon \times I_a}{A_m + R_d})) - R_d \quad (6.5)$$

With

$$R_d = \frac{A_m}{9} \quad (6.6)$$

$$\epsilon = \epsilon_0 \times \frac{C_i - \Gamma}{C_i + 2\Gamma} \quad (6.7)$$

Where R_d is the rate of dark respiration, ϵ is the quantum use efficiency, ϵ_0 is the maximum quantum use efficiency and I_a is the amount of light reaching the leaves (PAR).

The leaf conductance to CO_2 g_{sc} can be finally calculated as:

$$g_{sc} = g_{sc}^* + E \times \frac{M_a}{\rho_a M_v} \times \frac{C_s + C_i}{2 * (C_s - C_i)} \quad (6.8)$$

With

$$g_{sc}^* = \frac{A_n - A_{min} \frac{D_s(A_n + R_d)}{D_{max}(A_m + R_d)} + R_d \left(1 - \frac{A_n + R_d}{A_m + R_d}\right)}{C_s - C_i} \quad (6.9)$$

$$A_{min} = g_m(C_{min} - \Gamma) \quad (6.10)$$

$$E = \rho_a g_s D_s \quad (6.11)$$

Where C_{min} represents the value of the leaf CO_2 internal concentration for $D_s = D_{max}$, M_v and M_a represent the molecular mass of water and air, E is the leaf transpiration.

The leaf conductance to water vapour g_s is calculated as:

$$g_s = 1.6 \times g_{sc}^* + g_c \quad (6.12)$$

Appendix B: Supplementary figures of Chapter 5

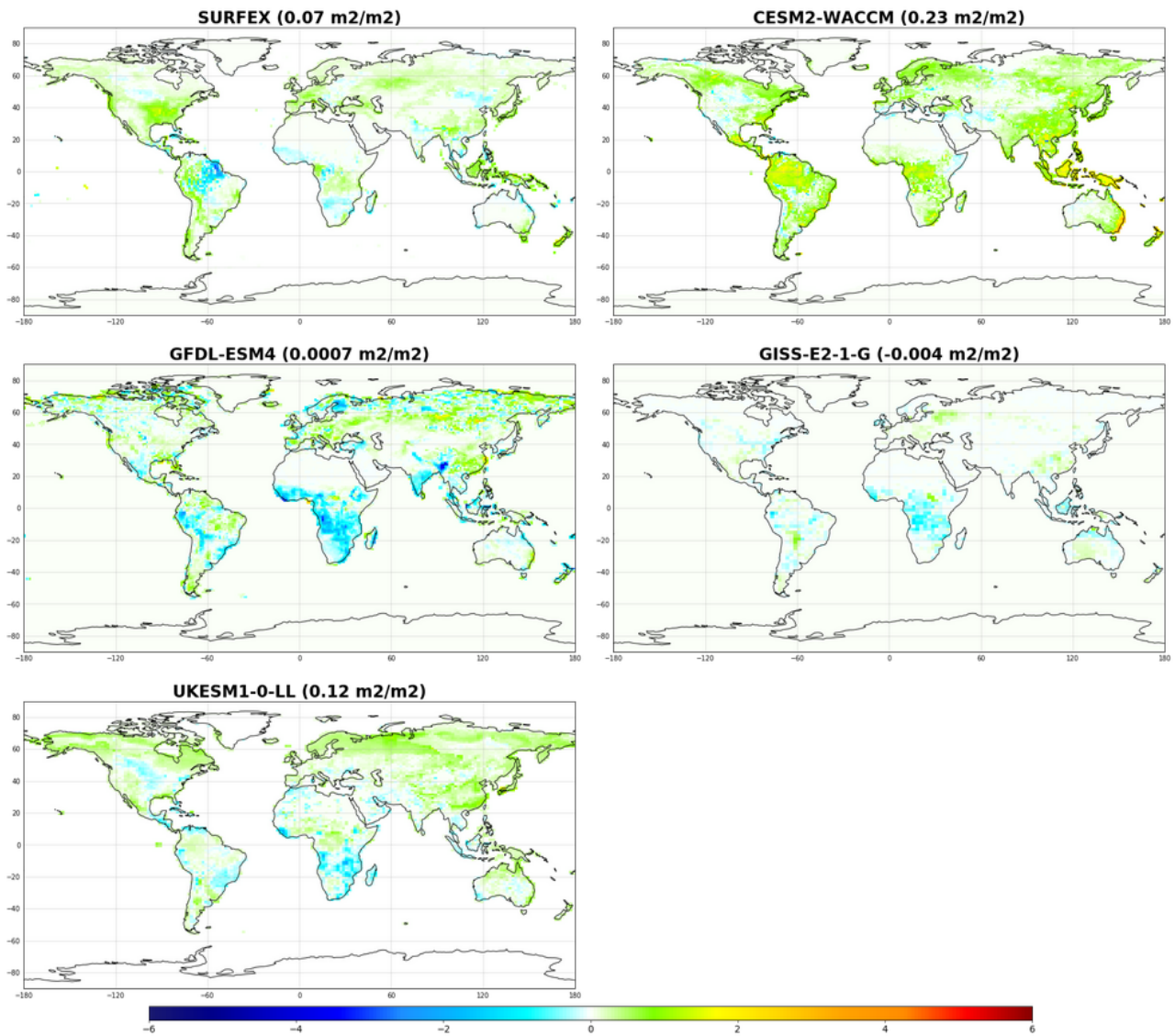


Figure B.1: Leaf area index absolute difference between 2046-2050 and 2010-2014 for the coupled model SURFEX-MEGAN and the 4 CMIP6 models: CESM2-WACCM, GFDL-ESM4, GISS-E2-1-G and UKESM1-0-LL.

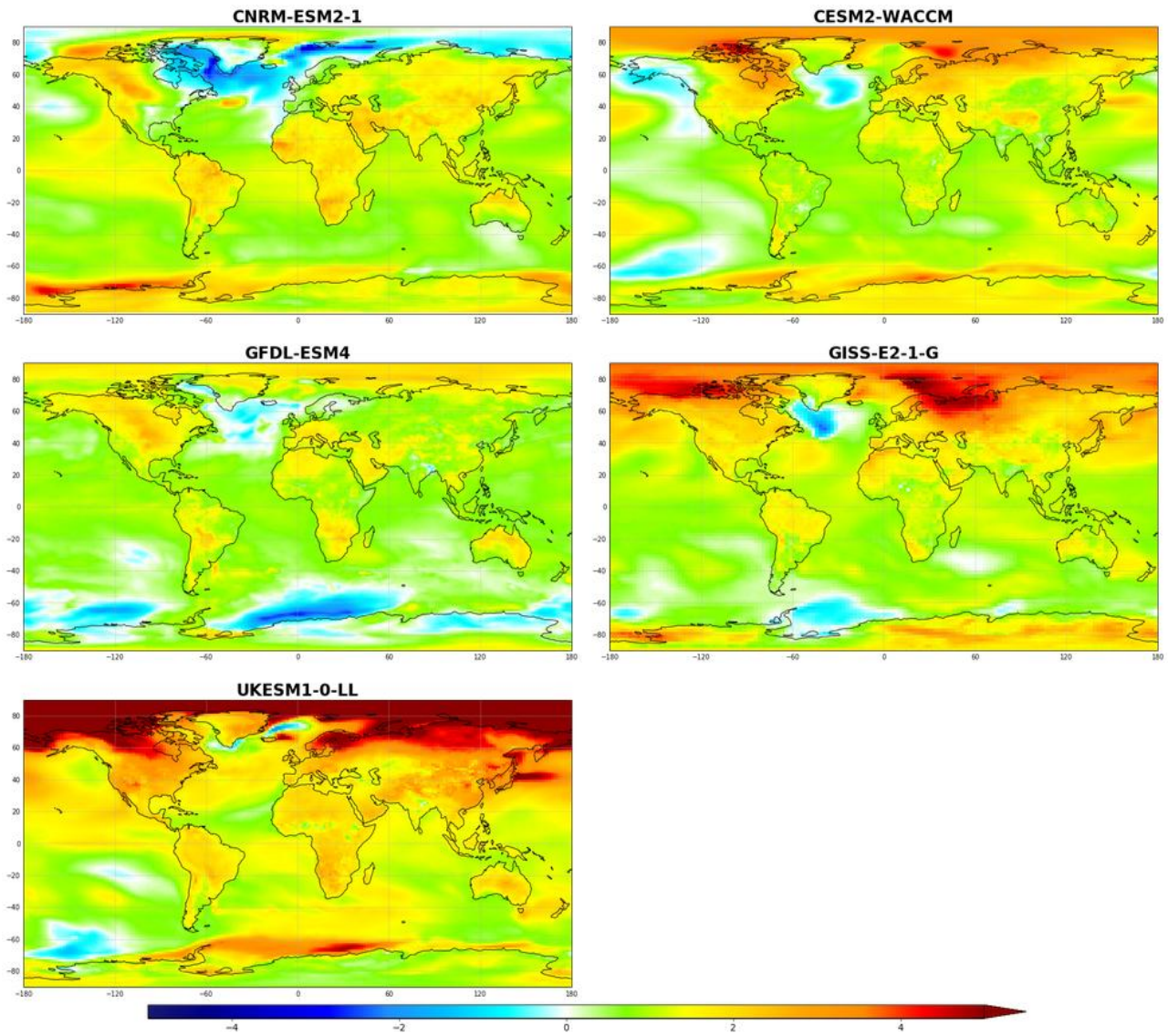


Figure B.2: Temperature absolute difference between 2046-2050 and 2010-2014 for the 5 CMIP6 models: CNRM-ESM2-1, CESM2-WACCM, GFDL-ESM4, GISS-E2-1-G and UKESM1-0-LL.

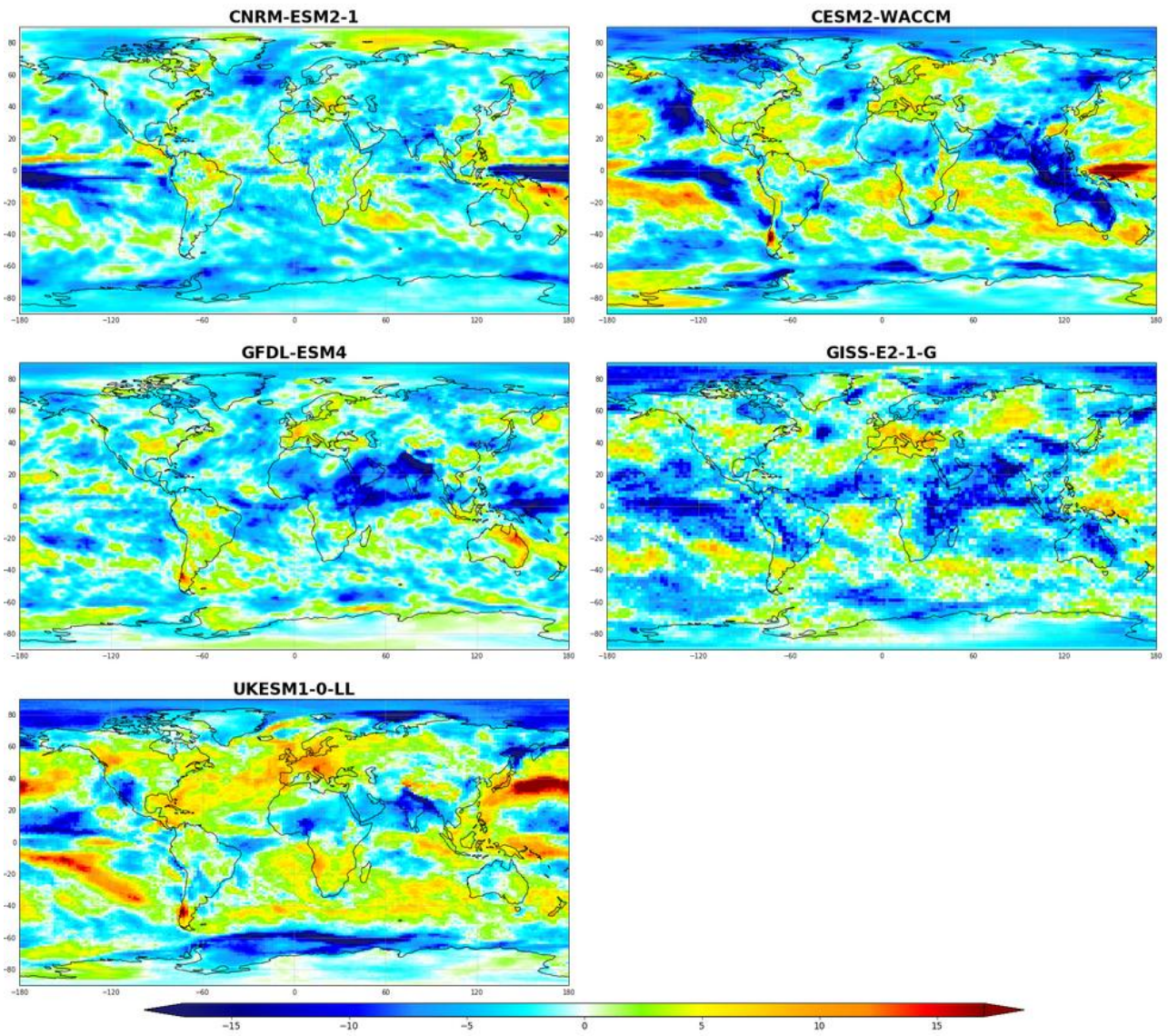


Figure B.3: Solar radiation absolute difference between 2046-2050 and 2010-2014 for the 5 CMIP6 models: CNRM-ESM2-1, CESM2-WACCM, GFDL-ESM4, GISS-E2-1-G and UKESM1-0-LL.

”My quest has taken me to the
physical,
the metaphysical,
the delusional and back.”

John Forbes Nash

Titre : Impact d'un climat à +2°C sur les émissions des composés biogéniques volatils et sur la qualité de l'air

Mots clés : qualité de l'air, composés biogéniques volatiles, changement climatique, ozone, isoprène, MEGAN

Résumé : Une fois que les composés organiques volatils (COV) sont libérés dans l'atmosphère, ils jouent un rôle majeur dans l'altération de sa chimie et de sa composition, impactant ainsi le climat mondial. Les COV émis par des sources naturelles représentent 90% du total des COV émis, ce qui fait des composés organiques volatils biogéniques (COVB) un contributeur clé à la formation de plusieurs polluants atmosphériques. L'influence des COVB va au-delà des préoccupations liées à la qualité de l'air, car ils peuvent affecter le climat par la formation d'aérosols ayant un effet de refroidissement et de gaz à effet de serre ayant un effet de réchauffement, impactant ainsi le forçage radiatif net de la Terre. À l'inverse, le climat peut influencer la libération des espèces biogéniques par le biais du réchauffement climatique, des changements de couverture et d'utilisation des sols, de la sécheresse et de l'augmentation des concentrations atmosphériques en CO₂. Le présent travail vise à évaluer comment les émissions de COVB évolueront dans des conditions de changement climatique de +2°C et comment ce changement affectera la qualité de l'air dans le futur. À cette fin, un travail conséquent a été entrepris pour coupler les modèles SURFEX (SURface Externalisée) et MEGAN (Model of Emission of Gases and Aerosols from Nature). Le modèle couplé SURFEX-MEGAN permettra la simulation des émissions futures d'espèces biogéniques ainsi que d'autres facteurs clés d'émission tels que l'indice de surface foliaire (LAI), l'humidité du sol, la température du sol, etc. L'impact du changement climatique sur les émissions d'isoprène a été évalué en réalisant deux simulations globales représentant les conditions climatiques actuelles et futures sur la période 2010-2014 et 2046-2050, respectivement. Les résultats de cette étude indiquent une augmentation globale des émissions d'isoprène de 13% (40 Tg). Cette variation prend en compte l'effet de la température, du rayonnement solaire et des concentrations atmosphériques en CO₂. La température a l'effet positif le plus élevé. Le rayonnement solaire a un effet négatif car il diminue selon le scénario SSP3-7.0, et les concentrations de CO₂ ont à la fois des effets positifs et négatifs. Le premier résulte de l'effet de fertilisation par le CO₂ et le second de l'effet d'inhibition du CO₂. Les résultats de SURFEX-MEGAN ont été confrontés à d'autres projections provenant des modèles CMIP6. La plupart des modèles ont prédit une tendance positive pour les émissions futures d'isoprène. Les disparités dans les résultats des modèles sont attribuées aux variations dans les schémas d'isoprène, la résolution, la distribution et la densité de la végétation, mais surtout, les sorties de température et de rayonnement solaire de chaque modèle différaient, malgré l'utilisation du même scénario SSP. L'étude de l'impact du changement climatique sur les niveaux futurs d'ozone a montré que la charge d'ozone augmentera de 5% en 2050 par rapport à 2013. Ce changement est principalement dû à la modification des émissions anthropiques de NO_x et de COV. Bien que la sensibilité de l'ozone à l'isoprène soit élevée, l'inclusion des changements futurs dans les émissions d'isoprène n'a qu'un effet marginal sur les tendances globales de l'ozone. Cependant, cet effet est significatif à l'échelle régionale et locale, où l'ozone est positivement et négativement corrélé aux tendances de l'isoprène dans les régions à forte et faible concentration de NO_x, respectivement. L'impact des émissions d'isoprène sur la qualité de l'air future est le plus significatif lorsque l'on néglige l'effet inhibiteur du CO₂ sur les émissions d'isoprène. Dans ce cas, la qualité de l'air était prévue s'améliorer à l'échelle globale et particulièrement dans les régions tropicales dans le futur, par rapport à un scénario climatique futur avec des émissions d'isoprène correspondant au climat actuel.

Title: Impact of a +2°C climate on the emission of biogenic volatile organic compounds and on air quality

Key words: air quality, biogenic volatile organic compounds, climate change, ozone, isoprene, MEGAN

Abstract: Once Volatile Organic Compounds (VOCs) are released into the atmosphere, they play a major role in altering its chemistry and composition, consequently impacting the global climate. VOCs released from natural sources account for 90% of the total emitted VOCs, which makes Biogenic Volatile Organic Compounds (BVOCs) a key contributor to the formation of several air pollutants. The influence of BVOCs goes beyond air quality concerns, as they can impact the climate through the formation of aerosols which have a cooling effect and greenhouse gases which have a warming effect, thus effecting the Earth's net radiative forcing. Conversely, climate can effect the release of biogenic species through global warming, land cover and land use change, drought and increasing atmospheric CO₂ concentrations. The present work aims to evaluate how BVOCs emission will evolve in a +2°C climate change conditions and how this change will effect air quality in the future. For this purpose, a consequent work was undertaken to couple the SURFEX (SURface Externalisée in French) and MEGAN (Model of Emission of Gases and Aerosols from Nature) models. The coupled model SURFEX-MEGAN will allow the simulation of future emissions of biogenic species along with other important emission key drivers such as leaf area index, soil moisture, soil temperature, etc. The impact of climate change on isoprene emissions was assessed by conducting two global simulations representing present- and future-climate conditions over 2010-2014 and 2046-2050, respectively. The results of this study indicate a global increase of isoprene emissions by 13% (40Tg). This change account for the effect of temperature, solar radiation and atmospheric CO₂ concentrations. Temperature have the highest positive effect. Solar radiation have a negative effect as it decreased under the SSP3-7.0 scenario and CO₂ concentrations have both positive and negative effects. The former arises from the CO₂ fertilization effect and the latter from the CO₂ inhibition effect. The SURFEX-MEGAN results were confronted to other projections from CMIP6 models. Most of the models predicted a positive trend in future isoprene emissions. The disparities in model results are attributed to variations in isoprene schemes, resolution, vegetation distribution, and density, but most importantly, each model's output of temperature and solar radiation differed, despite employing the same SSP scenario. The study of the impact of climate change on future ozone levels showed that the ozone burden will increase by 5% in 2050 compared to 2013. This change is mainly due to the change in human-induced NO_x and VOC emissions. Although ozone's sensitivity to isoprene is high, the inclusion of future changes in isoprene emissions have only a marginal effect on global ozone trends. However, this effect is significant at regional and local scales, where ozone is positively and negatively correlated to isoprene trends in high and low NO_x regions, respectively. The impact of isoprene emissions in future air quality is most significant when neglecting the inhibitory effect of CO₂ on isoprene emissions. In this case air quality was predicted to improve at a global scale and in tropical regions particularly in the future compared to a future-climate scenario with present-climate isoprene emissions.